

Annual Report 2018-19

Institute of Seismological Research
Department of Science and Technology
Government of Gujarat

Contributors

Group & Principal Investigator	Scientist/ Researcher
Near Real Time Seismology PI: Dr. Santosh Kumar, Scientist-D	Dr. P.Mahesh, Scientist-B Dr. A.P.Singh, Scientist-B Dr. Pavan Kumar Gayatri, Scientist-B Mr. Ketan Singha Roy, Scientist-B Ms. Vishwa Joshi, Scientist-B Ms. Vandana Patel, Sr Geophysicist Mr. Alla Sateesh, Sr Geophysicist Ms. Monika Bhatia, JRF
Seismic Hazard Assessment and Microzonation PI: Dr. Sumer Chopra, Scientist-G	Dr. Kapil Mohan, Scientist-C Dr. Pallabee Choudhury, Scientist-C Dr. Madan Mohan Rout, Scientist-C Dr. B. Sairam, Scientist-B Dr. Pavan Kumar Gayatri, Scientist-B Dr. Vasu Pancholi, Scientist-B Dr. Archana Das, Scientist-B Ms. Vandana Patel, Sr Geophysicist Mr. Naveen Kumar, Sr Geophysicist Mr. Vinay Kr Dwivedi, Sr Geophysicist Mr. Tarun Solanki, Sr Geophysicist Mr. Peush Chaudhary, Geophysicist Mr. Pruthul Patel, Geophysicist Mr. Dilip Singh, Geophysicist Mr. Mehul Nagar, Geophysicist Ms. Charu Kamra, JRF Ms. Shruti Dugar, JRF Ms. Neha Tanwar, JRF Mr. Akash Solanki, PF Mr. Russi Modi, PF
Solid Earth Geophysics PI: Dr. M.Ravi Kumar, Distinguished Scientist	Dr. A.P. Singh, Scientist-B Dr. Jyoti Sharma, Scientist-B Dr. Pavan Kumar Gayatri, Scientist-B Dr. G. Srijayanthi, Scientist-B Dr. Chinmay Halder, Scientist-B Dr. Himangshu Paul, NPDF Mr. Avinash Chauhan, Sr. Geophysicist Mr. Mayank Dikshit, Geophysicist

	<p>Mr. Arjav Shukla, Geophysicist Mr. Mehul Nagar, Geophysicist Mr. Dilip Singh, Geophysicist Mr. Virender Kumar Singh, JRF Ms. Indu Chaudhary, JRF Ms. Monika Bhatia, JRF Mr. Gaurav Dave, JRF Mr. Rakesh Nikam, PF Mr. Dinesh Singh, PF</p>
<p>Earthquake Precursory Research PI: Dr. K.M. Rao, Scientist-D</p>	<p>Mr. M.S.B.S.Prasad, Scientist-B Mr. C.P.Simha , Geophysicist Mr. Sushant Sahoo, Geophysicist Mr. Shivam Joshi, JRF Ms. Archana Radhakrishnan, PF</p>
<p>Active Tectonics PI: Dr. Pallabee Choudhury, Scientist-C</p>	<p>Dr. Siddharth Prizomwala, Scientist-B Dr. Girish Kothiyari, Scientist-B Dr. Falguni Bhattacharya, Scientist-B Dr. Rakesh Dumka, Scientist-B Dr. Rajeev Kr. Yadav, Scientist-B Dr. Archana Das, Scientist-B Mr. Tarun Solanki, Sr.Geologist Mr. Nisarg Makwana, Geophysicist Mr. Durga Prasad, JRF Mr. Raj Sunil Kandergula, JRF Ms. Sneha Mishra, JRF Ms. RiyankaTalukdar, JRF Ms. Neha Joshi, JRF Ms. Pratishtha Narian, JRF Mr. D. Suribabu, JRF Ms. Aashima Sodhi, JRF Mr. Chintan Vedpathak, PF</p>
<p>Commercial Research and Development PI: Dr. Kapil Mohan, Scientist-C</p>	<p>Dr. Siddharth Prizomwala, Scientist-B Dr. Vasu Pancholi, Scientist-B Mr. Naveen Kumar, Sr Geophysicist</p>

Contents

		Page No.
RESEARCH HIGHLIGHTS		1
RESEARCH CONTRIBUTIONS		4
1. NEAR REAL TIME SEISMOLOGY		4
1.1	Earthquake Monitoring and Seismicity Patterns in Gujarat	4
1.2	Description of Earthquakes in Different Parts of Gujarat	4
1.3	Description of Recorded Earthquakes in Different Parts of Gujarat since inception of the network till 2015	9
1.4	Development of Python based Software to analyse the Low Frequency Passive Seismic data for hydrocarbon exploration	11
1.5	Study on Earthquake Swarms in Palghar District, Maharashtra	15
1.6	Earthquake swarms in South Gujarat	17
1.7	Study on moment release and mechanical coupling between fault systems	19
1.8	Earthquake data processing and interpretation of MEQ data collected during Jan-July 2018 for study of seismogenic sources around the Subansiri Lower Hydro Electric (HE) Project, Arunachal Pradesh	20
2. SEISMIC HAZARD ASSESSMENT AND MICROZONATION		21
2.1	An Assessment of Peak Horizontal Ground Acceleration from Intraplate Earthquakes in Kachchh, Gujarat, India	21
2.2	A review of Seismic hazard assessment of Gujarat: a highly active intra-plate region	21
2.3	Influence of Local Site Effects in the Ahmedabad Mega City on the Damage due to Past Earthquakes in Northwestern India	22
2.4	Comparison of earthquake source characteristics in the Kachchh Rift Basin and Saurashtra horst, Deccan Volcanic Province, western India	24
2.5	Simulation of strong ground motion in the Rapar city using Neo-Deterministic Seismic Hazard Assessment (NDSHA) approach	26
2.6	Impact on seismic hazard of Kachchh due to change in dip of Kachchh Mainland fault	28
2.7	Deterministic Seismic Hazard Assessment (DSHA) of Khavda (Kachchh), Gujarat	29
2.8	Seismic Microzonation of Bhuj City, Kachchh (Gujarat)	30
2.9	Uncertainty/ Parametric Analysis for Ground Motion Estimation in Bhuj City	31
2.10	Comparative seismic hazard assessment in southern part of Gandhinagar (GIFT City, Gujarat) and Andheri (Mumbai, Maharashtra)	32
2.11	Kachchh Mainland Fault: Characterization and associated seismic hazard	33

		Page No.
2.12	Rapid Visual Screening (RVS) of RC frame buildings in Ahmedabad, India	34
2.13	Seismic Risk and Loss Assessment in Bhachau City	35
2.14	MT survey in Dudhai (Kachchh) for subsurface mapping	36
2.15	Magnetotelluric investigation in Little Rann area of Kachchh region	38
2.16	Dimensionality and Directionality analysis of MT data in the Kachchh Mainland Upliftment (KMU)	39
2.17	Magnetotelluric investigations in the western part of Narmada Son lineament zone	40
2.18	Magnetotelluric study in the Talala region of Saurashtra	41
2.19	Study of Lineaments and faults in Dadra and Nagar Haveli, western India	43
2.20	Palaeochannel Study in Dadra and Nagar Haveli	44
2.21	Trigger Mechanism for soft sediment deformation structures in Dadra and Nagar Haveli region	45
3. SOLID EARTH GEOPHYSICS		48
3.1	Site response study in and around the Bhuj City	48
3.2	Estimation of Shallow Structure beneath the Saurashtra region by array microtremor measurements and horizontal to-vertical spectral ratio method	49
3.3	Investigation of spatial and temporal variability of site response in the Arunachal Himalaya using ambient seismic noise and earthquake waveforms	50
3.4	Feasibility study on Low Frequency Passive Seismic (LFPS) survey in NELP Block WB-ONN-2005/4, MBA Basin	51
3.5	Investigation of Groundwater resources in the Kachchh district, Gujarat using Transient Electromagnetics	52
3.6	Integrated geophysical studies to delineate the structural features in the Ambaji mineralization zone, Gujarat, NW India	52
3.7	Tectonic trends and new crustal structure of the North Cambay rift basin, India deduced from integrated study of gravity, magnetic and seismic data	53
3.8	Delineation of lineaments in the Cambay rift and surrounding regions of NW India utilizing satellite derived EIGEN6C4 gravity data	55
3.9	Structural interpretation over the epicentre zone of 1819 Allah-Bund earthquake, North-western India using gravity data	56
3.10	Magnetotelluric imaging of the Allah-bund Fault: Seismotectonic implications on the Kachchh intraplate region, Western India	58
3.11	Magnetotelluric investigations in Eastern part of the Kachchh rift basin	59
3.12	Music of subterranean Seismic Signals recorded in Gujarat Region	60
3.13	Low - frequency microtremor anomalies at Mansa and Jotana areas in western India	62

		Page No.
3.14	Seismicity and décollement geometry beneath the Sikkim Himalaya using Local earthquake tomography	63
3.15	Radial Anisotropy study for the crustal and upper mantle structure beneath the Deccan Volcanic Province (DVP)	65
3.16	Identification of anomalous velocity features by cluster analysis	66
3.17	Evidence of seismic anisotropy in the D" layer using waveform data from Gujarat seismic stations	67
3.18	Widespread crustal magmatism in the Kachchh region– Evidence from shear wave velocity contrast across Moho	67
4. EARTHQUAKE PRECURSORY RESEARCH		69
4.1	Atmospheric and Ionospheric perturbations associated with the 6 th Feb 2018 Taiwan earthquake	69
4.2	Observation of abnormal thermal and infrasound signals prior to the Taiwan earthquake (M6.4) on Feb 6, 2018	71
4.3	Preliminary results of Magnetic survey at Desalpar	74
4.4	Diurnal variation of the Geomagnetic field (H component) near low latitude sites	76
4.5	Estimation of influence of Prompt penetration effects on Equatorial Electrojet (EEJ) in the Indian sector	78
4.6	Preliminary results of Magnetic survey at Badargadh	80
4.7	Anomalous Total Electron Content (TEC) before the Taiwan earthquake	81
4.8	Geomagnetic data characterization and analysis of seasonal trend of solar quiet time current at low latitude sites of Indian sector during different phase of solar cycle-24	84
4.9	Identification of suitable sites for two new magnetic stations	89
4.10	Study of Geomagnetic Pulsations using Induction Coil Magnetometer at MPGOS	90
4.11	Ionospheric Response with the Seismic Wave disturbance at the Madagascar	91
4.12	Characteristics of prompt penetration effects on EEJ from the Indian sector	93
4.13	Statistical characteristics of low latitude Pc4s: insights from Solar wind and IMF parameters in India	96
4.14	Magnetic survey at Amrapar and Kalyanpar	98
4.15	Study of Geomagnetic pulsations in association with the earthquake on 16 April 2013	99
5. ACTIVE TECTONICS		101
5.1	Deformation study of Gujarat	101
5.2	Deformation Study of Uttarakhand Himalaya	101
5.3	GPS measurement of rapid subsidence of Gandhinagar, Gujarat (western India) due to groundwater depletion	102

		Page No.
5.4	Geodetic evidence of high compression across seismically active Kachchh paleo-rift, India	102
5.5	Strong seismic coupling underneath Garhwal-Kumaun region, NW Himalaya, India	102
5.6	Crustal deformation and strain analysis along IBF and ABF	104
5.7	Observation of Holocene Tectonic activity along KHF	105
5.8	New insight into recent earthquake activity in the North Cambay basin, western India: A linkage between seismicity, focal mechanism and geodetic strain rate	105
5.9	Morpho-Structural evidence of Neotectonic activity along the Vigodi Fault, Kachchh, India	106
5.10	New insight into some coastal Harappan sites, Saurashtra, Western India: Implications in human-landscape relationship	106
5.11	Cycles of aggradational and incisional events from the Valley fill sequences, South- eastern Saurashtra	106
5.12	Characterizing the nature and extent of dryland fluvial response to extrinsic parameters since the Last glacial period: An example from Shetrunji basin (western India)	108
6. COMMERCIAL RESEARCH AND DEVELOPMENT		110
6.1	Magnetotelluric survey in the South Cambay basin	110
6.2	Estimation of Mesozoic sediment thickness in the western part of Kachchh	112
6.3	Estimation of sediment thickness (including Mesozoic) considering multiple Magnetotelluric data inversion techniques in the western central part of the Kachchh Basin	113
6.4	Site specific seismic hazard assessment and development of ground response spectra for Ammonia Storage tanks at HURL compound Barauni (Bihar)	115
6.5	Seismic hazard assessment and development of site specific ground response spectra for Ammonia Storage tanks at HURL compound Sindri (Jharkhand)	116
6.6	Delineation of freshwater layer at the selected sites in the Anjar Taluka of Kachchh using Time Domain Electromagnetic Survey	118
6.7	Delineation of Freshwater layer at the selected sites in the Lakhpat, Abdasa and Banni areas of Kachchh using Time Domain Electromagnetic Survey	121
6.8	Geophysical survey (Electrical and Time Domain Electromagnetic) for Delineation of groundwater in the Majivana Taluka of Porbandar	122
PUBLICATIONS		124
NOTABLE EVENTS		130
SOCIETAL OUTREACH		136
CAMPUS NEWS AND EVENTS		139

RESEARCH HIGHLIGHTS

- ✦ Epicentral parameters of 2015 earthquakes, in the magnitude range of M_L 0.5-4.8, which occurred in Gujarat in 2018, are estimated. Of these, 890 earthquakes are from Kachchh, 1046 earthquakes are from Saurashtra and 79 earthquakes are from the Mainland.
- ✦ Micro earthquake study for the Subansiri Lower Hydro Electric (H.E) Project, for the period Jan-July 2018 reveals that majority of the earthquakes are considerably away from the dam site in the vicinity of NNE-SSW striking thrusts.
- ✦ Seismological investigation of Swarms in South Gujarat suggests a causal relation with the Indian summer monsoon, associated with the phenomenon of hydro-seismicity.
- ✦ A comprehensive assessment of peak horizontal ground motion was carried out using waveform data of earthquakes in the Kachchh region, through a new prediction equation and spatial correlation model for PGA.
- ✦ The maximum peak ground acceleration (PGA) of $\sim 1g$ is estimated at the B/C boundary considering the actual shear wave velocity values in Bhuj city, and effects from all the major faults.
- ✦ Simulations reveal a 30-47% increase in seismic hazard in the northern region of the Kachchh Mainland fault (KMF) and 14-38% decrease in the southern part, considering a northward dip of the fault.
- ✦ The PGA estimated through DSHA has been found to be slightly higher than the PGA estimated through PSHA for 10% probability of exceedance, and lower for 1% & 2% probability of exceedance in 50 years in the Sindri (Jharkhand) region.
- ✦ The site specific response spectra at HURL compound Barauni has been generated, for design of Ammonia Storage tanks.
- ✦ Seismic risk and loss assessment at the locations of the buildings collapsed during the 2001 Bhuj earthquake reveals that most of the new buildings constructed may suffer moderate damages in the event of a major earthquake.
- ✦ Low-Frequency Passive Seismic (LFPS) survey has been carried out in the Jotana (Mehsana) and Mansa (Gandhinagar) regions to understand the characteristics and alterations of the microtremor signals, for hydrocarbon detection. Obtained results demonstrate the efficacy of the technique for identifying sweet spots for exploration, as validated by the data from the drill holes of ONGC.
- ✦ Attributes derived from Low Frequency Passive Seismic (LFPS) data of NELP Block WB-ONN-2005/4, MBA Basin enabled discrimination of wells that produce oil/gas and those that are dry.
- ✦ Three potential sites for fresh water at a depth $> 200m$ are suggested in the Anjar Taluka using Time Domain Electromagnetic measurements.
- ✦ The depth of groundwater is found to be $>65m$ at Majivana (Porbandar Taluka & District).
- ✦ In the Bhuj city, the predominant frequency is found to vary between 0.4 and 2.0 Hz. The low amplification values at few a sites indicate that the sites are situated on a

compact platform of Cretaceous sandstone of Bhuj formation, with no other soft rock deposits lying over or in contact with it.

- ✦ Shallow structure beneath the Saurashtra region is imaged by array microtremor measurements.
- ✦ Magnetotelluric investigations reveal a Mesozoic sediment thickness of 1.8-2.0 km in the western part of Kachchh (from Hazipir to Lathedi villages).
- ✦ Magnetotelluric investigations reveal a basement depth of 4.0 km in the Talala region of Saurashtra.
- ✦ The subsurface structure of the western great Rann of Kachchh is imaged through transient electromagnetic (TEM) and wideband (10000Hz-1000s) magnetotelluric (MT) studies.
- ✦ The Girnar fault in the Talala region of Saurashtra is characterized using Magnetotellurics.
- ✦ The first geophysical image of the Allah Bund Fault (ABF) was provided and imaging the subsurface structure in the western Great Rann of Kachchh is attempted through transient electromagnetic (TEM) and wideband (10000Hz-1000s) magnetotellurics (MT) studies.
- ✦ The crustal structure of the North Cambay rift basin, India is investigated using gravity, magnetic and seismic data. A new gravity map for the North Cambay rift basin was prepared, showing a variation of – 40 to +28 mGal.
- ✦ The lineaments in the Cambay rift basin, northwestern India, are delineated using satellite-derived EIGEN6C4 gravity data. Majority of the lineaments trend in the NW-SE and NE-SW directions, with their source depth in the range of 4.4 and 15 km. The NE-SW trending Diyodar and Tharad ridges in the Cambay rift basin are also identified for the first time, using gravity data.
- ✦ The 3-D seismic velocity structure of the Sikkim Himalaya was mapped using Seismic tomography method. Heterogeneous velocity structures, with low and high velocities (V_p and V_s) zones at different depth ranges, are imaged. Results reveal clear evidence for a gentle, north dipping décollement plane at ~20km depth, in terms of significant velocity perturbations across this interface.
- ✦ **The shear wave velocity contrast across the Moho ($\delta\beta_M$) is estimated all over the Gujarat region. The $\delta\beta_M$ values vary spatially from 0.15 to 0.86 km/s.**
- ✦ Anisotropic Surface Wave Tomography study has been performed to investigate the crustal and upper mantle anisotropy in northwestern India.
- ✦ High resolution ($1^\circ \times 1^\circ$) seismic images of the crust and upper mantle beneath the Deccan Volcanic Province (DVP) are obtained through nonlinear inversion of the observed group velocities of Rayleigh and Love waves.
- ✦ The presence of high velocities near the core-mantle boundary beneath all the major geoid lows is revealed by cluster analysis of global tomographic models. Besides this, low velocity structures are observed in the upper mantle (350-800 km) beneath all the geoid lows except Central Asia Geoid Low.
- ✦ Atmospheric and Ionospheric perturbations associated with the 6th Feb 2018 Taiwan earthquake, are studied. An abnormal thermal and infrasound signal was noticed prior to its occurrence.

- ✦ Analysis of the horizontal component of the Geomagnetic data near low latitude sites clearly shows a diurnal trend of 30-40nT.
- ✦ The influence of prompt penetration effects (PPEF) on Equatorial Electrojet (EEJ) using **99 PPEF events is estimated to be $\geq \pm 4$ nT in the Indian sector. The amplitude variation in PPEF on EEJ with longitude indicates that PPEF is influenced by the local ionization.**
- ✦ The response of the ionosphere to the anomalous Seismic Wave disturbance at Madagascar, on 11th Nov 2018 was studied.
- ✦ The seasonal trend of solar quiet time current at low latitude sites of Indian sector is characterised during different phases of the solar cycle-24.
- ✦ The statistical characteristics of low latitude Pc4s and its relation with Solar wind and IMF Parameters in India are determined.
- ✦ The geomagnetic pulsations in association with the earthquake on 16th April 2013 are studied.
- ✦ Magnetic survey in the Badargadh region and detailed analysis of the data indicate that the subsurface material is magnetically homogenous.
- ✦ Various scientific inputs were compiled to identify suitable locations for two new magnetic observatories.
- ✦ The continuous GPS measurements in the Garhwal-Kumaun Himalaya provide the rate of shortening as 18 ± 1 mm/yr and width of the locked frontal portion of the Main Himalayan Thrust (MHT) as 100 ± 15 km. The slip-deficit budget suggests that the brittle part of decollement has a deficit of ~ 4 -meter slip since the last major earthquake (1803 earthquake) in the Garhwal-Kumaun Himalaya.
- ✦ A new insight into the recent earthquake activity in North Cambay basin, western India was provided through a linkage between seismicity, focal mechanisms and geodetic strain rate. The study suggests that the complex geodynamics created around the northern part of the Cambay rift due to various movements along several faults, presence of basement ridges and sub-surface plutonic bodies in a failed rift are creating stresses, causing earthquakes in this part of the rift.
- ✦ Geological, Geomorphological and Tectonic maps of the Junagadh and Bhavnagar districts are prepared on a GIS platform.
- ✦ Higher density of NNE-SSW oriented linear structures along the Panvel flexure is evidenced geologically. The presence of seismicity along these linear trends signifies the active nature of the Panvel flexure.
- ✦ The signature of neotectonic activity is observed in Dadra and Nagar Haveli regions.
- ✦ Lithostratigraphy of the Shetrunji River basin was prepared from the valley fill Quaternary sequences.

RESEARCH CONTRIBUTIONS

1. NEAR REAL TIME SEISMOLOGY

1.1 Earthquake Monitoring and Seismicity Patterns in Gujarat

(Santosh Kumar, P Mahesh, A P Singh, Ketan Singha Roy, Vandna Patel)

The Gujarat State Seismic Network operated under the aegis of the Institute of Seismological Research, Gandhinagar is well maintained since July 2006. The network consists of 60 Broadband Seismograph Stations (BBS) spreadout in the state and neighboring areas (Fig.1.1). The data from almost 45 BBS is transmitted to the Institute of Seismological Research through VSAT, where the earthquake activity is monitored in near real time (24x7). Further, 54 Strong Motion Accelerographs (SMA) are also deployed at the BBS locations. The network has a detectability of M 2.0 in the Kachchh active area and M 2.5 in other areas of Gujarat.



Fig. 1.1: The distribution of BBS and SMA stations of the Gujarat State Seismic Network. The blue triangles represent the 15 standalone BBS; aperture antenna symbols are the 45 BBS connected through VSAT for online data transfer and red diamonds are the 54 SMA stations.

During 2018, the network recorded 2857 earthquakes out of which the epicentral parameters of 2015 local earthquakes were determined. Additionally, 28 regional earthquakes from other Indian states were also recorded. Some 245 distant earthquakes of M 5.0 or greater were recorded by the GSSN stations, including M 8.2 Fiji earthquake of 19 August 2018.

1.2 Description of Earthquakes in Different Parts of Gujarat

(Santosh Kumar, P Mahesh, A P Singh, Ketan Singha Roy, Vandna Patel)

Magnitude-wise distribution of earthquakes in the three regions of Gujarat during 2018 is given in Table 1.1. In the Kachchh region, 890 shocks were located of M0.5- 4.8. In the Saurashtra region, 1046 shocks of M 1.1 -3.7 were located. In the Mainland, 79 shocks of M1.0 – 3.7 were located (Fig. 1.2).

Table 1.1: Regional distribution of earthquakes located in the Gujarat during 2018

Region	M 0.5 - 1.9	M 2.0 - 2.9	M 3.0 - 3.9	M 4.0 - 4.9	Total
Kachchh	630	227	30	3	890
Saurashtra	806	237	3	0	1046
Mainland	39	33	7	0	79
Total	1475	497	40	3	2015

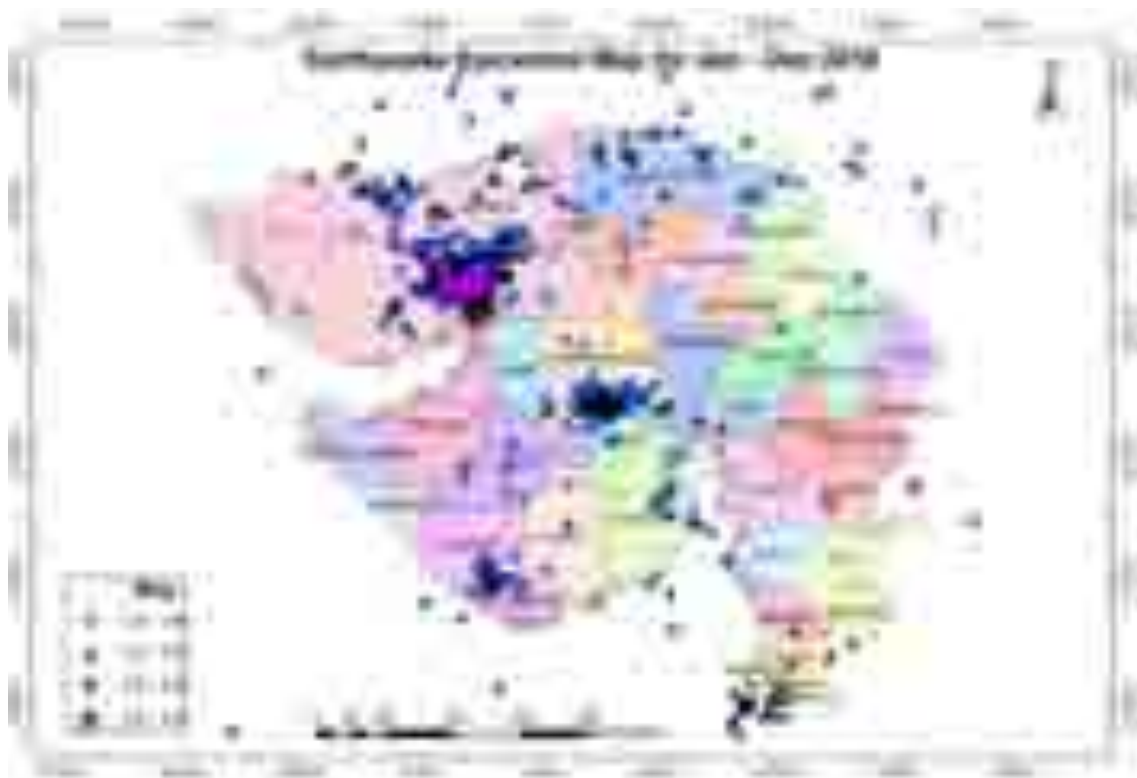


Fig. 1.2: Epicenters of earthquakes of M0.5-4.8 that occurred in Gujarat in 2018, and neighbouring regions.

Seismicity in Kachchh

This year in Kachchh there were 890 shocks out of which 630 are of M0.5-1.9, 227 shocks are of M2.0-2.9, 30 shocks are of M3.0-3.9, **and 3 shocks is of M≥4.0. The largest magnitude earthquake of M4.8 occurred on 28 March 2018 in this year ~22 km ESE from Bhachau, Kachchh.**

Seismicity in Saurashtra

This year there were 806 shocks of M < 2.0, 237 shocks in the range of M2.0-2.9, and 3 shocks of M3.0-3.9. The earthquake with largest magnitude M3.7 occurred on 23 January

2018, 16 km ENE from Talala, Junagarh. Details of earthquakes of magnitude $M \geq 3.0$ in Saurashtra during 2018 are shown in Table 1.2

Table 1.2: List of earthquakes with magnitude $M \geq 3.0$ in the Saurashtra region during 2018

Year	MO	DD	HR	MM	Sec	Latitude	Longitude	M
2018	01	23	13	2	9.9	21.077	70.689	3.7
2018	01	29	22	3	42.5	21.092	70.662	3.4
2018	02	10	9	29	10.2	20.902	71.474	3.2

Earthquakes in the Mainland Gujarat

In the Mainland, 79 shocks of $M1.0 - 3.7$ were located by the ISR network. Out of these, 7 shocks are of $M \geq 3.0$. A shock of $M3.7$ occurred on 11th August 2018 at 38 km ESE from Bharuch in South Gujarat.

Table 1.3: List of earthquakes having magnitudes $M1.0-3.7$ in the Mainland region during 2018

Year	Month	Date	HR	MM	Sec	Latitude	Longitude	Depth	MI
2018	1	6	0	34	57.6	20.381	73.141	11.6	1.9
2018	1	9	11	17	47.9	24.607	71.734	15	1.6
2018	1	19	8	47	48	24.256	71.736	8.2	1.8
2018	1	22	14	25	28.3	21.522	74.696	1.1	2.9
2018	1	30	3	44	13.8	24.461	71.734	3.3	2.3
2018	2	10	9	14	33.2	24.5	72.461	15	1
2018	2	20	23	37	46.7	19.985	73.079	1.2	2.3
2018	3	7	3	51	28.3	24.128	71.551	24.6	1.7
2018	3	17	19	54	26.4	23.918	71.902	11.7	1.6
2018	4	21	11	26	33.9	21.674	73.469	16.8	3.7
2018	4	24	7	58	58.3	24.202	74.281	1.1	2.4
2018	5	9	4	6	54.1	24.483	71.794	10	3
2018	5	11	8	17	57.3	24.921	73.414	1.5	1.9
2018	5	16	2	43	52	24.822	72.255	5.7	2.5
2018	5	27	16	33	28	24.661	72.187	0.6	2.2
2018	6	1	3	26	13.2	24.227	71.061	15	1.5
2018	6	6	8	9	19.7	23.968	74.398	15	1.7
2018	6	6	23	41	32.2	24.057	71.258	22.7	1.6

2018	6	7	11	12	6.8	24.569	72.801	1.3	2
2018	6	8	6	35	57	24.135	72.81	8.2	1.2
2018	6	8	7	21	37.5	24.153	72.845	12.3	1.6
2018	6	10	19	52	10.3	23.302	71.079	21.8	1.6
2018	7	1	9	15	6.2	23.072	73.076	24.1	1.1
2018	7	1	12	42	10.2	22.85	73.279	42.3	1.7
2018	7	1	20	54	53.6	22.287	72.547	172.7	2.3
2018	7	2	12	13	47.4	23.686	71.73	11.9	1.6
2018	7	6	0	20	32.8	23.341	71.076	19.5	1.7
2018	7	11	8	17	50.8	24.488	73.771	27.4	1.5
2018	7	16	7	50	31.3	24.088	72.921	15	1.3
2018	7	17	6	57	39.2	24.121	72.788	3.1	1.8
2018	7	17	7	32	28.7	23.937	72.732	16.8	1.2
2018	7	17	8	6	4.3	23.842	74.397	15	1.4
2018	7	20	11	52	4	24.366	73.684	11.4	1.5
2018	7	21	7	54	33.1	24.308	73.776	12.7	1.7
2018	7	24	0	46	19.5	20.457	73.469	38	3.1
2018	7	24	3	28	55.2	20.663	73.173	5.9	2.1
2018	7	28	18	53	7.7	20.556	73.657	2.2	2
2018	8	1	19	47	1.1	23.474	73.756	15	2.1
2018	8	6	4	31	44.3	19.982	72.983	1.2	2.4
2018	8	11	13	27	13	21.797	74.206	79.3	3.7
2018	8	14	5	1	31.2	24.269	73.121	20.6	2.4
2018	8	18	7	16	0.8	24.09	72.772	15.2	1.5
2018	8	19	0	15	27.2	24.212	73.257	6.6	1.6
2018	8	20	17	2	41.4	24.014	71.382	22.4	1.5
2018	8	21	10	21	46.3	24.459	72.377	15	1.1
2018	8	30	4	46	28.8	23.893	71.434	19	1.7
2018	9	12	8	31	3.8	24.312	73.754	22.5	1.6
2018	9	26	23	3	4	25.096	72.102	1.2	2
2018	10	2	21	7	30.3	24.485	71.507	8	2
2018	10	3	5	52	58.2	24.389	71.532	2.2	1.4

2018	10	3	6	41	1.8	24.97	73.51	1.2	2
2018	10	9	16	11	18.4	24.497	71.504	6	1.3
2018	10	22	19	49	56.6	23.882	71.296	11.7	1.4
2018	11	5	0	36	6.1	23.55	71.721	16.8	2.8
2018	11	7	11	0	52.7	24.457	72.378	15	1.7
2018	11	17	19	43	28	24.098	71.16	12.5	3.2
2018	11	24	9	18	33.6	24.138	72.085	3.4	2.3
2018	11	27	8	8	53.7	20.007	72.758	2.1	1.9
2018	12	1	15	54	17.1	20.087	73.041	17.3	1.6
2018	12	1	20	8	35.4	20.1	72.972	1.2	3.5
2018	12	1	20	18	49.3	24.414	72.433	9.6	2.7
2018	12	2	6	28	29.9	20.217	73.045	1.2	2.1
2018	12	2	6	58	30.3	24.244	73.051	13.4	1.5
2018	12	4	3	12	4.9	19.983	72.901	2.4	2
2018	12	4	4	59	17.9	20.137	72.986	4.1	2.1
2018	12	4	5	15	58.8	20.032	72.922	7.3	2.1
2018	12	4	9	43	45	20.063	72.721	10.8	1.9
2018	12	4	9	49	18.7	19.965	72.643	41.1	2.4
2018	12	4	9	58	7.4	19.919	72.622	41.9	2.4
2018	12	4	15	54	42.5	19.842	72.688	7.4	2.4
2018	12	4	17	3	16.8	20.071	72.796	4.9	2
2018	12	8	14	18	25.7	24.636	72.012	16	2.1
2018	12	8	18	0	40.9	24.518	71.521	8.6	2
2018	12	14	10	3	27.1	20.032	72.713	1.2	2.8
2018	12	14	15	15	56.6	21.216	72.598	12	3.5
2018	12	17	9	57	42.3	24.411	71.803	6.2	2.1
2018	12	19	16	15	46.9	20.112	72.732	1.2	2.3
2018	12	20	19	7	54.6	20.175	72.65	1.2	2.1
2018	12	26	23	50	13.6	24.617	71.926	19.6	1.5

Strong Motion Accelerograph data

During 2018, a total of 29 shocks in the magnitude range M1.7- 4.8 were recorded on strong motion accelerographs (Fig. 1.3). However, only 13 out of the total 29 shocks were recorded at three or more stations and the remaining shocks were recorded only at one SMA station.

In Kachchh, two tremors of M 4.1, and 4.8 were recorded by 5 and 9 SMA stations (Table 1.4 & Fig. 1.3).

Table 1.4: List of earthquakes of M ≥ 4 and number of SMA station triggered

M	Date	Time (GMT)	Lat	Long	Dep (km)	NST	Region
4.1	25-02-2018	11:06	23.14	70.45	16.9	5	23 Km SSE from Bhachau, Kachchh.
4.2	10-03-2018	11:44	23.41	70.43	19.3	3	15 Km NNE of Bhachau, Kachchh.
4.8	28-03-2018	22:33	23.23	70.53	27.5	9	22 Km ESE from Bhachau, Kachchh.

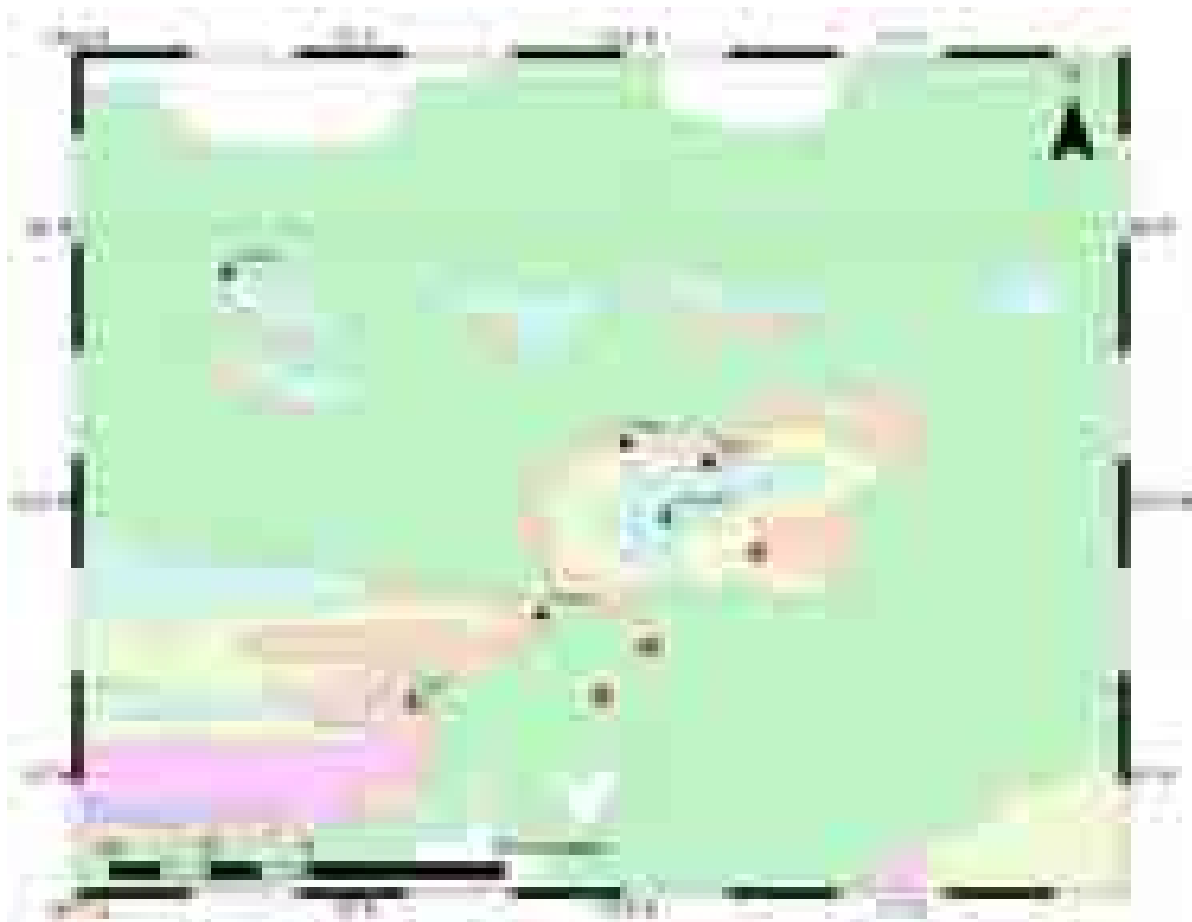


Fig 1.3: Earthquakes of M.4.0 recorded by SMA network in 2018

1.3 Description of Recorded Earthquakes in Different Parts of Gujarat since inception of the network

(Santosh Kumar, P Mahesh, A P Singh, Ketan Singha Roy, Vandna Patel)

Seismicity in Kachchh has consistently been lower since 2006 (Fig. 1.5 and Table 1.5) with ~ **60 earthquakes of M ≥ 3 annually**. The seismicity is slightly less than in 2017, since there are 31 shocks of M3.0 – 3.9 in 2018. There are two shocks of M 4.4 & M 4.8 in Kachchh, in 2018 (Tables 1.5 & Figure 1.4). During August 2006 to December 2018, 140 earthquakes of M 3-3.9, 8 earthquakes of M 4-4.9, and 2 earthquakes of M 5.0, M 5.1 were recorded from Saurashtra (Tables 1.6, 1.7 & Fig. 1.5).

Table 1.5: Annual distribution of earthquakes of $M \geq 3.0$ from the Kachchh region between the years 2006 and 2018 are listed in the table below

M	2006	2007	2008	2009	2010	2011	2012	2013	2014	2015	2016	2017	2018
3.0 - 3.9	405	143	66	73	52	62	56	59	45	70	49	47	31
4.0 - 4.9	20	6	5	4	1	3	2	3	1	1	2	5	3
≥ 5.0	4	0	0	0	0	0	1	0	0	0	0	0	0

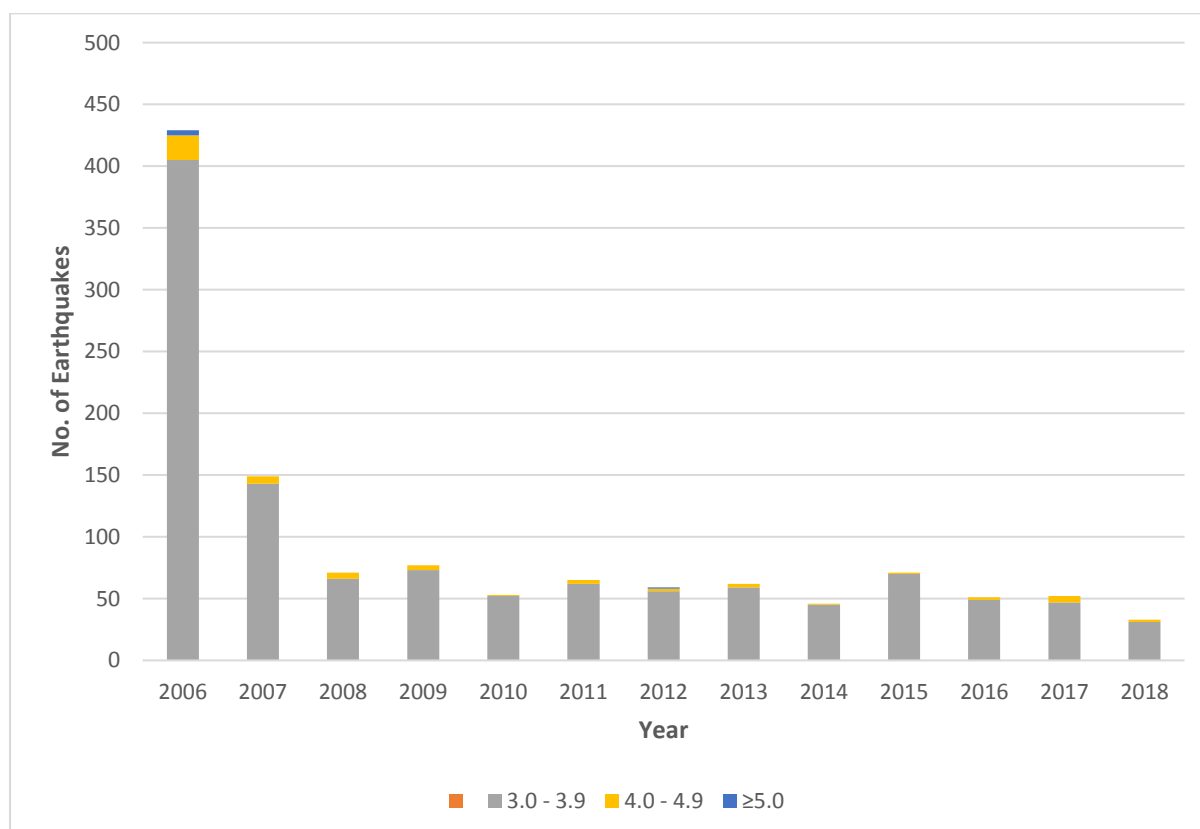


Fig. 1.4: Annual number of shocks in Kachchh from 2001 to 2018.

Table 1.6: Seismicity of $M \geq 3.0$ from Aug. 2006 to December 2018 in the Saurashtra region

M	No. of earthquakes
3.0-3.9	140
4.0-4.9	8
≥ 5.0	2

Table 1.7: Annual number of earthquakes of M 3.0 to 5.1 in Saurashtra region during 2007 to 2018.

Year	2007	2008	2009	2010	2011	2012	2013	2014	2015	2016	2017	2018
3.0 - 3.9	30	12	6	12	18	6	3	5	7	3	1	3

4.0 - 4.9	1	2	0	0	4	0	0	0	0	1	0	0
5.0 - 5.9	1	0	0	0	1	0	0	0	0	0	0	0
Total	32	14	6	12	23	6	3	5	7	4	1	3

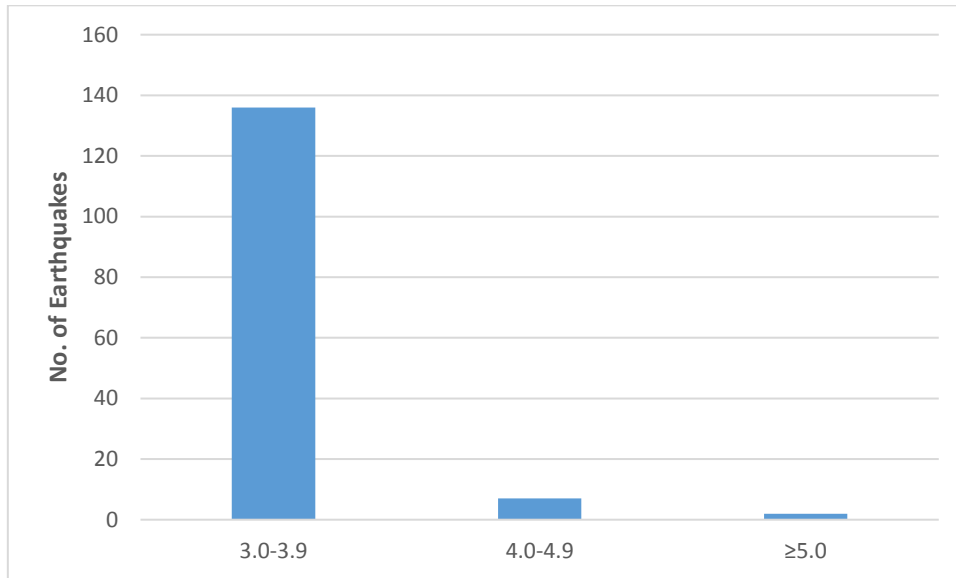


Fig. 1.5: Number of earthquakes in Saurashtra during year 2007- 2018 in three magnitude categories.

1.4 Development of Python based Software to analyse the Low Frequency Passive Seismic data for hydrocarbon exploration
(Ketan Singha Roy and A P Singh)

Ambient seismic background noise generates microvibrations, also known as microseismic noise, that travels through the solid earth. Such noise with frequencies above 1 Hz is usually referred to as microtremors (Bard 1999). Low-frequency (<10 Hz) spectral anomalies in surface microtremor signals have recently been used as hydrocarbon indicators. Dangel et al. (2003) investigated microtremor data to locate hydrocarbon bearing structures in the subsurface and found an empirical relationship between low-frequency spectral anomalies in microtremor wavefields and the presence of hydrocarbon reservoirs, mainly for sites in the Middle East. Motivated by these observations, a microtremor survey at two oil field regions, namely, Jotana and Mansa in Mehsana district, Gujarat was done in collaboration with ONGC. A python-based Graphical User Interface (GUI) software is developed to process the three component ground motion data, to analyze different spectral attributes and to display the results. The software consists of many modules, as shown in the below figures (Fig. 1.6-1.9).

Following Lambert et al. (2007), we computed V/H spectral ratios of three component ground motion data recorded at 134 sites (104 sites in Jotana and 30 sites in Mansa) and estimated the peak V/H amplitude and corresponding frequency. The 3-component data is recorded at 100 and 125 samples per second, and the data with abnormal spikes is discarded (Fig. 1.10). The selected data is then bandpass filtered in the frequency range of 0.5-10 Hz, and smoothed. Fig. 1.11 shows spectrograms of the three component time series recorded at two sites, one in Jotana (Z001) and the other in Mansa (X008). All the windowed spectra are averaged to form V, N and E spectra, and V/H ratios are calculated (Fig. 1.11). The frequency range of interest, which is 1-6 Hz, is shaded with gray colour in Fig. 1.11. Fig. 1.12 shows the distribution of peak amplitude over the study area. We then investigated the correlation between parameters obtained from microtremor signal and the reservoir location.



Fig. 1.6: Selection of different time windows to avoid anthropogenic noise

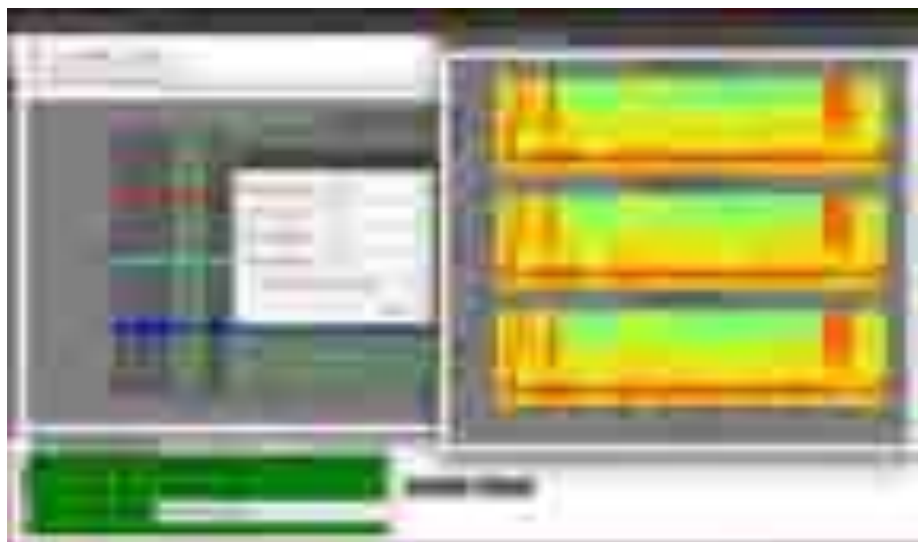


Fig. 1.7: Spectrogram analysis with variable signal length, % of overlap, cosine taper.

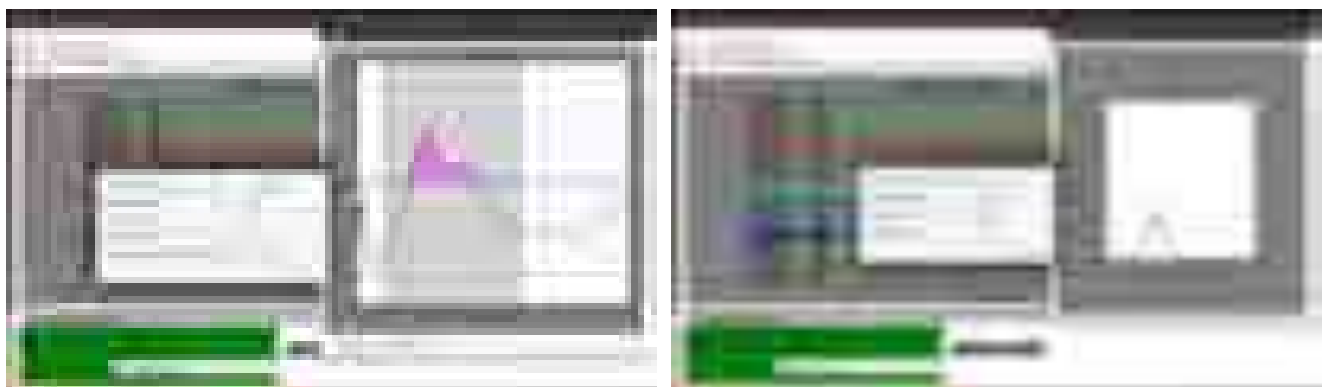


Fig. 1.8: Computation of V/H and Power Spectral Density

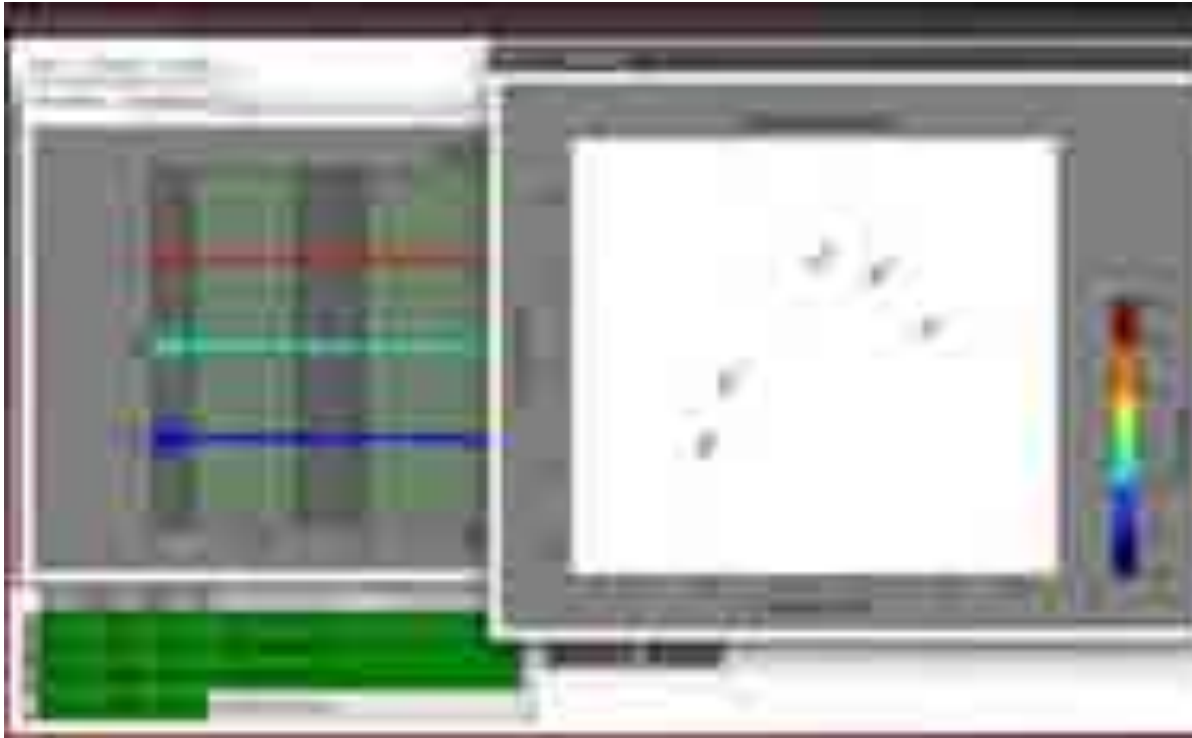


Fig. 1.9: Spatial distribution of peak frequency

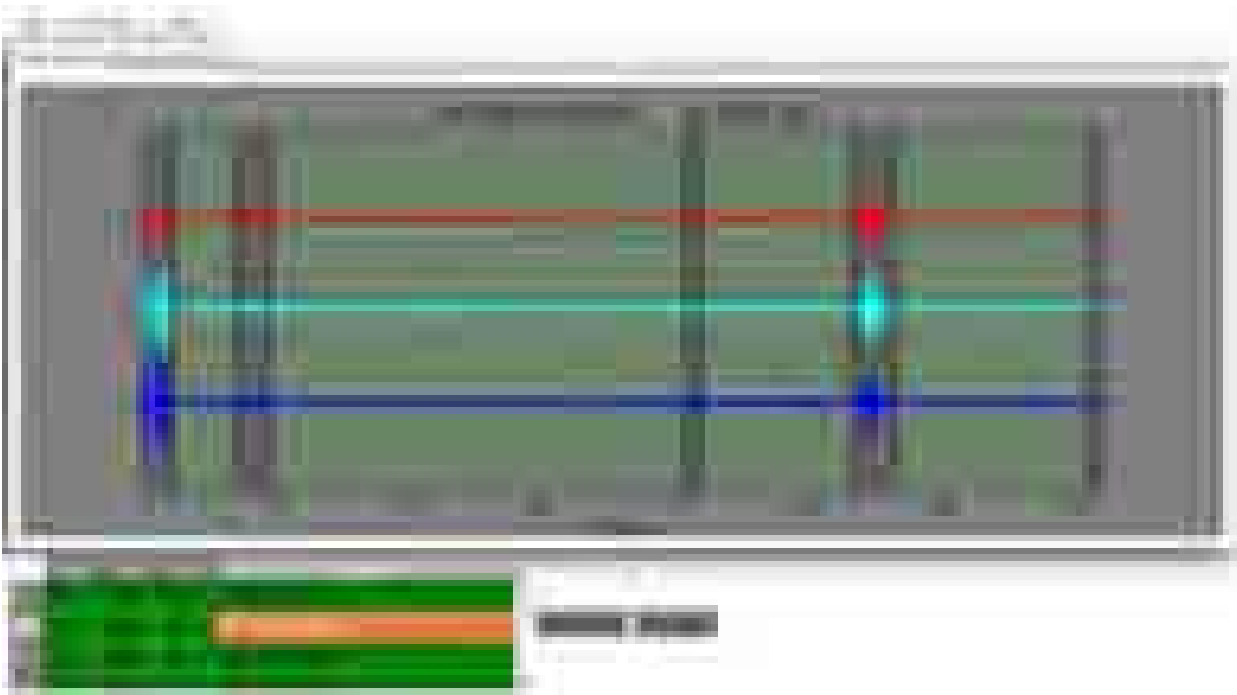


Fig. 1.10: Time series selection for site Z001. Green background colour indicates time-selection of three component ground motion for further processing.

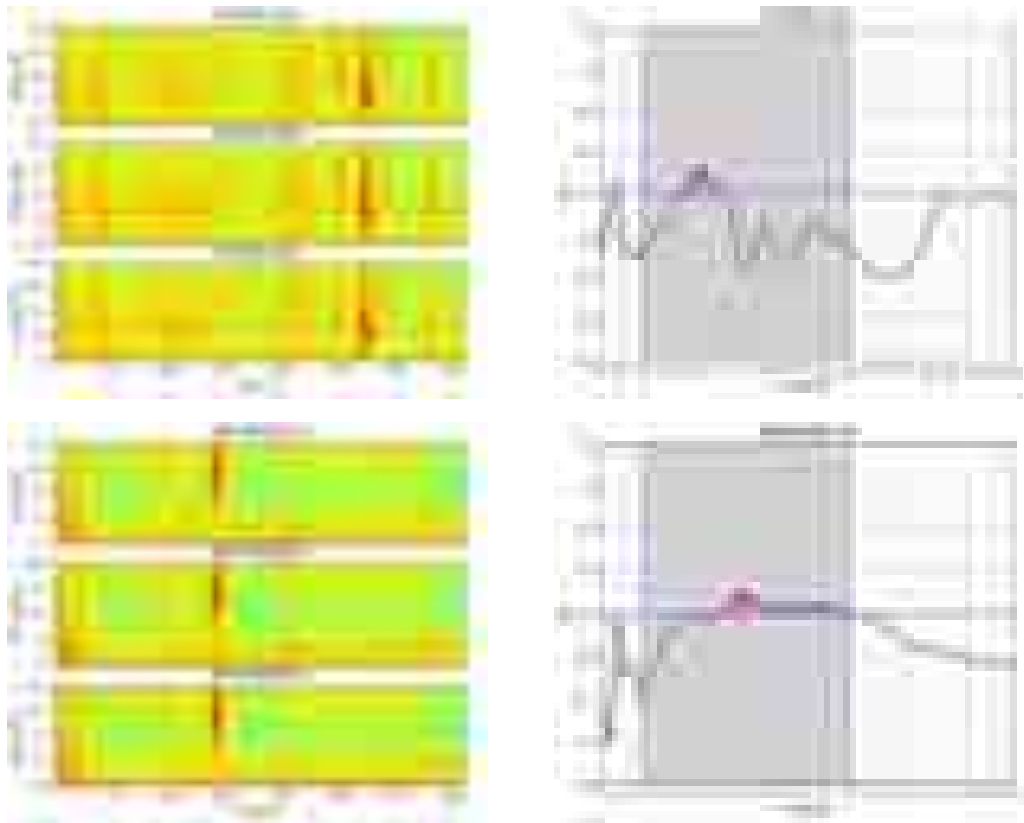


Fig 1.11: Spectrogram of three component ground motion data recorded at site Z001 and X008 (left) and the corresponding V/H spectral ratios (right). The shaded region represents area of the V/H curve where the amplitude exceeds unity, in the frequency range of 1 to 6. The red dot represents maximum V/H value at the station.

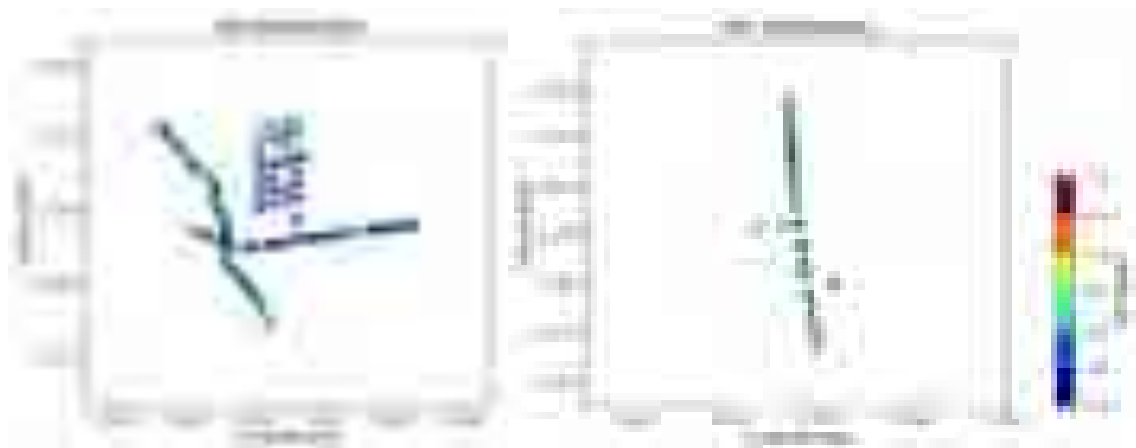


Fig. 1.12: Distribution of peak amplitude over Jotana (left) and Mansa (right) areas.

Microtremor measurements at two oil field regions, Jotana and Linch in Mehsana district, Gujarat have been done for ONGC. Further, to examine the quality of the recorded data, a new program module to evaluate the long-term seismic noise levels for checking the data quality of Microtremor instrument has been developed. The new noise processing software uses a probability density function (PDF) to display the distribution of seismic power spectral density (PSD) (Fig. 1.13) and can be implemented for any broadband seismic data with known instrument response.

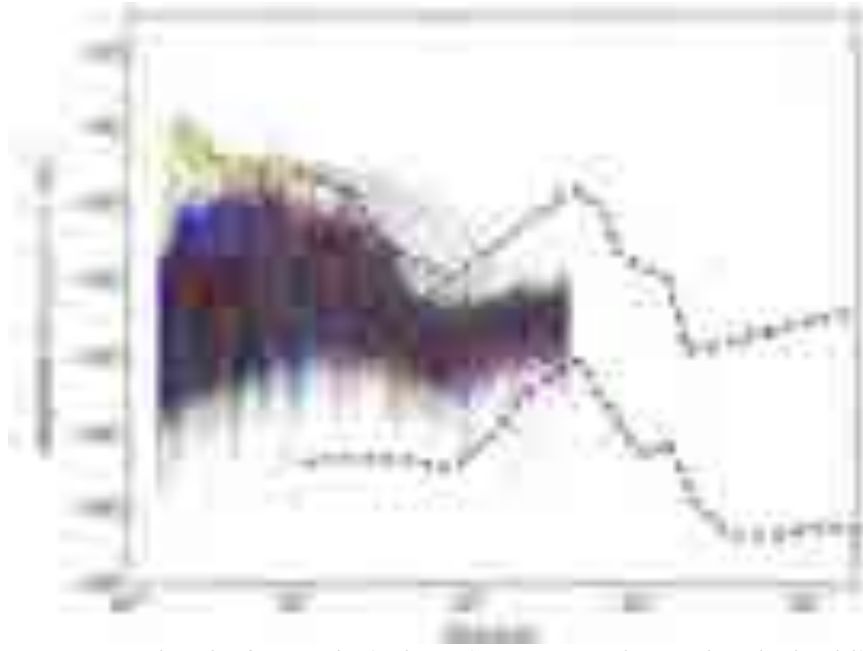


Figure 1.13: An example of PSD analysis for Microtremor data. The dashed lines represent the high and low noise models given by USGS.

1.5 Study on Earthquake Swarms in Palghar District, Maharashtra

(P Mahesh, Alla Sateesh, Charu Kamra, Santosh Kumar, Sumer Chopra, M Ravi Kumar)

The Palghar district of Maharashtra falls in zone III of the seismic zoning map of India. During the month of November 2018, a swarm activity started in the Palghar district of Maharashtra, which is still continuing. According to reports from the National Centre for Seismology (NCS), more than 1,000 earthquakes of mild-to-medium magnitude have occurred in the Dahanu and Talasari Talukas of Palghar district since November 3, 2018. The largest tremor of magnitude 3.7 was recorded on 1 February 2019, at 3.54 PM (IST). In the present study, data from 11 stations of GSNNet, in the proximity of earthquake swarm region are utilized (Blue triangles in Figure 1.14a). Initially, we located the earthquakes in near real time using the data from VSAT connected stations. Later, we incorporated the data from offline stations operated by ISR in the proximity of the observed swarm activity. We could locate earthquakes of magnitude 1.6 and above, with our GSNNet.

Initially, the earthquakes were located using the HYPOCENTER program, using the 1-D velocity model of the Narmada region (Joshi et al., 2017) and an average V_p/V_s ratio of 1.73. A total of 135 earthquakes in the magnitude (M_L) range of 1.6 to 3.7 were located in the Palghar district, from 3 November 2018 to 15 February 2019 (Figure 1.14b). Most of these earthquakes are in the depth range of 2 to 8 km. Further, these 90 earthquakes located using the data from both online and offline stations till 5 February 2019 were relocated using the hypoDD algorithm to improve the location accuracies (Figure 1.15). In order to decipher their association with the existing faults and lineaments, the earthquakes are plotted along a NE-SW cross section (A-B, as shown in Figure 1.15). We determined the focal mechanism solution of an earthquake of M_L 3.7 that occurred on 01/02/2019, using the ISOLA code (Sokos and Zahradnik 2008, 2013). The focal mechanism (Figure 1.15) shows strike-slip faulting. Interestingly, one of the nodal planes (NNW-NSE) have an orientation that is similar to the epicentral distribution. Therefore, the NNW-SSE near vertical plane can be considered as the fault plane, which coincides with the seismicity trend.

The relocated earthquake distribution shows that the swarm activity in Palghar follows a general NS trend, confined to an area of 10 km × 2 km, which is parallel to the trend of lineaments/dykes/basement faults present in the Panvel Flexure (Figure 1.15). Inset of Figure 1.15 shows the depth variation of earthquakes, within 5 km on either side of the NE-SW cross section A-B. The depths of the majority of hypocenters vary between 1.5 and 8.0 in the region (cross section A-B, Inset of Figure 1.15). This cross section reveals that the hypocenters of swarm earthquakes are on a near vertical plane. The computed focal mechanism (Figure 1.20) shows strike-slip faulting with a near vertical fault plane coinciding with the trend of the seismicity. The geological studies and satellite data also reveal NS to NW-SE trending lineaments/fracture zones in the study region.



Figure 1.14: (a) Regional tectonic map of Gujarat and Maharashtra, western India (modified after Biswas). Locations of historical earthquakes are taken from Chandra⁴ and Mohan⁵. The study region is marked by a rectangular box. ABF: Allah Bund fault, NPF: Nagar Parkar Fault, IBF: Island Belt Fault, KMF: Kachchh Mainland Fault, KHF: Katrol Hill Fault, GF: Gedi Fault, SWF: South Wagad Fault, NWF: North Wagad Fault, ECF: East Cambay Fault, WCF: West Cambay Fault, SNF: Son Narmada Fault, NTF: North Tapti Fault (b) The enlarged geo-tectonic map of the study region with epicentral distribution of earthquakes (open circles and stars) located by the HYPOCENTER program.

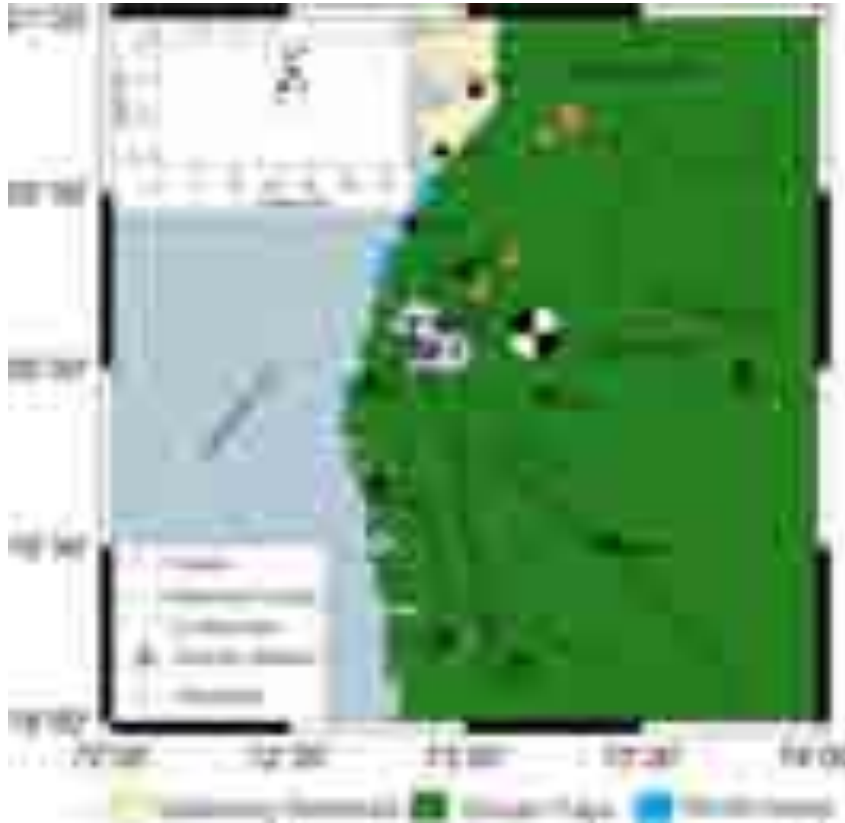


Fig. 1.15: Epicentral distribution of earthquakes (filled circles) relocated using the double-difference method (hypoDD). The fault plane solution of the earthquake of M_L 3.7 that occurred on 01/02/2019 is also shown. The A-B line shows the location of SW-NE cross-section used for showing depth distribution of earthquakes. The inset map shows the depth distribution of earthquakes that occurred within 5 km width on either side of the profile A-B.

1.6 Earthquake swarms in South Gujarat

(*P Mahesh, Alla Sateesh, A P Singh, Santosh Kumar*)

South Gujarat, a part of the northwest Deccan Volcanic Province of India has been experiencing episodic earthquake swarm activity with reports of sounds, whose association remains unclear. After the Indian monsoon period, during the month of September 2016, a swarm activity occurred around the Keliya dam in the Navsari district of South Gujarat and nearby villages in the Dadra and Nagar Haveli (DNH), which continued for about four months. Again, the swarm activity recurred during the month of August 2017 and continued for about five months till January 2018. Many of these events were accompanied by audible sounds, like blasting, that caused severe panic among local occupants. A local network of 4 stations was installed to monitor the swarm activity, in addition to the Gujarat state seismic network. A total of 1048 earthquakes were located around Keliya dam and 229 events in the DNH region from September 2016 to June 2018 (Fig. 1.16). In the present study, we performed spectrogram analysis of the events with associated sounds. The analysis revealed significant **energy at frequencies ≥ 20 Hz, in the audible frequency range**. The relocated earthquake distribution (Fig. 1.17) shows that seismicity in the Navsari district follows a \sim NW-SE trend, confined to an area of 13×2 sq. km with a depth extent of 3 km. The trend is similar in the DNH region, confined to an area of 15×2 sq. km, down to a depth of 6 km. The seismicity patterns seem to corroborate with the trends of the lineaments/dykes in the region. We

speculate that the present swarm activity follows the Indian summer monsoon season in time with some delay and this could be associated to the phenomenon of hydro-seismicity.

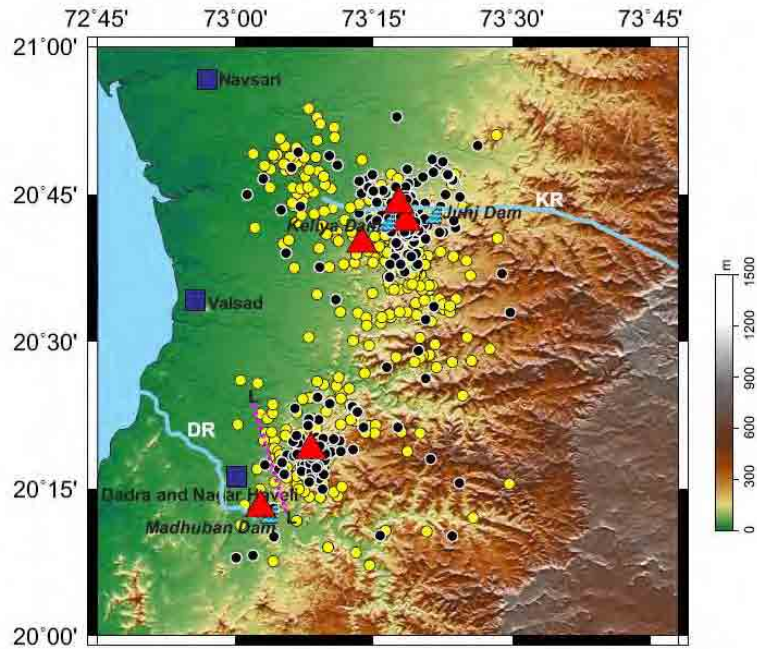


Fig. 1.16: Epicentral distribution of earthquakes (filled circles) located by the HYPOCENTER program (Lienert and Havskov, 1995). Black circles show epicenters located using records from a single station; yellow circles: recorded by three or more stations. L-L: Lineament inferred by Central Ground Water Board of India. KR: Kaveri River, DR: Damanganga River.

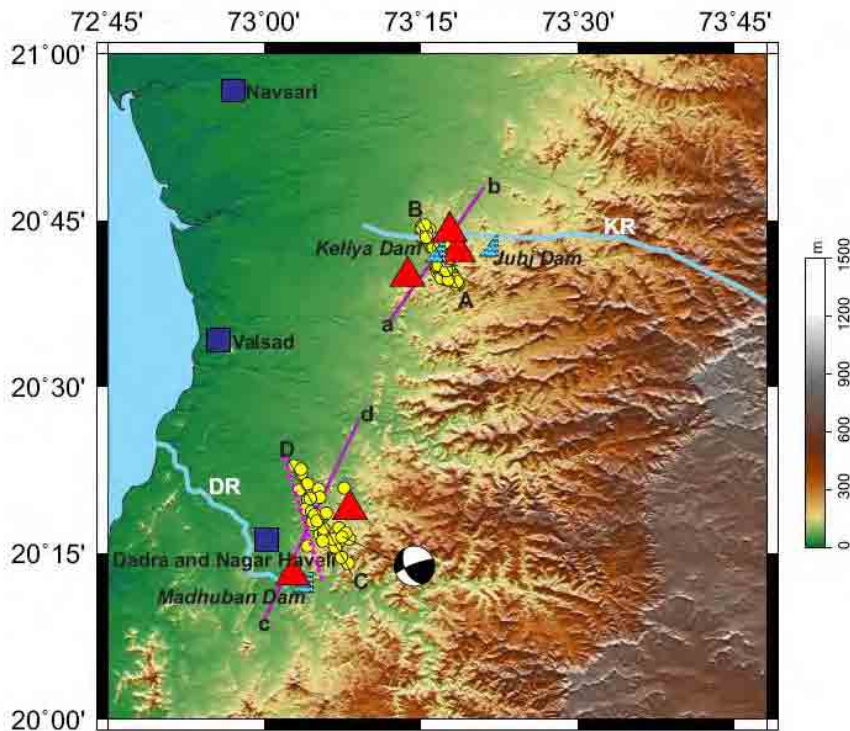


Fig. 1.17: Epicentral distribution of earthquakes (filled circles) relocated using the double-difference method (hypoDD). The fault plane solution of the earthquake of Mw 3.2 that occurred on 08/10/2017 in Dadra and Nagar Haveli (DNH) region is also shown.

1.7 Study on moment release and mechanical coupling between fault systems
(Vishwa Joshi and Sumer Chopra)

The aim of this study is to understand whether the complex spatiotemporal patterns of earthquakes in Kachchh are simply random effects of long recurrence times on different faults or could these migrating earthquakes reflect mechanical coupling between the fault systems. In this study, the seismic moment release along the fault systems is estimated. The **earthquakes which occurred from 1800 to 2018 having magnitude ≥ 4.0 in different active regions** are shown by different colours in fig. 1.18. We estimated the total moment release of these earthquakes (Fig. 1.19). An earthquake catalog is prepared using the information reported by different agencies like USGS, ISC, IMD, NGRI, and ISR. Thus, the information on earthquake size does not have a uniform magnitude scale. Therefore, to prepare a homogeneous catalog, relationships between different magnitude scales and moment magnitude (M_w) **for earthquakes having magnitude ≥ 4.0 have also been developed.** Further analysis is being done to understand whether the migrating earthquakes reflect mechanical coupling between the fault systems.

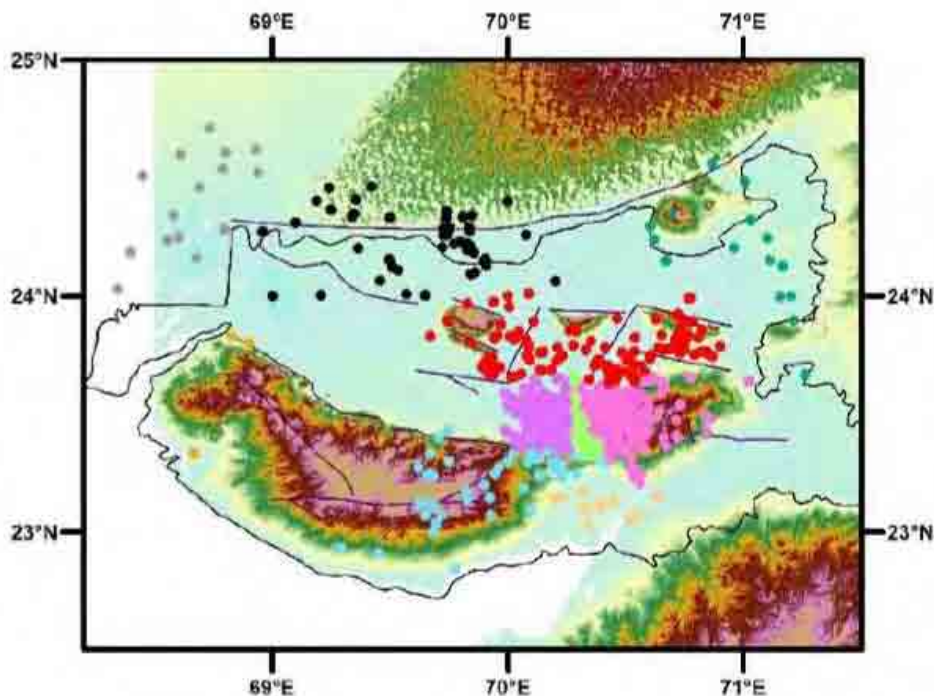


Fig. 1.18: Distribution of earthquakes in different active fault regions shown by different colours



Fig. 1.19: Total moment release (colour of the bar represents the area shown in figure 1.2).

1.8 Earthquake data processing and interpretation of MEQ data collected during Jan-July 2018 for study of seismogenic sources around the Subansiri Lower Hydro Electric (HE) Project, Arunachal Pradesh

(P Mahesh, Kunjal Parmar, Santosh Kumar)

NHPC Limited is carrying out micro-earthquake (MEQ) studies in Subansiri Lower HE Project, Arunachal Pradesh, since May 2006. The network consists of eight observatories in and around Subansiri Lower HE project. While data acquisition is undertaken by NHPC, the analysis of waveform data for local earthquakes and interpretation is entrusted to the Institute of Seismological Research. In a 300 km vicinity of the NHPC project site, 486 earthquakes were recorded during the period of January-July 2018. The magnitude of these earthquakes scaled between M 0.7 to M 4.8. The spatial distribution of earthquakes clearly shows 42 earthquakes (Fig. 1.20) of magnitude M 0.7- 2.7 within the 50 km radius of the dam site, with most of the earthquakes being in the depth range of 10-30 km. The earthquakes within 50 km radius of the dam site are all micro earthquakes having $M < 3.0$. Majority of these earthquakes are considerably away from the dam site and are either to the NW or SW of the dam site and near the thrusts T1, T2 & T3 (Fig. 1.20) trending NNE-SSW.

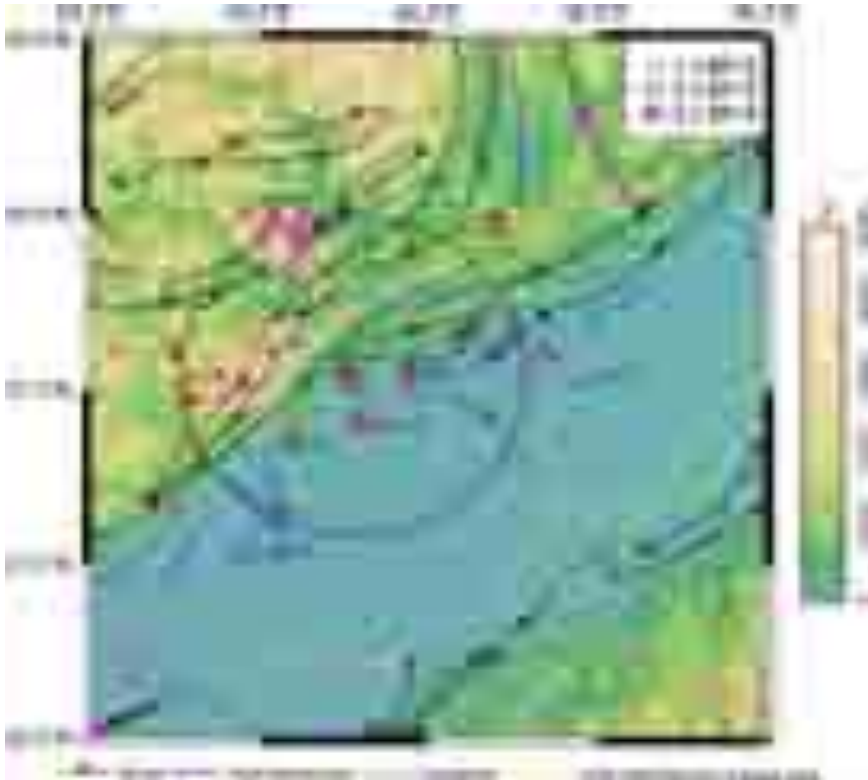


Fig 1.20: Distribution earthquake epicentres (S-P < 15 sec) recorded by 3 or more SLHEP network observatories during the period January to July 2018. MCT - Main Central Thrust, MBT - Main Boundary Thrust, MFT – Main Frontal Thrust, DT –Dauki Thrust. Rectangle (black) represents the dam location. Circle shows radius of 50 km from dam site.

2. SEISMIC HAZARD ASSESSMENT AND MICROZONATION

2.1 An Assessment of Peak Horizontal Ground Acceleration from Intraplate Earthquakes in Kachchh, Gujarat, India

(K. K. S Thingbaijam, P. Choudhury, and S. Chopra)

Understanding the ground-motions from small-to-moderate events ($M_W < 6.0$) is important for applications pertinent to critical facilities, early earthquake warning and induced seismicity. In the intraplate region of Kachchh, India, available strong motion recordings belong to this magnitude-range, besides a few records of the M_W 7.7 2001 Bhuj earthquake. Here, we evaluate the peak ground acceleration (PGA) at very-stiff to soft-rock sites, to develop a new prediction equation and a spatial correlation model. The derived equation is,

$$\log_{10} PGA = -2.0659 - 0.0198 M_W + 0.0523 M_W^2 - 0.0019 R - 0.6029 \log_{10}(R), \quad \sigma_{total} = 0.328$$

in which, $R = \sqrt{(R_{hypo}^2 + H_{eff}^2)}$, $h_{eff} = \max(1, 10^{-1.72+0.43M_W})$, R_{hypo} is hypocentral distance in km, and σ_{total} is the standard deviation. This equation suggests that the high-frequency ground motions in the region have weaker far-source attenuation than previously observed. Additionally, it predicts lower PGA, compared to very-shallow events with high stress-drop in the peninsular India. Nonetheless, we find a general similarity in the ground-motion scaling behavior, between the study region and Eastern North America. Likewise, the estimated spatial correlation model, $\rho(\Delta) = \exp(-0.0766\Delta)$ where Δ , the separation distance in km between the stations, is comparable to those reported for different regions across the globe. However, statistical resampling shows that empirical semivariogram is sensitive to source-station geometry, suggesting significant variability. These results would be relevant for seismic hazard assessment in the intraplate regions.

2.2 A review of Seismic hazard assessment of Gujarat: a highly active intra-plate region

(Pallabee Choudhury, Sumer Chopra and M Ravi Kumar)

Large intraplate earthquakes that occur in the interior of continental plates are rare and often very destructive. The Gujarat region of western India, that witnessed the deadly Mw 7.6 earthquake on January 26, 2001 and the Mw7.8 quake on June 16, 1819, is one of the most active intraplate regions of the world. The tragedy caused by the 2001 earthquake marked a turning point in the disaster awareness and preparedness in the region. In the aftermath of this earthquake, several workers investigated the important issue of mitigating seismic hazard through new knowledge based techniques of probabilistic and deterministic ground motion prediction, micro and macro zoning of vulnerable areas. This paper reviews the results of seismic hazard estimation in the Gujarat region from different methodologies. We note that the probabilistic seismic hazard estimates by different workers are not consistent even within the same region because of uncertainties in constraining the hazard parameters, akin to the global observations. Using a logical approach, we evaluate all the ground motion predictions from different methodologies and constrain the level of expected peak ground acceleration (PGA) by adjusting all the values onto a common platform. Our assessment reveals that the PGA values in Gujarat vary from 0.04 to 0.35g and 0.07 to 0.77g for 10% and 2% probability of exceedance in 50 years, at the engineering bedrock ($V_s=760$ m/s) level. The hazard values thus estimated in this study can be directly used to estimate the PGAs at the surface by incorporating local site effects, which in-turn can be utilized in planning and mitigating earthquake hazards. Further, the estimates of PGA from deterministic approaches range from 0.05 to 0.90g. We see that within Gujarat, the ground motion values obtained by deterministic

and probabilistic methodologies do not show much variation. We affirm that we need to undertake such a logical approach to arrive at realistic probabilistic hazard values that are in conformity with the estimates from deterministic assessment. We also advocate the need to upgrade the classical methods of probabilistic and deterministic hazard assessment and incorporate the source and site complexities while estimating the hazard. Further, a comparison of the hazard values of Gujarat with those from other intraplate regions of the world, reveals that the hazard level in Gujarat is higher than in Australia, Brazil and Western Europe and comparable to North China, Eastern Canada and the New Madrid Seismic zone.

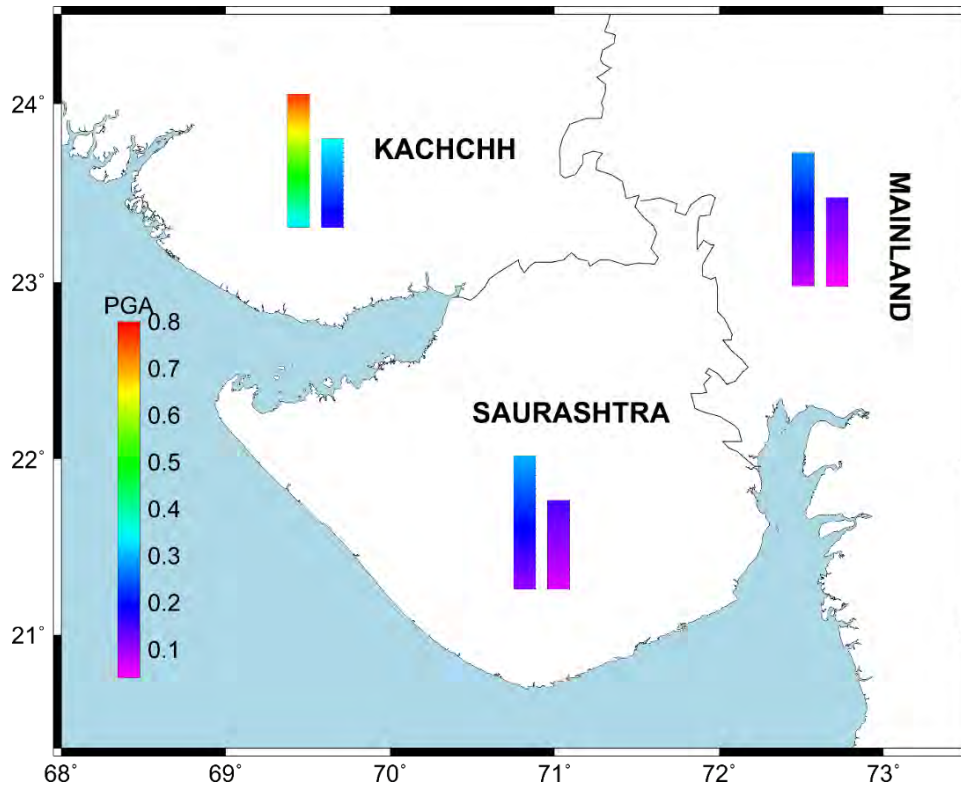


Fig. 2.1: The range of PGA (in g) values obtained in the present study for three different regions of Gujarat. The smaller and longer legends denote 10% and 2% PE in 50 years, respectively.

2.3 Influence of Local Site Effects in the Ahmedabad Mega City on the Damage due to Past Earthquakes in Northwestern India

(B Sairam, A.P. Singh, V. Patel, V. Pancholi, S. Chopra, V.K. Dwivedi, and M. Ravi Kumar)

The city of Ahmedabad of Gujarat in western India suffered severe damage during the 2001 Mw 7.7 Bhuj earthquake, despite being ~250 km away from the epicentre (Fig. 2.2). Similar damage patterns were also reported during the 1819 Allah Bund earthquake (Mw 7.8). To investigate the probable causes, we employed an integrated approach using multichannel analysis of surface waves (MASW), single and array microtremor measurements, broadband earthquake data, and geotechnical investigations. Significant differences in site characteristics are observed in both the damaged and undamaged areas. The investigations revealed shear-wave velocity values in excess of 320 m/s and less than 220 m/s in the undamaged and damaged areas, respectively, in the top 6 m of the subsurface. The refusal ($N_{1(60)}$) values are observed at 6–20 m and 20 m depth downward in the undamaged and damaged areas, respectively. The amplification factor in the damaged areas varies from 3.3 to 6.6 in the 1.5–2.0 Hz frequency range. On the other hand, the amplification factor in the undamaged areas

varies from 1.0 to 3.0 in the 0.7–1.5 Hz frequency range (Fig. 2.3; Table 2.1). Nevertheless, the damages were mostly restricted to mid-to-high-rise buildings, located in the western side of the Sabarmati River, where the presence of a paleochannel is reported, and in some southeastern parts of the city, along lakes and ponds. The low-rise buildings on the eastern side of the river in the old city area remained almost intact. Our study confirms that local site effects together with the poor quality of construction contributed to the damages.

Table 2.1: Comparison of Site Effects in the Damaged and Undamaged Areas of Ahmedabad

Location	Site Effect	Damage
Western side of Sabarmati River	High amplification (1.0 to 3.0) in the 0.7–1.5 Hz frequency range	Mid-to-high-rise buildings damaged
Southeastern parts of the city	High amplification (1.0 to 3.0) in the 0.7–1.5 Hz frequency range	Mid-to-high-rise buildings damaged
Eastern side of the river in the old city area	Low amplification (1.0 to 3.0) in the 0.7–1.5 Hz frequency range	Low-rise buildings almost intact

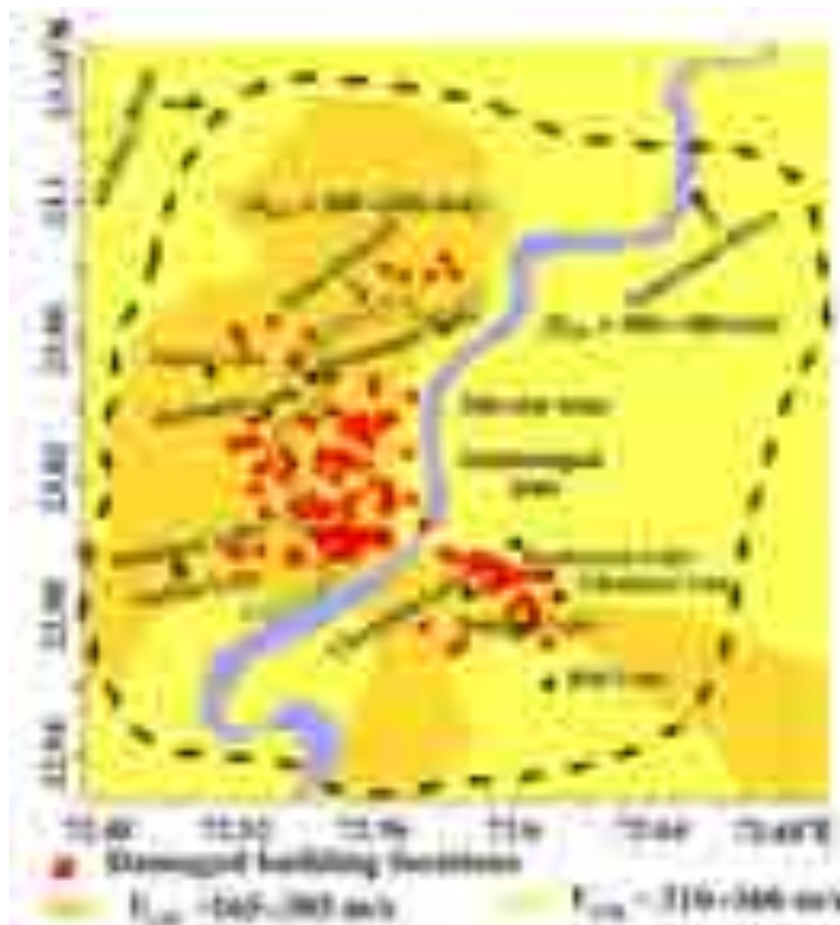


Fig. 2.2: Map showing the V_{s30} variation in the study area. Squares are the locations of the damaged or collapsed buildings due to the Bhuj earthquake.

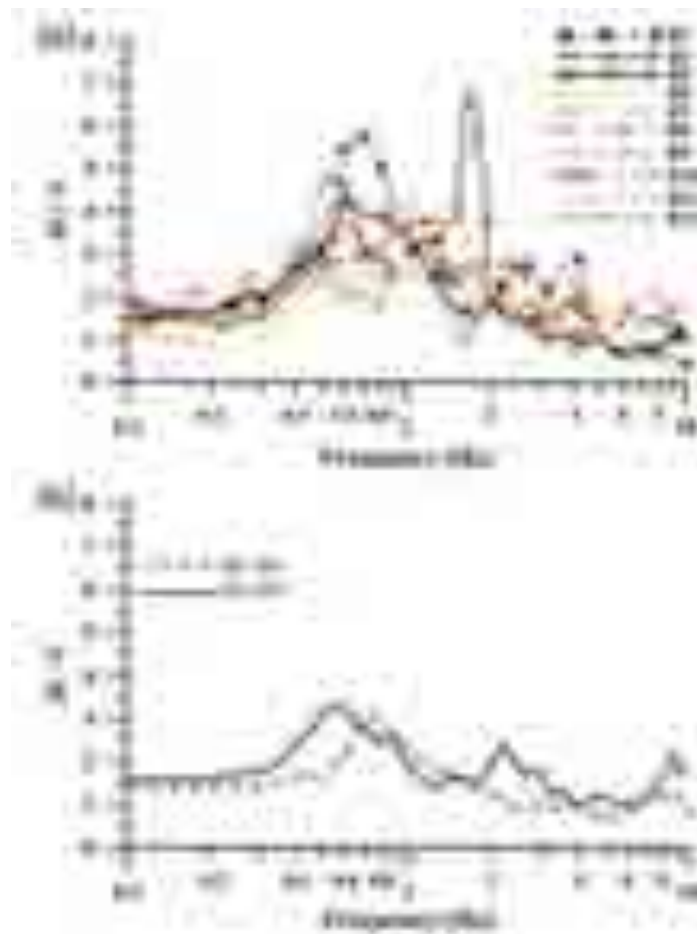


Fig. 2.3: Comparisons of HVSR in the (a) damaged area (sites B1 and B2) and (b) undamaged area (sites B3 and B4).

2.4 Comparison of earthquake source characteristics in the Kachchh Rift Basin and Saurashtra horst, Deccan Volcanic Province, western India (Sairam, B., Singh, A.P. and M. Ravi Kumar)

Seismic source parameters of small to moderate sized intraplate earthquakes that occurred during 2002-2009 in the tectonic blocks of Kachchh Rift Basin (KRB) and the Saurashtra horst (SH), in the stable continental region of western peninsular India, are studied through spectral analysis of shear waves. The data of aftershock sequence of the 2001 Bhuj earthquake (M_w 7.7) in the KRB and the 2007 Talala earthquake (M_w 5.0) in the SH are used for this study. In the SH, the seismic moment (M_0), corner frequency (f_c), stress drop ($\Delta\sigma$) and source radius (r) vary from 7.8×10^{11} to 4.0×10^{16} N-m, 1.0 to 8.9 Hz, 4.8 to 10.2 MPa and 195 -1480 m, respectively (Fig. 2.4). While in the KRB, these parameters vary from $M_0 \sim 1.24 \times 10^{11}$ to 4.1×10^{16} N-m, $f_c \sim 1.6$ to 13.1 Hz, $\Delta\sigma \sim 0.06$ to 16.62 MPa and $r \sim 100$ to 840 m (Fig. 2.4). The kappa (k) value in the KRB (0.025 to 0.03) is slightly larger than that in the SH region (0.02), probably due to thick sedimentary layers. The estimated stress drops of earthquakes in the KRB are relatively higher than those in SH, due to large crustal stress concentration associated with mafic/ultramafic rocks at the hypocentral depths. The results also suggest that the stress drop value of intraplate earthquakes is larger than the interplate earthquakes. In addition, it is observed that the strike-slip events in the SH have lower stress drops, compared to the thrust with strike-slip events in the Kachchh.

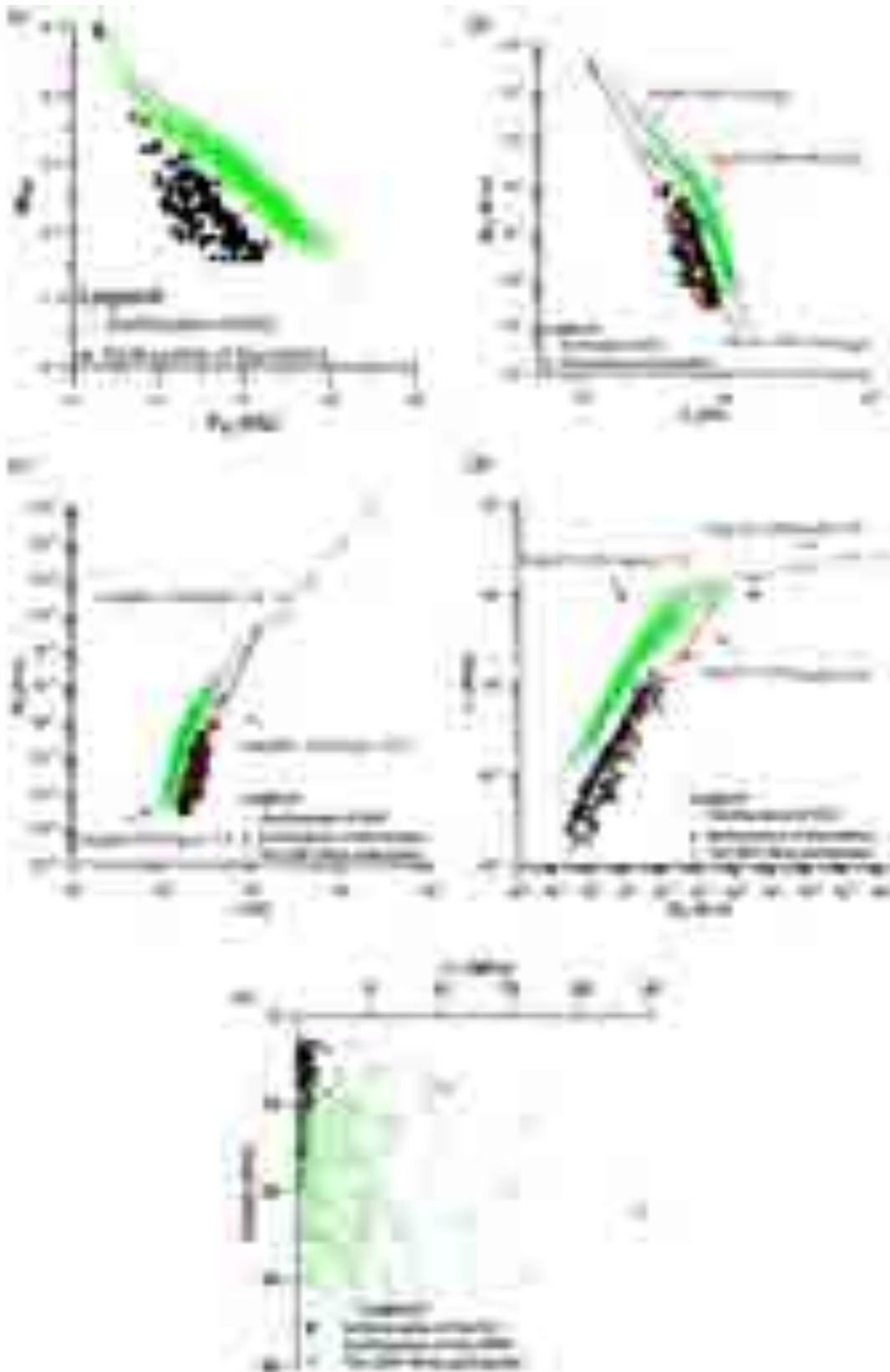


Fig. 2.4: Relation between (a) f_c and M_w , (b) f_c and M_o , (c) M_o and $\Delta\sigma$, (d) r and M_o , (e) depth-wise distribution of stress drops in the KRB and SH regions. The large $\Delta\sigma$ values, mostly confined in 15–30 and 3–8 km depths, respectively in the KRB and SH.

2.5 Simulation of strong ground motion in the Rapar city using Neo-Deterministic Seismic Hazard Assessment (NDSHA) approach (Neha Tanwar and Kapil Mohan)

Rapar is a city and a municipality in the Kachchh district, Gujarat. This area is called as Wagad (70.25°E to 71.167°E and 23.33°N to 23.75°N). Rapar is the main town in the Wagad region of the Kachchh and the easternmost town of the Kachchh district. The Kachchh region in western India has been affected in the past by large damaging earthquakes. In 1668, an earthquake of M 7 razed Samaji, a town 200 km west of Kachchh on the Indus delta in Pakistan (Chandra, 1977). In 1819, an earthquake of Mw 7.8, 100 km northwest of Bhuj created a 90 km long and 6 m high scarp along the Allah Bund fault (Bilhamand Gaur, 2000). In 1845, an earthquake of modified Mercalli intensity VIII hit Lakhpatt in the western part of Kachchh (Rajendran and Rajendran, 2001) and an earthquake of Mw 6 having intensity VIII struck Anjar in 1956, killing 115 people (Tandon, 1959; Chung and Gao, 1995). Nine damaging earthquakes of Mw 5–6 have been observed during the past 155 years, on an average, with an recurring period of 17 years, namely in the years 1864, 1903, 1940, and 1950. The devastating earthquake of Mw 7.6 occurred in 2001, causing 14,000 deaths and an economic loss of \$10 billion U.S. (Rastogi, 2004). This earthquake was felt up to Kashmir in the north, Kanyakumari in the south, and Nepal and Calcutta in the northeast. The most affected cities were Bhachau, Bhuj, Anjar, Rapar, Gandhidham and Kandla cities of Kachchh district (Narayan, 2004).

The strong ground motion data at Rapar city (70.6447°E, 23.573°N), Kachchh, Gujarat was simulated using the Neo-deterministic seismic hazard assessment (NDSHA) approach, considering three nearby major faults, i.e., South Wagad Fault (SWF), North Wagad Fault (NWF) and the eastern segment of Kachchh Mainland Fault (KMF-D). Literature survey comprising of the geological, geophysical and seismological aspects of the Rapar city (Kachchh, Gujarat) were conducted. The preliminary input parameters for the seismic hazard assessment (site specific) have been prepared. The magnitude, depth, strike, dip, rake, length and width are assigned based on past studies in the area (Mohan et al. 2014, Mandal et al. 2008, Chopra et al. 2010, Chopra et al. 2012, Yagi and Kikuchi, 2001, Mori et al., 2001, Kumar et al., 2017 and Azeez et al., 2018). The rupture parameters used for simulation of the ground motion are given in the Table 2.2. A velocity-density structure model proposed by USGS for 2001 Bhuj earthquake (Table 2.3) has been used in the present study.

The simulation of strong ground motion at the Rapar city is estimated using NDSHA. A peak ground acceleration (PGA) of 291 cm/sec² and peak spectral acceleration of 1502 cm/sec² at 0.140 sec are estimated due to a scenario earthquake of magnitude 7.6 along the NWF (Fig. 2.5 (a to c) and Fig. 2.5g); the PGA of 727cm/sec² and peak spectral acceleration of 1696 cm/sec² at 0.34sec are estimated due to a scenario earthquake of magnitude 7.6 along SWF (Fig. 2.5 (d to f) and Fig. 2.5h). The values of peak ground acceleration and peak spectral acceleration due to different fault segments for different scenarios are given in Table 2.4. The maximum PGA was obtained at Rapar city, which is due to the SWF. The Rapar city is situated at almost the eastern side of the NWF, therefore the obtained PGA is less compared to SWF.

Table 2.2: Preliminary input parameters of seismic hazard assessment for Rapar (70.6447, 23.573) city, Kachchh, Gujarat.

Fault	Long (°E)	Lat (°N)	Mw	Depth (km)	Strike	Dip	Rake	Length (km)	Width (km)	Vs (km/s)
SWF	70.68	23.45	7.6 ^{\$*}	17 ^{##}	280 ^{o##}	85 ^{o*}	180 ^{o^}	40 ^{\$*}	40 ^{\$*}	3.5
NWF	70.24	23.63	7.6 ^{##}	10 ^{##}	78 ^{o##}	58 ^{oS##}	81 ^{o##,##}	75 ^{##}	35 ^{##}	3.7

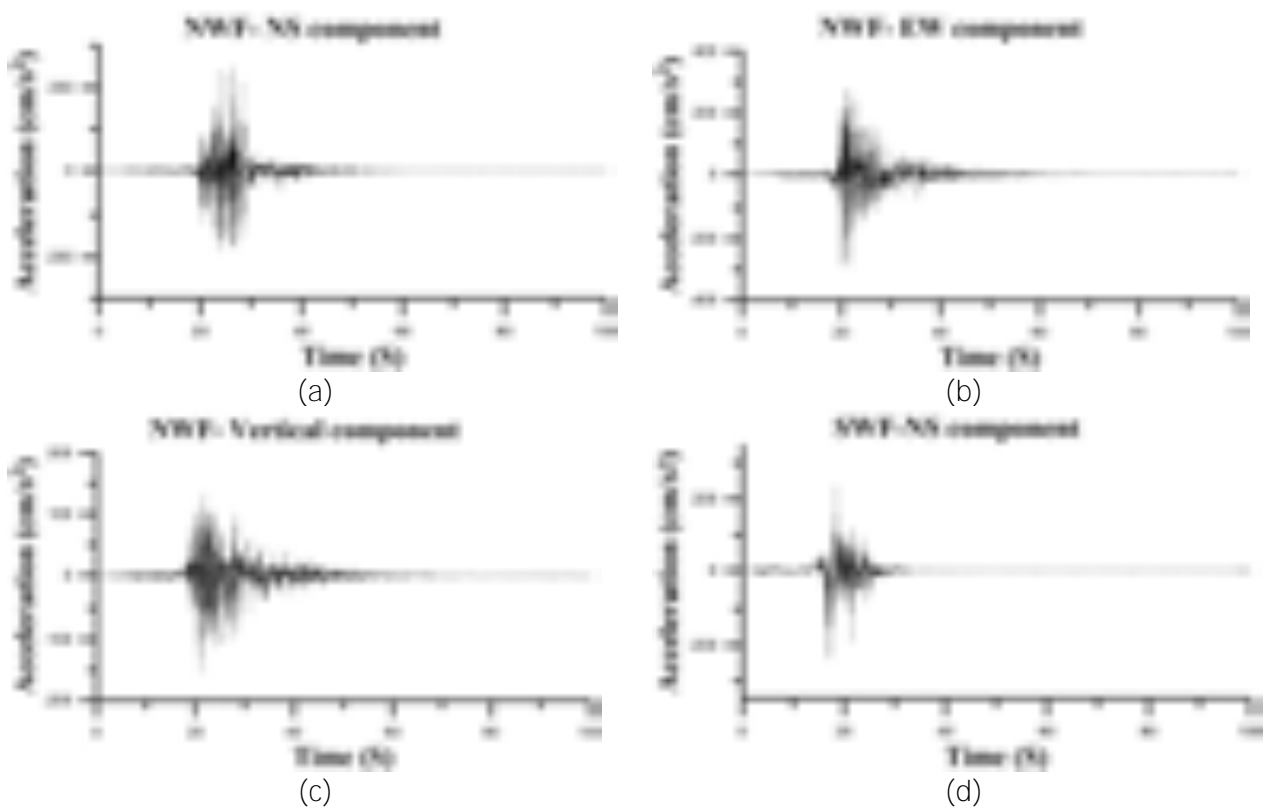
(*Mohan et al., 2014; #Mandal et al., 2008; \$Chopra et al., 2010; \$*Chopra et al., 2012; ##Yagi and Kikuchi, 2001 (<http://www.eic.eri.utokyo.ac.jp/index-e.html>); **Mori et al., 2001; ^Kothyari et al., 2015).

Table 2.3: A subsurface model proposed by USGS for 2001 Bhuj earthquake region

Depth (km)	P-vel (km/s)	S-vel (km/s)	Density (g/cm ³)	Q _p	Q _s
0.00	2.50	1.20	2.10	1000	500
0.50	6.20	3.60	2.80	1000	500
12.00	6.40	3.60	2.85	1000	500
24.00	6.80	3.80	2.95	1000	500
35.00	8.08	4.47	3.38	1200	500
231.00	8.59	4.66	3.45	360	140

Table 2.4: Peak ground acceleration (PGA) and Peak spectral acceleration (PSA) values estimated due to different scenarios using NDSHA.

Sr. No.	Fault	PGA (cm/s ²)	PSA (cm/s ²)
1	NWF	291	1502 at 0.14 sec
2	SWF	727	1696 at 0.34 sec



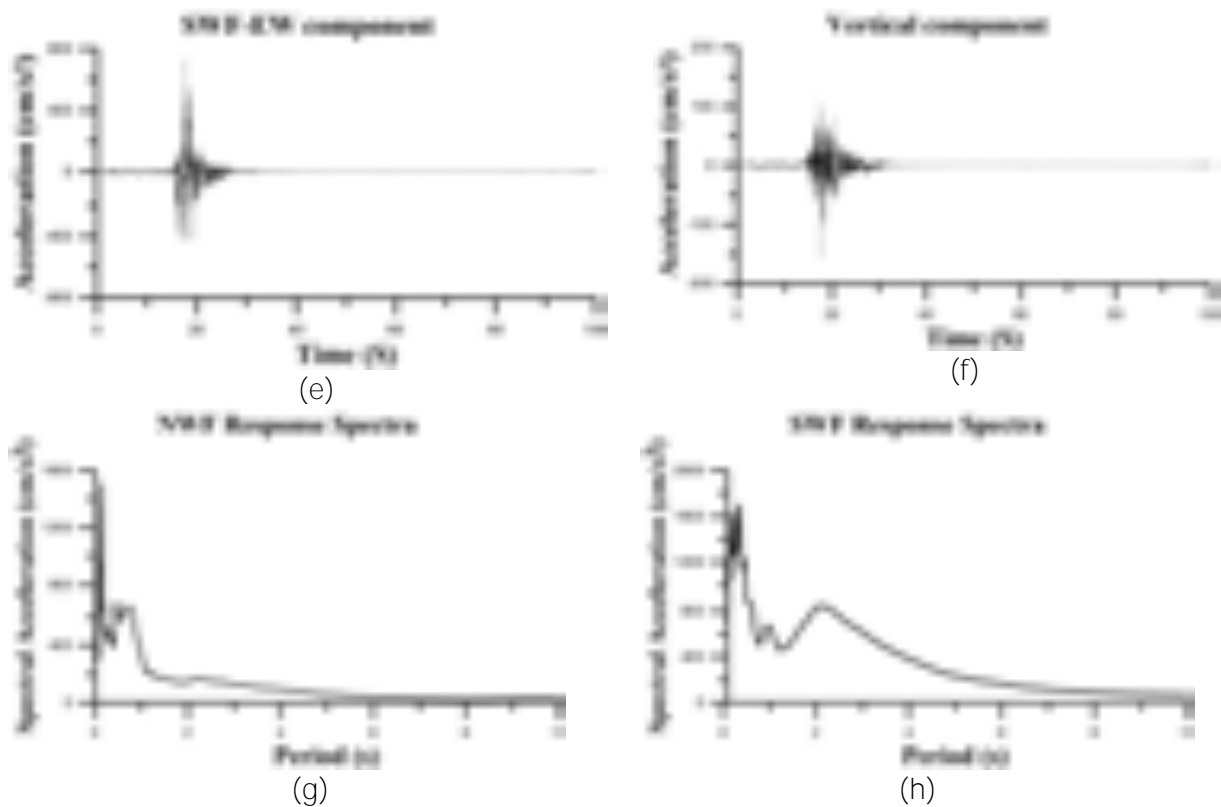


Fig. 2.5: (a) NS (b) EW and (c) Vertical accelerograms estimated at Rapar city due to a scenario earthquake of magnitude Mw 7.6 along NWF; (d) NS (e) EW and (f) Vertical accelerograms estimated at Rapar city due to scenario earthquake of magnitude Mw 7.6 along the SWF. Response spectra at Rapar city due to scenario earthquake of magnitude Mw 7.6 along (g) NWF and (h) SWF.

2.6 Impact on seismic hazard of Kachchh due to change in dip of Kachchh Mainland fault

(Kapil Mohan, Shruti Dugar and Sumer Chopra)

The KMF is an active fault (Malik et al., 2008; Morino et al., 2008) and is a major source of seismic hazard for Western India (Rastogi et al., 2012; Chopra et al., 2012; Mohan, 2014). The easternmost part of the KMF has been studied by Magnetotellurics (Mohan et al. (2010); Naganjaneyulu et al. (2010a); Chandrasekhar et al. (2012). Chandrasekhar and Mishra (2002), through modelling of Bouguer gravity data, suggested that the KMF is almost vertical, while KHF dips 50–60° south. Rastogi et al. (2014) suggested the KMF as a south dipping fault based on studies conducted in the eastern part of the KMF.

Mandal (2016) suggested a northward dip for the KMF from the relocated hypocenters of the earthquakes in the epicentral zone of 2001 Bhuj earthquake. Joshi et al. (2012), from five north-south ground penetrating radar (GPR) profiles along the KMF (east of Nirona to Amrapur village), suggested it as a north-dipping normal fault in three segments. Morino et al. (2008) through Paleo-seismological studies near Jhura (10 km east of Nirona), suggested that KMF is a low angle south inclination fault. Maurya et al. (2016) based on very shallow GPR study, suggested that KMF is a near vertical north-dipping fault that tends to become a steep southward dipping fault. Naganjaneyulu et al. (2010a) through MT studies suggested a south-dipping basement in the Samkhiali Basin. Mohan et al. (2010) suggested a south dipping fault 4 km north, a possible extension of KMF towards east near Bhachau. Chandrasekhar et al.

(2012) suggested a south-dipping reverse fault towards the north of KMF (F1 Fault), close to the location suggested by Mohan et al. (2010). Mohan et al. (2015) inferred KMF as a south-dipping fault located 5 km north of Dudhai (central portion) and 7 km NE of Bhachau (eastern portion). Sarkar et al. (2007) carried out a seismic survey in the eastern portion of the Kachchh and crossed both KMF and KHF and inferred a southward dip for both the faults. In a recent study, Mohan et al. (2018) have concluded that KMF is a north dipping fault which becomes south dipping in the vicinity of transverse faults cutting the KMF. On the basis of this finding, the seismic hazard assessment due to Kachchh Mainland fault has been conducted using Stochastic Finite-Fault Modelling technique (Motazedian and Atkinson, 2005) by dividing the entire Kachchh into 251 grid points and considering four different active segments of the KMF. The parametric testing has also been performed by considering a range of stress drop values, Kappa values, quality factors proposed by different studies in the area. From the current study, it is found that at sites south of the KMF (Bhuj, Bhachau, etc), the PGA decreases by 14-38% and on the sites north of KMF (Rapar, Khavda etc.), the PGA is increased by 30-47% at shear wave velocity of 520m/sec (Fig. 2.6), in comparison to the PGA estimated considering a southward dip of KMF.

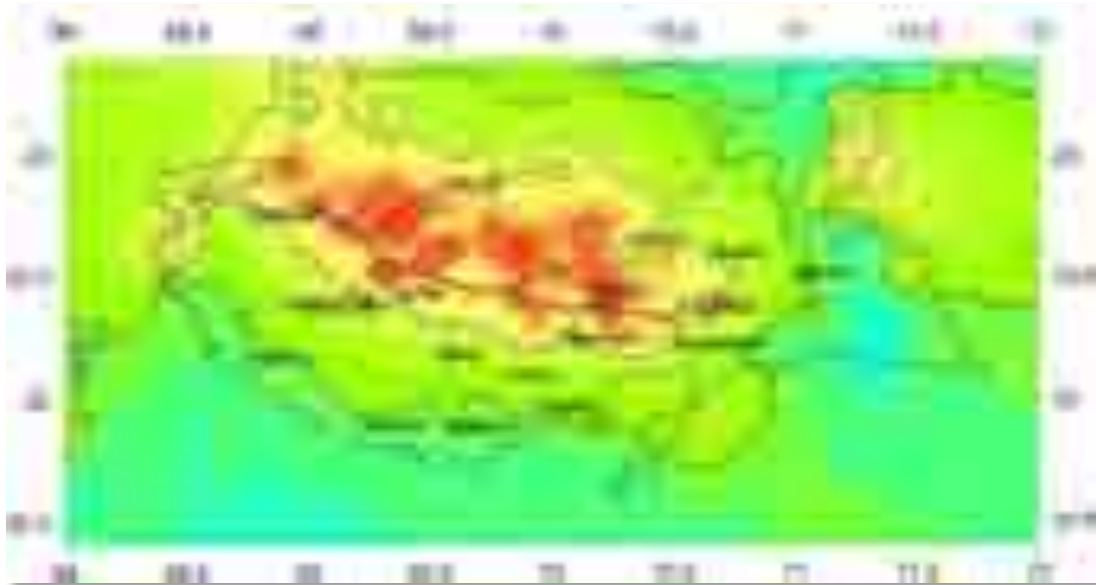


Fig. 2.6: PGA distribution maps due to a scenario earthquake of M_w 7.6 at V_s of 520m/sec, along KMF, considering a northward dip.

2.7 Deterministic Seismic Hazard Assessment (DSHA) of Khavda (Kachchh), Gujarat

(Kapil Mohan, Shruti Dugar and Sumer Chopra)

Khavda is a village in Kachchh district of Gujarat. It falls in Zone V in the seismic zonation map of India. Due to the proximity of many active faults and the ongoing commercial activities in this region, it is essential to estimate the seismic hazard for the Khavda and its surroundings. Khavda is bounded by several faults, such as the Allah Bund Fault (ABF) and Island Belt Fault (IBF) in the north; Kachchh Mainland Fault (KMF) and Katrol Hill Fault (KHF) in the south. The Gedi Fault (GF), North Wagad Fault (NWF) and South Wagad Fault (SWF) also fall in the neighbourhood. Therefore, an earthquake from any of these faults should be considered as a potential source of the seismic hazard in Khavda and its surrounding regions. Due to unavailability of the strong ground motion data from large magnitude earthquakes in Kachchh, the scenario earthquakes have been considered along these faults based on past earthquake catalog, to predict the ground accelerations. The Stochastic Finite-Fault Modelling technique

has been considered to simulate the strong ground motion. A magnitude of Mw 7.5 has been considered along KHF and IBF, Mw 7.6 along KMF, NWF, SWF and GF, and Mw 7.8 along ABF. Also, parametric testing has been conducted considering possible range of values for stress drop, Kappa and quality factors proposed for the region. The ground motions at 255m/s, 310m/s and 520m/s have been estimated. The highest value of mean Peak Ground Acceleration (PGA) of 0.81g is estimated due to an earthquake from the ABF. The mean PGA of 0.75g has been estimated due to earthquakes from IBF and KMF. A minimum PGA ~ 0.13g has been estimated due an earthquake from the GF.

2.8 Seismic Microzonation of Bhuj City, Kachchh (Gujarat)

(Kapil Mohan, Sumer Chopra, Vasu Pancholi, A.P. Singh, B. Sairam, Naveen Kumar, Shruti Dugar, Vinay Divedi, Vandana Patel and Arjav Shukla)

The Bhuj city (Fig. 2.7) falls in zone V of the seismic zoning map of India compiled by the Bureau of Indian Standard (BIS). Huge destruction was observed in the city due to the 2001 Bhuj earthquake. Therefore, the Ministry of Earth Science (MoES), New Delhi, sanctioned a project to ISR for seismic microzonation of the city. In this project, ISR has estimated the shear wave velocity values at 19 uniformly distributed sites in the Bhuj city. Under this project, ISR (i) prepared the site specific (local) geological map.(ii) prepared seismotectonic maps (1:2000 scale) (iii) drilled 28 boreholes, having depths of 3m to 21m. In all these boreholes, SPT tests for N-value were conducted every 3m and the disturbed /undisturbed soil samples were collected alternately every 1.5 m to measure the soil properties. Further, 2D soil profiles have been prepared, which help in soil modelling (iv) measured the shear wave velocity at 19 sites and prepared a Vs30 (average shear wave velocity up to 30m depth) map. (v) prepared the site response map using microtremor data, measured at 42 sites (vi) estimated the depth to the engineering bed layer (vii) estimated the response spectra at each borehole site in the Bhuj city,using ground response analysis. Liquefaction potential factor was also considered.

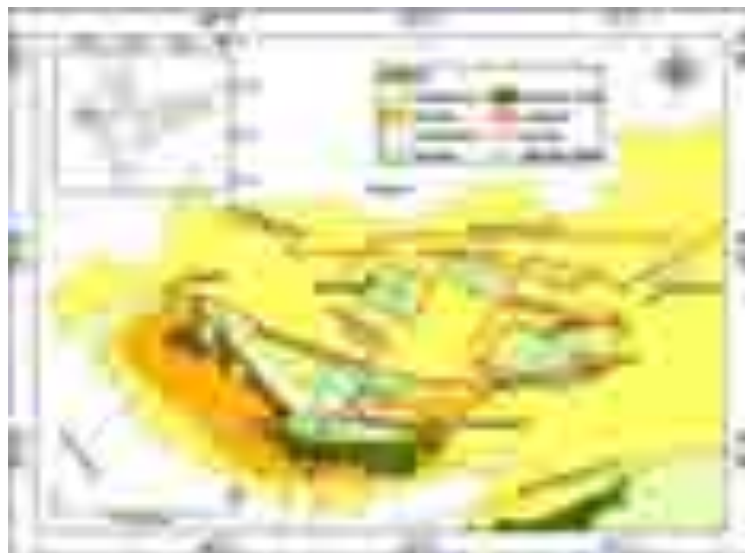


Fig. 2.7: The location of Bhuj City on Geology and Tectonic map of Kachchh (after Biswas, 2016).

Based on the geotechnical investigations and MASW surveys, the EBL is adopted as the layer with a Vs of 760 m/s. The depth to the EBL in Bhuj city varies from 12 to 28 m depth. It is shallower in the central and south-western parts and deeper in the north-western and the south-eastern parts. The Bhuj city is in the vicinity of major active faults like the Katrol Hill

Fault in the south, Kachchh Mainland Fault, Allahbund Fault, Island Belt Fault in the north and South Wagad Fault and North Wagad Fault in the north-east. The ground response analysis has been conducted to estimate the surface strong ground motion considering soil data from the drilled boreholes. A three-fold methodology has been adopted: (i) soil modelling and estimation of depth to the engineering bed layer (EBL) (ii) estimation of the ground motion at EBL (iii) estimation of ground motion at the surface by 1D ground response analysis. The soil models are prepared from the borehole data, shear-wave velocity measurements, and standard penetration test (SPT) N-values. The ground motion at EBL is estimated using the stochastic finite-fault source modelling technique by generating scenario earthquakes along major faults (of magnitude Mw 7.5 along the KHF and IBF, Mw 7.6 along KMF, NWF and GF, and Mw 7.8 along ABF) using the region specific ground model parameters. The ground motion was calculated for all scenario earthquakes at the location of 28 borehole sites at estimated Vs30. A total of 168 accelerograms were generated at each borehole site. The surface ground motion was estimated by passing the ground motion simulated at EBL (Fig. 2.8a) through prepared soil models at each site, using SHAKE. The highest mean PGA of ~1g is observed at the surface in the central-western part of the Bhuj city area where clay with high plasticity is present. The mean PGA amplification factor (between EBL and surface) is also calculated at all the boreholes, which is found to vary from 1.7 to 3.7.

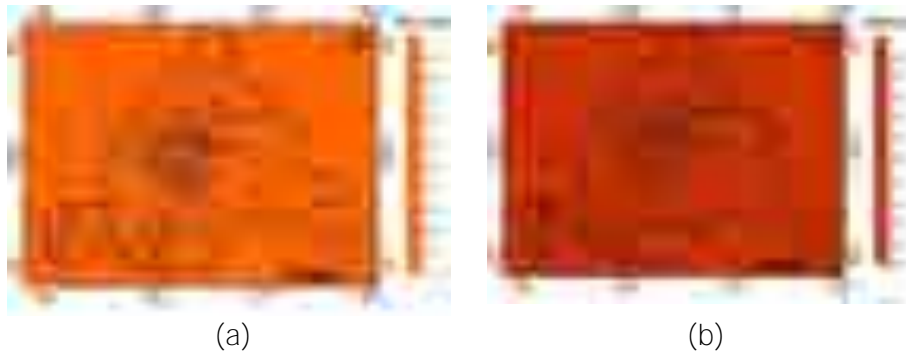


Fig. 2.8: The PGA distribution map of Bhuj city at (a) Engineering Bed layer and (b) Surface

2.9 Uncertainty/ Parametric Analysis for Ground Motion Estimation in Bhuj City
(Shruti Dugar, Kapil Mohan and Sumer Chopra)

In order to evaluate the variability of ground motion in the Bhuj city due to uncertainties in the input parameters, sensitivity analysis is performed considering variation in the stress drop (Fig. 2.9), Kappa (Fig. 2.10) and slip distribution (Fig. 2.11).

- a) Different stress drop (in bars) values: On increase of stress drop value from 100 bars to 140 bars, the maximum peak ground acceleration is increased by 27%.

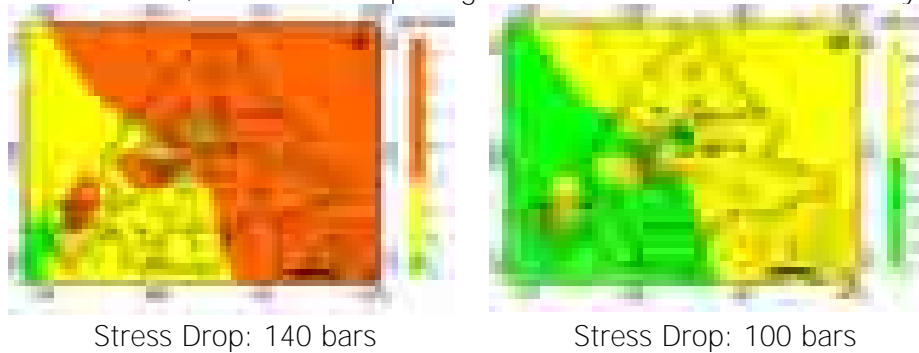


Fig. 2.9: The PGA distribution maps for different stress drop values

- b) Different near-surface attenuation factor (kappa): By increasing the kappa value from 0.02s to 0.025s, a ~30% decrease in the PGA is observed.

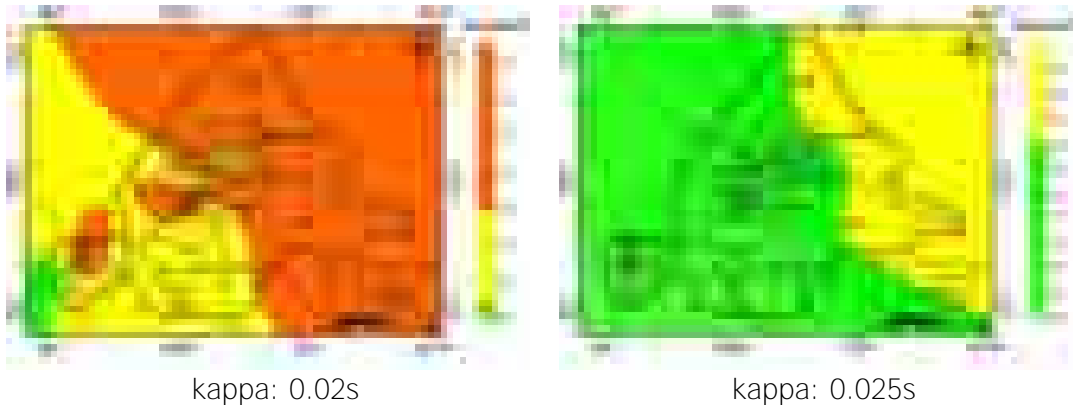


Fig. 2.10: The PGA distribution maps for different attenuation factors (kappa)

- c) Different slip distribution models for the Mw 7.6 earthquake: The maximum PGA value increases to 19% on using the slip model given by Yagi and Kikuchi (2001) in place of a random slip model.

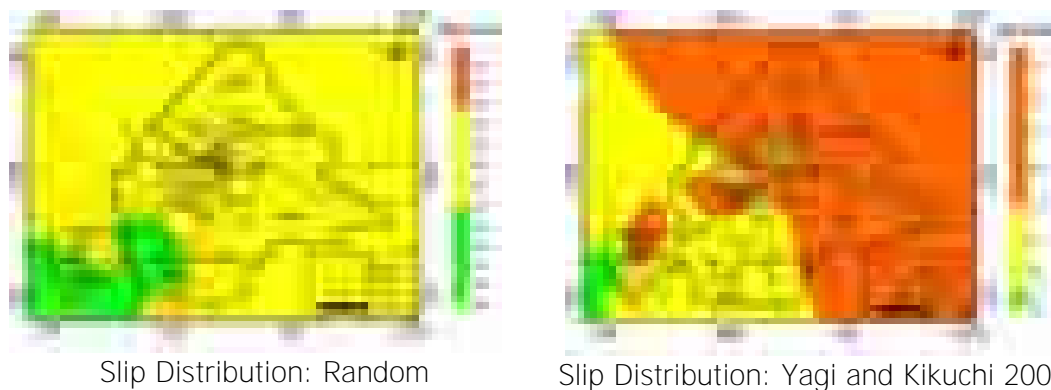


Fig. 2.11: The PGA distribution maps on different slip distribution

2.10 Comparative seismic hazard assessment in southern part of Gandhinagar (GIFT City, Gujarat) and Andheri (Mumbai, Maharashtra)
(Kapil Mohan, Shruti Dugar, Naveen Kumar and Sumer Chopra)

The Multi Commodity Exchange of India Limited (MCX) has invited ISR to conduct comparative seismic hazard assessments at Multi Commodity Exchange of India Ltd, Andheri, Mumbai and at some suggested locations in the GIFT City, Gandhinagar. Based on the past seismicity and tectonic settings of the areas, five different earthquake scenarios have been considered. These are (i) Mw 7.6 earthquake along the eastern part of the KMF (2001 Bhuj earthquake of Mw 7.6), (ii) Mw 6.0 earthquake along the East Cambay Fault (1864 earthquake of M 5.7, 100 km south of Gandhinagar city), (iii) Mw 6.0 along the Narmada Son Fault (1954 earthquake of Mw 5.4 at Bharuch)(iv) Mw 6.5 along the Panvel Flexure (1856 earthquake of Mw 5.0 in the Panvel Flexure seismic zone) and (v) an earthquake of magnitude Mw 7.0 along the Chiplun Fault (1618 earthquake of Mw 6.5, ~20km south of Mumbai in 1618).

The strong ground motions have been estimated at GIFT City, Gandhinagar and MCX, Mumbai considering these five different scenario earthquakes. The maximum PGA has been estimated due to the scenario earthquake of magnitude Mw 6.0 along the East Cambay Fault at GIFT City, Gandhinagar and scenario earthquake of magnitude Mw 7.0 along the Chiplun fault at

MCX, Mumbai. The accelerogram and response spectra at 5% damping estimated at GIFT city due to an earthquake of magnitude Mw 7.0 along the Chiplun fault are shown in Fig. 2.12. It is concluded that these PGA values can generate vibration/ cracking/damage at the individual sites but none of the scenario earthquakes have shown PGA, which could damage both the sites simultaneously.

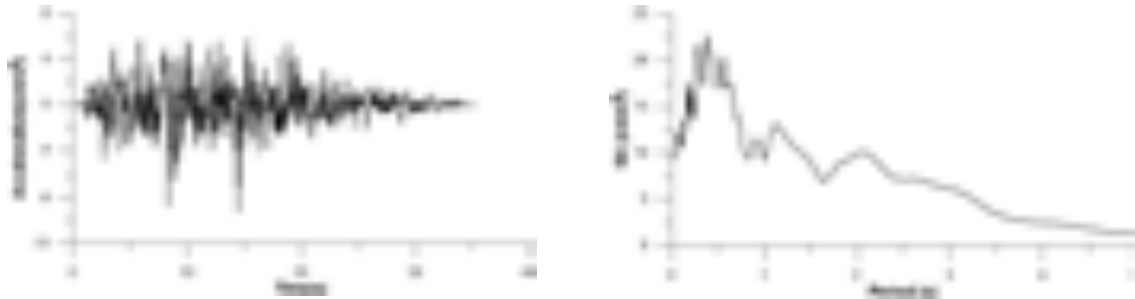


Fig. 2.12: The accelerogram (left) and response spectra (at 5% damping) (right) estimated at DRS, GIFT City due to a scenario earthquake of Mw 7.0 along the Chiplun fault.

2.11 Kachchh Mainland Fault: Characterization and associated seismic hazard (Kapil Mohan, Peush Chaudhary, Pruthul Patel, Shruti Dugar and Sumer Chopra)

The seismically active Kachchh Mainland Fault (KMF) is a WNW-ESE to E-W trending major fault, which is laterally displaced by NW-SE to NE-SW trending transverse faults. Various past studies suggested different dip directions, constrained by results from a suite of geophysical surveys, conducted mostly in its eastern part. The KMF was hitherto not studied throughout its entire length (especially the western part) by any deep geophysical survey. Due to its active nature and immense significance in seismic hazard of Kachchh, a Magnetotelluric survey across the KMF has been conducted covering two NS trending profiles, one from Luna village to Lathedi village (P1) and the other from Shervo village to Dujapar village (P2). For the characterization of the KMF in the western Kachchh, the profile lengths are chosen between 50 km and 80 km with an interstation spacing of 2-3 km. The geoelectric strike direction of these profiles varies from N55°W to N60°W. The 1D inversion of MT data (conducted by Occam and Bostic inversion techniques) constrains the sediment thickness to be about 2.0 km in the vicinity of the KMF. From 2D inversion of MT data, it is found that the KMF is steeply dipping south in the vicinity of the transverse faults near Profile P1 and dipping steeply north away from the transverse faults near Profile P2. Results from the present study correlate with the previous MT studies in the eastern part of KMF (Mohan et al., 2015).

The results from the MT study have been used to assess the seismic hazard due to KMF by dividing the entire Kachchh into 251 grid points and considering four different active segments of the KMF. The Stochastic Finite-Fault Modelling technique has been used to simulate strong ground motion at soft rock conditions considering a magnitude Mw 7.6 along each segment of KMF. The parametric testing has also been conducted by considering a range of stress drop values, Kappa values, Quality factors proposed by different studies in the Kachchh region. Considering the KMF as north dipping rather than south dipping, the peak ground acceleration estimates decreased by 14-38% at the sites falling to the south of KMF (like Bhuj, Bhachau etc.) and increased by 30-47% at the sites falling to the north of KMF (Rapar, Khavda etc.). Therefore, the dip of a fault plays a significant role in seismic hazard assessment across a fault. The present study gave realistic estimates of PGA as the dip of KMF was very well constrained and verified by detailed inversion of MT data.

2.12 Rapid Visual Screening (RVS) of RC frame buildings in Ahmedabad, India (Russi Modi and Kapil Mohan)

The RVS was carried out for the 67 RC frame type buildings that were reconstructed on the collapsed building sites, after the 2001 Bhuj earthquake. The performance score of the building is calculated based on the collected details such as the number of storeys, the presence of the vulnerability parameters such as soft storey, overhang, re-entrant corners, pounding and setbacks. For the surveyed buildings, the number of storeys ranges from 3 to 11. However, most (34) buildings have 5 storeys. 60 out of 67 buildings are of residential (Flat & Apartment) type. The calculated performance score ranges from 29 to 135. The mean and standard deviation for the set of obtained performance scores are 67.9104 and 22.3259. Most number of the buildings lie in the performance score range 46-90. However, there are some buildings in the low-performance score range 23-46, which may suffer severe damages in the event of an earthquake.

Fig. 2.13 shows the RVS statistics of the surveyed buildings. Higher the performance score, lesser is the vulnerability of the building to earthquakes. Fig. 2.13 shows the Gaussian distribution of the obtained scores of the surveyed buildings. The building damage states like no damage, slight damage, moderate damage, severe damage and collapse state are classified based on the $\mu-3\sigma$, $\mu-2\sigma$, $\mu-\sigma$, μ , $\mu+\sigma$, $\mu+2\sigma$, and $\mu+3\sigma$. Correlation of the damage state of a building with RVS score and PGA value of the region is also used to estimate the damage state of the surveyed buildings. Fig. 2.14 shows the generalized damage state of building w.r.t. RVS score and PGA for RC buildings (Sreerama et al., 2017). The PGA values considered for the damage grade estimation of a building are, surface PGA for near and far field earthquakes (Mohan et al., 2018 (ISR Annual report 2017-18, p. 28) and Zone Factor (IS 1893 Part I, 2016).

Based on the normal distribution, 60% of the surveyed buildings lie in the performance score range 46-90, which comes under the moderate damage state. Based on the above-given correlation in Fig. 2.15, 34% and 24% of the surveyed buildings fall under collapse and severe damage state respectively, when the nearfield earthquake surface PGA is considered. Around 58% of the surveyed buildings come under the moderate damage state when a zone factor value 0.16 and far-field earthquake surface PGA are considered. Fig. 2.15 shows an interpretation of the building damage state for the surveyed buildings based on the normal distribution curve, PGA of the region and RVS score of a building.

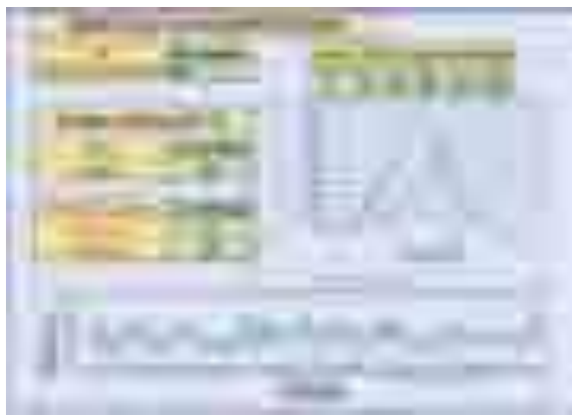


Fig. 2.13: RVS statistics for the buildings surveyed.

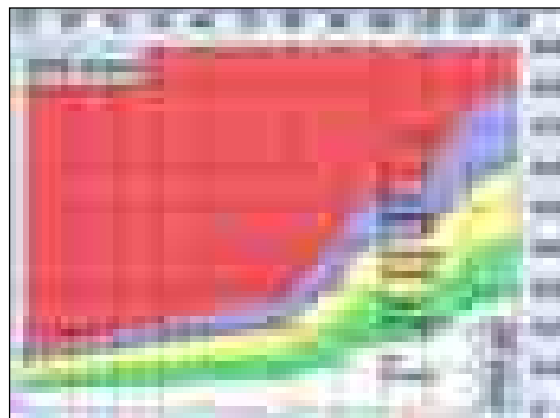


Fig. 2.14: Generalized damage state of building w.r.t. RVS score and PGA for RC buildings (Sreerama et al., 2017).

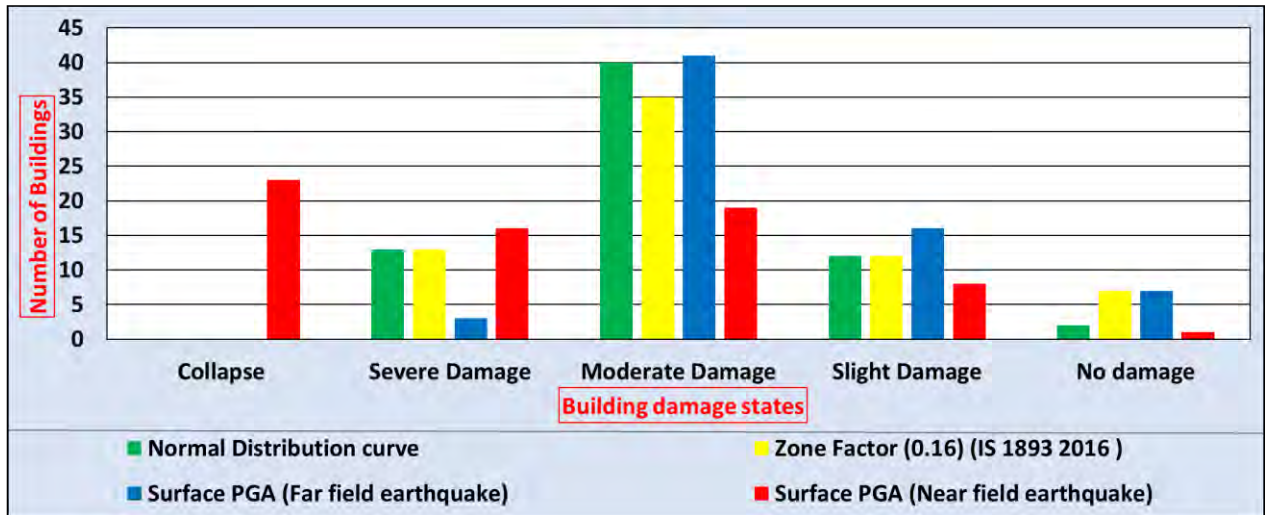


Fig. 2.15: Interpretation of the building damage state for the surveyed buildings based on the normal distribution curve, PGA of the region and RVS score of a building.

2.13 Seismic Risk and Loss Assessment in Bhachau City
(Akash Solanki and Kapil Mohan)

A total of 5600 buildings have been mapped for assessment of seismic risk in Bhachau city (Fig. 2.16). The mapping has been done in order to generate the total built up area in the city which can be distributed based on the type of structure and building use. Along with this, a preliminary estimate of seismic risk was done (direct economic loss) using available data on buildings in the city. Census 2011 data on housing was used for this purpose (Table 2.5). Four different hazard scenarios were considered based on nearby faults and the estimated PGAs were considered as primary input, as follows:

- Mw 7.6 scenario earthquake along Kachchh Mainland Fault (KMF) – 0.71g (Mohan, 2014)
- Mw 7.6 scenario earthquake along Katrol Hill Fault (KHF) - 0.20g (Mohan, 2014)
- Mw 6.5 scenario earthquake along South Wagad Fault (SWF) - 0.33g (Mohan, 2014)
- 2001 Bhuj Earthquake - 0.51g (Chopra et al., 2010)

The following assumptions were made while estimating the seismic risk as the census data did not fulfil every requirement.

- 100 sq mt area of each house
- 7700 Rs/ mt sq replacement cost for load bearing structures (Jantri, 2011)
- Most buildings have 2 story except for those having sloping type roofs.
- Only structural loss is estimated
- Type II: Medium Soil

Table 2.5: Building Stock classification using 2011 census housing data for Bhachau City (Source: Census 2011)

Particulars	Nos.
Total No. of census houses in Bhachau	10902
Total No. of census houses with residential and residential + other uses	8483
Total No. of census houses with other than residential uses	2419
Total No. of brick masonry with flat RC roof houses (only residential and residential + other uses)	4417
Total No. of brick masonry with GI sheet roof houses (only residential and residential + other uses)	1383

Total No. of brick masonry with sloping tiles roof houses (only residential and residential + other uses)	1981
---	------



Fig. 2.16: The mapped 5600 buildings (in white colour) in Bhachchau city. The surveyed buildings are shown with black colour.

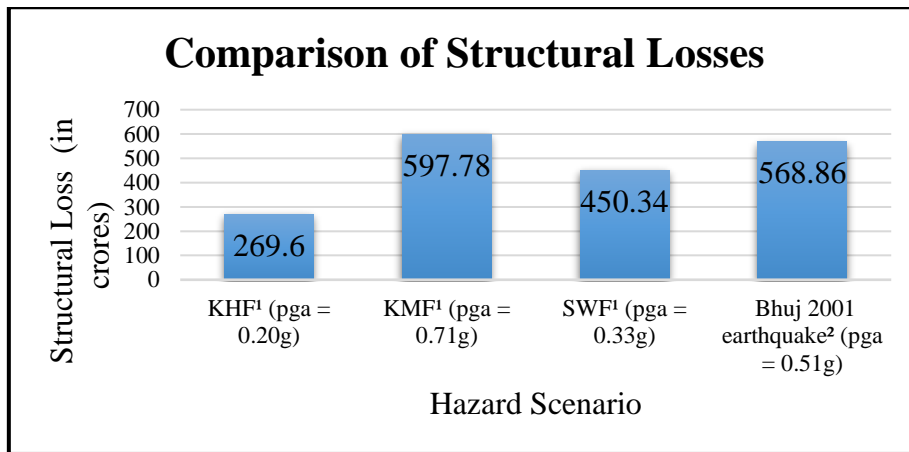


Fig. 2.17: Comparison of estimated structural losses considering 4 different PGA values and Census 2011 residential housing data for Bhachchau city considering Jantri rates for 2011 (KHF: Katrol Hill Fault, KMF: Kachchh Mainland Fault, SWF: South Wagad Fault, ¹Mohan, 2014, ²Chopra et al., 2010)

It may be observed from Fig. 2.17 that structural losses are highest (INR 597.78 crores) for the scenario considering the earthquake at Kachchh Mainland Fault (PGA- 0.71g) and lowest (INR 269.6 crores) considering the earthquake from the Katrol Hill Fault (PGA- 0.20g).

2.14 MT survey in Dudhai (Kachchh) for subsurface mapping
(Peush Chaudhary, Pruthul Patel and Kapil Mohan)

A Magnetotelluric (MT) survey has been conducted in Dudhai (Kachchh) and surrounding regions for subsurface mapping. Data at a total of seven MT sites has been acquired with ADU-07e recording units of M/s Metronix, Germany. The recording period of the MT data ranges from 2-3 days with an interstation spacing of 6-7 km. The profile length was ~ 50 km along a near N-S direction. The magnetic field measurements were made using MSF-06e coils, and the electric field measurements were made using the Pb-PbCl₂ electrodes. The electric field was measured in two components (Ex and Ey) while magnetic field was measured in three components (Hx, Hy, and Hz). The electrode separation of 80 m was maintained to

measure the electric field at each site. The location map with acquired sites is shown in the Fig. 2.18.

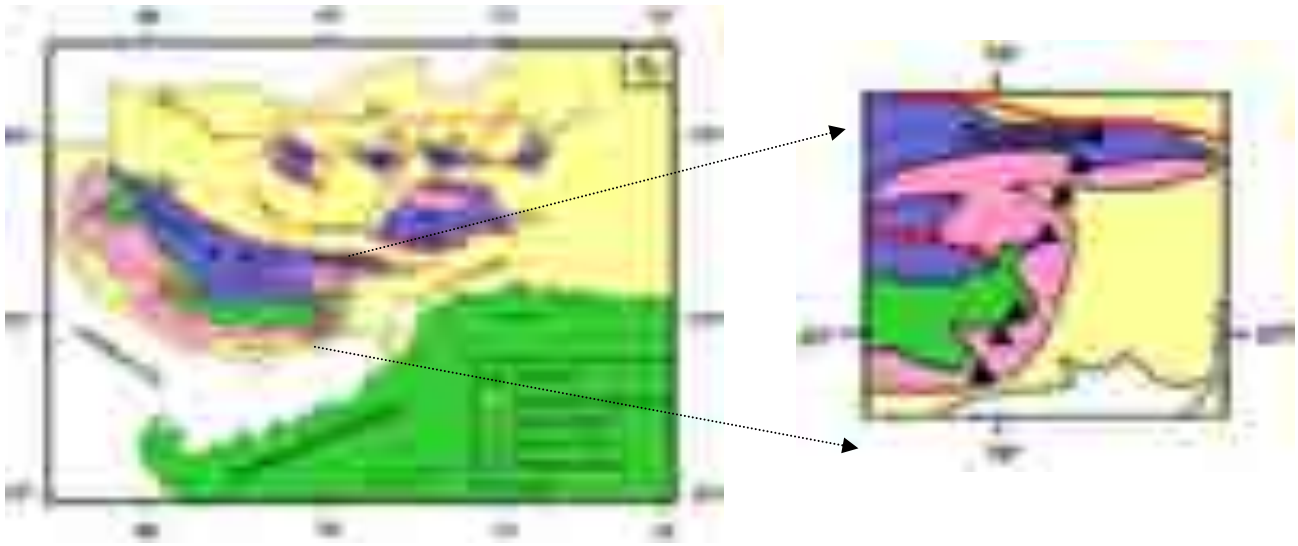


Fig. 2.18: Geological map of the study region Duhai. The black triangles show the locations in Duhai where MT survey was carried out.

MT data is processed with the help of MAPROS processing software to obtain the apparent resistivity and phase curves. In processing, the noisy part is masked to obtain smooth MT curves. However, due to the heavy industrialization, cultural noise and presence of power grid, MT data is noisy at some sites (Fig. 2.19). The 1-D MT data inversion has been performed using the Occam algorithm (Constable et al., 1987). The geoelectric depth section prepared from the 1D inversion is shown in Fig. 2.20. From 1D inversion of MT data, the basement has been found at a depth of ~4km. The basement has been found fractured due to the presence of faults below sites 1, 3 and 5 (Fig. 2.20).



Fig. 2.19: MT data curves (apparent resistivity and phase).

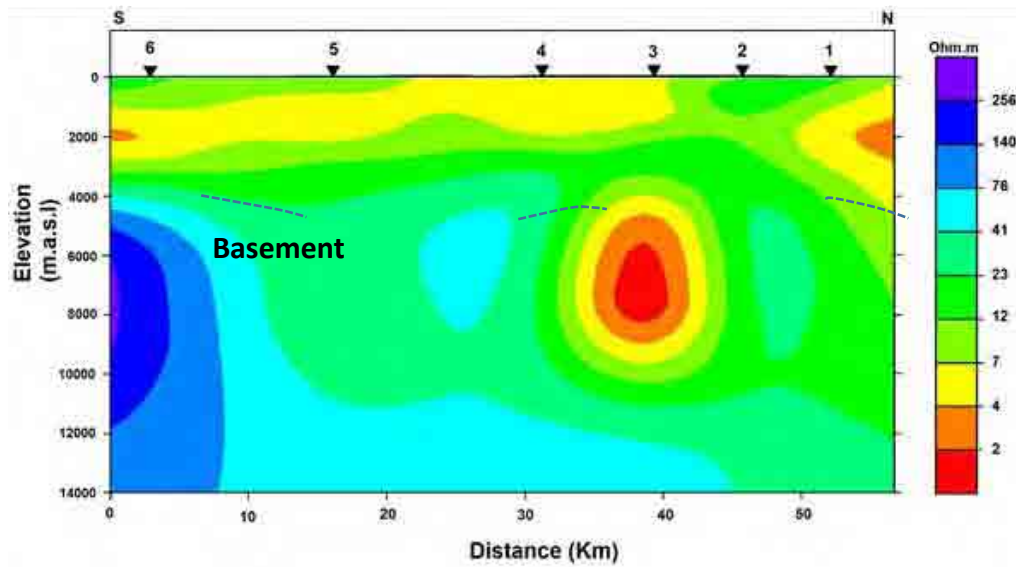


Fig. 2.20: The geoelectric depth section generated from 1D inversion.

2.15 Magnetotelluric investigation in Little Rann area of Kachchh region
(Peush Chaudhary and Kapil Mohan)

Data from 17 MT sites were acquired in the Little Rann area in the eastern part of Kachchh. The 2D subsurface geoelectrical section is shown in Fig. 2.21. In the present study, three faults have been inferred based on conductors C1, C2 and C3. C1 is located at the proposed location of Kanmer fault (eastern extension of South Wagad Fault) which was formed during the rifting process in Kachchh. The large sediment thickness in the northern part (north to Kanmer fault) confirms the northward tilting of Wagad Uplift, as suggested by Biswas (2005). Conductor C2 is located at the contact of Kachchh and Saurashtra peninsula, at the proposed location of North Kathiawar Fault. This north dipping conductor is interpreted as NKF, the southern boundary of the Kachchh rift. Conductor C3 has been inferred as the sub-parallel fault formed during the rifting process. Based on the information extracted from the geoelectric depth model, a geological model is also proposed for the study area and shown in Fig. 2.22.

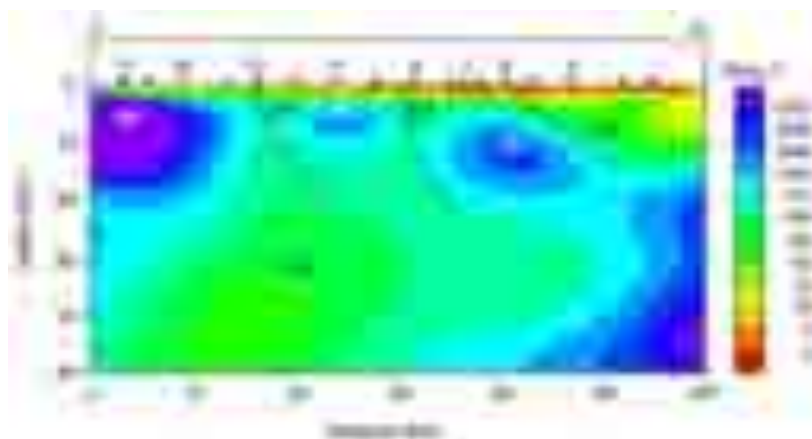


Fig. 2.21: Geoelectric depth section obtained after 2D inversion of tipper, TE and TM modes data along the profile.

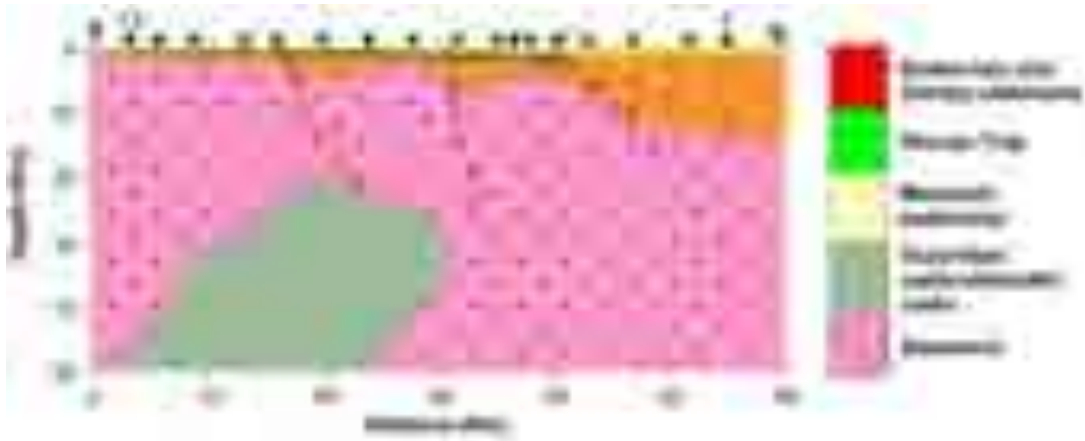


Fig. 2.22: Geological model proposed based on 2D geoelectric depth section.

2.16 Dimensionality and Directionality analysis of MT data in the Kachchh Mainland Upliftment (KMU)

(Pruthul Patel and Kapil Mohan)

To estimate the sediment thickness including that of the Mesozoics, an MT survey has been carried out along an E-W profile of ~90 km length, with an interstation spacing of 2-3 km, in the Kachchh Mainland Upliftment (KMU) area from Nagviri village in the west to Chapredi village in the east (Fig. 2.23). Data at a total of 25 stations of broadband MT data (period range 0.003-3000 s) was acquired along the EW profile. The time series data has been **processed and dimensionality analysis has been carried out using the Swift's and Bahr's skew techniques. The Swift's skew plot (Fig. 2.24) shows major skew values below 0.2° . The Bahr's skew plot (Fig. 2.25) shows skew values less than 0.3° for periods less than 30 s suggesting the 1D/ 2D nature of MT data below 30s.**

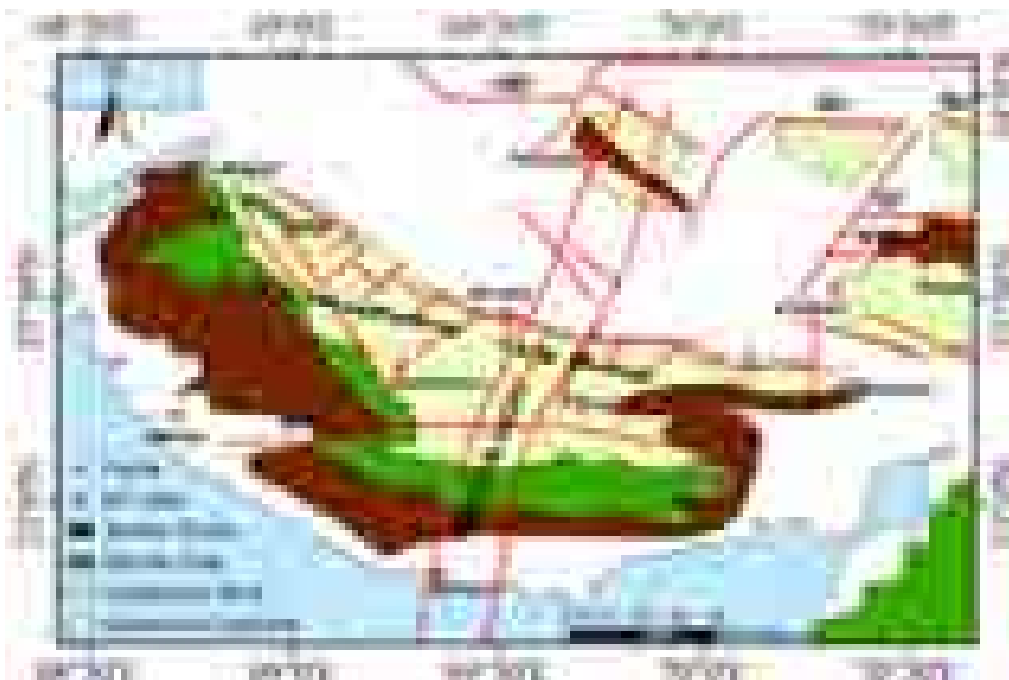


Fig. 2.23: MT station acquired points in Kachchh district



Fig. 2.24: The dimensionality conducted using Swift's skew technique.



Fig. 2.25: The dimensionality conducted using Bahr's skew technique.

2.17 Magnetotelluric investigations in the western part of Narmada Son lineament zone (Peush Chaudhary and Kapil Mohan)

Magnetotelluric data at 8 sites along N-S profile in the Bhadbhut area (Bharuch) were acquired to map the Son Narmada Fault (Fig. 2.26).



Fig. 2.26: Map showing the location of stations where the MT data was acquired (after Naganjaneyulu & Santosh, 2011).

An interstation spacing of 3-4 km has been maintained during the survey with a recording period of 3-4 days. The acquired data was processed with the help of MAPROS processing software, to obtain the impedance tensor. A geoelectric strike direction of $N88^{\circ}E$ was obtained with the current MT data using the Becken & Burkhart (2004) approach. The data was then decomposed into the TE mode (parallel to strike) and TM mode (perpendicular to strike). After the decomposition of data into TE and TM modes, the MT data is subjected to 2D modeling

with the help of WinGLink software. The preliminary 2D geoelectric depth section down to 25 km depth, is given in Fig. 2.27. The 2D geoelectric depth section indicates an upper layer of resistivity from 1 to 5 Ohm-m. This layer may represent the Tertiary sediments having maximum thickness in the southern part of the profile followed by the granitic basement. A conductive feature (C1 in Fig. 2.27) in the southern part of the profile below the sites 6 and 7 might be the Son Narmada fault (SNF). However, these results are preliminary in nature and more MT measurements are required in the southern part of the study region for a high resolution image of the Son Narmada Fault.

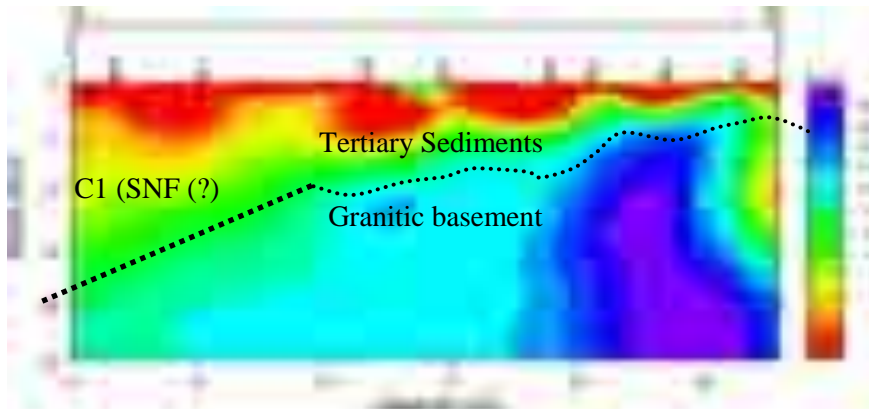


Fig. 2.27: 2D geoelectric depth section of the MT data along the profile (Figure 2.26).

2.18 Magnetotelluric study in the Talala region of Saurashtra
(Dillip Kushwaha and Kapil Mohan)

The Talala region of Saurashtra in western India witnessed three moderate sized earthquakes of Mw 4.8 (2007), Mw 5.0 (2007) and Mw 5.1 (2011) in the past and studies indicated the causative fault as the Girnar Fault (Rastogi et al., 2012). Magnetotelluric (MT) investigations were carried out in Saurashtra near Talala along a NW-SE profile (62km) from Sendarda in the north to Hadmatiya village in the south, for characterizing the Girnar fault (Figure 2.28). Data from 16 MT stations was acquired from October to November 2018. The data was acquired in a broad period range of 0.001 to 1000 sec., for ~48 hours. In the present study, the MT data acquisition system ADU-07 was used. The magnetic field measurements were made using MFS-06e induction coils and the electric field measurements were made using Pb-PbCl₂ electrodes.

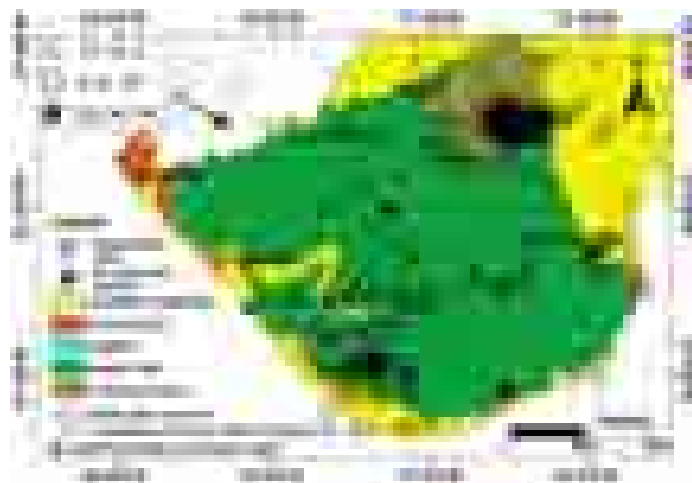


Fig. 2.28: Geological map of the study area along with the Magnetotelluric stations. The seismicity is plotted for 2018 year (catalog from ISR).

The strike analysis of the acquired data has been carried out using Becken & Burkhardt as well as Groom-Bailey techniques for both the broad period range and various period bands. The regional strike estimated at all the 16 sites is found to be in good agreement with the tectonic setting of the study area. The dimensionality analysis of the MT data was conducted using swift skew, Bahr skew and phase tensor analysis technique. **The Swift's skew plot shows values less than 0.2° for a broad period range, indicating 1D and 2D nature of the subsurface structure. The Bahr's skew plot shows values less than 0.3° for periods less than 10sec, suggesting 1D/2D nature of the subsurface structure below 10 sec. The phase tensor ellipses from 0.01 to 100 sec are close to a circle with a moderate skewness value, suggesting a 1D nature of the subsurface structure. The distortion parameters estimated through Groom-Bailey decomposition technique for the broad period band as well as various period bands suggest the 2D nature of the subsurface structure. The plot of real induction arrows indicates a low resistive zone between stations TL5 and TL7, which could be attributed to a fault.**

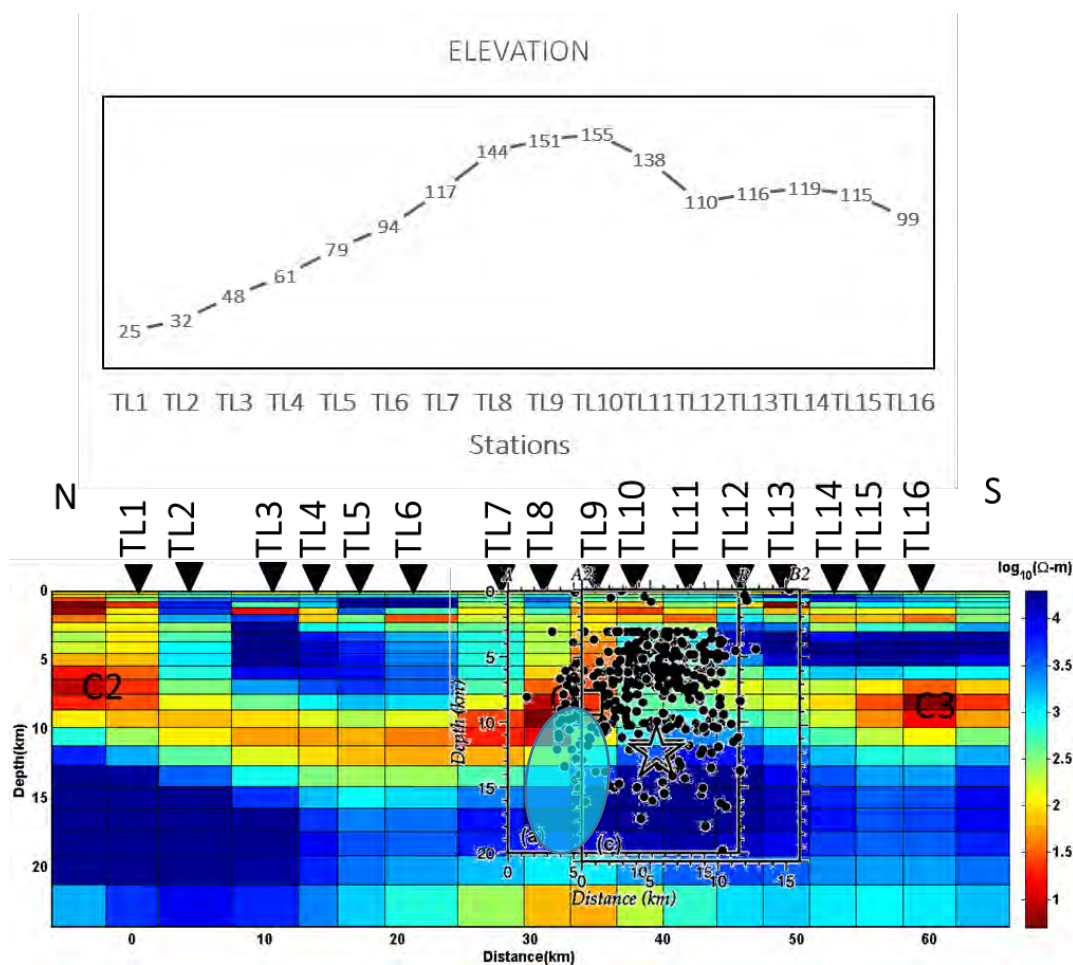


Fig. 2.29: 2D inversion model of joint TE and TM mode data along with seismicity in the area.

We performed 2D inversion of the MT data using the code MT2DInvMATLAB (Lee et al. 2009). In this program, the smoothness-constrained least-squares inversion is adopted for solving the regularized inverse problems (Siripunvaraporn and Egbert 2000; Mehanee and Zhdanov 2002). It uses the reciprocity method to calculate the Jacobian matrix to reduce computational time. In the inversion process, a spatially variable regularization parameter algorithm suggested by Yi et al. (2003) was adopted for smoothness-constrained least-squares inversion with an active constraint balancing algorithm to obtain an optimal smoothness constraint. The model obtained from the inversion of the joint TE and TM mode data is given in Fig. 2.29. The

final root mean square misfit is ~ 0.4 for TM mode inversion and ~ 0.5 for both TE and joint mode inversion. From 2D inversion of MT data, an almost vertical conductive zone has been observed at the centre of the profile (between stations TL8 and TL9) (Fig. 2.29) with a resistivity of 5–50 Ω -m. This conductor has been interpreted as the Girnar Fault. It matches well with the location proposed by seismic reflection survey (Rao and Tewari, 2005) and the linear trend of Gravity low (Mishra et. al., 2004) by Rastogi et al. (2012). The result matches well with the strike slip mechanism suggested by Yadav et al. (2007).

2.19 Study of Lineaments and faults in Dadra and Nagar Haveli, western India (Naveen Kumar, Kapil Mohan)

The study of lineaments and faults has been carried out in an area of ~ 8000 km² in Dadra and Nagar Haveli (19.83° N-20.52° N and 72.68° E-73.67° E), western India using the photo geological interpretations, followed by field investigations on a 1:50,000 scale. The structural features are recognized using the false colour composite and SRTM-DEM based products like slope aspect, shaded relief, drainage network and drainage profiles. The seismotectonic map has been prepared identifying the linear features and seismicity of the area since 1856.

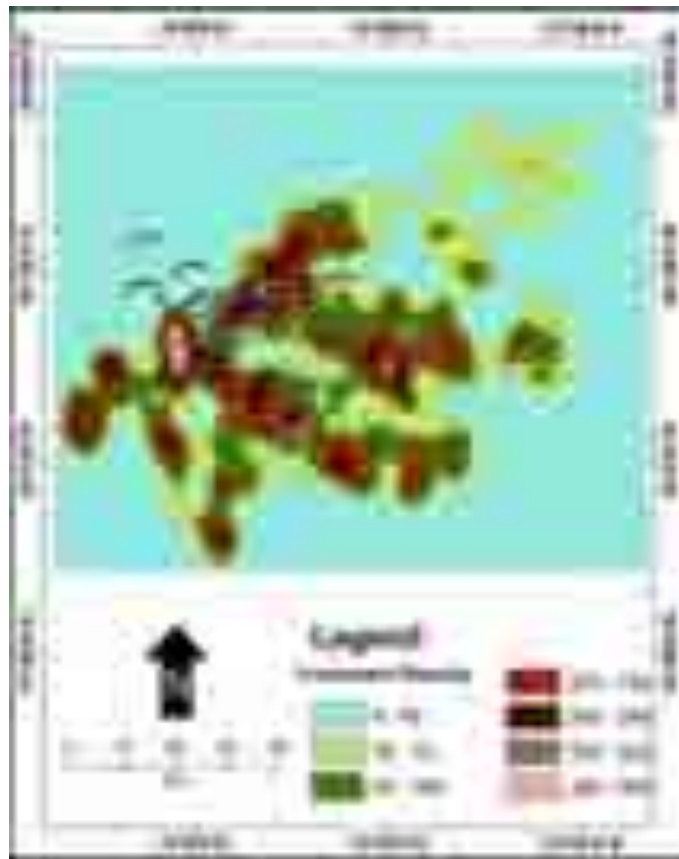


Fig. 2.30: Lineament density map in Dadra and Nagar Haveli.

By combining results of all the remote sensing processed images, the final lineament map was produced. The structures that have maximum relevance of structures like roads, canals and railway tracks were filtered during the image processing. The latitude, longitude and direction of lineaments were stored during digitization. The field survey was conducted with an aim to validate the observed lineaments and relate them to the existing geological structures in the field. Based on physical characteristics of the linear feature map and field verification, various lineaments with structural indications were observed at different places in the study area.

However, during the field work, preference was given to the geological lineaments that have the potential to produce seismic hazard. Analysis of lineament density showed a high lineament density towards the central portion of the study area (Fig. 2.30) and low lineament density in the alluvial part, which may be due to obliteration and siltation processes. These lineaments are seen in maximum numbers with a dominance in the NNE-SSW direction, similar to the Panvel flexure, a major tectonic feature in the study area (Fig. 2.30). Regional tectonic structures surrounding the area are having the same direction as the NNE-SSW trending linear structures. Higher density of linear structures in the central portion of the study area, presence of seismicity along these NNE-SSW trending linear structures further pointed out the active nature of the Panvel flexure.

2.20 Palaeochannel Study in Dadra and Nagar Haveli

(Naveen Kumar and Kapil Mohan)

The Damanganga River is the major river in Dadra and Nagar Haveli, which originates from the Sahyadri mountain range from an elevation of ~683m. The alignment of stream channels in the upper middle and lower elevation levels reveals that the river basins are controlled by lineaments and faults. The drainage of Damanganga River in the upper region follows the NNE-SSW and E-W trending lineaments. Further, the sharp turn of the river in Dadra and Nagar Haveli indicates the tectonically controlled structural conformation of the Damanganga River. The palaeochannel along the Damanganga River is well preserved and can be easily identified in the field. It is possible to trace the channel over a distance of 1.50 km length and ~1.0 km width and the palaeochannel is being used for the most cultivated land in the area. During the geological mapping in this region it has also been noticed that the ground water is present along the palaeochannel which confirms the presence of aquifers in the sandy layers of alluvium. The sediments underlying the palaeochannel are sandy gravels, sandy silt and silty clay, the uniformity being seen in sediment deposition (Fig. 2.31a). The lithological sections of right and left limbs of the palaeochannels are plotted (Fig. 2.31 b, c, d & e). In order to determine the geometry of the palaeochannel and the present day channel, a geological traverse survey was undertaken using GPS. The surveyed data was used to plot the geometry of the palaeochannel and the present channel (Fig. 2.31f). From E-W cross section (Fig. 2.31f), it is evident that the palaeochannel is present in this part of study area. The E-W cross section across the palaeochannel reveals a steep drop of 8.0 m (Fig. 2.31f). A N-S profile (Fig. 2.31f) has been plotted across the palaeochannel and the current channel which reveals a steep elevation difference of 12-15 m between the palaeochannel and the current river channel.

During geological investigations conducted in river bed, an E-W trending normal fault has been inferred (Fig. 2.31a). The fault surface is marked by remarkable development of slickensides (Fig. 2.31g). The slickenside surface was well exposed at a depth of 10-15 cm and 5-10 m in length. The slickensides were steeply inclined (68°) in south-south west direction on the fault surface (Fig. 2.31g). The slickenlines are smooth to the touch in the downward direction and rough in the upward direction. This suggests that the missing block moved down (Doblas 1998; Argles 2010). The amount of down throw is not determinable because of homogeneous strata, but an attempt is made to correlate the present topographic levels of the left and right banks along the river. The N-S cross section reveals that there is a difference of 3.0 m in the topography of right and left banks along the river (Fig. 2.31f), this suggests that the amount of down throw could be ~3.0 m.

In summary, the presence of a palaeochannel at an elevation higher than the present river channel (Fig. 2.31f) (12-15m) in the study area reveals that it has been influenced by tectonic activities in the form of faulting (Fig. 2.31g) (slickensides surfaces) or may have undergone

an episode of upliftment, which results in the down-cutting of river channel by the Damanganga River. The rate of river channel incision was very high because the river incised the basaltic bedrock at a depth of 10-15m. The higher rate of incision in a rocky terrain also suggests that the faulting is followed by incision.



Fig. 2.31: (a) Palaeochannel and present day channel of River Damanganga with associated faults and lineaments, (b) Palaeochannel deposits exposed on the right limb of the fossil river, (c) The stratigraphy of alluvial deposits exposed in the right limb Palaeochannel of Damanganga River, (d) Palaeochannel deposits exposed on the left limb of fossil river, (e) The stratigraphy of alluvial deposits exposed in the left limb Palaeochannel of Damanganga River, (f) E-W and N-S Geological cross sections along Palaeochannels and Damanganga River, (g) Slickenside fault surface.

2.21 Trigger Mechanism for soft sediment deformation structures in Dadra and Nagar Haveli region

(Naveen Kumar, Kapil Mohan, Rakesh K. Dumka and Sumer Chopra)

In the Dadra and Nagar Haveli region, different kinds of soft sediment deformation structures have been analysed from several outcrop sections during the field investigation. These structures were mainly observed in sandy silt, silty clay and sandy gravels. The soft sediment deformation structures recorded mainly are sandy silt dykes & sills, slump structures, suspended sandy silt, sandy gravel blocks, convolute bedding and load structures. By reviewing the available worldwide literature on soft sediment deformation structures, the most reliable and suited trigger mechanism has been worked out for the soft sediment structures reported in Dadra and Nagar Haveli region. Most mechanisms propose that the soft sediment

deformation structures (SSDS) are initiated **by the action of "trigger"**. Numerous possibilities of trigger mechanisms have been described for soft sediment deformation structures. The most known are (i) sediment loading (Moretti and Sabato, 2007; Lowe and LoPiccolo, 1974; Anketell et al., 1970), (ii) the turbiditic currents (Alfaro et al., 2002; Molina et al., 1998; Dalrymple, 1979), (iii) collapse structures (Moretti et al., 2001; Waltham and Fookes, 2003; Moretti et al., 2011), (iv) liquefaction through pre-existing cracks (Holzer and Clark, 1993; Guhman and Pederson, 1992), and (v) seismic shaking (Rodríguez-Pascua et al., 2000; Rossetti, 1999; Alfaro et al., 1999; Vanneste et al., 1999; Calvo et al., 1998; Lowe, 1975; Sims, 1975; Seilacher, 1969; Moretti et al., 2011). Though the sediment loading, the turbiditic currents, collapse structures, liquefaction through pre-existing cracks can be triggering mechanisms for the formation of the soft sediment structures, these could be insignificant in the study region due to the following reasons:

- i) The sediment loading induced SSDS are mostly formed in lacustrine environments and induced by the density currents. Since the sediments are of fluvial origin and in the absence of thick piles of sediments over the horizon of SSDS, the theory of overburden loading as the cause for the formation of SSDS can be discarded (Obermeier, 1996).
- ii) The turbidity currents are generally formed in the deep sea near the continental shelf regions with high slopes. The study area being a flat terrain with an average elevation between 30- 40m, the role of turbidity in the formation of SSDS can be overruled.
- iii) The study area is located in the Konkan coastal belt in the western part of Deccan Volcanic Province and the signatures of karst topography are not present in this region. Therefore, the SSDS could not have been formed due to the collapse structures.
- iv) The soft sediment deformation structures along the cracks are only limited to the sand boils in a linear pattern along the linear cracks. However, in the present study a wide variety of SSDS are recognized from the different parts of the study area with wide distribution that do not show any linear pattern. Therefore, these SSDS were not formed due to the liquefaction along the cracks.

Since the Quaternary sediments in the study area are of fluvial origin and a wide extent of the soft sediment deformation structures are identified, active role of a regional triggering mechanism compared to the mechanisms described above (i to iv), is clearly indicated. Seismic shaking could be the most plausible triggering mechanism that might have led to the formation of the observed SSDS in the study area considering its proximity to the Son-Narmada and the Panvel seismic zone (Chandra, 1977). Further, the study area is surrounded by faults (west coast fault, Panvel flexure fault) and Western Ghats escarpment which was formed as a result of the upliftment (Kale et al., 2016). These tectonic features played a significant role in sculpturing the landscape of the study area. The seismicity along the Panvel flexure with earthquakes of magnitude M 6.5 in 1618 (Rao, 2005; Rao and Rao, 1984), M 5.7 in 1856 (Chandra, 1977), M 5 in 1935 (Bansal and Gupta, 1998), M4.1 in 1989 (ISC) and a low-intensity earthquakes between M 1 to 3.9 in the study area (>200) supports the tectonically active nature of the region. Moreover, the earthquake catalog data (Fig. 2.32) validates the presence of a large number of recent earthquakes in the study area. Also, the high density of earthquake epicentres in the NW are in concordance with the tectonic features present in the region (Fig. 2.32). The studies in Deccan upland region like Nashik, Nanded and Osmanabad districts of Maharashtra state have documented the presence of seismites, flexures, warping, folding, offsets and deformation in the alluvial sediments (Kale et al., 2016; Kaplay et al., 2016 & 2013; Dole et al., 2002; Rajendran, 1997) similar to the SSDS of Damanganga River in Dadra and Nagar Haveli. According to Rajendran (1997), the magnitude of the paleo-earthquake, which caused deformation in sediments at Ter, was estimated to be similar to the 1993 Killari earthquake. All these locations are in Deccan Trap Province mainly in the Deccan upland region, where the sediment deformational structures are reported, and these locations exhibit the bedrock of basaltic flow covered by the alluvial sediments and soil.

The similarity of this geological framework with that in the present study area is significant. The SSDS recorded from Quaternary sediments are incontrovertible evidences of neotectonic deformation in the study area. The presence of these structures in sediments also suggests that such events occurred at different locations in different intervals. The presence of microseismicity, soft sediment deformation structures and historic earthquake records lay emphasis on the occurrence of a major earthquake event (>5 Magnitude) in the area along the axis of Panvel flexure during Quaternary period.

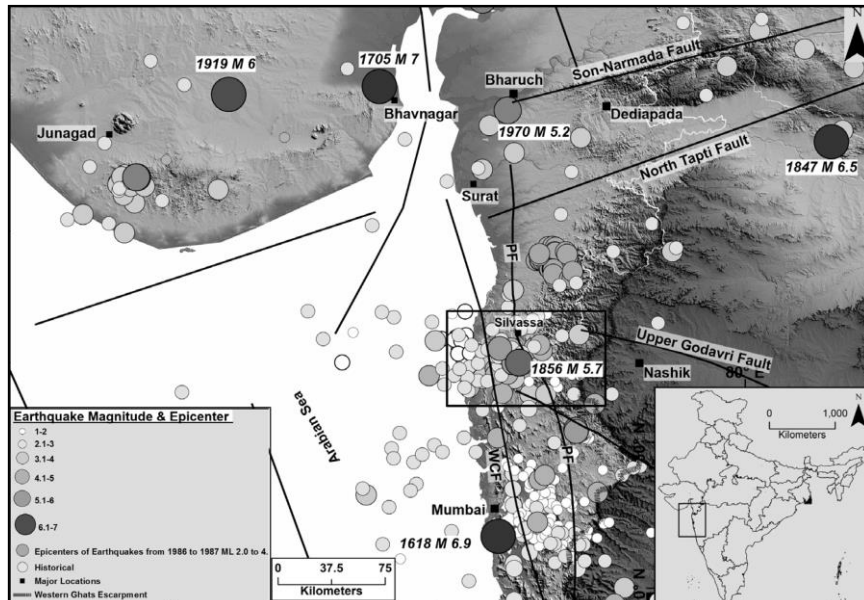


Fig. 2.32: Seismotectonic map of the study area (shown in black box) (Earthquakes plotted from 1856 to January 2019), PF-Panvel flexure, WCF-West coast fault.

3. SOLID EARTH GEOPHYSICS

3.1 Site response study in and around the Bhuj City

(Arjav Shukla)

In the present study, ambient noise was recorded at nearly 42 sites of Bhuj city to determine the site amplifications. This technique uses low frequency ambient vibration generated due to the ocean tides and winds, while local cultural noise is avoided. The observations were made for an hour at each site. For reliable experimental conditions, we followed the guidelines proposed by Koller et al. (2004) in the framework of SESAME (WP02 of SESAME Project). Single station measurements were made using the City Shark – II digitizer and recorder. The data were recorded during early morning, evening and night time on continuous mode at a sampling rate 100 samples/s. The data was recorded for a 40 minute time length window. The data was processed using open source software Geopsy and represented here in form of H/V profiles (S1 - S42). The H/V ratio is calculated using at least 40 to 60 second time windows, overlapping one another by 5%. A FFT is applied to the signal of the three components to obtain the spectral amplitudes. The spectra are then smoothed following the approach of Konno and Ohmachi (1998).



Fig. 3.1: Satellite imagery of Bhuj area showing locations of the microtremor survey (Black and white circles)

The single station HVSRs of ambient noise (microtremors) were estimated at 42 sites (Fig. 3.1) in and around the Bhuj city. The H/V ratio curves obtained for all sites in Bhuj show very close similarity in terms of their shape and spatial distribution. The shape and values of peak frequency and amplitude are nearly same for all locations, except a few, which is due to the similar geology of the city. The resultant HVSR curves match with the local geological conditions at sites. It is observed that most of the curves exhibit broad, plateau shaped peaks at very flat, low to moderate amplitude values in a confined low frequency range between 0.4 and 2.0 Hz.

The sites with low amplitude values at lower frequencies <3 Hz are situated on a compact platform of Cretaceous sandstone of Bhuj formation with no other soft rock deposits lying over or in contact with it. A few sites, i.e., S8, S13, S25, and S41 are found to have comparatively high amplitude values >4, indicating soft and unconsolidated Quaternary and basaltic body beneath the sites. These sites are located near plaeo river/lack flows and old city areas. For all the sites, the observed peaks with low/high amplitude values at low/high frequencies suggest velocity/impedance contrast at deeper/shallower depths. Some sites are found with two or multiple peak amplitudes at different frequencies, indicating multiple

impedance contrasts at different depths. The Bhuj City overlies sandstones and no much amplification is observed except at a few sites. The H/V spectral ratios reveal that most of the sites have predominant frequencies in the range of 0.4 - 5.0 Hz without any sharp peak. The **dominant frequency ≤ 1.2 Hz is noticed** at most of the sites.

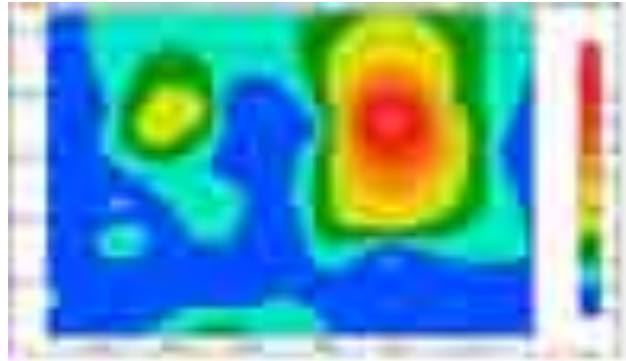


Fig. 3.2: Predominant frequencies obtained by single microtremor measurements in and around the Bhuj City

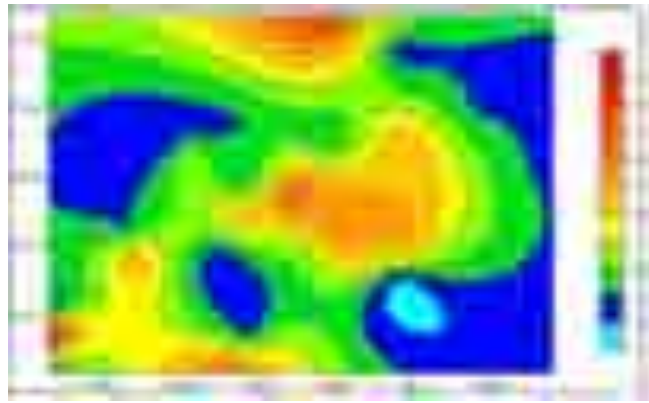


Fig. 3.3: Amplifications estimated by single microtremor measurements in and around the Bhuj City

3.2 Estimation of Shallow Structure beneath the Saurashtra region by array microtremor measurements and horizontal to-vertical spectral ratio method (AP Singh and Gaurav Dave)

The microtremor measurements have been carried out at 50 well distributed sites in an area of 170 km² to determine the site amplification corresponding to the amplified frequencies and the relevant shear wave velocity profile. The results show a plateau like shape with no sharp peak. The phase velocity dispersion of Rayleigh wave is calculated from array data using spatial autocorrelation method, and a 1-D wave velocity structure is determined by means of inversion process, based on the neighbourhood algorithm. H/V spectral ratios at all the sites indicate amplification between 2.9 to 3.5 and 2.0 to 2.2 in the frequency bands of 1.8 - 2.5 Hz and 4.0-6.0 Hz, respectively. A three layer model (one soil layer with the power law variation of the velocity over the substratum) was used as the initial model for the inversion. It was observed that the upper most layer up to 12 m has a low shear wave velocity between 175-400 m/s. The second layer is at 25-40 m depth with shear velocity 450-800 m/s and the third layer at 70-80 m depth with shear velocity 850-1350 m/s (Figure 3.4). The results of single and array measurements have been compared with the results of multi-channel analysis of surface wave (MASW). The estimated shallow subsurface shear wave velocity structure in the city shows a good correlation with the geomorphological data.



Fig. 3.4: (a) HVSR curve at the Rajkot site (b) Velocity profile obtained through forward modelling. Three-layer model is used and the V_{s30} value is estimated to be 516m/s.

3.3 Investigation of spatial and temporal variability of site response in the Arunachal Himalaya using ambient seismic noise and earthquake waveforms (A. P. Singh, M. Ravi Kumar, Abhay Pandey, Ketan Singha Roy)

The Arunachal region that constitutes the easternmost segment of the Himalaya has experienced two great earthquakes in the past. This portion is geologically and seismotectonically unique compared to the other parts of Himalaya. In this study, the ambient seismic noise and earthquake waveforms registered at 34 broadband seismograph stations with a flat frequency response between 120s and 0.02s are analyzed to understand the stability and reliability of the Horizontal to Vertical Spectral Ratio (HVSR) method. Also, we use the bootstrapping method to estimate the uncertainty and variations in the HVSR in different seasons. Although the predominant frequency does not show any seasonal variation, the amplitudes reveal a slight dependence. The predominant frequencies in the area mainly vary from 1.1 Hz to 7.0 Hz. At a few sites, two peaks well separated in frequency, indicate shallower and deeper layers with impedance contrast. Our results show that the average predominant frequencies are around 3.5 Hz for the undifferentiated granite gneiss, 4.3 Hz for the Bomdila granite gneiss, 2.1 Hz for the Bomdila Group of rocks (paleoproterozoic), 2.8 Hz for the *Gandise batholiths*, 2.6 Hz for the Gondwana succession and 1.8 Hz for the Abor formation. The amplification estimated by the site to reference method, varies between 1.5 and 6.2, which is lower than that obtained from the HVSR method. Validation of the results from ambient seismic noise was performed by comparing them with those from the earthquake waveforms and correlation with local geology.

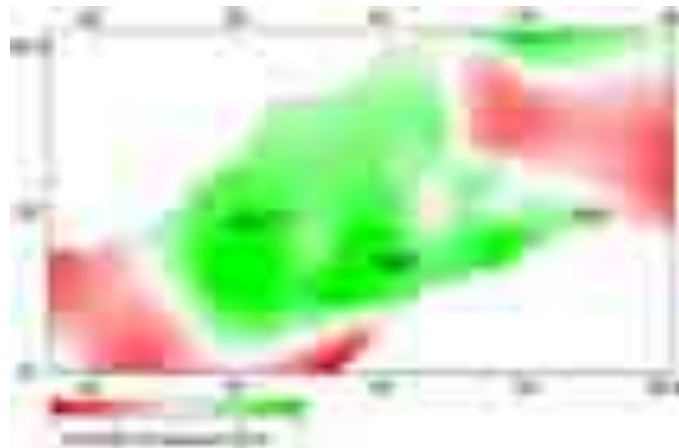


Fig. 3.5: Spatial distribution of predominant frequency (Hz) in the Arunachal Himalaya. The frequency scale is shown in the map. The major tectonic features are also shown.

3.4 Feasibility study on Low Frequency Passive Seismic (LFPS) survey in NELP Block WB-ONN-2005/4, MBA Basin
(A.P Singh, Harsh Limbachiya, Jay Pandit, Ketan Singha Roy)

The Oil and Natural Gas Corporation (ONGC), Mumbai has made a request to the Institute of Seismological Research (ISR), Gandhinagar to carry out a feasibility study on Low Frequency Passive Seismic (LFPS) survey in the NELP Block WB-ONN-2005/4, MBA Basin. The data acquisition started on 23 November 2018 and completed by 29 November 2018. The data acquisition was usually done in two shifts starting from early morning 06:00 hrs to 16:00 hrs. LFPS data were collected at 30 locations for 4-6 hours in each of the two shifts. The sensors were planted in ~1ft deep pits. The results show very distinctive V/H ratio >1.5 for Ashokenagar#1 (oil/Gas well), as compared to low values at Jaguli#1 (Dry well). Higher V/H ratios are also observed near the proposed drill location. Their values change in different directions. The LFPS survey in a 3D grid pattern around the proposed locations is recommended for optimal positioning of the drill holes. The doublet response, instead of a single peak, observed in the V/H plots needs to be critically analysed to ascertain their sources. It may lead to some additional potential zones.

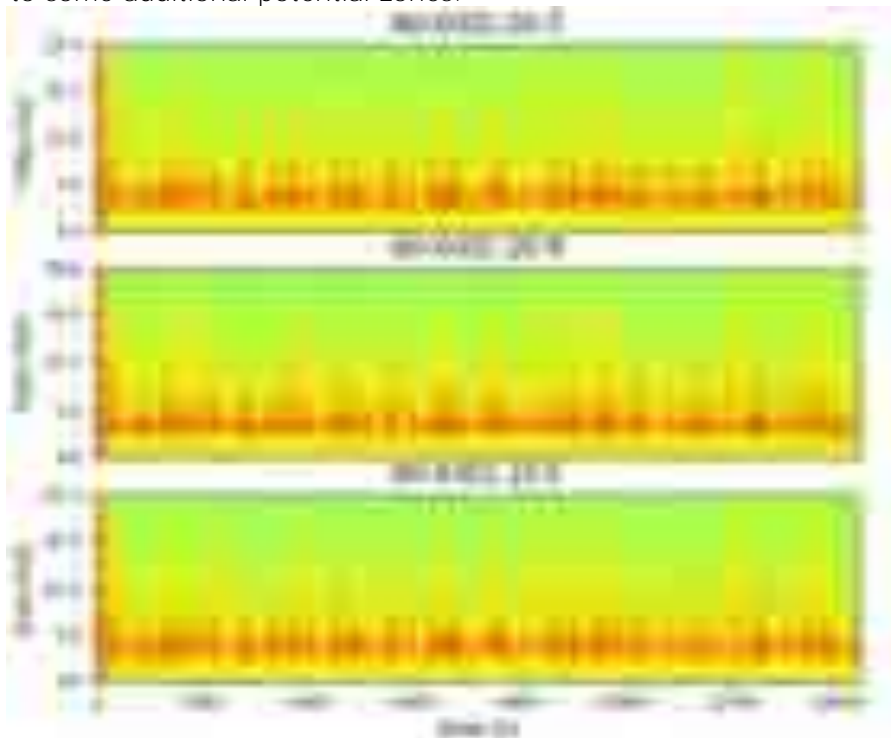


Fig. 3.6: Spectrogram of all three components of LFPS data (4 hrs) at observation point 8.



Fig. 3.7: Distinct anomalies of V/H Ratio attribute over oil/gas well and dry well.

3.5 Investigation of Groundwater resources in the Kachchh district, Gujarat using Transient Electromagnetics

(Pavan Kumar, Indu Chaudhary, Mehul Nagar, Himanshu Chaube, Rakesh Nikam, Dinesh Singh, Durga Prasad and Siddhartha Prizomwala)

In-loop transient electromagnetic (TEM) survey at nearly 100 locations in the Bhachau taluka of Kachchh district is carried out to assess the depth of the groundwater table and to identify deep potential aquifers and understand the aquifer characteristics. The one dimensional resistivity information is calibrated and validated with the existing lithologs in the region. The TEM resistivity sections infer variable groundwater level ranging from 15- 150m and suggest a multi-layered aquifer system. The resistivity sections across fault zones in the region indicate a confined aquifer at 50-90m depth that possibly terminates near the fault zone. A change in groundwater level and quality is observed over different geological setups. The analysis of self-potential values suggests the active role of the fault zone in the infiltration and the groundwater outflow. A large amount of infiltration from the Rann/coastal areas at shallow levels could be a possible cause for the high salinity observed in the ground water in this region. From the study, it is suggested that the groundwater in the alluvial covered regions is more contaminated compared to the rocky terrains with the Tertiary to Mesozoic formations. The variations in the infiltration and the salinity in the groundwater correlate well with the geomorphology of the region. A potential freshwater aquifer is delineated at 100-120m depth, that is associated with a palaeochannel in the region. From the present study, we propose that the geotectonic setting and depositional environment has a strong influence on the aquifer dynamics and quality of the groundwater.

3.6 Integrated geophysical studies to delineate the structural features in the Ambaji mineralization zone, Gujarat, NW India

(Avinash Kumar Chouhan, Dinesh Singh, Himanshu Chaube, Rakesh Nikam, Mehul Nagar and G. Pavan Kumar)

To understand the complex tectonic setting and its linkage to origin of mineralization of the Ambaji and its surrounding area, gravity (~ 650 points) and magnetic data (~200 points) are collected at a station interval of 4-5 km, and analysed. Bouguer gravity anomalies are obtained using a Bouguer slab of density 2.67 gm/cc. Bouguer anomaly (BA) values range from -30 to 30 mGal (Fig.3.8a). Total magnetic anomaly values of the study area are calculated after correcting for diurnal variation and International Geomagnetic Reference Field (IGRF), which show a variation from -770 to -30 nT (Fig.3.8b). Upward continuation of gravity data is done to image the subsurface extension of regional tectonic features. Gravity and magnetic data have been analysed for delineation of structural features using different derivative techniques like, total horizontal derivative (THD), Tilt angle derivative, Theta map and Analytical Signal techniques.

The derivative analysis delineated major NE-SW trending lineaments, such as, Chambal-Jamnagar Lineament (CJL), Pisangan-Vadnagar Lineament (PVL) and the NW-SE oriented Jaisalmer-Barvani Lineament (JBL). The high gravity anomalies in the western part of the study region indicate a shallow basement. Residual Bouguer anomaly is obtained by subtracting the regional field from the observed Bouguer anomaly. The residual BA shows a pattern almost similar to the observed BA, with little changes in the amplitude. The Magnetic high in the south-western part that correlates with the JBL possibly indicates the deep rooted nature of the lineament. An E-W structural trend that appears to be continued from the northeastern part of the region represents the Delhi-Aravalli trend. The presence of Aravalli is below the northern alluvial plains is also supported by previous regional geophysical studies in the region.

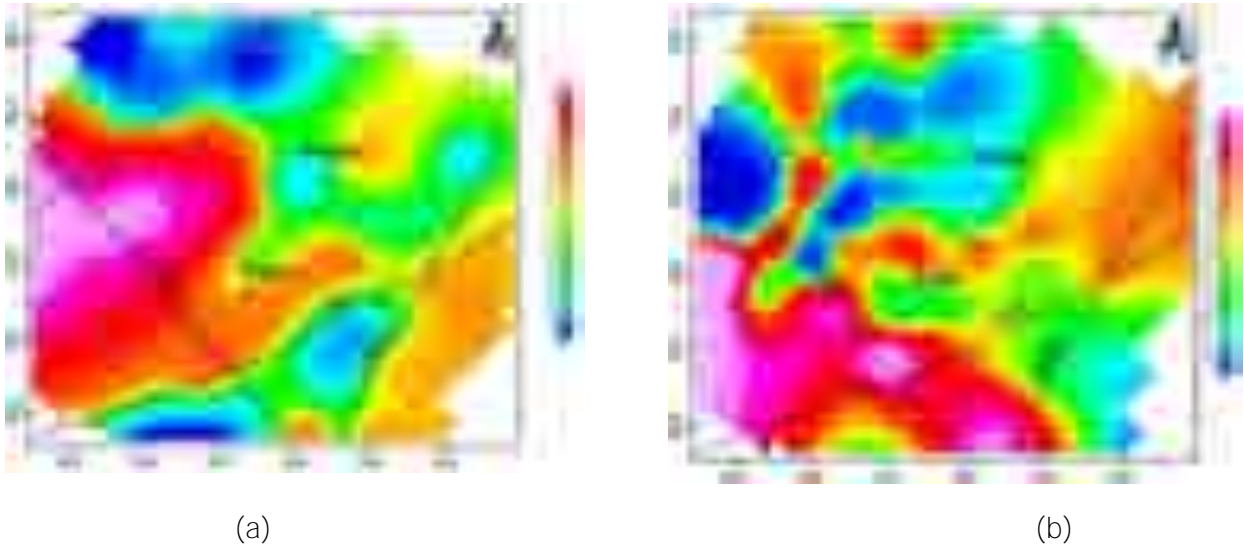


Fig. 3.8: (a) Bouguer anomaly map of the Ambaji area. (b) Magnetic anomaly map of the Ambaji area. CJL- Chambal Jamnagar Lineament, JBL- Jaisalmer Barwani Lineament, PVL- Pisangan Vadnagar Lineament. Dots show the gravity and magnetic stations.

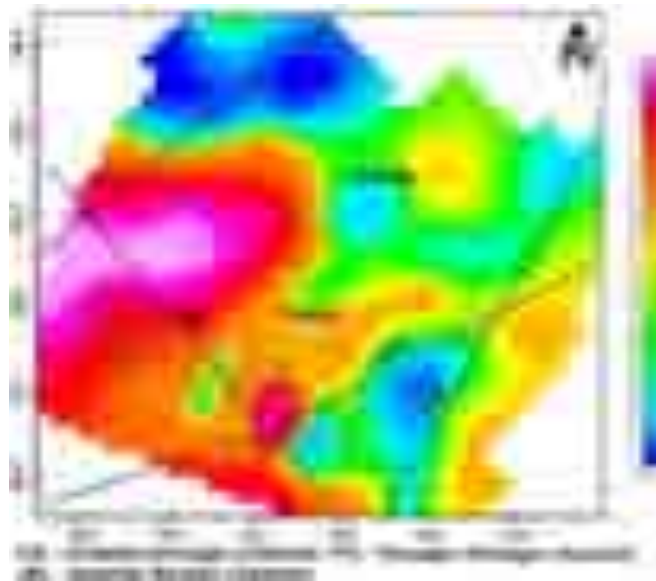


Fig. 3.9: Residual Bouguer anomaly map of the Ambaji area showing gravity measurement points (block dots)

3.7 Tectonic trends and new crustal structure of the North Cambay rift basin, India deduced from integrated study of gravity, magnetic and seismic data (Avinash Kumar Chouhan)

The Cambay rift basin (CRB) is an intracratonic rift basin, which is a well-established hydrocarbon province of the western part of India that has experienced several earthquakes of magnitude greater than 5 in the past. To understand the detailed crustal geometry, both gravity and magnetic surveys are carried out and a new gravity map is prepared, which shows a variation of -40 to $+28$ mGal. Further, the NW-SE oriented lineaments and faults are delineated by studying the total horizontal derivative and tilt derivative of magnetic and gravity

anomalies. Spectral analysis suggests three layers at a depth of 15, 5.5 and 2 km. In the present study, we have given the revised locations of the Eastern Cambay Fault (ECF) and Western Cambay Fault (WCF) using residual-Bouguer anomaly, total horizontal derivative and tilt derivative of the Bouguer anomaly. The present residual Bouguer and magnetic anomaly map also shows previously unnoticed gravity features like, NE-SW trending Unhawa ridge and N-S trending Mehsana uplift. To study the crustal structure, five gravity models have been constructed using inputs from previous studies like Deep Seismic Sounding (DSS), wells and seismological data. The crustal architecture in terms of sedimentary and Deccan Trap thickness, varies from 0.5-6 m and 0.5-3 km respectively. Evidence of magmatic underplating layer in the lower crust is also found, which has the largest thickness in the central part of the basin. The Moho depth varies between 31 and 34 km in the study area. Gravity models also show the presence of ECF and WCF in the middle crust, which is supported by the regional-Bouguer anomaly map. On the basis of these evidences, we can say that both the marginal faults are deep rooted in nature.

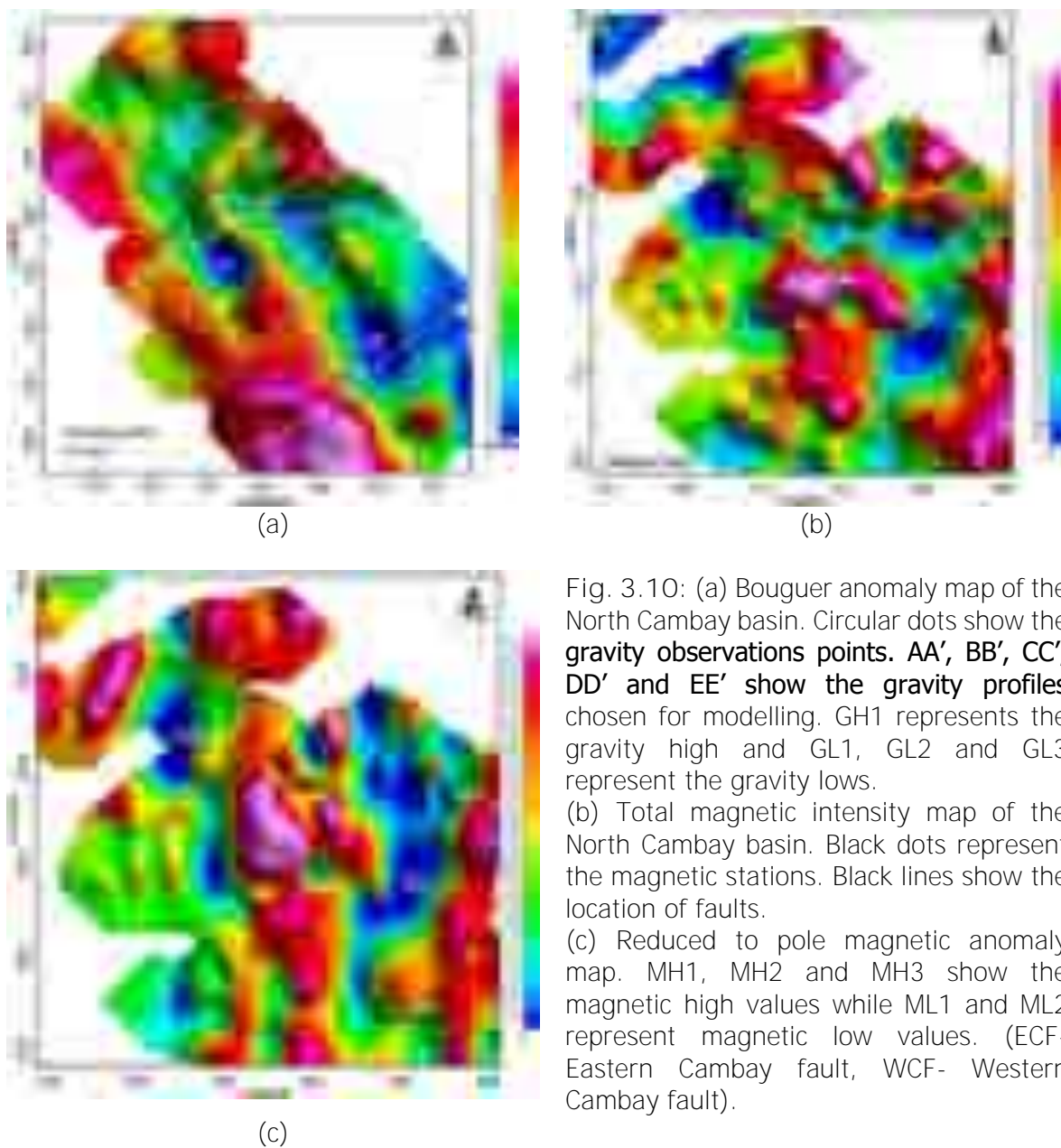


Fig. 3.10: (a) Bouguer anomaly map of the North Cambay basin. Circular dots show the gravity observations points. AA', BB', CC', DD' and EE' show the gravity profiles chosen for modelling. GH1 represents the gravity high and GL1, GL2 and GL3 represent the gravity lows. (b) Total magnetic intensity map of the North Cambay basin. Black dots represent the magnetic stations. Black lines show the location of faults. (c) Reduced to pole magnetic anomaly map. MH1, MH2 and MH3 show the magnetic high values while ML1 and ML2 represent magnetic low values. (ECF- Eastern Cambay fault, WCF- Western Cambay fault).

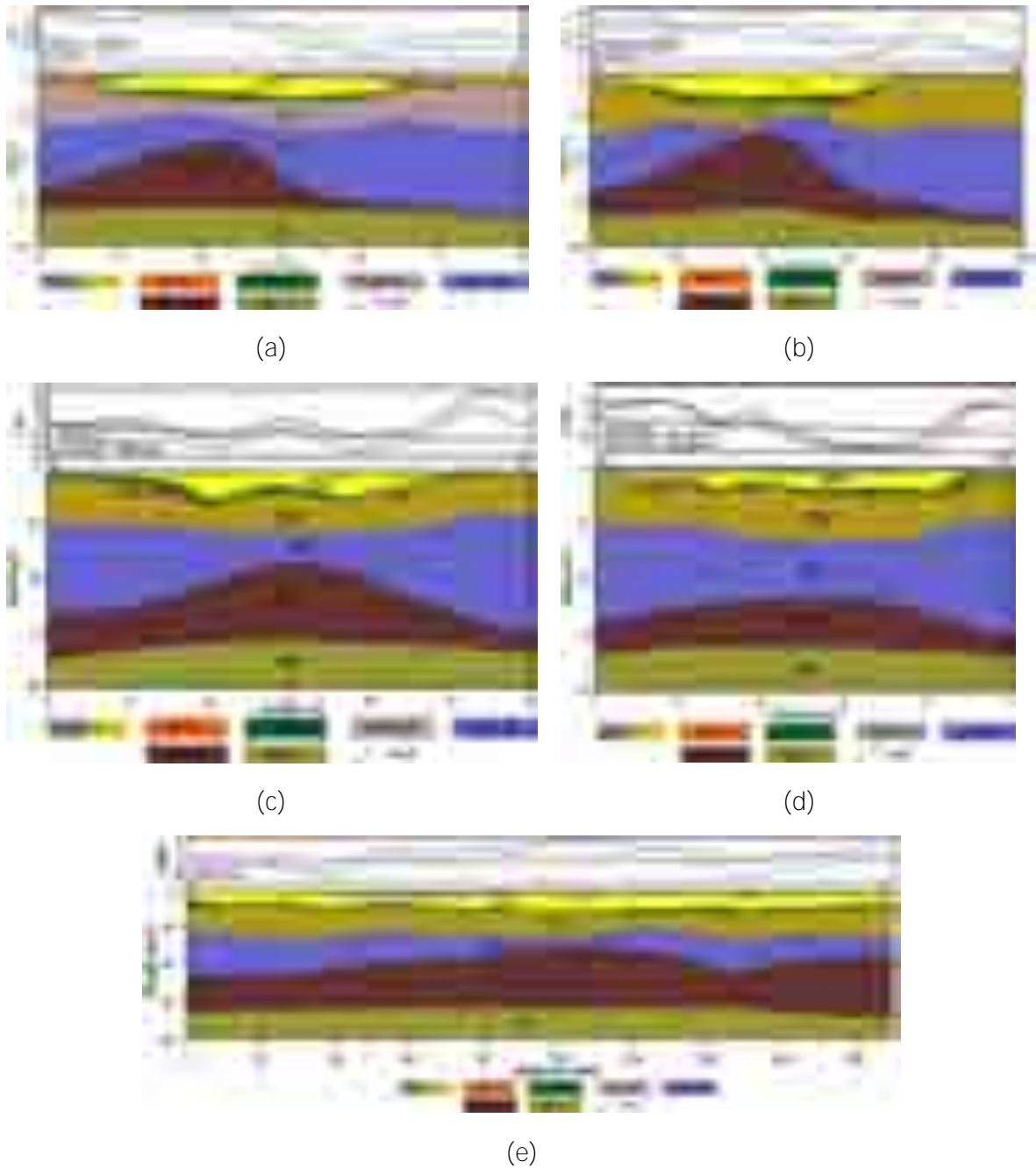


Fig. 3.11: The geological cross section and 2.5D gravity modelling (a) along profile AA', (b) along profile BB', (c) along profile CC', (d) along profile DD', and (e) along profile EE'. Observed, calculated, regional and residual Bouguer anomalies are shown by dots, black, red and blue lines in figure. Stratigraphic units QTS- Quaternary and Tertiary sediments, MS- Mesozoic sediments, DT- Deccan trap, PCB, Pre Cambrian basement, MC- Middle crust, MU- Magmatic underplating layer and UM- Upper mantle. Eastern and Western Cambay faults (ECF and WCF) are represented by dotted lines on the model. Density (in gm/cc) of each stratigraphic layer is shown in the legend.

3.8 Delineation of lineaments in the Cambay rift and surrounding regions of NW India utilizing satellite derived EIGEN6C4 gravity data
(Avinash Kumar Chouhan, Dinesh Singh, Pallabee Choudhury, S K Pal)

The present study is an attempt to delineate the lineaments in the Cambay rift (CR), northwestern India, using satellite-derived EIGEN6C4 gravity data. A comparative study between the EIGEN6C4 and in-situ Bouguer anomaly over the CR is done to validate the satellite data and a good correlation is observed between them. Modern gravity data processing techniques (Total Horizontal Derivative, Analytical Signal, Tilt Derivative, and Euler deconvolution) are used to delineate the lineaments and their source depth estimation. The majority of the identified lineaments trend in the NW-SE and NE-SW directions and their source depth ranges between 4.4 km and 15 km. The NE-SW trending Diyodar and Tharad ridges in the CR are identified for the first time using gravity data. Based on the result of the present study, an updated tectonic map of the study area is prepared (Figure 3.12).

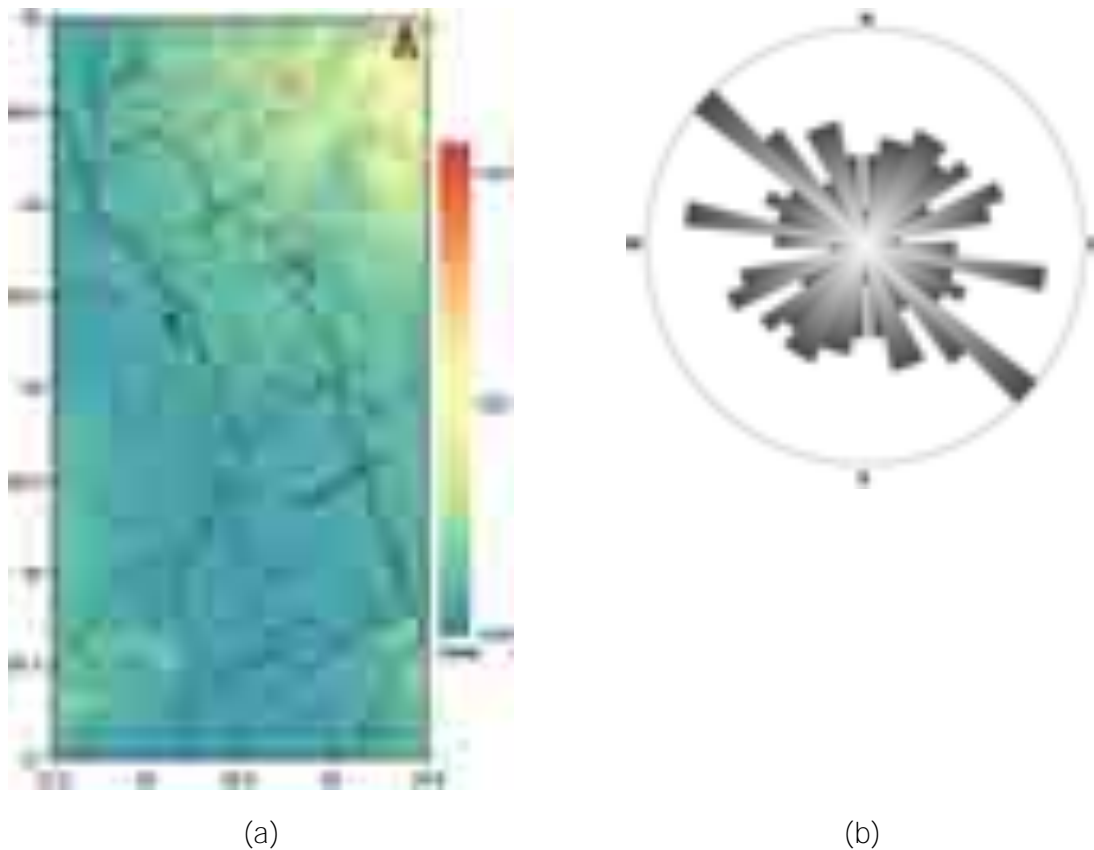


Fig. 3.12: (a) The new structural map of the study area showing combination of lineaments/faults over the Digital elevation model. Solid and dashed black lines represent lineaments/faults marked using THD and Analytical signal, respectively. ECF and WCF are the eastern and western Cambay faults represented by black dotted lines. (b) Synoptic rose diagram representing marked lineament/fault trends over the study area.

3.9 Structural interpretation over the epicentre zone of 1819 Allah-Bund earthquake, North-western India using gravity data (Avinash Kumar Chouhan and Sumer Chopra)

The 1819 Allah-Bund earthquake that occurred in the north-western part of the Kachchh rift, India, was one of the deadliest intraplate earthquakes of the nineteenth century. In this work, we have used EGM 2008 satellite derived gravity data to understand the tectonic framework in the epicentral zone of the 1819 Allah-Bund earthquake and surrounding regions (Fig. 3.13). Total horizontal derivative analysis of the Bouguer anomaly is carried out to map major lineaments in the study area (Fig. 3.14). The logarithmic amplitude spectra of the Bouguer anomalies provide an average depth of 13 km between the interface of the upper crust and

the basement, while the basement-sediment interface is found at 1.6 km. The residual anomaly (Fig. 3.15), which is obtained by applying a high pass filter with a cut-off wavelength of 100 km, shows high value with a NW-SE trend, sympathetic with the trace of the Allah-Bund (AB) on the surface. Moho in the region is found NW dipping as shown in the regional anomaly map (Fig. 3.16). The upper crustal geometry of the region is provided for the first time by performing 2.5D forward gravity modelling, constrained by seismological and well-log data, along two profiles (Fig. 3.17). It is inferred from the present model that the upper crustal thickness increases towards AB. The basement is undulating, which is uplifted by 1-2 km over AB. The present study provided the first geophysical evidence of the ABF and it is inferred that the fault is shallow in nature and dipping in the SW direction.

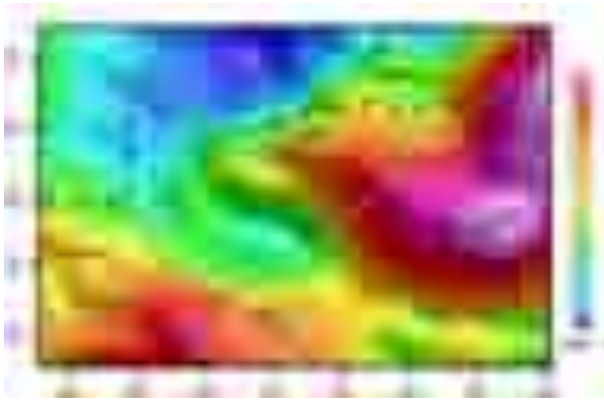


Fig. 3.13: Bouguer anomaly map over epicentre zone of the 1819 Allah-Bund earthquake and surroundings. H1 and H2: gravity highs and L1: gravity low. The white lines AB and CD are the profiles along which gravity modelling is done. The black lines show locations of inferred faults. The open circles represent earthquakes ($M > 3$) that occurred between 2008 and 2017.

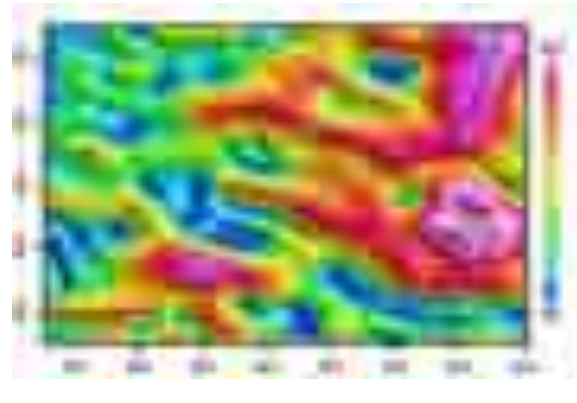


Fig. 3.14: Total Horizontal derivative (THD) calculated from EGM 2008 Bouguer anomaly over the epicentral zone of the 1819 Allah-Bund earthquake and surroundings. The lineaments are identified on the basis of the anomalous THD characteristics. Lineaments show a NW-SE trend.

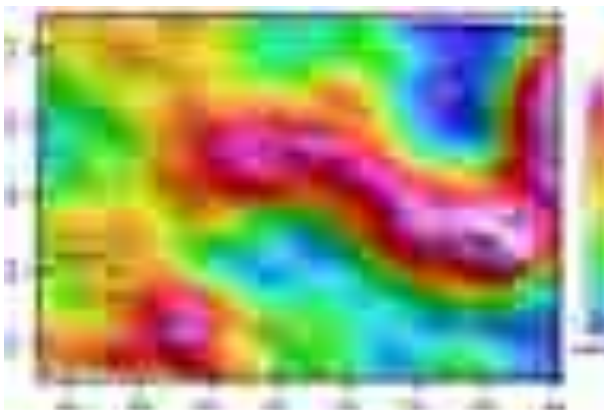


Fig. 3.15: Residual Bouguer anomaly with cut-off wavelengths of 100 km over the epicentre zone of 1819 Allah-Bund earthquake and surroundings, obtained by applying a high pass filter. The white dashed line shows the location of Allah-Bund fault inferred from the present study.

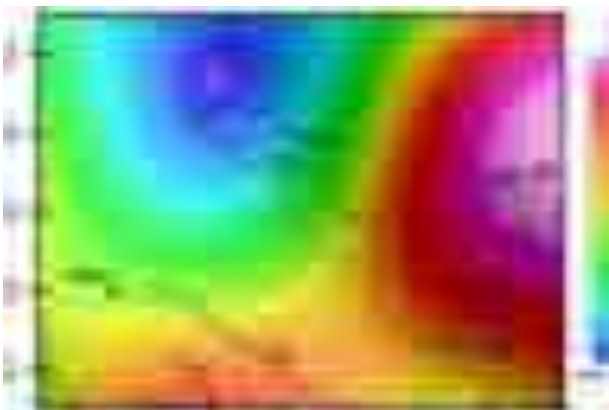


Fig. 3.16: Regional Bouguer anomaly obtained by subtracting the residual from the Bouguer anomaly. The black lines show the locations of faults.

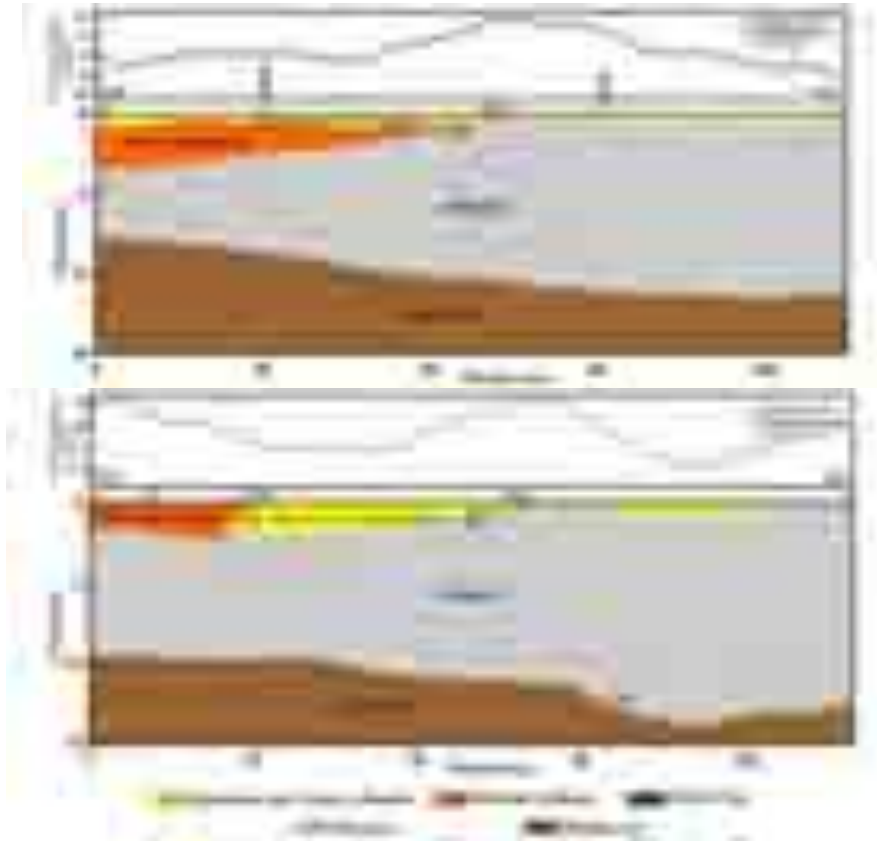


Fig. 3.17: The geological cross section and 2.5D forward modelling of the residual Bouguer anomaly along profiles AB and CD down to 15 km depth over the epicentre zone of the Allah-Bund fault. The constraints are derived from power spectrum analysis, seismological and well data. The black dashed lines F1 and F2 represent the ABF where basement uplift of 1-2 km is noticed and F3 represents the KMF. F4 is the dipping structure in the upper crust. The densities of the layers are given in gm/cm^3 that are shown in the legend.

3.10 Magnetotelluric imaging of the Allah-bund Fault: Seismotectonic implications on the Kachchh intraplate region, Western India

(G. Pavan Kumar, Mehul Nagar, Rakesh Nikam, Indu Choudhary and Sumer Chopra)

Data from 26 TEM sites along three NE-SW profiles with an inter-station spacing of 0.8-1km and 13 MT sites along a NE-SW profile with a site separation of 1.8-2km are acquired in the western part of the Great Rann of Kachchh (Fig. 3.18). The TEM resistivity sections show a minimum of 15-25m thick Rann sediments overlain on Tertiary deposits that slightly thicken towards north. A vertical resistivity contrast along which displacement of the tertiary blocks with a cumulative throw of 25-30 m is observed. 2-D modelling of the MT data reveals the sedimentary thickness to be 1.5-2.5km in the region. Importantly, a low angle ($< 45^\circ$) south dipping high conductive zone ($< 5 \Omega.m$) terminating at shallow to mid-crustal levels ($> 15-18\text{km}$) adjoining a high resistive zone ($> 1000 \Omega.m$) is imaged, representing presence of the ABF. In conjunction with the occurrence of the micro to moderate seismicity in the north of the ABF scarp, we postulate that the 1819 event and the present seismicity could be associated with the south dipping Nagar Parkar Fault (northern margin of the Kachchh basin) and the ABF might be a listric sympathetic splay of the basin margin, indicating the ongoing Holocene deformation in the region.

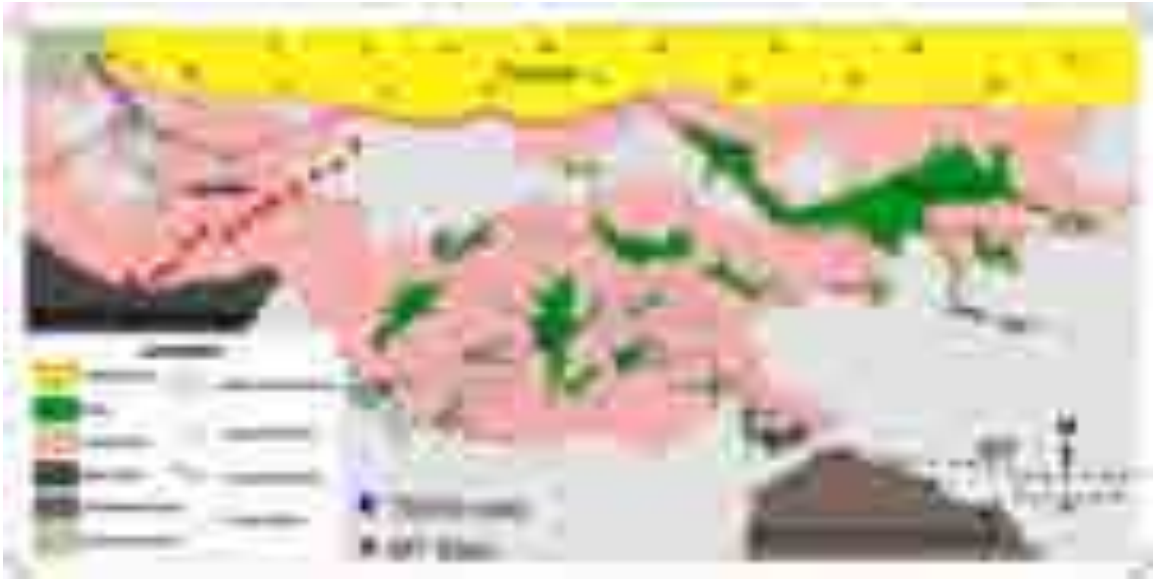


Fig. 3.18: Resistivity section across the profile.

3.11 Magnetotelluric investigations in Eastern part of the Kachchh rift basin (Pavan Kumar, Mehul Nagar, Rakesh Nigam and Himanshu Chaube)

To understand the crustal electrical resistivity structure of the eastern Kachchh region, we acquired MT data from 15 sites across the KHF and KMF. At each site, we acquired the natural time varying secondary electromagnetic signals in a broad frequency range (0.01-4096s) with 4 days recording duration. The interstation spacing is about 3-4km. The acquired MT sites are shown in Fig. 3.19. Data of 15 sites have been processed and earth response functions in wide frequency band are estimated. The processed data are then analysed for amount of distortions present and calculation of the geoelectric strike direction (N71E).



Fig. 3.19: Map showing location of the acquired MT sites (violet squares)

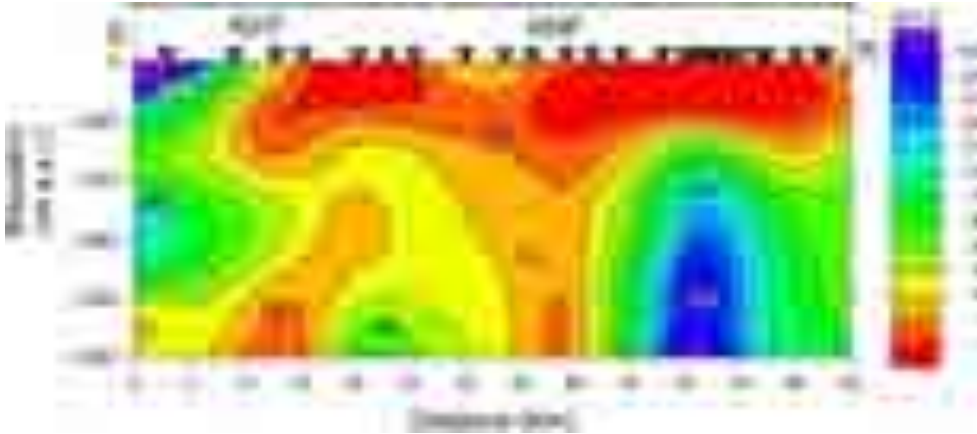


Fig. 3.20: Resistivity section across the profile

One-dimensional inversion is carried-out to estimate the sedimentary thickness and the basement architecture. The 1-D section along the profile is shown in Fig. 3.20. From the section, it can be seen that the northern part of the profile is more conductive compared to the southern part. The high conductive zone (C1) ($< 5 \text{ ohm.m}$) observed in the model could represent the quaternary and tertiary sedimentary deposits (clay and sand) in the region. The moderate conductive zone (C2) underlain by the quaternary and tertiary sediments might indicate the presence of the Mesozoic formations that comprise sandstone and shale. In the northern portion, the sedimentary layer is overlain on a resistive layer ($\sim 500 \text{ ohm}$), representing the basement. The high resistive zone (R2) ($> 1000 \text{ ohm.m}$) at depth of 6-7km might indicate the basaltic intrusion, representing the remanence of Deccan Volcanism about 65My ago, that occurred in the region. In the southern portion of the profile, we observe resistive layers (R3 & R1) at shallow depths, indicating the presence of Deccan traps in the region. Interestingly, the 1-D model yields two conductive zones (C3, C4) down to greater depths ($\sim 10\text{km}$). The surface location C3 coincides with the Kachchh Mainland Fault (KMF). We therefore suggest that the C3 zone represents the subsurface image the KMF. In the southern portion, we observe a good resistive contrast (R3 & C2) that represents the presence of Katrol Hill fault (KHF). The model also shows a high conductive zone at 8km below the KHF zone. We speculate that this conductive zone might be the fluid filled fracture zone. However, detailed 2D/3D modelling will be required to further confirm the presence of this high conductive zone.

3.12 Music of subterranean Seismic Signals recorded in Gujarat Region (*Mayank Dixit*)

Earthquake sounds are one of the most common effects observed during or immediately before a seismic event. The increased popularity of animation movies and you tube videos change the format of how information is distributed. Tapping into an alternative approach of information exchange, the seismic data has been shifted and converted into audible range by time compression known as **"Sonification"** or **"Audiofication"**. This investigation used the waveform data of 2012 Mw5.1 Dholavira Earthquake, 2011 Mw 9.1 Honshu, Japan Earthquake, and 2012 Mw8.6 Sumatra Earthquake recorded by thr Seismic Network of Gujarat (SeisNetG), installed and maintained by the Institute of Seismological Research (ISR). The findings of this investigation not only improve the perceptibility of patterns in the data but also foster an interest for common people in seismology.

The seismogram trace changes from light to dark as a time indicator progression line (Vertical Magneta line) moves from left to right. Transverse component velocity seismogram (Top), 2-8 Hz bandpass filtered seismogram (Middle), and the Spectrogram (Bottom).

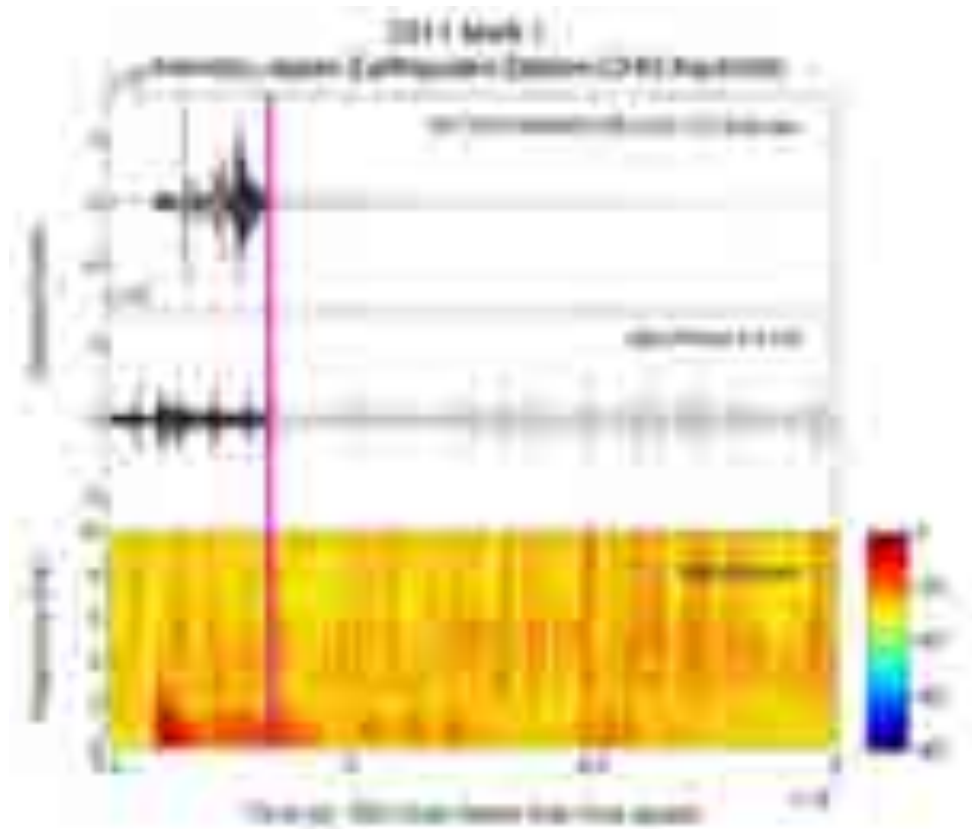


Fig. 3.21: Snapshot from a sample video of the transverse component of data from the 2011 Mw 9.1 Honshu, Japan Earthquake, recorded at station CHO in Kachchh.

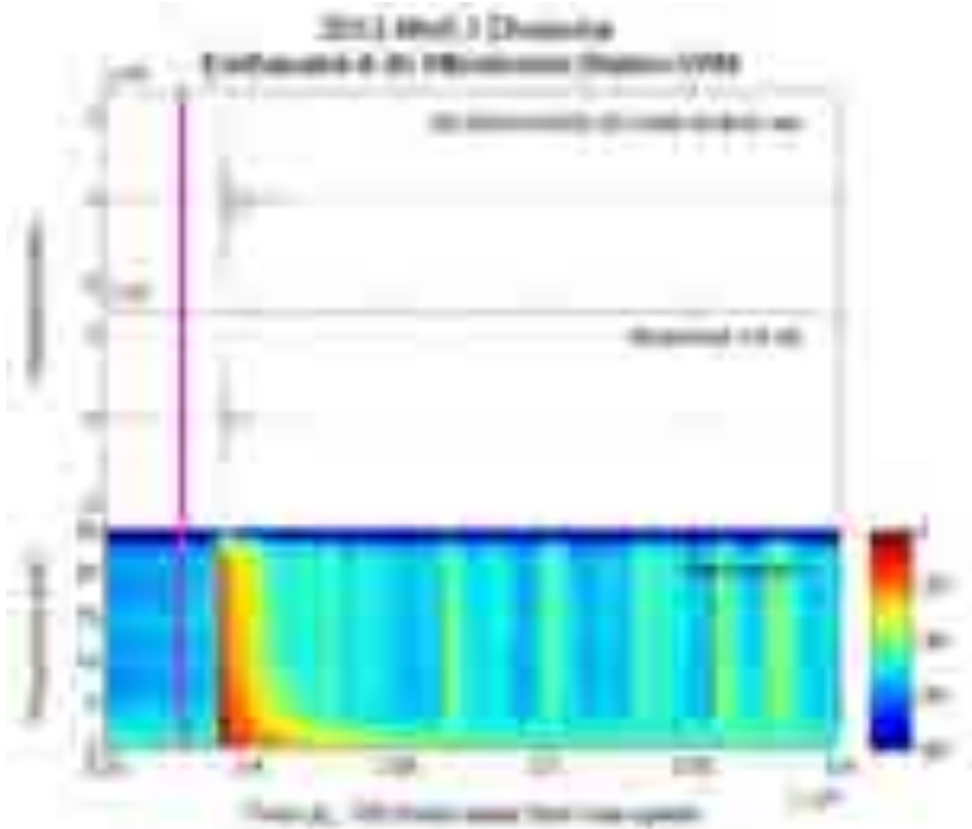


Fig. 3.22: Same as figure 3.21 for 2012 Mw 5.1 Dholavira Earthquake recorded at station VAM in Kachchh.

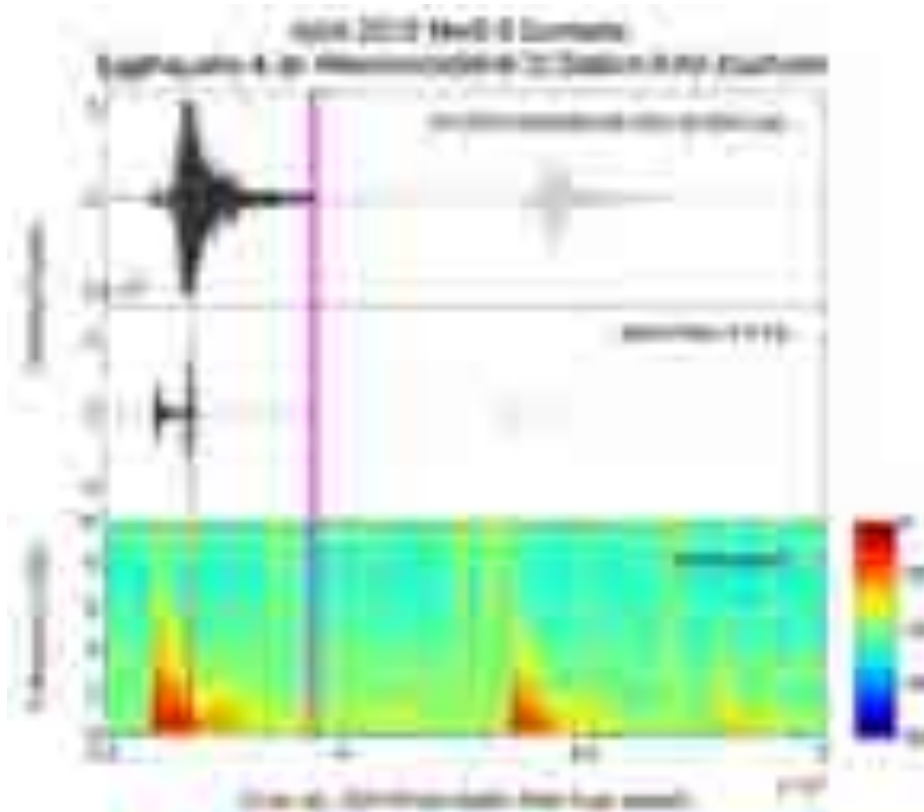


Fig. 3.23: Same as fig. 3.21 for April 2012 Mw8.6 Sumatra Earthquake recorded at station KAV in Kachch.

3.13 Low - frequency microtremor anomalies at Mansa and Jotana areas in western India

(Mayank Dixit, Arjav Shukla, A. P. Singh, Ketan Singha Roy, Sumer Chopra and M. Ravi Kumar)

Low-Frequency Passive Seismic (LFPS) Surveys have been carried out at Jotana (Mehsana) and Mansa (Gandhinagar) regions. The purpose of this survey was to determine the characteristics and alterations of the microtremor signals and to investigate whether these signals can be used as proxies for hydrocarbon detection. Single station LFPS survey has been carried out in both the regions to establish the low frequency passive seismic attributes in hydrocarbon reservoirs areas. Ambient noise data from 136 sites has been acquired under LFPS survey using Lennartz LE3d (5s), Tromino 3g (10s) and Broadband Seismograph (120s). The surveys were carried out during early morning and night time, to avoid the cultural noise.

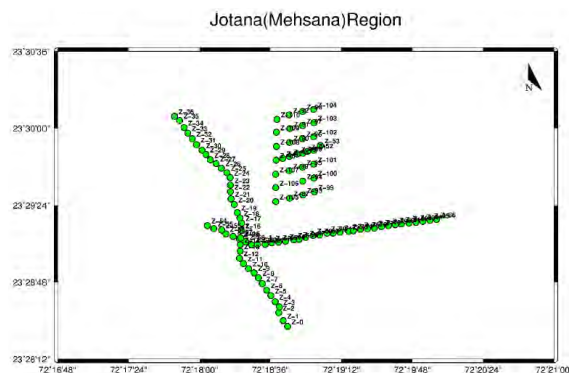


Fig. 3.24: Maps show the sites covered in the LFPS survey

3.14 Seismicity and décollement geometry beneath the Sikkim Himalaya using Local earthquake tomography (A. P. Singh, O. P. Mishra)

We have analysed about 1250 events that are recorded by 18 broad band seismic stations in the Sikkim Himalaya area during 2007–2011. Heterogeneous velocity structures with low and high velocities (V_p and V_s) zones at different depth ranges are imaged. A well resolved low velocity zone is consistently observed down to a depth of ~ 20 km. Results reveal clear evidence for a gentle, north dipping décollement plane at ~ 20 km depth, in terms of significant velocity perturbations across this interface. The geometry and depth of the décollement surface seem to vary laterally, the deepest being ~ 25 km. Most of the past moderate sized earthquakes occurred at the junction of high and low velocities (V_p and V_s). However, the larger earthquakes occurred mostly below the décollement plane where high velocities are observed. Further, the shallower LVZ (0-10 km) is identified with higher V_p/V_s , and the mid crustal HVZ with lower V_p/V_s . We suggest that the shallower LVZ is associated with sediments.

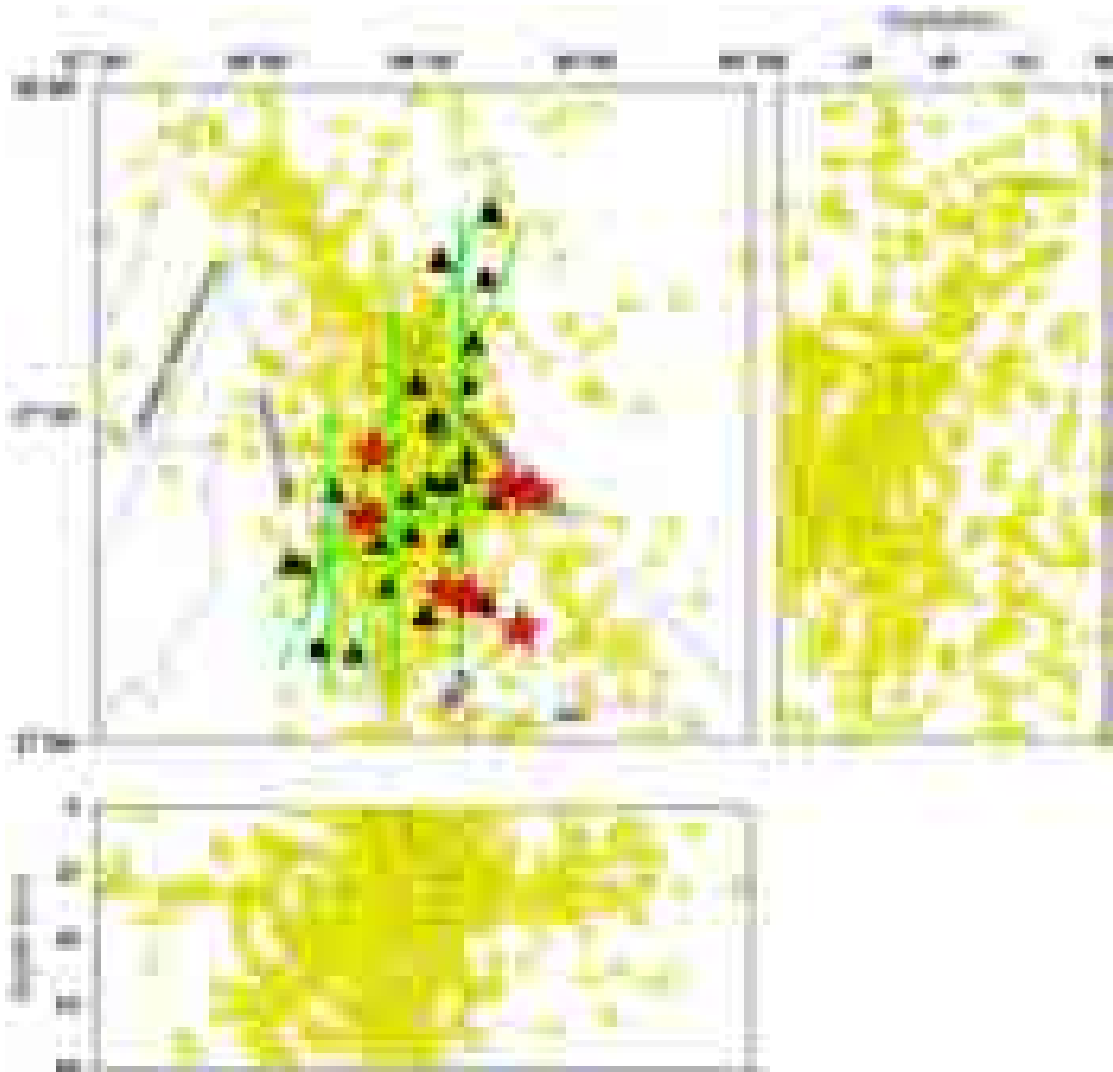


Fig. 3.25: Epicentral distribution of earthquakes and seismic stations used in this study region are shown by open circles and solid triangles, respectively. In cross sectional view with depth, the left side shows the distribution of events along latitude, while the lower one shows the distribution along longitude.

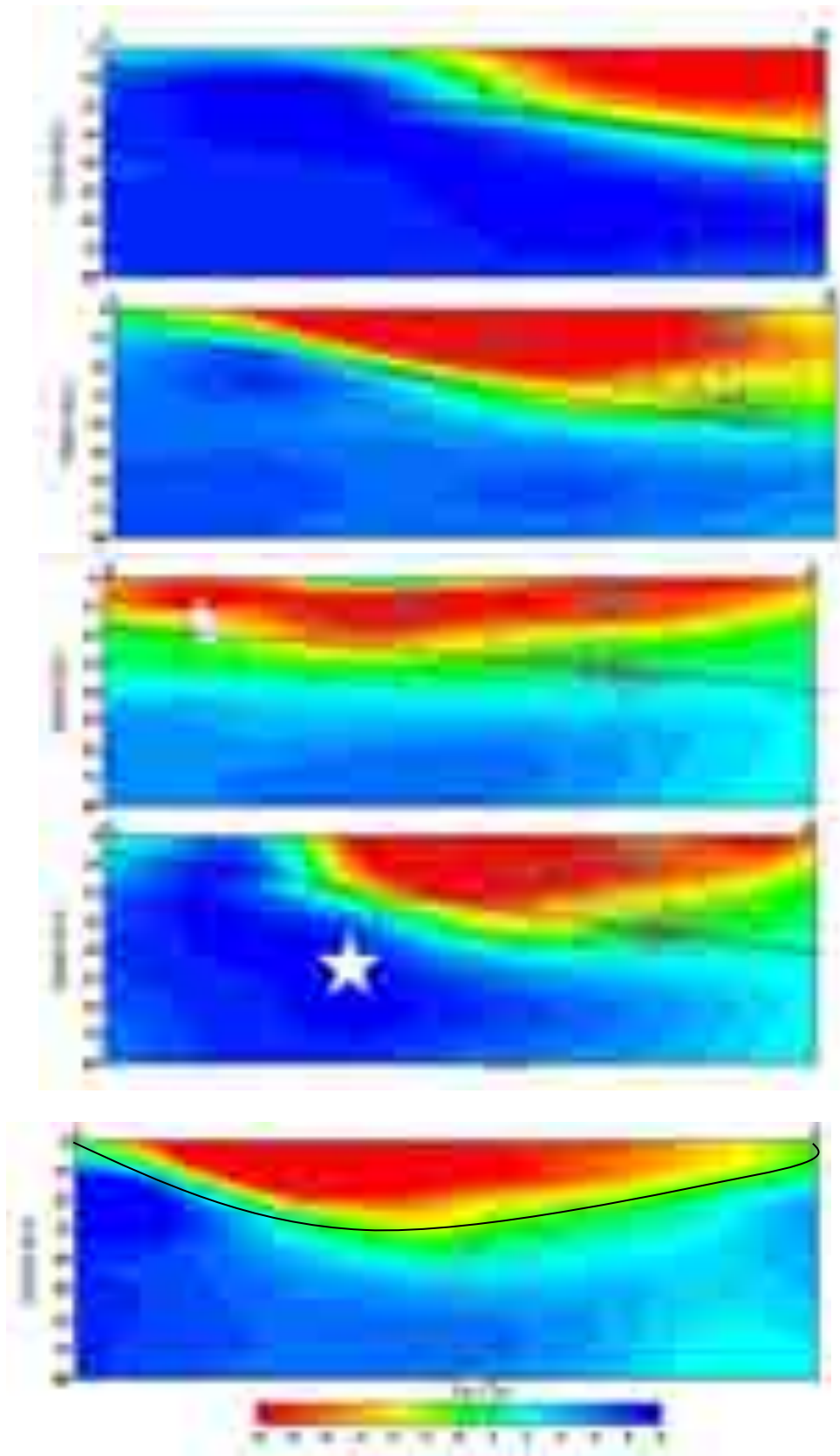


Fig. 3.26: Vertical cross sections of P wave velocity models with topography, along profiles (AB-IJ). White dots show the seismicity. Dotted lines show the locations of possible décollement in each cross section, which are marked based on earlier and the present study. The scale is also shown at the bottom.

3.15 Radial Anisotropy study for the crustal and upper mantle structure beneath the Deccan Volcanic Province (DVP) (Jyoti Sharma)

In the present study, we obtained a high resolution ($1^\circ \times 1^\circ$) crustal and upper mantle velocity structure beneath the DVP through nonlinear inversion of the observed group velocities of Rayleigh and Love waves, obtained along 1286 event-station paths. A total of 2572 dispersion curves are obtained within the period range of 6 to 100s from Rayleigh and Love waves recorded on the vertical and transverse components, respectively. The selected group velocity curves are obtained along different source-station paths and source zones (Himalaya region, Nicobar Islands, Bay of Bengal, Carlsberg Ridge, Hindu Kush region, Katawaz Basin and Northern India), and vary from 1.8 to 4.6 km/s for Rayleigh waves and 2.2 to 4.9 km/s for Love waves.

The observed group velocities along different paths are then used to obtain the regionalized maps, to calculate the local group velocities for a set of periods, using the 2D seismic tomography technique (Yanovskaya and Ditmar, 1990). Thereafter, the inversion is performed to obtain the shear wave structure, V_{sv} and V_{sh} using Rayleigh and Loves waves, respectively. **Radial anisotropy coefficient (ξ) is also calculated for the study region at 1° by 1° resolution for 33 grid cells (Fig. 3.27).**

$$\xi(\%) = \frac{V_{SH} - V_{SV}}{(V_{SH} + V_{SV})/2} * 100$$

Signature of a radially anisotropic lithosphere is observed in terms of variation in V_{sv} and V_{sh} velocities. The sharp decrease in S -wave velocities (V_{sv} and V_{sh}) below the lid is considered as the Lithosphere-Asthenosphere Boundary (LAB). We have also observed negative radial anisotropy at an average depth of ~ 166 km, which may indicate presence of partially molten material beneath the Kutch Seismic Zone, Cambay, Saurashtra and Narmada rift regions. The LVZ could be a result of plume thermal anomaly. Moreover, negative radial anisotropy is encountered at shallow depths (~ 128 km) beneath the west Narmada region (Fig. 3.28) in comparison to other parts of DVP, which may be due to thermal erosion of the lithosphere or could be representative of transition zone of oceanic and continental regions.

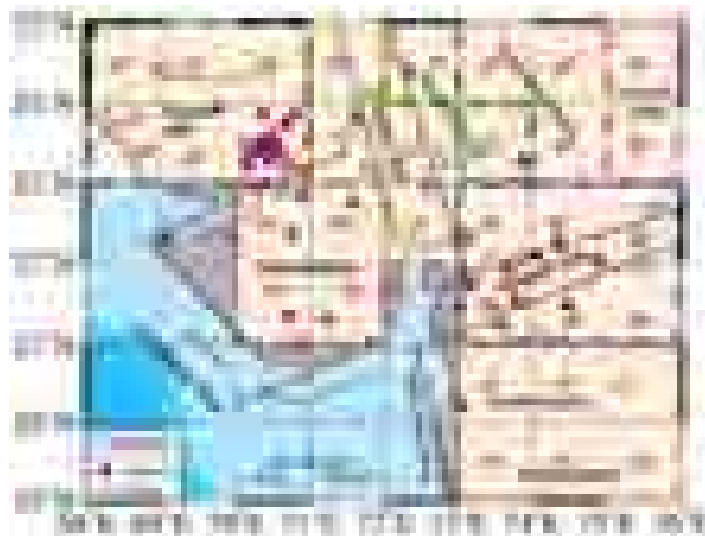


Fig. 3.27: Regionalized map of the DVP region with $1^\circ \times 1^\circ$ grid cells. The main tectonic features (brown lines) are also indicated. The coloured polygons represent different sub-regions of DVP.

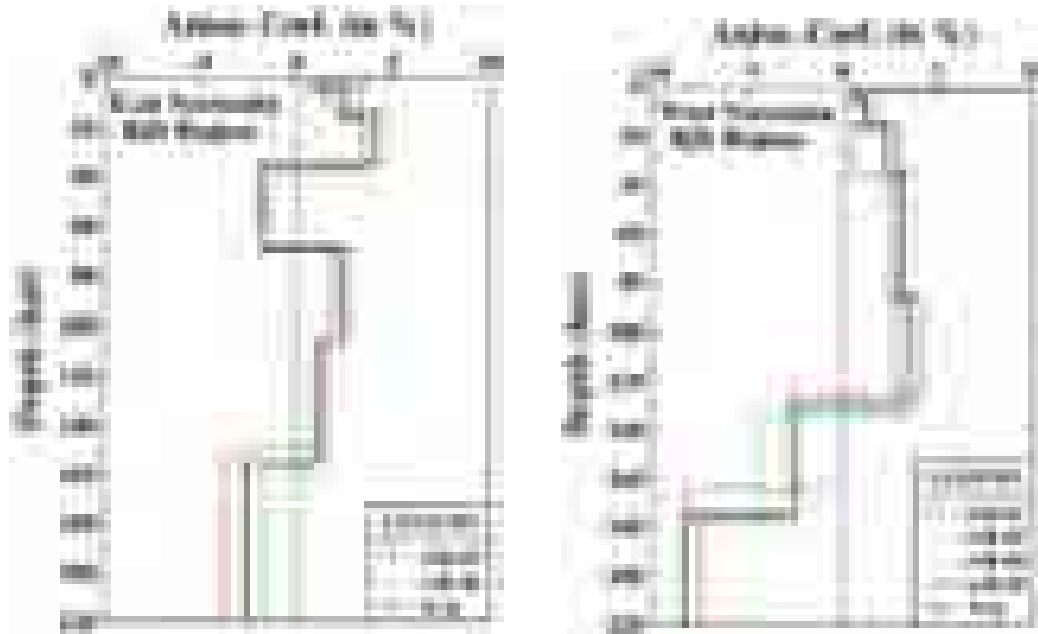


Fig. 3.28: Anisotropy coefficient (ξ) estimated for the east and west Narmada regions of DVP at 1° by 1° grid cells.

3.16 Identification of anomalous velocity features by cluster analysis (Himangshu Paul)

K-means clustering is a statistical method to organize large datasets into groups. K-means divides 'n' elements into 'K' groups such that each element falls into the group whose characteristic is similar to the element itself. In other words, similar characteristic elements are grouped together. When this concept is applied to velocity perturbations, small velocity variations are ignored and geographical extent of similar velocity regions are obtained. This methodology is also called Tectonic Regionalization as the velocity regionalization can be related to the tectonic structures. Density structure of the earth is the most important component influencing the geoid and the density structure is proportional to the velocity structure. Therefore, global tomographic models can be utilized to investigate the causes of geoid anomalies. We investigate geoid lows because their cause, especially that of the large negative amplitude of Indian Ocean Geoid Low (IOGL), is not understood well. Other major geoid lows reside over the Ross Sea, NE Pacific, West Atlantic, Central Asia and Hudson Bay. To perform cluster analysis at all depth ranges, the lithosphere and mantle structure is divided into five depth division or groups.

Cluster analysis results reveal the presence of high velocities near the core-mantle boundary beneath all the major geoid lows, distributed across various depth ranges. The highest distribution range is of 1200 km beneath the Ross Sea Geoid Low and the least is 650 km beneath the Indo-Australian Plate. Besides high velocity structure, low velocity structures were observed in the upper mantle (350-800 km) beneath all the geoid lows except Central Asia Geoid Low. These low velocity structures are dominant at a depth 400 km to 700 km beneath the IOGL and 400 km to 1000 km beneath the remaining geoid lows. The velocity perturbation of these low velocity structures is least for IOGL with a magnitude of -0.7% to -1.0% V_s . For other geoid lows, the magnitude varies from -0.2% to -0.7% V_s . Beneath Central Asia and Hudson Bay Geoid Lows and Indian Shield, high velocity structures were found within the

lithosphere. Additionally, high velocity structures were also found in the mid mantle (depth 800-1600 km) beneath the Indian Shield and Hudson Bay Geoid Low.

3.17 Evidence of seismic anisotropy in the D'' layer using waveform data from Gujarat seismic stations

(Srijayanthi G)

The D'' layer ~200 km above the core-mantle boundary is believed to play an important role in mantle geo-dynamic processes. The present study is an attempt to understand the character of seismic anisotropy of the D'' layer sampled by the teleseismic earthquake waves recorded by the 78 temporary and permanent seismological stations under the aegis of ISR, Gujarat. The core refracted seismic phases (SKS and SKKS) sample almost the same path in the upper mantle and crust for the same source-station configuration. However, the raypaths are significantly different in the lowermost mantle. Therefore, discrepancies in the SKS-SKKS shear wave splitting (seismic anisotropy) emerged as strong evidence for the presence of seismic anisotropy in the D'' layer.

In the present study, we extracted the teleseismic SK(K)S waveforms from 243 events having an epicentral distance of 84° to 145° . The Splitlab analysis software was utilised for the shear wave splitting analysis (Wüstefeld et al., 2008). A total of 5 discrepant SKS-SKKS measurements were observed by analysing the waveform data from 68 stations. An example of such discrepant measurement is shown in the figure 3.29. Further, shear wave splitting analysis from 10 stations has to be added to the present results to improve the understanding of seismic character of the D'' layer anisotropy.

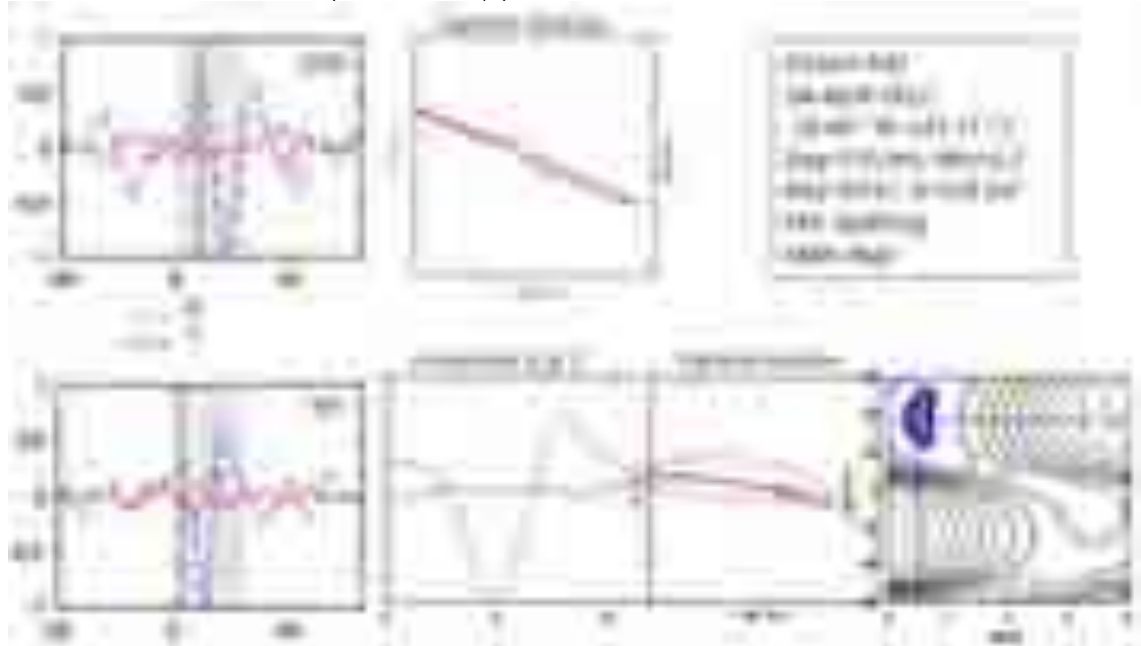


Fig. 3.29: Example of SKS-SKKS seismic anisotropy measurement at station RAJ.

3.18 Widespread crustal magmatism in the Kachchh region— Evidence from shear wave velocity contrast across Moho

(Chinmay Haldar)

To estimate the shear wave velocity contrast across the Moho ($\delta\beta_M$) we have used the waveform data recorded at 27 broadband stations (12 are in Kachchh, 9 are in Saurashtra and 6 are in Mainland region) spread all over the Gujarat region. The estimated $\delta\beta_M$ values

vary spatially from 0.15 to 0.86 km/s (Fig. 3.30) in the study region. For the **Kachchh rift**, $\delta\beta_M$ varies from ~ 0.15 to 0.58 km/s with the average values being lower for most of the stations compared to those in Saurashtra and Mainland Gujarat. For the **Saurashtra region**, $\delta\beta_M$ varies from ~ 0.44 to 0.86 km/s and for Mainland Gujarat, it varies from ~ 0.32 to 0.74 km/s. Lower $\delta\beta_M$ values are predominantly observed in the Kachchh region having large number of faults and sutures with concentrated seismicity. The intrusion of magma which causes the seismic activity at depths of 35-45 km continuously alters the crust, which is reflected as low shear wave velocity contrast. Further, the observed low values in shear wave velocity contrast correspond to the tectonic regions of Kachchh rift that are characterised by basaltic underplating in the lower crust and in the upper mantle.

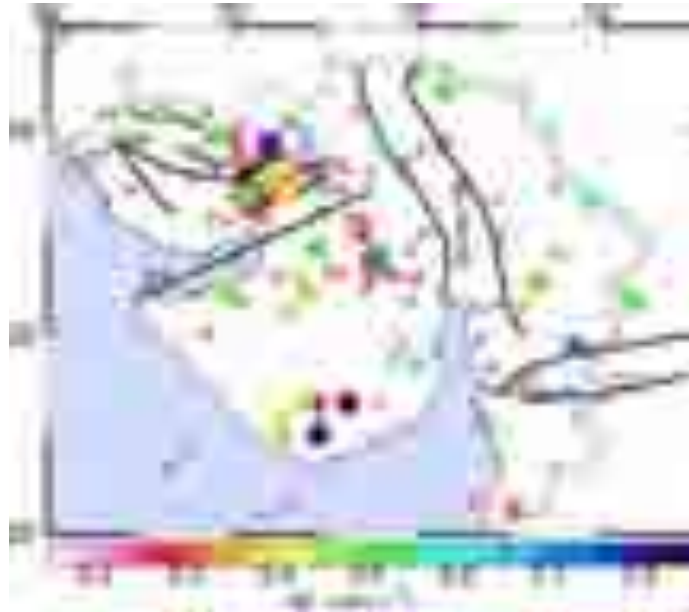


Fig. 3.30: Shear-wave velocity contrast map across Gujarat with three regions i.e., Kachchh, Saurashtra and Mainland Gujarat superimposed on the tectonic map. Thick lines show the faults in the region. Different colour codes for the solid circles show the estimated shear wave velocity contrast ($\delta\beta_M$) across the Moho. Red open circles indicate the seismicity plots of the Gujarat region with earthquake hypocenters within the depth range of ~ 35 -45 km. NKF: North Kathiawar Fault; KMF: Kachchh Mainland Fault; VF: Vigod Fault; BF: Banni Fault; SWF: South Wagad Fault; NWF: North Wagad Fault; IBF: Island Belt Fault; GF: Gedi Fault. It is interesting to **note that the dense seismic region is characterized by lower value of $\delta\beta_M$ ($< \sim 0.5$ km/s).**

4. EARTHQUAKE PRECURSORY RESEARCH

4.1 Atmospheric and Ionospheric perturbations associated with the 6th Feb 2018 Taiwan earthquake

(Prasanna Simha and K.M.Rao)

In this study, we examine the perturbations of atmospheric and ionospheric parameters in association with the Taiwan earthquake, which occurred on 6th Feb 2018 with magnitude 6.4 and depth around 23 km. Two IGS GPS stations, namely, TWTF and CKSV are used in this study. These stations are within the preparatory zone of the earthquake. The Ionospheric and atmospheric parameters such as VTEC, Sea Level Pressure, and SST have been analyzed during the period 1st Jan- 28th to Feb 2018 (59 days). During this earthquake, we observe the raise of diurnal variations 5-8TECU just few days before the event. The distortion of the diurnal variation of TEC in association with the earthquake has been witnessed for the two stations. A drop of 6 TECU is observed. The frequency response of TEC in the Ionosphere within the ULF range has been evaluated by computing the Fractal Dimensions for the frequency of 0.01Hz, which are more effected over the seismo electromagnetic emissions. Sea surface level pressure is very prominent on the event day of the earthquake, which is noticed with a rise of 300 mbar.



Fig. 4.1: Variation of VTEC for the two month period

GPS TEC data has been retrieved from IGS GPS network to investigate the ionospheric anomalies prior to the event. The atmospheric parameters such as OLR, sea surface pressure, sea surface temperature (SST) have been obtained from NCEP/NCAR NOAA, for the above mentioned period. The 24hour TEC variations for the two stations TWTF and CKSV are shown in Fig. 4.1. The diurnal values vary from 5 to 20 TECU during normal days without the influence of either far field or near field inferences. However, the diurnal TEC values have raised to 30-40TECU. To explore the reason behind such abnormal rise in the ionospheric component, we tried to look for solar terrestrial activity based on the Dst, Kp and Sunspot number values. Interestingly, just two days before the earthquake where Kp is 10 and Dst is -4 nT, which is considered to be a quiet condition, diurnal variations have increased above normal. The rise of 5-8TECU has been observed just one day before the earthquake for the two stations. The upper and lower quartile along with VTEC 7 days before and two days after the event are shown as Fig. 4.2.

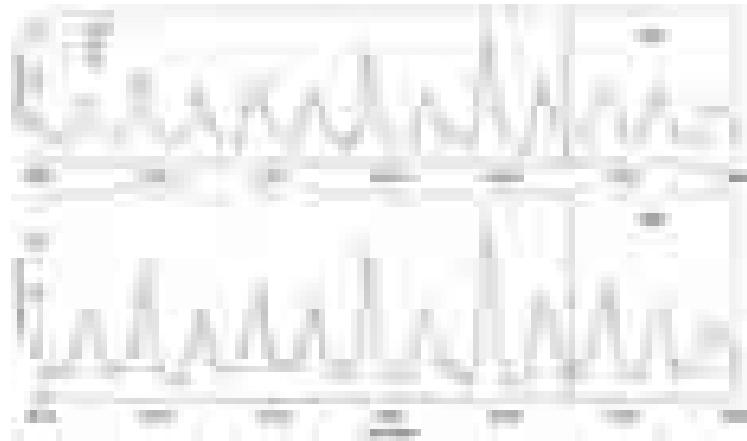


Fig. 4.2: Upper and lower quartile along with VTEC 7 days before and two days after the event.

The observed TEC values are found to be lower than the LQ during the period, which indicate that VTEC values have changed from the upper and lower limits at the two stations. In order to examine the variations of TEC during quiet and disturbed days, we plotted TEC values 5 days during quiet and disturbed periods, in Fig. 4.3.

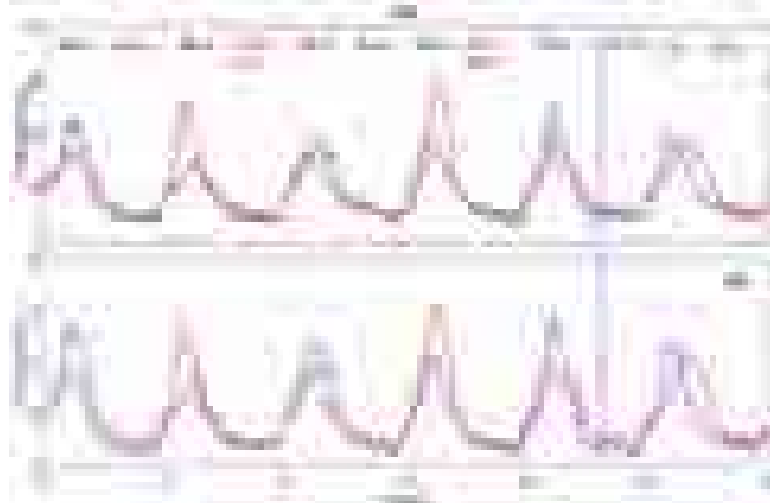


Fig. 4.3: TEC values during quiet time period (blue line) and earthquake disturbed periods (red line)

The delta TEC, third principal values (Pc3) and fractal dimension values are shown in Fig. 4.4. The delta TEC has been computed by taking the difference between the maximum and minimum values for every sixty minutes (Pulinets et al 2009). The delta TEC values show a rise of the signal before the event regime. The third principal values (Pc3) and fractal dimension values are observed to increase two days prior to the earthquake.

Apart from the meteorological cycle, we noticed the rise of sea surface level pressure during winter season (Fig. 4.5). The sea surface pressure shows very prominent variations just during the event regime (Ozounov et al 2004). This enables sudden pressure release with the effect of release of energy along the fault line. This parameter is seen to be one of the most promising tools for the present atmospheric analysis.

The pressure values increased above 2sigma level before and within the event regime. 300mbar pressure variations have been evidenced during the present event. Similarly, the SST variations are clearly seen in the Ocean water. A 0.5°C value is observed within the area

of the event. Such variations have not been observed just a day prior to the earthquake. Diurnal variations of SST from 1st Jan to 28th Feb 2018 within the epicentral zone of the event also show a 0.5°C rise just before and during the event regime.



Fig. 4.4: Delta TEC, Pc3 and Fractal Dimensional values of TEC for the CKSV station

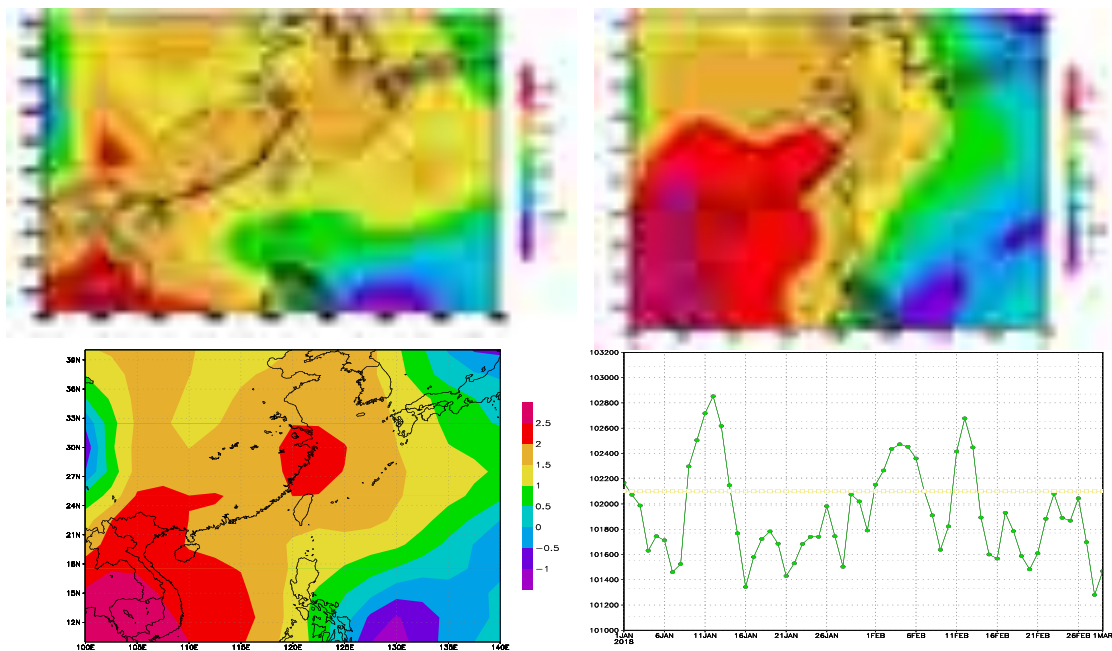


Fig. 4.5: Sea surface pressures from 1st Jan to 28th Feb 2018 near the epicentre of the earthquake

4.2 Observation of abnormal thermal and infrasound signals prior to the Taiwan earthquake (M6.4) on Feb 6, 2018

(Prasanna Simha, N. Venkatanathan and K.M.Rao)

From the analysis of surface latent heat flux (SLHF) in the Hualien, Taiwan region during the period November 6, 2017- February 6, 2018, an anomalous flux in latent heat was observed in two phases. The first phase was observed on December 8, 2017 with a value of 400.835 W/m², more than ten **year’s average of the latent heat flux value** (Fig. 4.6a). The anomalous **index of 3.3356 was recorded, which is above the 3σ level** (Fig. 4.6b). Similarly, the second phase was observed for two days (Feb 3 and 4, 2018) with a flux value of 333.895 W/m² & 362.780 W/m². On February 3, 2018 the anomalous index value of 3.3558 was observed

above 3σ level and for the next day (February 4, 2018) the anomalous index of 3.135 was observed above the 3σ level.

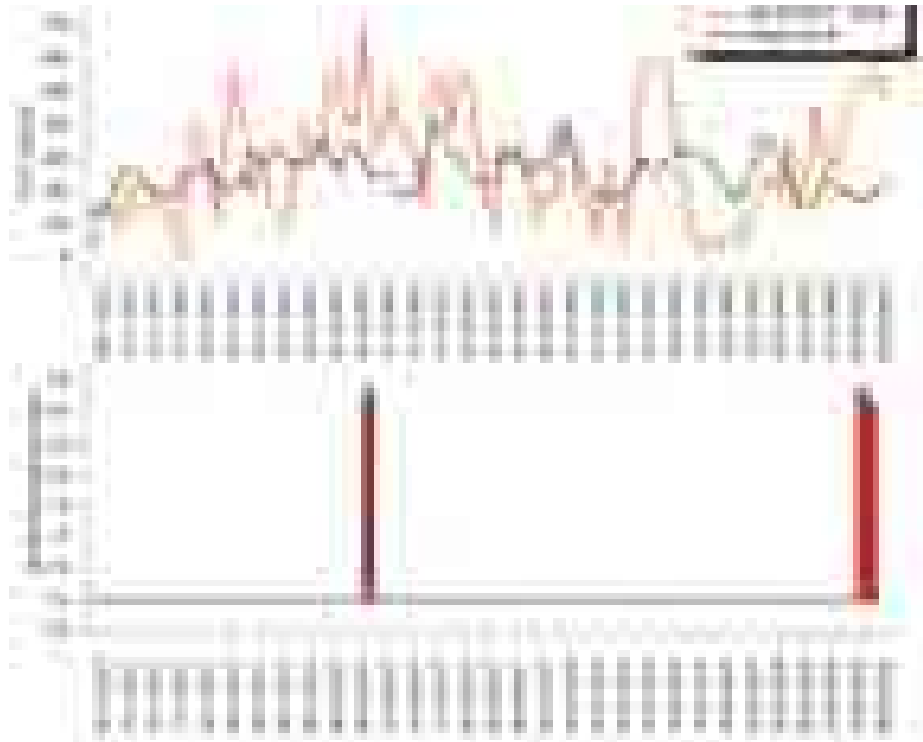


Fig. 4.6: Graph showing (a) current SLHF variations and mean SLHF calculated for the past 10 years. (b) anomalous spikes in SLHF observed twice prior to the earthquake on Dec 8, 2017 (first phase) and February 3 & 4, 2018 (2nd phase).



Fig. 4.7: OLR Flux index scenario observed on November 16, 2017. The black concentric circle represents the epicentre of the February 6, 2018 earthquake and red patch indicates the anomalous OLR flux.

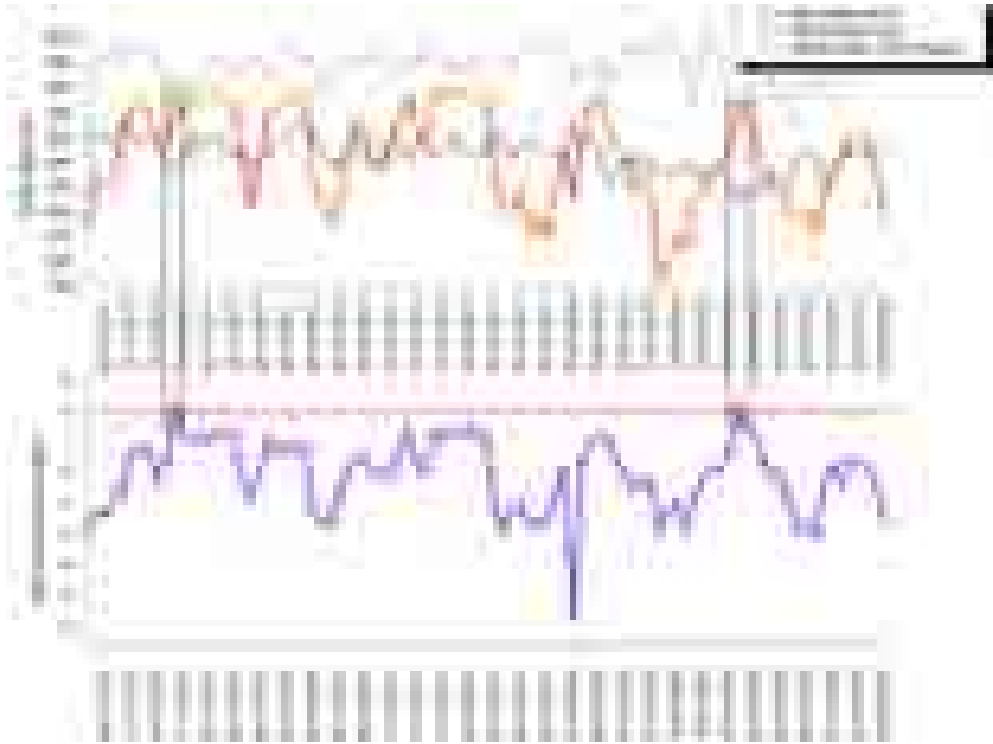


Fig. 4.8: Graph representing (a) OLR flux scenario prior to the February 6, 2018 Hualien, Taiwan region earthquake b) anomalous energy index ($\Delta\epsilon_t$) prior to the earthquake and anomaly observed on November 16, 2017 and January 20, 2018.



Fig. 4.9: OLR Flux index scenario observed on January 20, 2018. The black concentric circle represents the epicentre of the February 6, 2018 earthquake and red patch indicates the anomalous OLR flux.

By analyzing the OLR flux value for the Hualien, Taiwan region, prior to the occurrence of the earthquake on Feb 6, 2018, it was found that the OLR flux was anomalous for two days. The first anomaly was recorded on November 16, 2017 (Fig. 4.7), with the OLR flux value of

309.915 W/m²(Fig 4.8a), which is 5.679 W/m² more than the 2 σ level and the anomalous energy index ($\Delta\epsilon_T$) value is 2.174 (Fig. 4.8b). The second anomaly was observed on January 20, 2018, with a OLR flux value of 299.336 W/m², which is 4.887 W/m² more than the 2 σ level (Fig. 4.9) and the anomalous energy index ($\Delta\epsilon_T$) observed this time is 2.114. The anomaly that appeared second time was lesser compared to the first anomaly observed on November 16, 2017 (Fig. 4.8 a and b).

4.3 Preliminary results of Magnetic survey at Desalpar (Archana R.K, Shivam Joshi, Prasanna Simha and K.M.Rao)

Ground magnetic survey at Desalpar and Badargadh has been conducted in order to evaluate the magnetic homogeneity of the subsurface. An area of 100x100 m has been covered with 5x5m gridding using overhauser GSM 19. The contour plot of total field (around 286 points) within existing observatory region and proposed site is shown in Fig 4.10. The diurnal variation on the days of survey is nearly 40 nT (45610-45650 nT, obtained from DFM measurements). The observed total field variations greater than 50 nT can be considered as anomalous values. A base station was established at 23.7426°N and 70.6861°E using another overhauser GSM-19. The average total field (F) value obtained from the base station is around 46860nT, which is higher than the expected by a value of 700nT (possibly due to the presence of dolerite dykes). Hence, the recorded base station values are not used in the data processing. A contour plot of total field (F) inside the compound of Desalpar MPGO is shown in Fig 4.10. The proposed site for the relocation of Desalpar magnetic observatory is situated few meters away from the backside of the MPGO compound. The observed total field along the two sites varies between 44500-46400nT, indicating the magnetic heterogeneity of subsurface materials. For further clarifications, horizontal and vertical gradient of total field are derived and plotted. Figs 4.12 and 4.13 show the horizontal and vertical gradients of the total magnetic field.

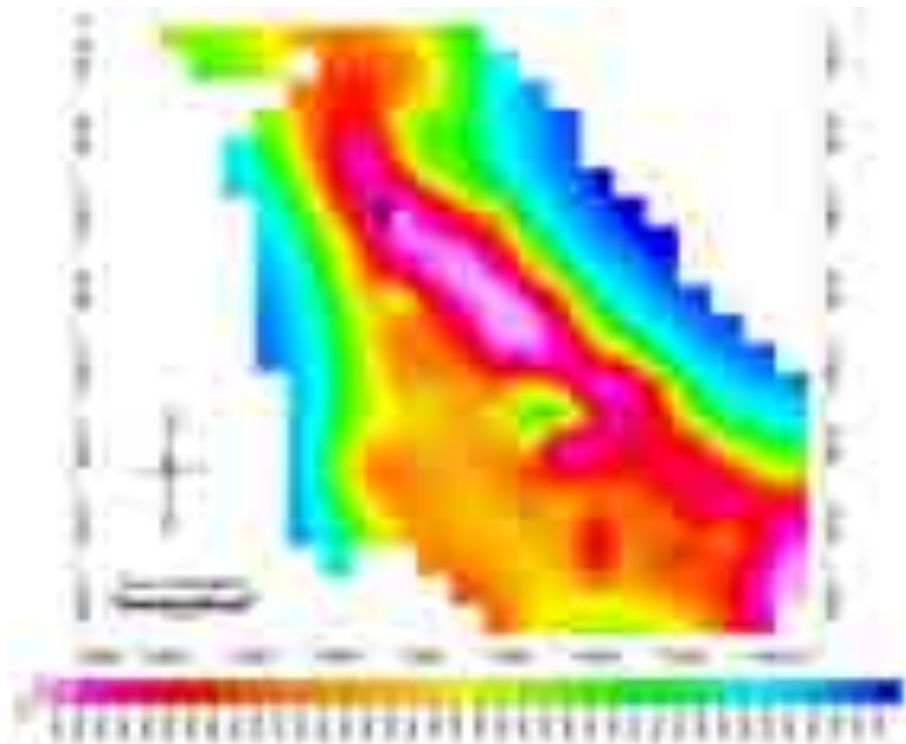


Fig. 4.10: Total magnetic field at Desalpar observatory area. The black star shows the position of the base station.

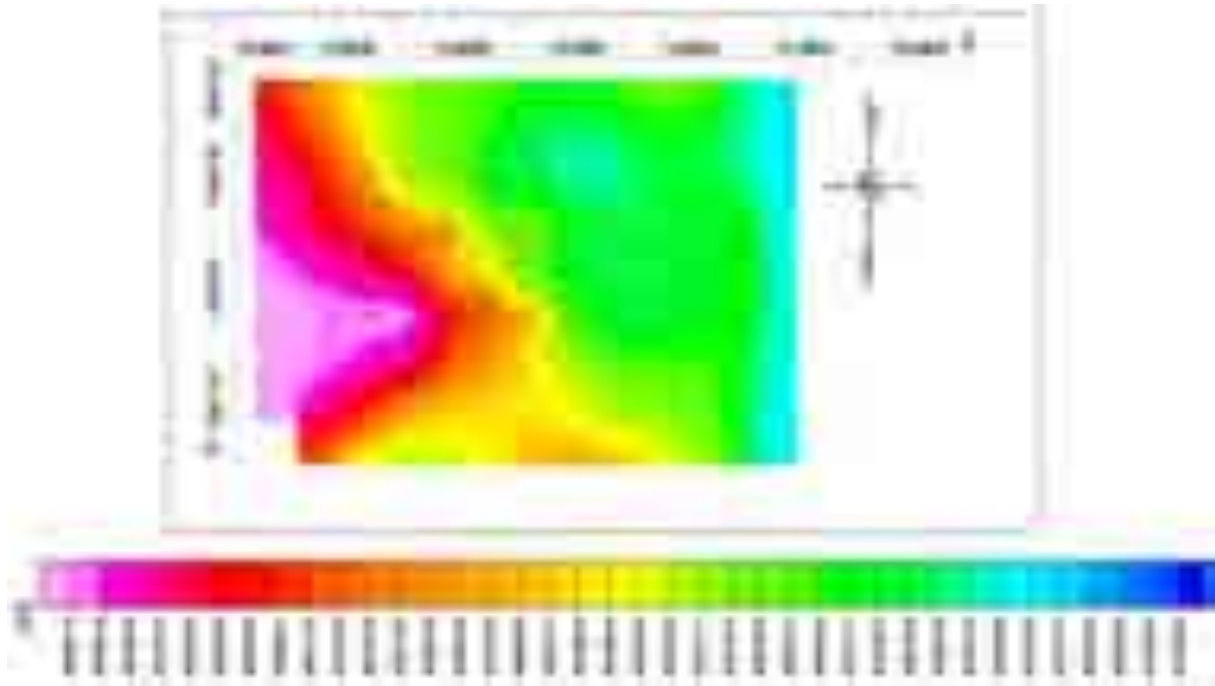


Fig. 4.11: Total field map obtained for the proposed site at Desalpar

The artificial magnetic pollution is relatively less in the new proposed site compared to the existing site, but still, the observed horizontal magnetic gradient shows higher values $\sim 100\text{nT/m}$. The horizontal gradient values indicate that the campus is highly magnetically polluted, probably due to presence of towers, buildings and magnetic rocks. The gradient of total magnetic field intensity along the vertical direction is estimated and shown in Fig 4.13. A gradient of $100\text{-}150\text{nT/m}$ is observed within the existing MPGO site and the proposed site. A nominal vertical gradient is observed outside the campus along the N-E direction, being around $15\text{-}20\text{nT/m}$.

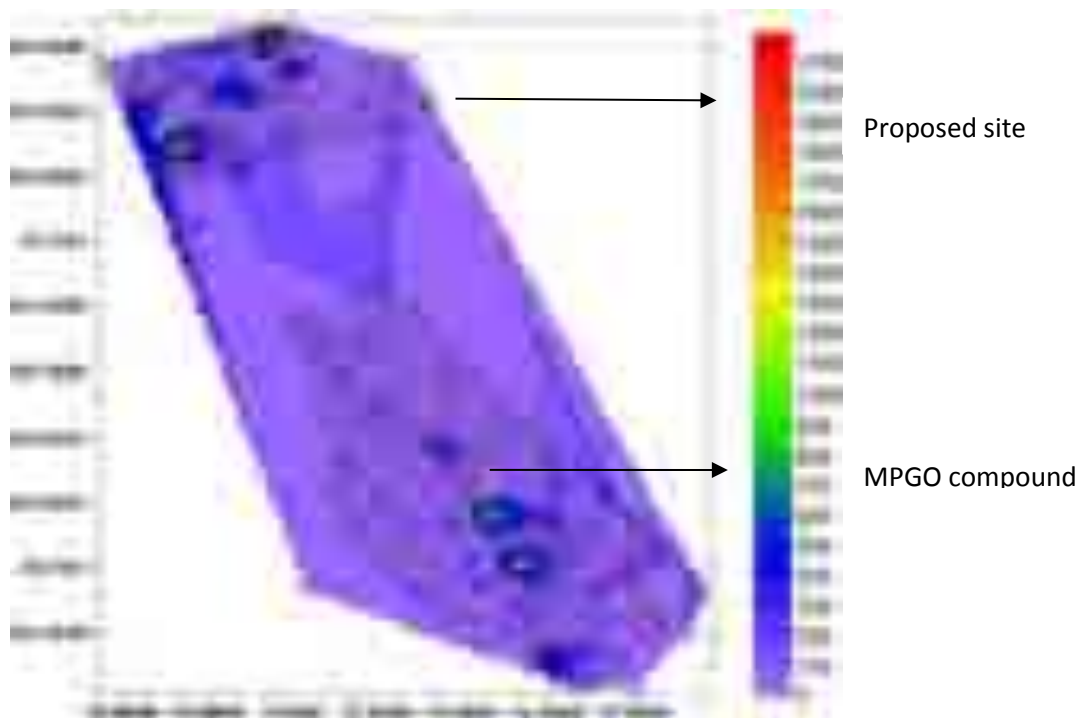


Fig. 4.12: Horizontal gradient map of the total magnetic field inside and outside the Desalpar MPGO

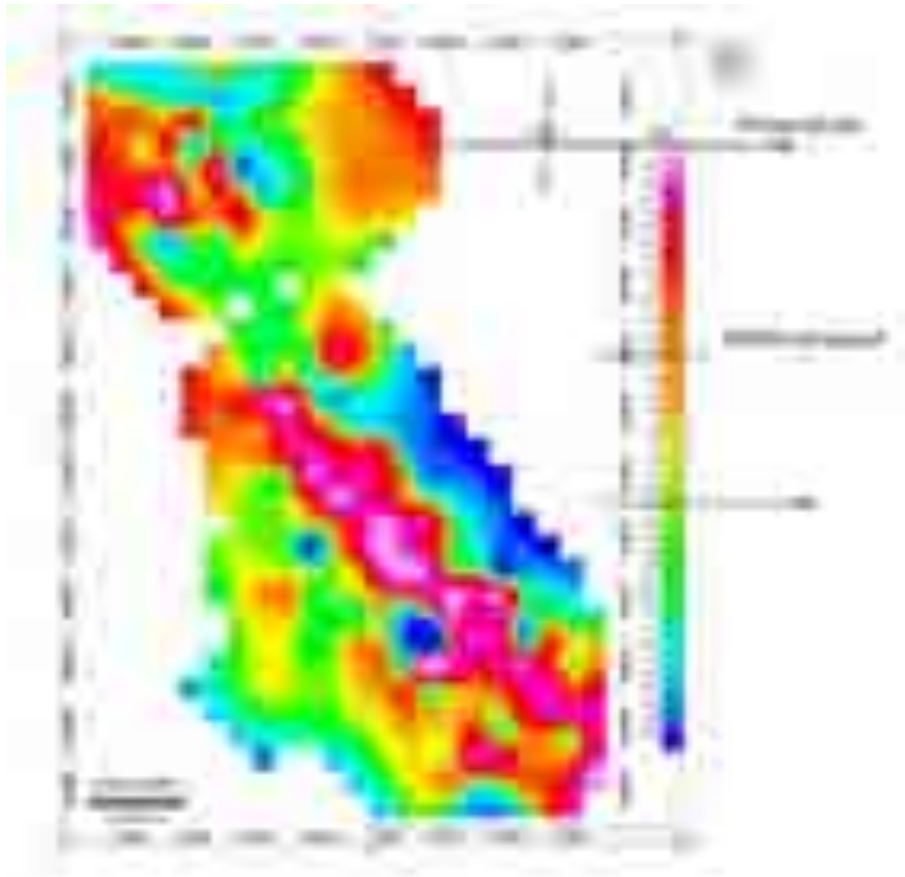


Fig. 4.13: Vertical gradient of the Total Magnetic Field intensity inside and outside the Desalpar campus

4.4 Diurnal variation of the Geomagnetic field (H component) near low latitude sites

(Archana Radhakrishnan and K. M. Rao)

Geomagnetic data (horizontal component) from Desalpar (DSP) and Alibag (ABG, INTERMAGNET site) have been analyzed for the period of 3 months (February- April 2009). The quality of the data has been checked by the first difference method and spikes are removed from the data before processing. One second sampled horizontal (H) component raw data from the site DSP is shown in the Fig. 4.14. The data shows a clear diurnal trend of 30-40nT, when the spikes are removed. The data has been converted to hourly by averaging 3600 data points in their respective local time. To obtain the diurnal pattern, midnight mean values of each day are calculated and removed from the corresponding day.

The diurnal variation is caused by the solar quiet current (Sq) flowing in the E layer of the ionosphere. At the low latitude and equatorial regions, the H component shows larger variation than the other components. The H component at the lower latitudes rises with solar insolation and reaches its peak when the sun is exactly above the site (i.e. at local noon time) and decreases back to the base value by evening. It is assumed that during local midnight hours, the ionosphere is inactive, the measurements at this time correspond to the absolute field strength at the site. The midnight hours (00.00, 01.00 23.00 and/or 24.00 hours) values are averaged for each day and subtracted from corresponding day to visualize the diurnal variations. The hourly means of diurnal variation of the H component at DSP and ABG are shown in Fig. 4.15. The trend of diurnal variations at both the sites are similar. However, at

station ABG, the amplitude is slightly higher. The higher amplitude at ABG is attributed to its proximity to the equator by 5°, compared to DSP.



Fig. 4.14: Geomagnetic H component data at DSP for the month of March 2009.



Fig. 4.15: Diurnal variations of H component at DSP (red line) and ABG (blue line) for the month of March 2009.

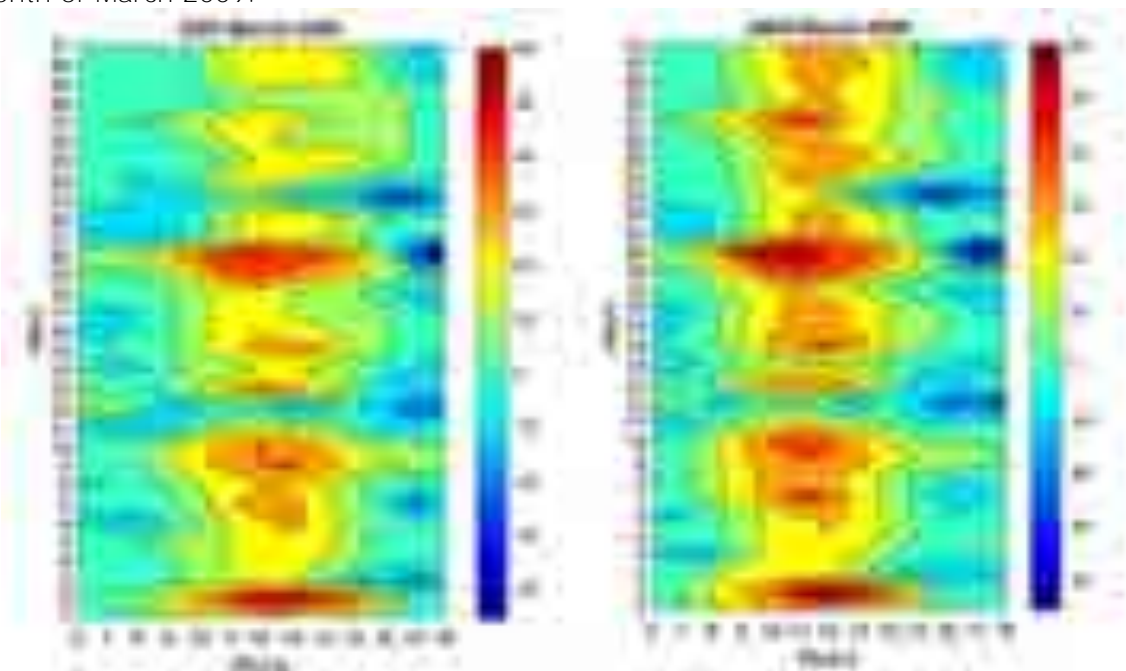


Fig. 4.16: Observed Sq-H variations during day light hours at sites DSP and ABG.



Fig. 4.17: The difference between Sq-H daily peaks at ABG and DSP sites for the month of March 2009

The daily patterns of Sq-H component at DSP and ABG for the month of March 2009 have been plotted for day light hours (6.00-18.00) in local time, in Fig. 4.16. The variation in the Sq-H at DSP and ABG is similar for majority of the days in March 2009. The amplitude variations till mid of March reach the peak at the noon time at both the sites. However, during the last 10 days between 21st and 31st March the noon time peak remains high ~30-50nT at ABG but DSP shows weak peaks around 15-25nT. The difference in the noon time peak between the sites is not consistent.

The observed average difference between the ABG and the DSP daily peaks for the month of March 2009 is 6nT. During certain days, it has been observed that ABG shows higher peak than the DSP (after 20th March, Fig. 4.4). The observed irregular variations may be due to the influence of atmospheric winds, which is more effective in equatorial regions. To observe the seasonal trends between the sites, more data from these sites need to be processed.

4.5 Estimation of influence of Prompt penetration effects on Equatorial Electrojet (EEJ) in the Indian sector

(Archana Radhakrishnan, Jayashree, Kusumita Arora and K.M.Rao)

Studies on Prompt penetration effects on Equatorial Electrojet (EEJ) during magnetically quiet period are limited. In the present study, we focus on the Prompt penetration effects (PPEF) on EEJ from three sites separated at 5°, 15° and 20° longitude, in the Indian sector. It would be interesting to identify the fluctuations in the EEJ strength at different longitudinal separations caused by interplanetary electric field. Therefore, it is essential to isolate the disturbances in EEJ resulted by ionospheric and interplanetary origin. The principal objectives of the present study are (i) identification of Prompt penetration effects on EEJ (ii) observe the longitudinal difference in the PPEF on EEJ at close separations (iii) isolation of fluctuation in EEJ due to interplanetary effects and ionospheric disturbances. We used concurrent ground based magnetic observations from three pairs of sites to derive the EEJ strength, (1) Minicoy (MNC)-Alibag(ABG) at 72°E, (2) Vencode (VEN)-Hyderabad (HYB) at 77°E and (3) Campbell bay (CBY)- Nabagram (NBG) at 93°E. Five minute sampled EEJ strength at MNC, VEN and CBY are compared with the solar wind electric field from OMNI site. The dawn dusk component of interplanetary electric field (E_y) is calculated by $E_y = V_x * B_z$, where V_x is the solar wind velocity component in the sunward direction and B_z is the vertical component of the interplanetary magnetic field in Geocentric- Solar-Magnetospheric (GSM) coordinates. The OMNI data sets are time shifted to bow-shock nose region. The five minute sampled EEJ strength at each station is correlated with the E_y component for each hour with overlapping

of 90% of the data points. The obtained correlation coefficient is validated by statistical P and T tests. The events with correlation coefficient greater than 0.7 are considered as Prompt penetration.

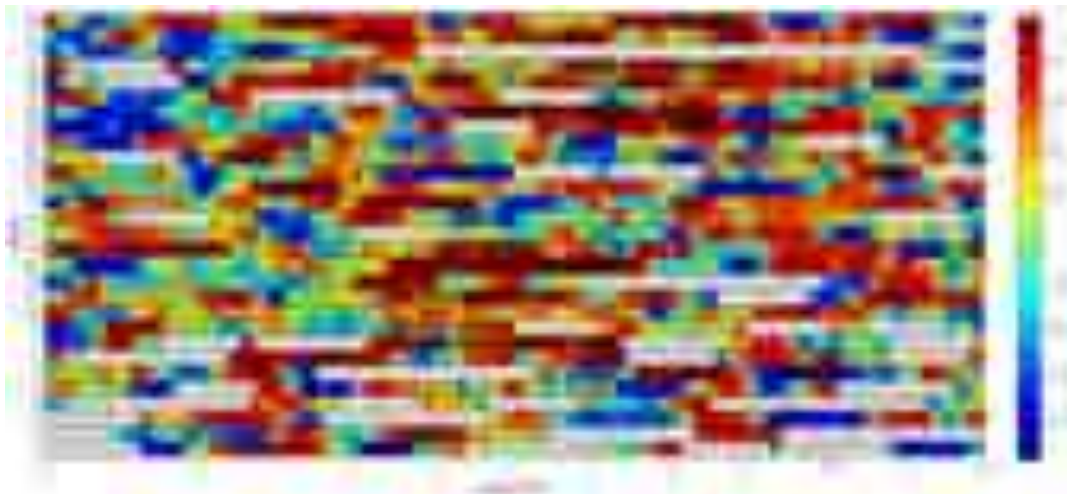


Fig. 4.18: Correlation coefficient between EEJ and E_y at MNC for the month of June 2015.

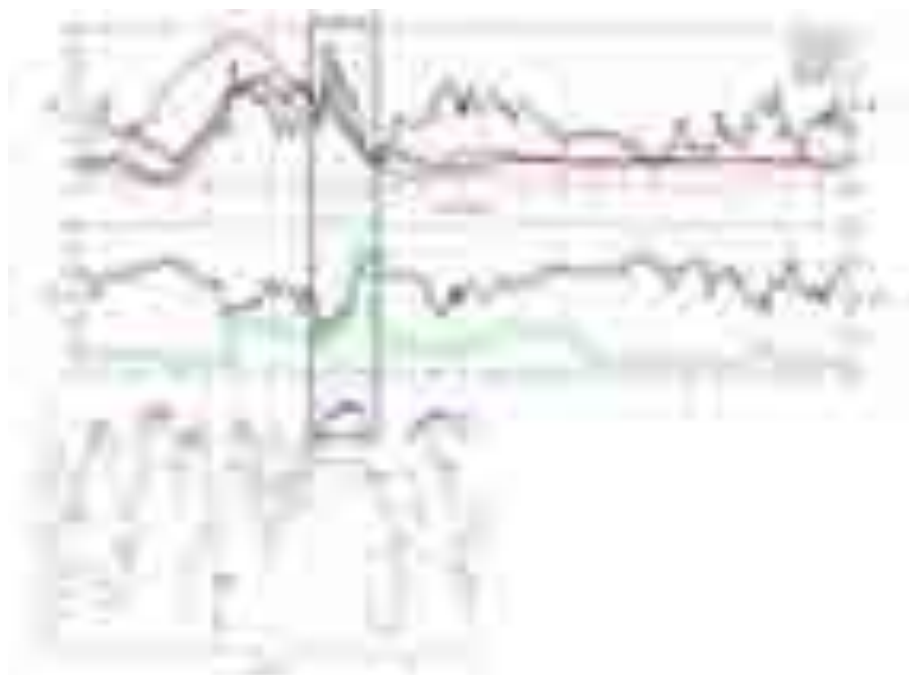


Fig. 4.19: EEJ, E_y , AE and Bz components on 29 June 2015. The corresponding high correlation coefficients are presented in the bottom panel. The penetration event is highlighted by a rectangular box.

Correlation coefficient between EEJ and E_y at MNC for the month of June 2015 is presented in Fig.4.18. The high correlation, which resulted in a variation of ± 4 nT in EEJ is considered as the PPEF events, marked by black arrows. The arrows directing right indicate under shielding (-ve PPEF) and left indicate over shielding (+ve PPEF). The blank spaces are the points where E_y data was missing and the correlation coefficients could not be calculated. The Prompt penetration effect is high on June 29 ($K_p=1.125$). The EEJ, E_y , AE and Bz components on 29 June 2015, corresponding to high correlation coefficients, are presented in Fig 4.19. It clearly indicates a sudden change in E_y that resulted in decrease as well as increase in EEJ, up to 14 nT, 11 nT, 7 nT at MNC, VEN and CBY. A strong correlation of 0.8 is observed at all the three

sites during the period and the average K_p value is less than 2, which indicates that it is a magnetically quiet day.

A total of 99 PPEF events were identified, which resulted in ± 4 nT changes or more in EEJ at three sites MNC, VEN and CBY. All the observed events are concurrent at three sites, with a slight difference in the amplitudes. Out of the total 99 PPEF events, 14 events show higher amplitudes at MNC than CBY, 19 events show higher amplitudes at CBY than MNC (>5 nT) and the remaining 66 events have similar amplitudes. Further, 57 events occurred when $K_p < 3$ and 42 events occurred when $K_p \geq 3$, which resulted in amplitude variation within ± 10 nT and greater than ± 10 nT respectively. The events observed during $K_p < 3$ indicate that the ionosphere is vulnerable to interplanetary electric field at any time. The variation in E_y greater than ± 1 mV/m can result in PPEF which can change the EEJ strength by ± 5 nT. The amplitude variation in PPEF on EEJ with longitude indicates that PPEF is influenced by local ionization.

4.6 Preliminary results of Magnetic survey at Badargadh (Shivam Joshi, Archana R.K, Prasanna Simha and K.M.Rao)

Ground magnetic survey has been conducted at Badargadh in order to evaluate the magnetic homogeneity of the subsurface. An area of 75x85 m has been covered with 5x5 m gridding, using two Overhausers, GSM 19, one for base station with sampling interval of 30s and other in survey mode. The base station was established at 70.57°E, 23.47°N after conducting a preliminary survey by taking measurements along 10 points, which gave a gradient less than 4nT. The base station recorded continuous F values with a sampling period of 30 seconds. The location of the survey area and the base station are shown in Fig. 4.20. The contour plot of total field (around 208 points) within the proposed site before and after necessary correction is shown in Fig. 4.21.



Fig. 4.20: Locations of the proposed sites, base station and existing MPOG lab are marked.

The diurnal correction for the TMF values acquired through survey mode is done by subtracting the base station TMF values at the time of acquiring the gridded values. The anomaly map shown in Fig. 4.21 indicates that the base values are 30-60nT more than the gridded values. The horizontal gradient map shows that the values are minimum (0-5 nT/m) at most points except little high values (~ 20 nT/m) at the center of the grid, which indicates that the subsurface material is magnetically homogenous beneath the survey area. The vertical derivative of the TMF along the z direction is shown in Fig. 4.22. The gradient is very small in the 5th, 9th and 12th lines. The vertical gradient values are in the range of -2 to 2.2 nT/m. Thus, the gradient of the site is minimal or very small. Further, the vertical gradient is

consistently low in the 5th line zone. Such a feature is not noticed in the other zones of the grid. Point to point gradient of the observed total magnetic field is not more than 2 nT.

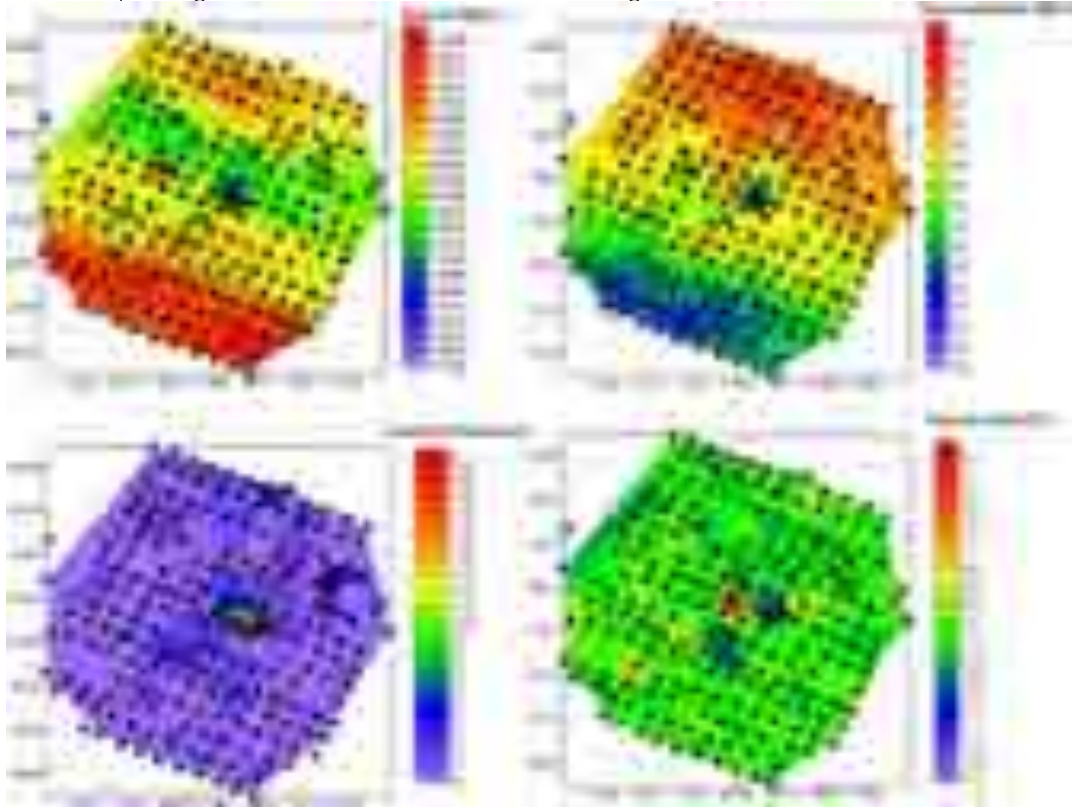


Fig. 4.21: Magnetic anomaly maps a) observed TMF at each point of the grid b) observed TMF and base TMF at the time c) horizontal gradient d) first difference between each point of the grid.

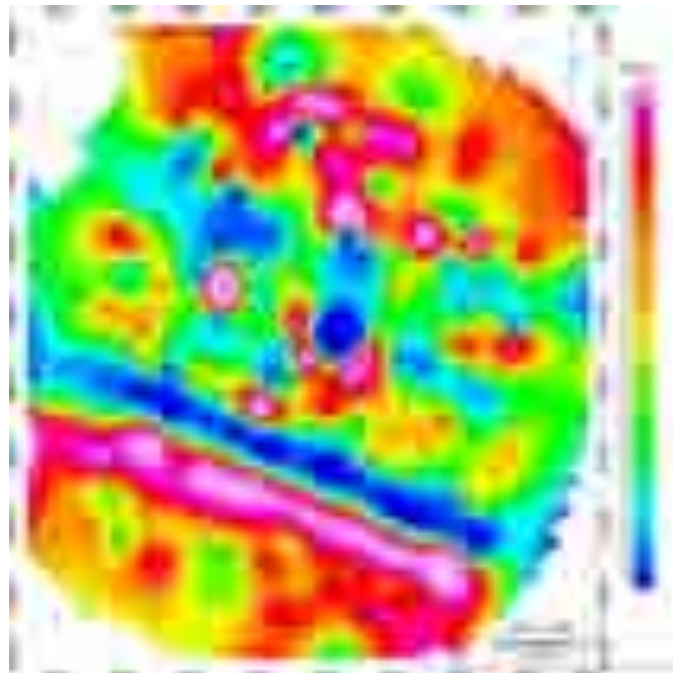


Fig. 4.22: Vertical Gradient of TMF at the observed grid.

4.7 Anomalous Total Electron Content (TEC) before the Taiwan earthquake
(Prassanna Simha and K. M. Rao)

On 6 February 2018 at 15:50:43 (GMT), an earthquake of magnitude Mw 6.4, depth 17.0 km occurred in the north-east coastal zone of Taiwan (to the north-north east of the Hualian city, Taiwan). The earthquake is characterized by oblique strike slip mechanism and the location is in proximity to the plate boundary between the Philippine Sea and the Eurasian plate. Globally, few studies reported changes in different ionospheric/atmospheric parameters before and after large magnitude earthquakes. Therefore, in the present study we are attempting to understand whether large earthquakes are associated with any ionospheric changes as a precursory signature. In order to identify the precursory signatures, data from two GPS stations TWTF and CKSV are analysed in the present study. The TEC values have been derived from the standard algorithms adopted from Kolbuchar et al., 1986 and Schaertal et al., 1998. Dst, Dst anomaly, TEC values from the TWTF and CKSV stations during 1 January 2016-25 March 2018 are shown in Fig 4.23.

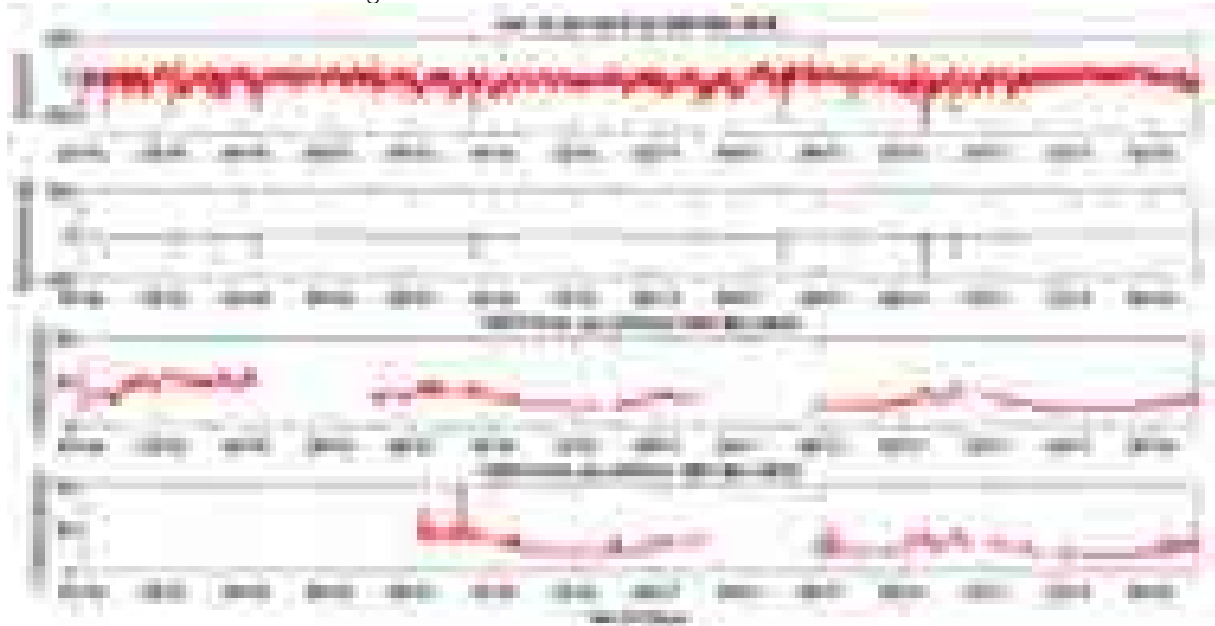


Fig. 4.23: Dst, Dst anomaly, TEC values at TWTF and CKSV stations during 1 January 2016-25 March 2018.

The diurnal variations of the TEC at station TWTF for different months during January 2016 to February 2018 are shown in Fig. 4.24. In this study, we concentrated in two time periods, winter and equinox. Equinox variations have been 25% more than the winter seasonal variations for the two stations. Taiwan lies at the EIA zone and the Tropic of Cancer passes through the center of the Taiwan zone. The possible fountain effect at this region may be influenced because of the interaction of equatorial electrojet with the N-S geomagnetic field at the equator, which gives rise to the upliftment of plasma to higher altitudes during most of the day time. **Dst, Δ Dst, Kp and Δ Kp Values for 33 days with reference to this earthquake are shown in Fig. 4.25.**

The Dst index shows some fluctuations prior to this earthquake during magnetic storms. The Dst time-series showed that the geomagnetic activity was relatively violent on the 23rd day, 14th day, 12th day and 11th day before the earthquake, and the corresponding Dst indices are -20 nT, -15 nT, -15 nT and -10 nT. These fluctuations indicate that geomagnetic storms might have happened on these days. After **the sliding detection, the Δ Dst values show negative anomalies mainly on 23rd day, 14th day, 12th day and 11th days before the earthquake. A similar trend is also observed in Kp and Δ Kp. The possible ionospheric earthquake signatures have been identified with upper and lower bounds using sliding interquartile method (Liu et al**

2009). As per the solar rotation of 27 days, we tried to examine the ionospheric anomaly with a 33 day window (i.e., 28 days before and 4 days after the event) (Fig 4.26). Both the stations TWTF and CKSV have shown positive anomalies before the Taiwan earthquake (Fig. 4.27). The correlation between Kp index and TEC at stations TWTF and CKSV is calculated. However, no obvious correlation between these indices was observed before the earthquake, which means TEC was not affected by the geomagnetic activity.



Fig. 4.24: Diurnal variations at TWTF for different months from January 2016 to February 2018.

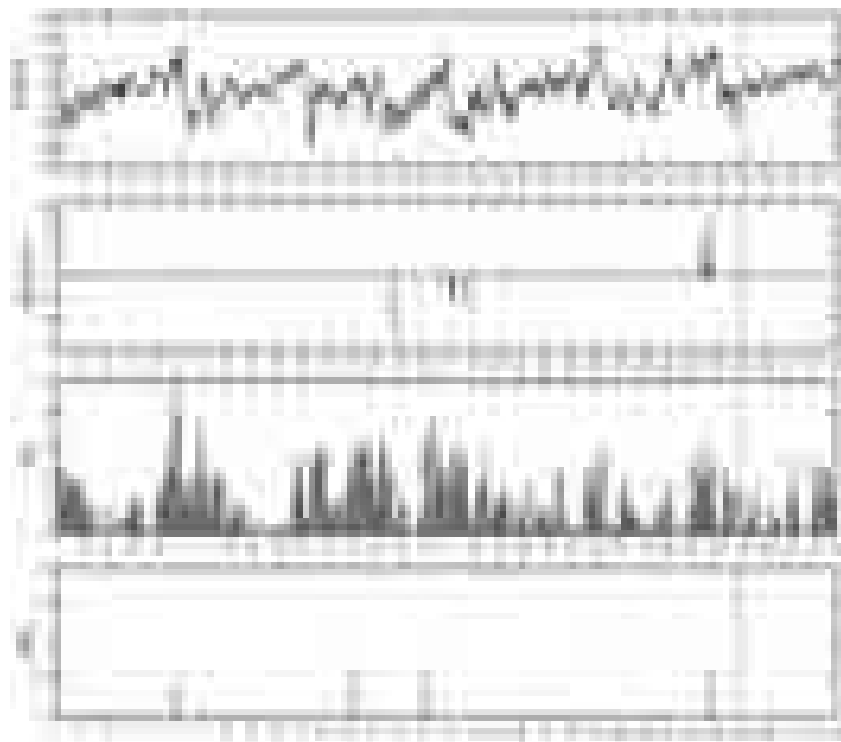


Fig. 4.25: Dst, Δ Dst, Kp and Δ Kp values for 33 days. The dashed red line indicates the time of the earthquake.

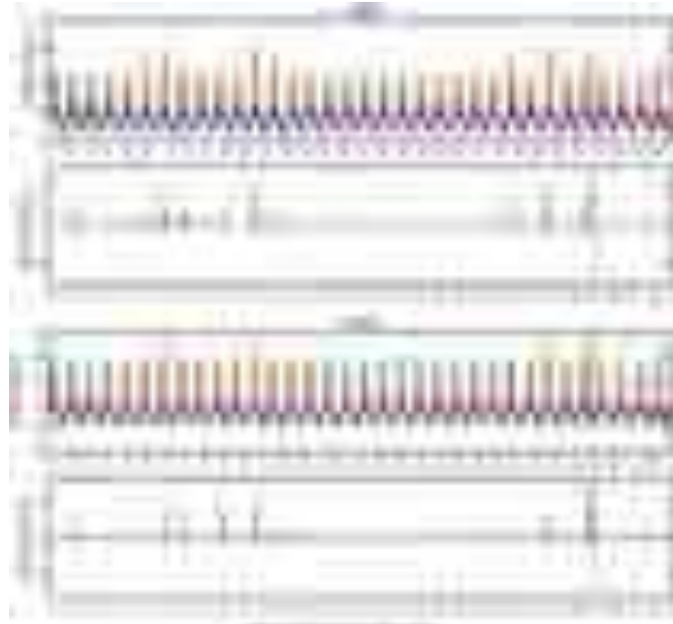


Fig. 4.26: VTEC time series and the anomalies of Δ VTEC time-series (28 days before and 4 days after the event) at TWTF and CKSV stations.

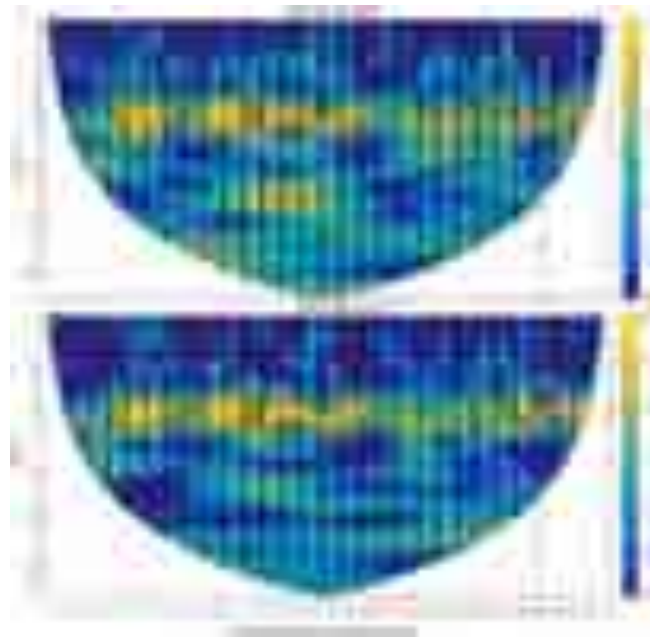


Fig. 4.27: Cross wavelet analysis for correlations between Kp index and TEC at stations TWTF and CKSV.

4.8 Geomagnetic data characterization and analysis of seasonal trend of solar quiet time current at low latitude sites of Indian sector during different phase of solar cycle-24

(Archana Radhakrishnan and K. M. Rao)

To obtain seasonal trends of solar quiet time current (Sq) at Desalpar (DSP) Kutch region, the geomagnetic three component (X, Y and Z) data recorded by a Digital Fluxgate Magnetometer at one second sample interval, have been analysed for 2009 and 2012. The spikes in the DSP data are identified by first difference method and are removed from all the components. The

calculated total field (F) at DSP has been compared with a nearby INTERMAGNET site (ABG-Alibag) in order to verify the trend of diurnal pattern at the site. The verified data have been used to obtain the diurnal variation of H component and its seasonal pattern. The observations are compared with ABG, HYB and JAI sites (Fig. 4.28) which provide latitudinal variations of Sq current with seasons. It has been observed that Sq current shows clear variations in its amplitude with season, higher in E and lowest in D. The observed seasonal trend is enhanced during the peak phase of solar cycle-24 (2012) compared to the initial phase (2009).

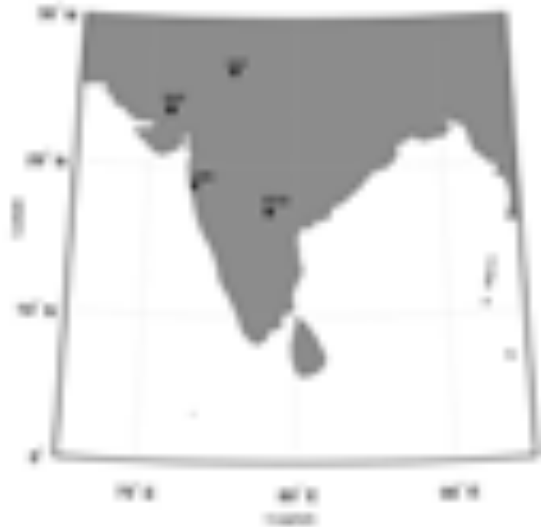


Fig. 4.28: Locations of the magnetic stations used in the study.



Fig. 4.29: Flow chart for the data characterization at DSP.

Table 4.1: The geographic coordinates of the magnetic observatories

Site	Geographic Latitude	Geographic Longitude	Geomagnetic Latitude	Geomagnetic Longitude	Inclination
JAI	26.92°	75.80°	18.28°	150.27°	41.949°
DSP	23.74°	70.68°	15.60°	145.13°	36.550°
ABG	18.62°	72.87°	10.45°	146.89°	26.478°
HYB	17.40°	78.6°	8.75°	152.29°	23.617°

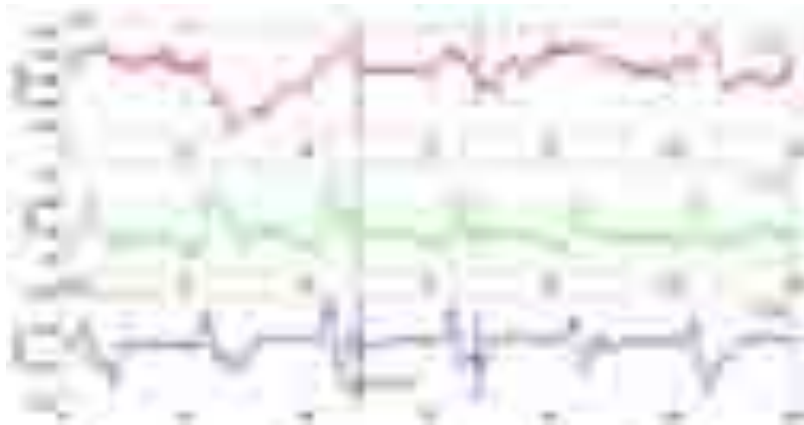


Fig. 4.30: The raw X, Y and Z component data from Desalpar (DSP) from 2nd to 7th January 2009.

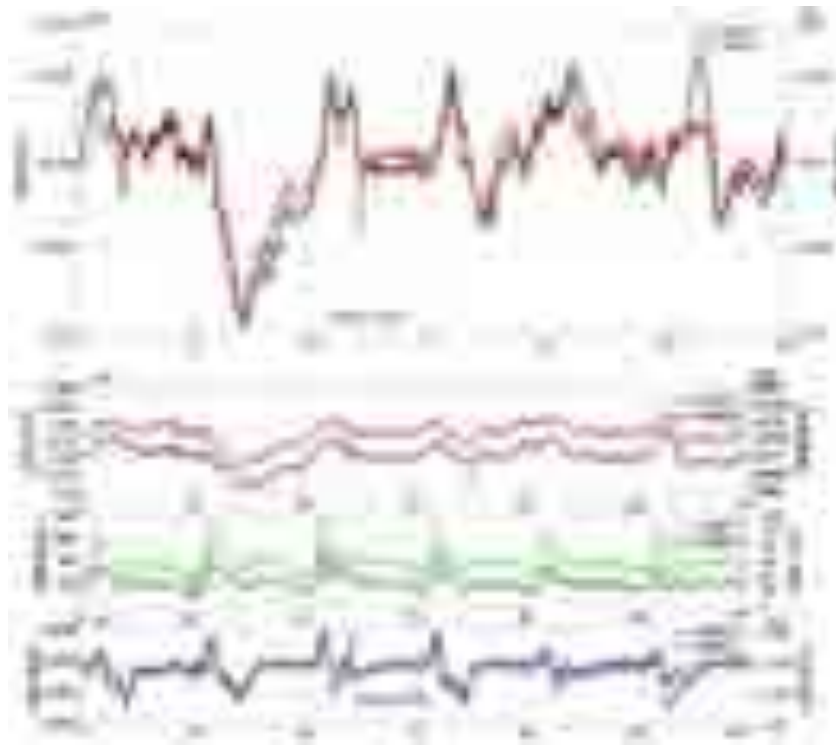


Fig. 4.31: Calculated F component at DSP and ABG from 2nd to 7th January 2009 (top panel), one minute sampled X, Y and Z components at DSP and ABG for the same period.

The primary objectives of the present study are geomagnetic data characterization and rectification of ISR magnetic observatories and comparison of seasonal pattern of Sq current during ascending and peak phase of solar cycle in the Indian sector. The Desalpar (DSP) magnetic observatory of ISR is situated in the Kutch region, western India and all the other magnetic observatories are run by IIG, Mumbai and NGRI, Hyderabad (Fig. 4.28). The geographic location and geomagnetic coordinates are given in Table 4.1. The data from other magnetic observatories are available online and can be downloaded from the INTERMAGNET website (<http://www.intermagnet.org/data-donnee/download-eng.php>). The algorithm to characterize the geomagnetic data from Desalpar (DSP) has been presented as a flow chart in Fig. 4.29. A sample of raw X, Y and Z data from the DSP station is shown in Fig. 4.30, the variation pattern is verified by comparing with the raw data from Alibag (ABG) shown in Fig.4.31.

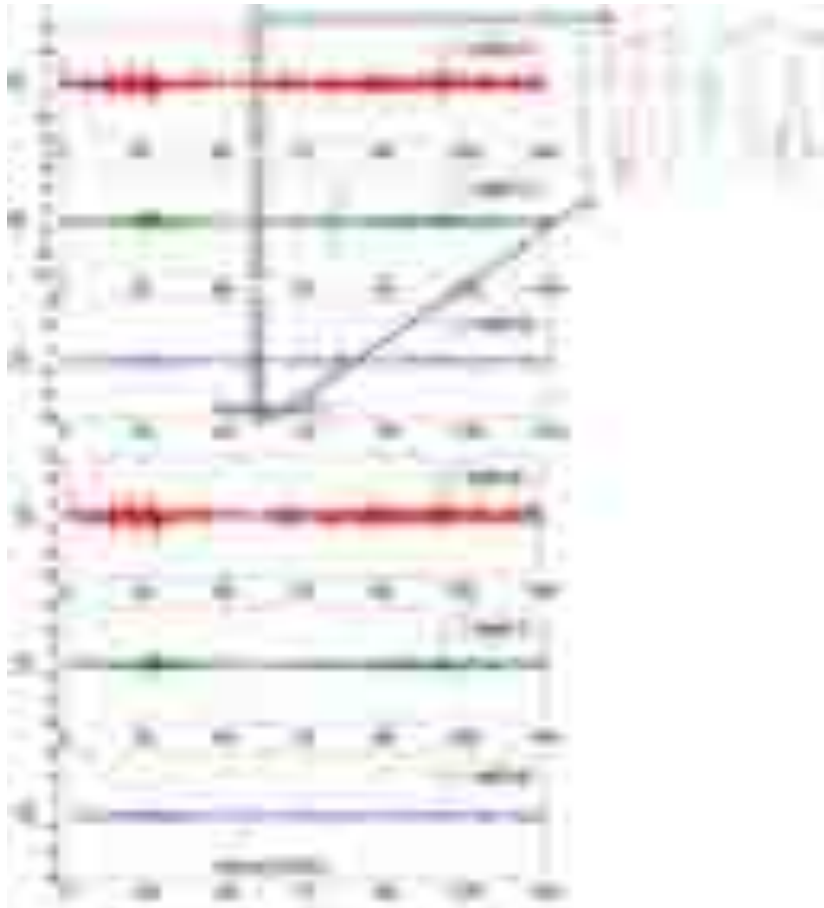


Fig. 4.32: First difference of the data from 2nd to 7th January 2009. Large amplitude of first difference is highlighted by a black box and the corresponding spike data is shown. The first difference of the same data after spike removal is shown in the bottom panel.

The data at DSP is recorded every 1 second whereas the sampling interval at the ABG station is 1 minute. Therefore, in order to compare the patterns, the DSP data is also converted into 1 minute averages. The calculated F at DSP and ABG are plotted together in Fig. 4.31 (top panel) and individual components from both the stations are also plotted in the bottom panel. The daily pattern of the X, Y, Z and F at DSP matches well with ABG.

The spikes in the data have been identified by plotting the first difference of the X, Y and Z components. The spikes with larger amplitudes are even visible in the raw data plots (Fig. 4.30). The first difference plots of one minute sampled raw data at two stations are shown in Fig. 4.31 and after spike removal, in Fig. 4.32. The time window highlighted with black rectangle indicate the data points with large amplitude in the first difference and the corresponding signal from all the three components are visualised (Fig. 4.32). The irregular sudden large variations indicate that it is an artificial signal which needs to be removed. The first difference of all three components of the same data after removal of spikes is shown in the bottom panel, where amplitudes are within $\pm 2nT$.

The dynamo region in the E-layer of the ionosphere results in Pederson current at ~ 130 km, which flows in an eastward direction at the equatorial and low latitude sites and westward in the high latitude regions. The variation in the geomagnetic field due to atmospheric dynamo is known as a Solar quiet time current (Sq), which results in geomagnetic variations with a period of 24 hours (Diurnal tide).

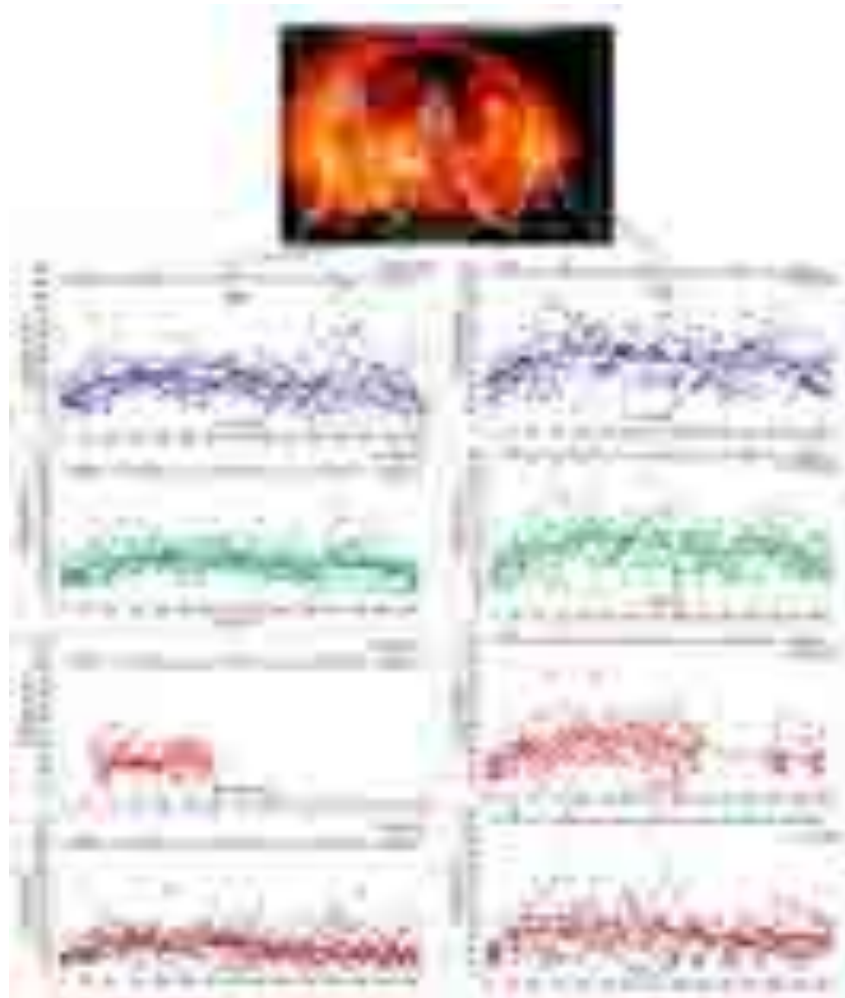


Fig. 4.33: The Sq peaks at each sites plotted against Julian days for 2009 and 2012. A polynomial fit is shown in black line.

It is assumed that during midnight hours, the ionosphere is inactive and the measured geomagnetic field represents the Core + Lithospheric field at the location. The average of the midnight hour i.e. 00:00, 01:00, 22:00 and 23:00 at the respective local time of the site for each day is calculated and subtracted from the remaining time series data to derive the diurnal variations. The diurnal variations of H/X i.e. Sq are derived at all the sites for the years 2009 and 2012. The peak value of Sq for each day has been noted. The pattern of daily peak values of Sq at each site are presented in Fig. 4.33, for the years 2009 and 2012. A polynomial of order 6 has been fitted to the data, which indicates the seasonal pattern of the Sq variations, high in E and J (Equinox and Summer solstice) and low in D (Winter solstice).

The diurnal variation of solar quiet (Sq) time current has been obtained at four low latitude sites in the Indian sector. The Sq daily peaks for each day at all the stations (DSP, ABG, HYB and JAI) are calculated for the years 2009 and 2012. A seasonal variation in all the four stations is evident and it is observed that all four sites coherently show higher peaks during E and low during D seasons. A difference of 15-20 nT is observed between D and E seasons for the year 2012 (solar cycle peak) whereas the difference reduces to nearly 5-10 nT for the year 2009, which marks the solar ascending phase. A weak seasonal trend is observed at station JAI compared to other sites, possibly due to latitudinal effects. This study has to be extended for a few more years to get a complete picture of latitudinal effects and the influence of solar cycle on seasonal trend of Sq.

4.9 Identification of suitable sites for two new magnetic stations
(Archana Radhakrishnan, Prassanna Simha, Shivam Joshi and K.M.Rao)

In order to identify two new sites to establish magnetic observatories in Kutch, Gujarat, a thorough review of geological and geophysical information of the Kachchh region is compiled and a few areas were selected. Further, detailed magnetic surveys are conducted to establish a site. The present locations of MPGOs at Badargadh and Desalpar are shown in Fig.4.34.



Fig. 4.34: The current locations of the MPGO sites in Desalpar and Badargadh.

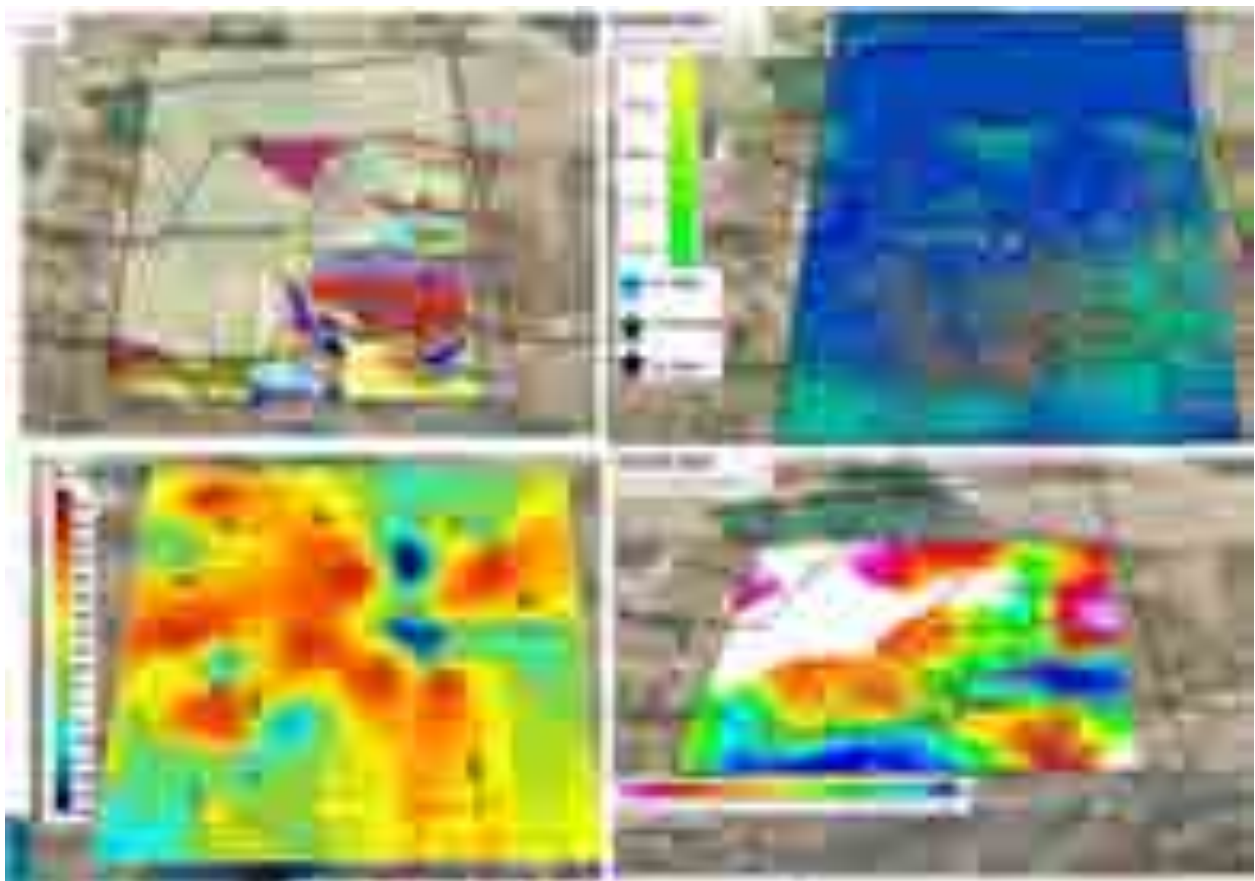


Fig. 4.35: The compiled image of the KMZ files of the selected area in Kutch.

A KMZ file has been prepared for the newly selected area (Fig. 4.35), which contains the following layers of information.

- MPGO- location of existing observatories; Desalpar (DSP), Badargadh (BDG) and Vamka.
- Selected area- The proposed area and selected seven villages.

- SIO MPO- Survey of India MAP along with the existing MPO lab and the six newly proposed sites.
- MT- MT and 2D resistivity maps along two profiles.
- Geology of the area, from geological map of GSI (2001), structural geology from Kothyari et. al. 2016 and 2018 (localised faults, domes, anticlines), Intrusive- from Kothyari et. al. 2018, local faults (there is a possibility of ± 2.5 km error).
- SRTM data.
- Gravity-BA- Bouger anomaly map.
- GPS studies- GPS sites, velocity, directions (ISR annual reports).
- Dykes- GSI 2001.
- Earthquakes before relocation and after relocation (Mahesh et. al.)
- Aeromagnetic MAP- Its a sample map provided by Macphar that includes (i)Horizontal gradient, (ii) Reduction to pole total field (iii) Second Vertical Derivative of the IGRF Corrected TMI (2VD) (iv)Analytic Signal of the IGRF Corrected TMI (AS).
- BBS- Broadband Seismic stations.
- Magnetic Anomaly map- from Chandrasekhar et. al., 2005.

4.10 Study of Geomagnetic Pulsations using Induction Coil Magnetometer at MPOs

(C P Simha and K M Rao)

Geomagnetic Pulsations are classified as Pulsation Continuous (Pc) and Pulsation Irregular (Pi). These geomagnetic pulsations are generated either by external or internal geomagnetic disturbances in the ULF waves. The ULF waves are in the frequency range of 0.001-5 Hz. Pulinets et. al. (2009) and Hayakawa et. al. (2012) reported the relation between these geomagnetic pulsations and earthquakes. Saito (1969), Tamao, (1964) and Jacob et. al. (1960) have linked the geomagnetic pulsations with the magnetosphere. In this study, we attempted to identify various geomagnetic pulsations recorded at our LEMI 30 instruments installed at Badargadh and Desalpar (MPOs).

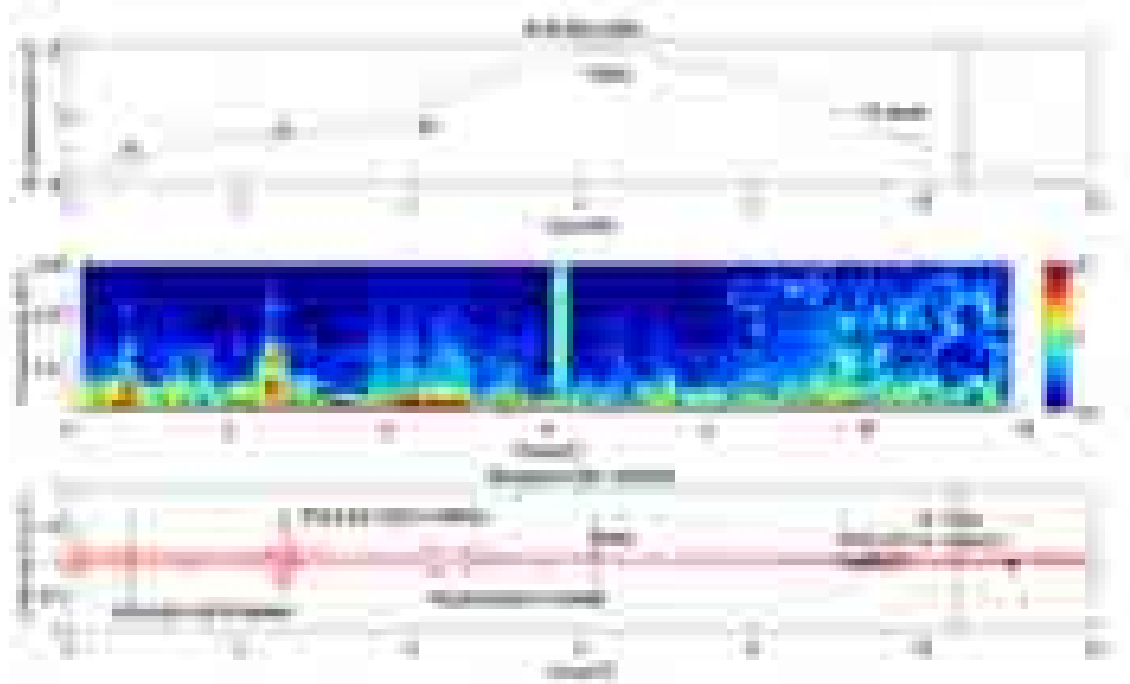


Fig. 4.36: 16th Apr 2013 D Component Geomagnetic Pulsations during 00-12UT.

One example of pulsation identification is shown in Fig.4.36 for the earthquake of M 7.7 on 16 April 2013 in Iran at 10:44 UTC. The epicentral distance from our observation site is about 1000 km. Here, we clearly notice two PIs (0.3-0.6 and 2.2 - 2.5 UT with peak to peak amplitude of 1.2 nT and frequency from 8 to 15 mHz) and one Pc (4-4.8 UT, 0.8 nT and 4 mHz) and very feeble PC during the event time. We noticed that PI2 and Pc5 were identified just before the event. The Kp value is zero and Dst is around 3nT during 00-12UT on 16 April 2013. These values are considered to be normal. We may speculate that the pulsations are observed for this earthquake as the magnetosphere conditions are normal. We identified all magnetic pulsations during 2013 at Badargadh. Now, we are processing the Desalpar site.

4.11 Ionospheric Response with the Seismic Wave disturbance at the Madagascar.

(C P Simha and K M Rao)

Mysterious seismic waves have been rolled around the world on 11 November 2018 at around 09:30 UT. The Seismic waves began 15 miles off the shore of Mayotte, a French Island sandwiched between Africa and the Northern tip of Madagascar. In this study, we analysed the ionospheric response in association with these mysterious seismic waves. Five IGS GPS stations have been selected for the present analysis, which are shown in Fig. 4.37.



Fig. 4.37: IGS GPS Sites selected on the Seismic Disturbance.

The seismic disturbance has travelled from MAYG in the south direction. The GPS derived VTEC data have been synthesized from 1 January to 15 December 2018. The raw data of the VTEC for this duration is as shown in Fig. 4.38. The seasonal variations in the TEC values can be clearly noticed from Fig. 4.38. To understand the disturbance caused by the magnetosphere, the Kp, Ap, Dst values are also analysed during the corresponding period (Fig.4.39). During the geomagnetic storms, the conductivity in the ionosphere increases with the disturbance caused in the magnetosphere by solar winds and intrusion of charged particles through north and south poles (Danilov and Belik, 1992). The storms have been noticed on the April, May and September period and we noticed clear raise in the VTEC compared to the average on quite days.

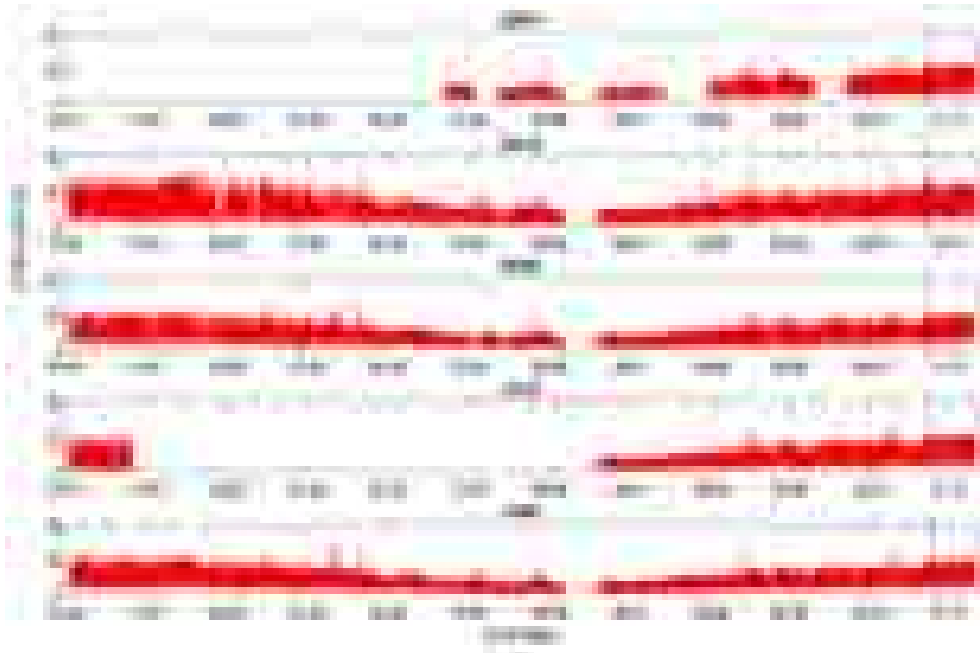


Fig. 4.38: VTEC values from 01st Jan to 15th Dec 2018 for the five stations.

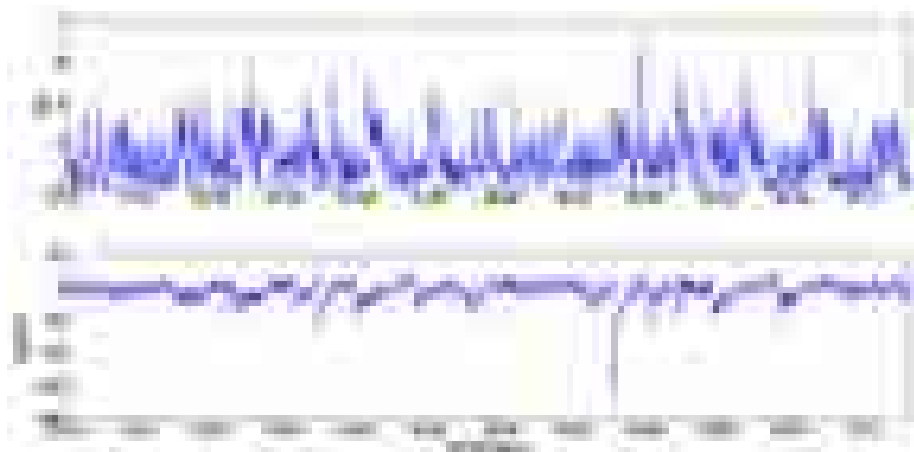


Fig. 4.39: Geomagnetic Activity Index (Kp and Ap) along with Dst from 1 January to December 2018.

The descriptive statistical methods such as mean and median and standard deviations have been calculated to understand and study the background variations during the period to detect the pre earthquake ionospheric anomalies (Pulinets et al., 2005; Dautermann et al., 2007; Li et al., 2014). The pre, during and post earthquake periods are analysed considering any variation in the observed parameters from the background level. The solar radiation effects such as storms and tail currents, have an impact on the solar rotation and one complete solar rotation is 27 days (Rich et al., 2003). Hence, we tried to study the ionospheric parameters before 27 days and after 4 days of any seismic disturbance (i.e. from 1 October to 15 November 2018). The anomaly in the signal is calculated with the sliding averaged TEC of 27 days before the earthquake (Li et al., 2014, J Guo et al 2015).

The VTEC values with the UB and LB are computed and plotted in Fig. 4.40. An anomalous signal has been found from 06 November onwards. Its background geomagnetic variations have been shown in Fig. 4.40. Further, we observed two magnetic storm conditions during the 45 day period from 08 October to 05 November 2018 but there was no significant enhancement in the TEC (no variation above or below the UB & LB). Interestingly, we noticed

some rise of the signal 06 days prior to the disturbance at four IGS stations which are near to the earthquake location. Therefore, this anomaly could be attributed to the seismic signal observed on the 11 November 2018. The raw data plot of VTEC for 15 days period from 01 November to 15 November is shown in Fig. 4.41. The values enhanced to 6-8 TECU on the 6 November, which could give the message of anomalous signal for the 11 November 2018.

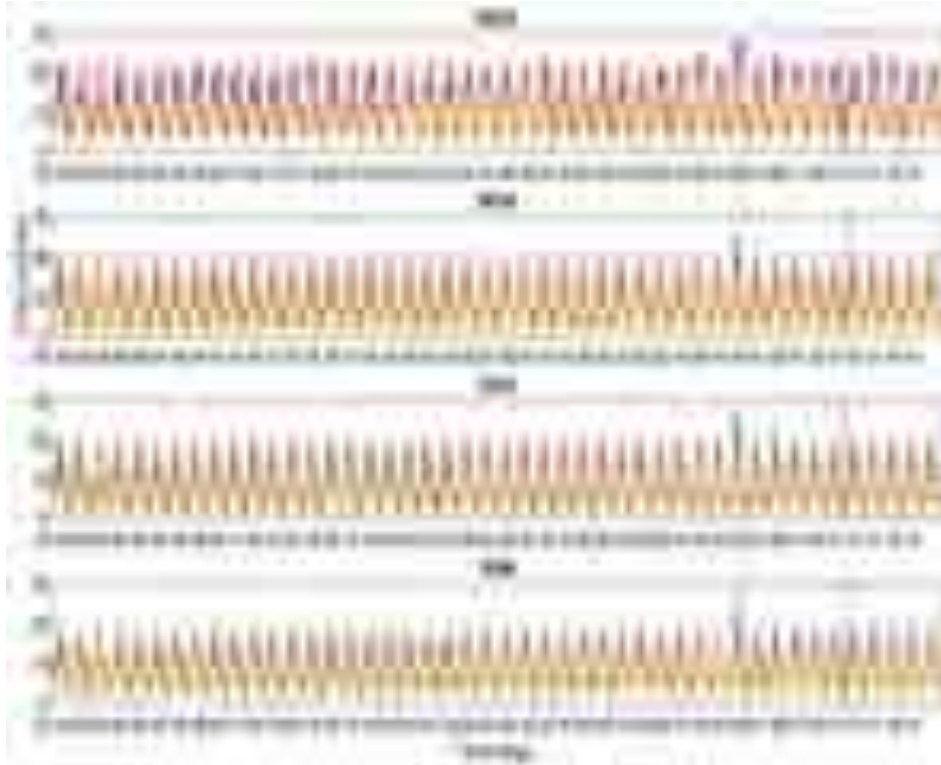


Fig. 4.40: The 45 days VTEC values with UB, LB computed from Sliding averaged method; red corresponds to UB, Blue to VTEC and Pink to LB.

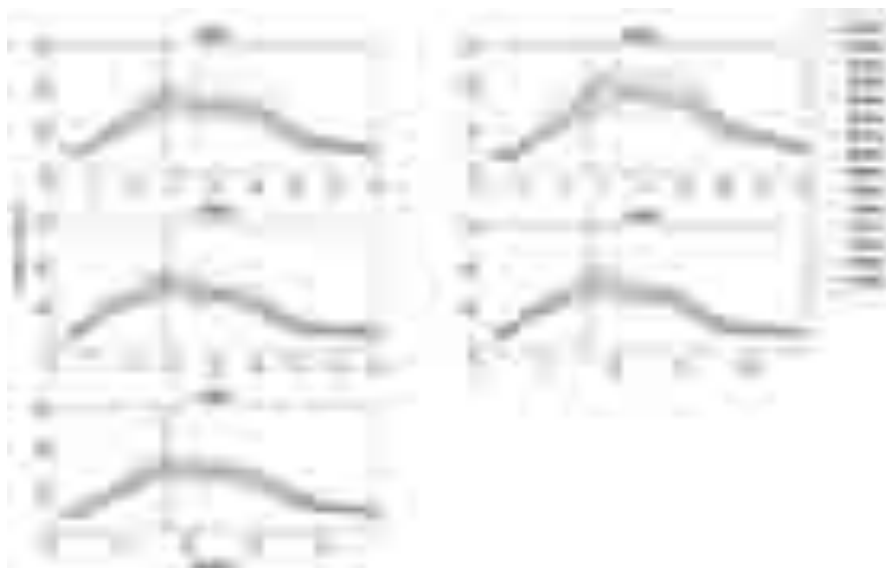


Fig. 4.41: Diurnal variations of VTEC from 01 November to 15 November 2018.

4.12 Characteristics of prompt penetration effects on EEJ from the Indian sector (Archana Radhakrishnan, Kusumita Arora and K.M.Rao)

Prompt penetration (PP) is the penetration of interplanetary electric field, that is, the electric field related to the solar wind to equatorial region through high latitude. To identify the PP events, a new method has been introduced using five minute sampled Equatorial Electrojet (EEJ) data and E_y data, which can further be verified using the AE index and a linear relationship between EEJ peak to peak amplitude and E_y amplitude for the identified events. The strength of EEJ is obtained at MNC (Minicoy, 72°E), VEN (Vencode, 77 °E) and CBY (Campbell bay ,93°E) using their longitudinally paired low latitude site ABG (Alibag, 72 °E), **HYB (Hyderabad, 77°E) and NBG (Nabagram 93 °E)**. The ΔH variation at all the sites and EEJ strength at the equatorial sites is shown in Figure 4.42 for the month of April 2015.

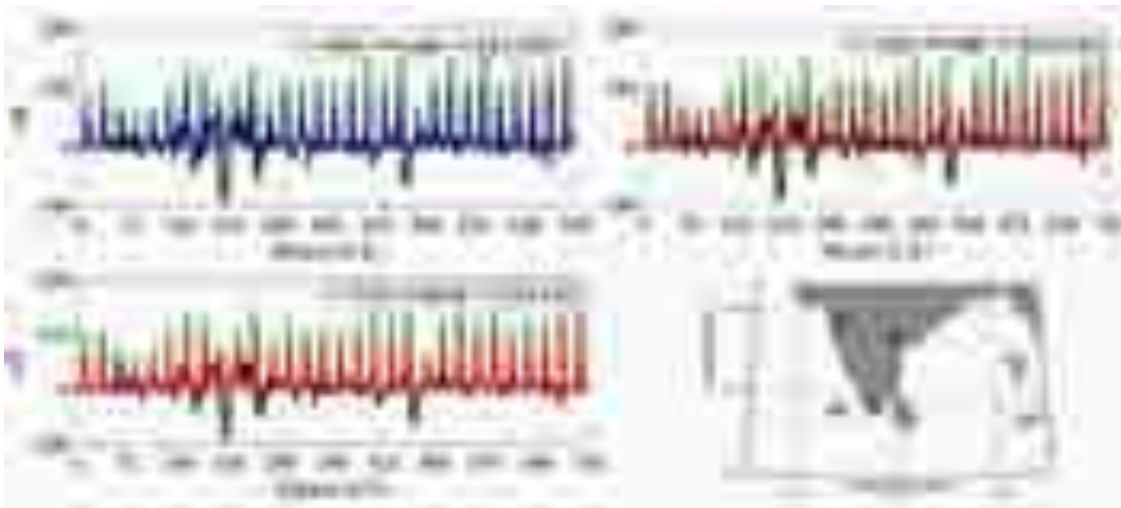


Figure 4.42: ΔH variation at MNC, VEN, CBY (green), at ABG, HYB, NBG (black) EEJ strength MNC (blue), VEN (red), CBY (brown) for the month of April 2015.

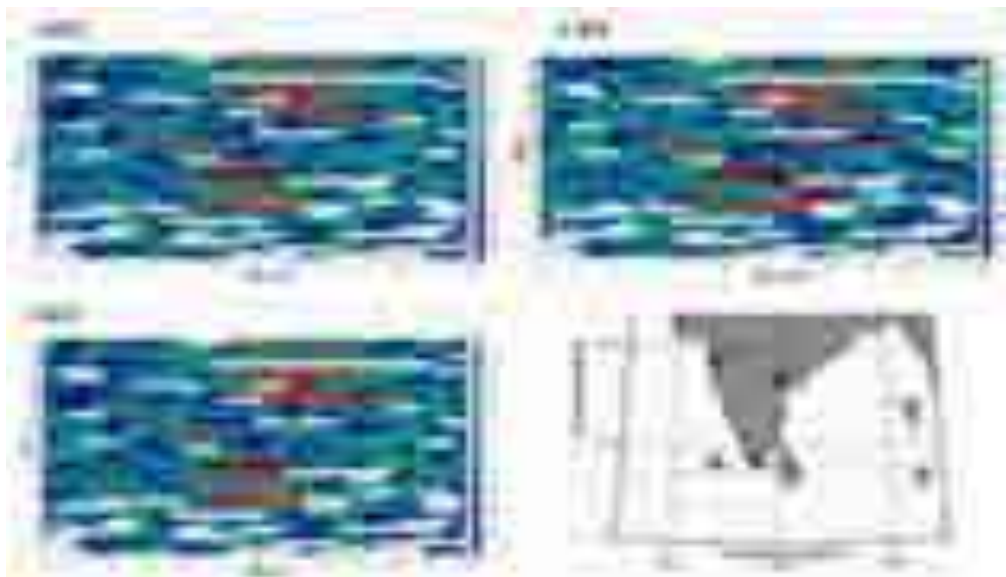


Figure 4.43: Correlation coefficient obtained at MNC, VEN and CBY for June 2015, westward PP is highlighted using a red arrow and the eastward PP is highlighted using black arrows, the white colour indicates missing data.

In order to investigate penetration efficiency of PP during IMF-Bz turning and local time at a site continuous EEJ data from VEN for five years (2011-2015) has been used in this study. To look at the PP events at different longitudinal separation, concurrent data for 2011, 2012 and 2015 of VEN and CBY are used, which are separated at 15° longitude. Concurrent data of VEN

and MNC for 2014 & 2015 are also used to investigate the PP effects at a separation of 5° longitudes. It is evident from figure 4.44 that the PP events have higher efficiency during Bz northward turning, showing over shielding effect. The amplitude of EEJ strongly decreases when Bz is northward and increases when the Bz is southward turning (under shielding). The Kp value is less than 3 during the quiet period.

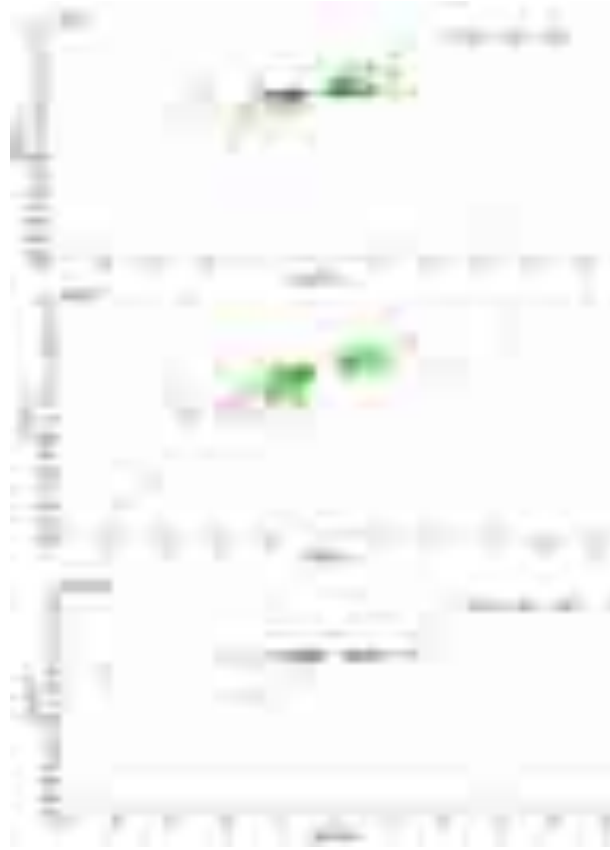


Figure 4.44: PP events identified from VEN during 2011-2015, peak to peak EEJ and Ey amplitude during PP events categorized according to the time of occurrence (morning-1-5UT, 6-9.55 LT), (noon-5-9UT, 10-14LT), (afternoon and evening hours 10-12UT, 15-17LT).

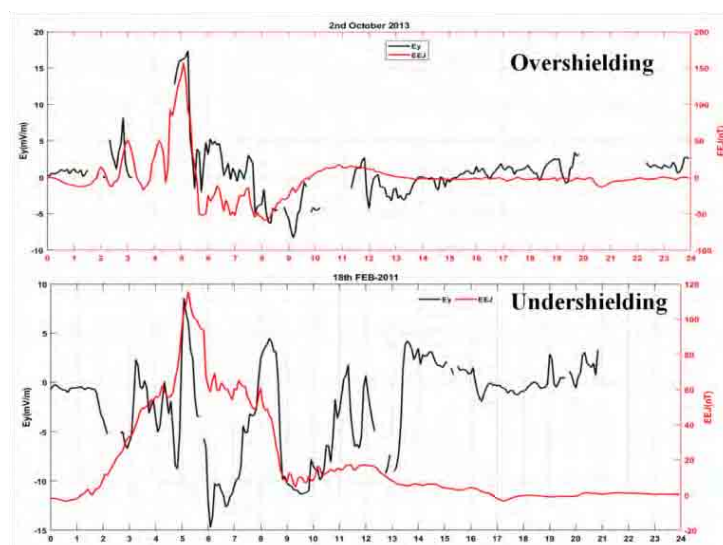


Figure 4.45: Example of over shielding and under shielding effects.

Figure 4.45 shows the strongest PP over shielding and under shielding event during 2011-2015. The bottom panel of the figure 4.46, shows that during the under shielding effect, the E_y increases from -9 mV/m to 9 mV/m, which causes eastward penetration of the electric field in the equatorial region resulting in an increase in EEJ amplitude up to 59 nT.

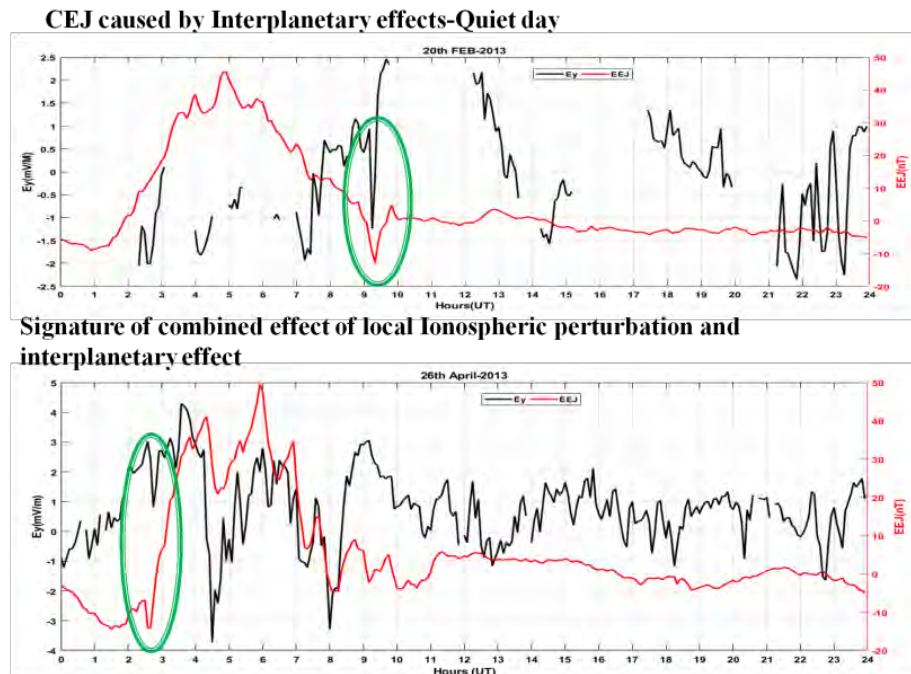


Figure 4.46: An example of the equatorial counter electrojet caused by PP during magnetically quiet time (event is highlighted by green circle in the top panel), an example of combined effect of interplanetary and localised ionospheric perturbation presented in the bottom panel (highlighted by the green circle).

4.13 Statistical characteristics of low latitude Pc4s: insights from Solar wind and IMF parameters in India

(Prassanna Simha, Jayshree Bulusu, Kusumita Arora and K.M.Rao)

The present work focuses on the Pc3-4 geomagnetic pulsations in the year 2013 from low latitude station Desalpar (DSP), operated by the Institute of Seismological Research (ISR). The Pc4 extracted from north-south and east-west components of Induction coil magnetometer (LEMI 30) are investigated along with the background IMF parameters and the activity indices. During 2013, many Pc4 events and merely two Pc3 were identified. The Pc4 events are predominantly observed during the local midnight and pre-noon sector in both the x and y components. The maximum number of Pc4(s) have been observed during the solar wind speed of 300 - 400 km/s and average IMF B field of 3 - 6 nT. The amplitude of Pc4s at DSP show that they have been controlled by the solar wind speed, number density, dynamic pressure and average B field. In addition, with IMF and solar wind parameters, they have been varying in association with the geomagnetic activity index (Kp). Based on our investigation, we conclude that Pc4s at very low latitude differ in frequency than those of mid and high latitudes. The interplanetary parameters can alter the amplitudes of Pc4s but no noticeable change is observed in Pc4 frequency. The clock angle dependence of Pc4 at low latitude is reported here for the first time, which clearly demonstrates the control of southward component of IMF on Pc4 frequency. However, as the frequency does not show any dependence on IMF parameter, we speculate that the observed Pc4s are of internal origin.

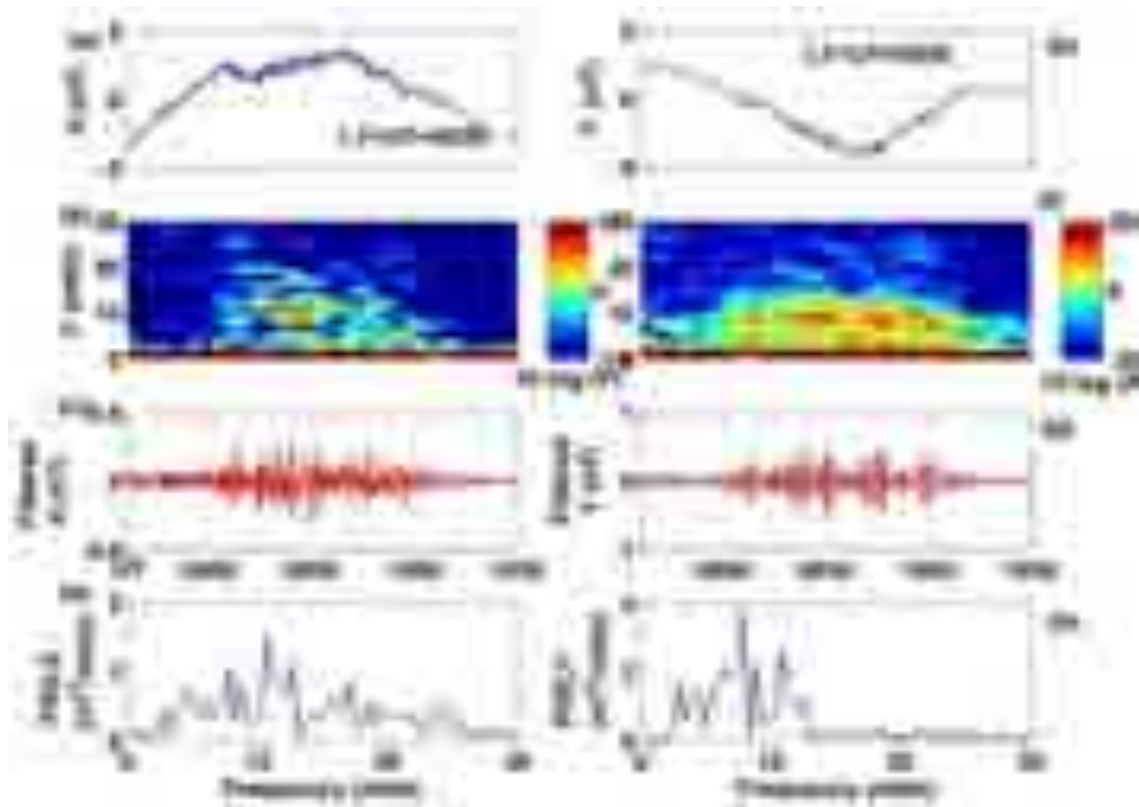


Figure 4.47: Raw and spectral estimates of X and Y components on 12 Jan 2013. (a) and (e) raw data, (b) and (f) spectrogram, (c) and (g) band pass filter (2-30MHz), (d) and (h) power spectral density estimates (PSD) of X and Y component, respectively.

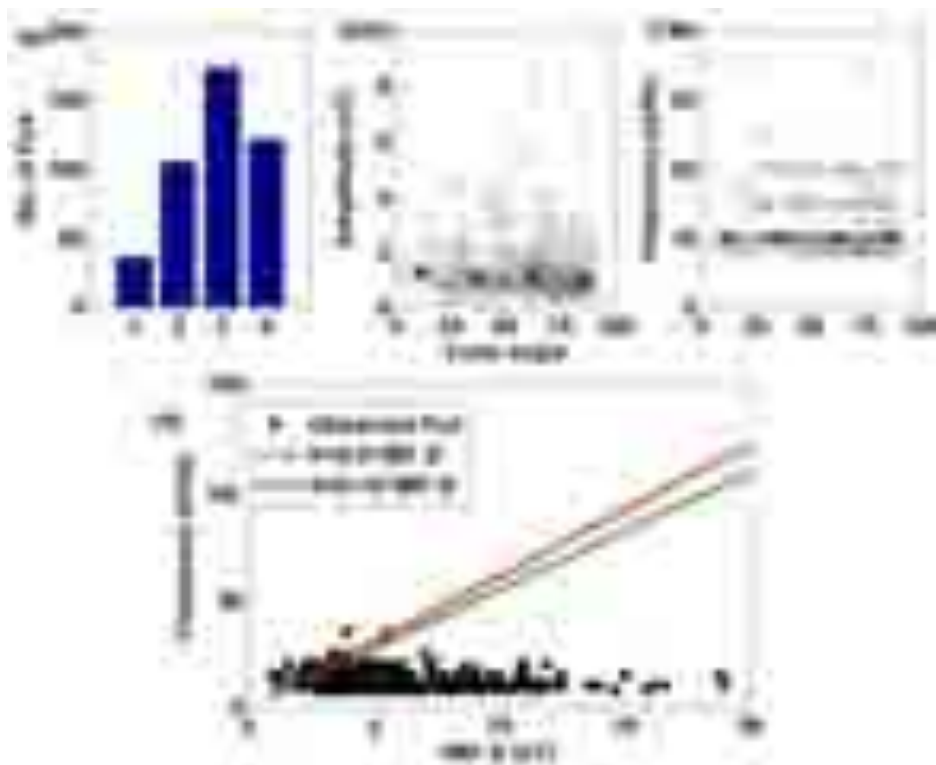


Figure 4.48: Variation of Pc4 as a function of cone angle in bins of 25 degrees (a) occurrence pattern (b) amplitude and (c) frequency of Pc4 (d) theoretical and observed Pc4 frequency estimates.

Figure 4.47 shows a typical event of Pc4, observed on 12 January 2013. The presence of an oscillatory signature is clearly seen in the raw data of X (Figure 4.47a) and Y (Figure 4.47e) respectively. This feature is identified as a scattered weak signature in spectrogram of X (Figure 4.47a) and as a continuous patch in Y (Figure 4.47e). The presence of Pc4 pulsation during 0900-1030 UT (LT=UT+05:30) is evidenced from time-frequency analysis. As the event is present below 30 mHz (Figure 4.47b and 4.47f), a band pass filter in 2-30 mHz was applied and is reflected in the filtered components in figure 4.47c and figure 4.47f respectively. Peak to peak amplitude of 0.6 nT in the X component (Figure 4.47c) and 0.8 nT in the Y component (Figure 4.47g) was observed. A dominant peak of around 10 mHz and 7 mHz in the X and Y component respectively are seen (Figure 4.47d, h). The events are classified into bins of 25 degrees each and contradictory results are evident with maximum number of Pc4 in 50-75° bin (Figure 4.48a). Very less number of events are observed in cone angle limit of 25°. Amplitude and frequency of Pc4s are independent of cone angle (Figure 4.48b and c). Further, the dependence of Pc3-4 on average B field is only evident in the lower limit ($B_{avg} < 5$ nT) (Figure 4.48d). The Pc4 frequencies are completely independent of average B field. Theoretically computed Pc3-4 frequencies from earlier numerical relations are superimposed on individual samples of Pc3-4s. It is observed that the numerical fits cannot explain the observed Pc4 distribution.

4.14 Magnetic survey at Amrapar and Kalyanpar (Prassanna Simha, Archana and K.M.Rao)

The ground magnetic surveys have been conducted at Amrapar near Dholavira and Kalyanpar, Rapar. The site is situated 6 km from Amrapar village and surrounded by lands which could be useful for agricultural work. Rocky structure is seen in the area. Kalyanpar Mitti Jameen is located 1-2 km from the Kalyanpar village.

The data have been archived using Gemlink Overhauser using walking mode at 1 sec sampling interval. The rough and spurious values have been removed from the data before preparing the contour plots. The signal strength while acquiring the data was also scrutinized very carefully; data with signal strength below 99 have been discarded for further analysis.

Figure 4.49(a) shows the TMF values at each point of the line at Amrapar site. The TMF values vary from 45303 nT to 45380 nT over the length of 484 m. The TMF values in the N-E portion of the area seem to be high compared to other areas. The values decrease when we move to the northwest direction and the values vary uniformly within 5nT for the length of around 140 m. The point to point variations derived using the First Difference between the points are in the range of -1 to 1 nT/m over the entire area. The TMF values in Kalyanpar area vary from 45084 to 45135 nT. The point to point variations of TMF are very high. The first difference between the points are computed and plotted on a contour map in figure 4.49(d). The gradient is ~ 2 to -2 nT/m in this area. From this study, we observe the following:

- TMF values at Amrapar are more homogenous compared to those at Kalyanpar.
- Point to point difference obtained from the two sites showed that Amrapar site has less variations compared to Kalyanpar.
- Amrapar site is a rocky area and Kalyanpar appears like soft soil.

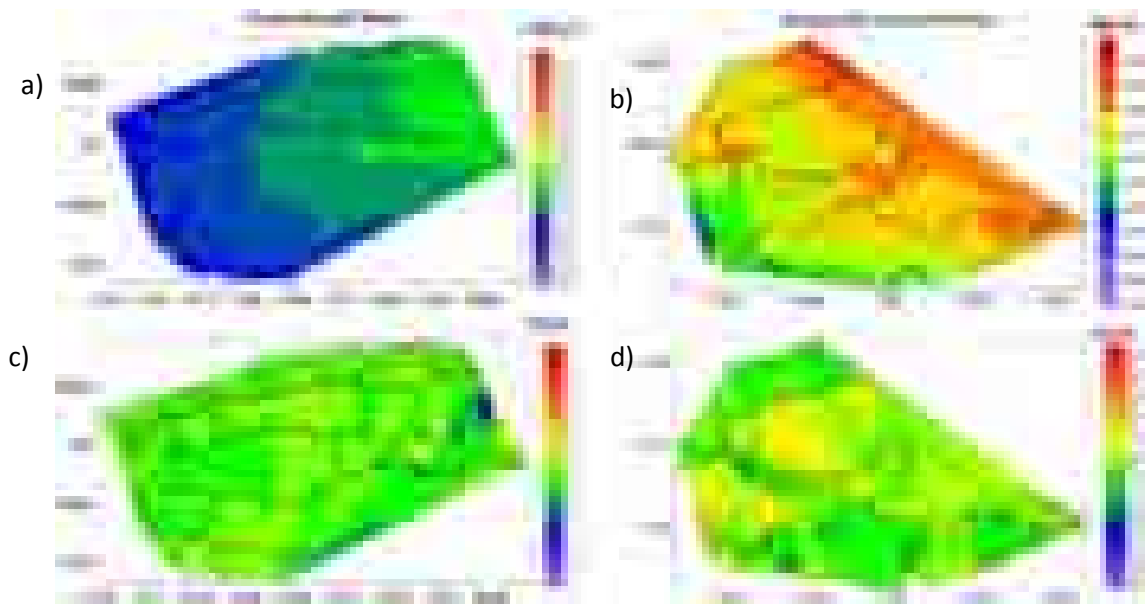


Figure 4.49: The TMF values at each point of the grid a) Amrapar site b) Kalyanpar, and one to one difference between the values at c) Amrapar d) Kalyanpar

4.15 Study of Geomagnetic pulsations in association with the earthquake on 16 April 2013

(Prassanna Simha and K.M.Rao)

We identified various geomagnetic pulsations in the magnetic data of LEMI 30 instruments installed at Desalpar MPO. We observed more Pc4 and Pi2 and very less Pc5 and Pi2 at both the sites. In this study, we studied the magnetic pulsations during the time of an earthquake of Magnitude 7.7, that occurred on 16 April 2013 at 10:44 UTC at 28.033N, 61.996E, 83 km E of Khash, Iran. This earthquake is located 980 km from Desalpar.

The magnetic pulsations observed on 16 April 2013 are depicted in Figure 4.50. We noticed two PIs (0.3-0.6 and 2.2 and 2.5 UT with peak to peak amplitude of 1.2nT and frequency from 8 to 15 mHz) and one Pc (4-4.8UT, 0.8nT and 4mHz) and very feeble Pc during the event time. These pulsations are identified as Pi2 and Pc5. In order to identify the global impact, we looked at the response of Kp and Dst values on 16 April 2013. We found Kp is zero and Dst is around 3nT during 00-12 UT. These values are at the normal level and cannot be attributed as causes for generating these Pi and Pc pulsations. Further, we also looked at the relation between IMF and solar wind in the magnetosphere with these pulsations. Interplanetary Magnetic Field (Bz and Bx) along with Solar wind speed and density in association with the Pc4 and Pi2 amplitude are shown in Fig 4.51.

During high solar wind, the hydrogen density is high in the solar wind and Pc4 signature is witnessed. Moreover, we noticed Pi2 during the abrupt changes in IMF and solar parameters. So, we can relate the generation of these pulsations with changes in Solar wind and IMF parameters. We clearly see that even if Kp value is less, we cannot relate the magnetic pulsations with earthquake. We have to carefully look for solar wind velocity and solar wind Hydrogen density. We speculate that these geomagnetic pulsations are related to ULF waves in the magnetosphere, and not with the earthquake processes.

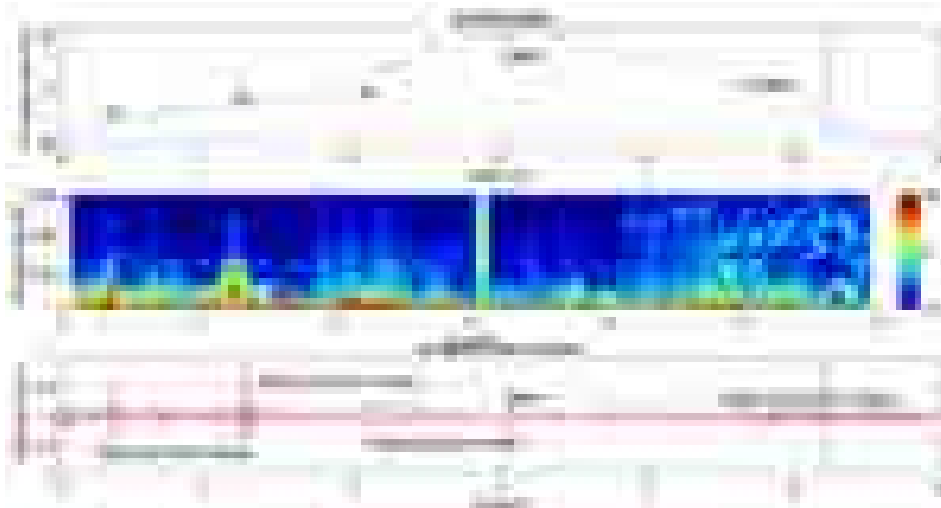


Figure 4.50: D Component Geomagnetic Pulsations during 00-12UT on 16 April 2013.



Figure 4.51: Interplanetary Magnetic Field (B_z and B_x) along with Solar wind speed and density in association with the Pc4 and Pi2 amplitudes.

5. ACTIVE TECTONICS

5.1 Deformation study of Gujarat

(Rakesh K Dumka, D. SuriBabu, P. Narain)

For the deformation analysis of Gujarat region, GPS data of all the permanent as well as campaign mode sites of ISR network is processed using GAMIT-GLOBK software. For a better understanding of the deformation pattern of the region, velocities of all the sites were also calculated in the Indian Terrestrial Reference Frame. Analysis indicates maximum amount of strain accumulation in the Kachchh region and significant level of strain accumulation in the Narmada region. To analyse the deformation pattern along the Allah Band Fault (ABF), we used three GPS stations, KHAV, KUAR and VKOT and calculated strain using the best fit calculation, after giving equal weightage to all the three sites. The calculated deformation of sites indicates that the region has an average deformation rate of 2.11 ± 0.63 mm/yr. The site KHAV, which is the southernmost site in this region indicates maximum amount of deformation (2.46 ± 0.26 mm/yr). Strain analysis along the Allah Band Fault (ABF) indicates 0.018μ strain/year and shows maximum compression in the NE-SW direction. Detailed analysis reveals that the segmented IBF has a maximum deformation rate of 2.9 mm/yr towards the Pachham Island and minimum towards the Khadir Island. The computation shows a maximum seismic moment (M_0) of 2.1×10^{24} dyne-cm in this part, which corresponds to an **earthquake of $\approx M_w$ 6.0**. The calculated maximum strain of 0.04 micro-strain/year is low but significant in an intra-plate region. The postseismic deformation, after the M_w 7.7, 2001 Bhuj earthquake is estimated to be low in this part. The reverse along with strike-slip motion of faults builds up stress in the area, accumulating more strain.

5.2 Deformation Study of Uttarakhand Himalaya

(Rakesh K Dumka, D. SuriBabu, P. Narain)

We present the geodetically estimated crustal strain rates in the Uttarakhand Himalaya, a region which has long been considered as a part of the seismic gap. The GPS data, obtained from the sites covering all the tectonic units from the Sub Himalaya in the south to the Tethys Himalaya in the north, including the major Himalayan thrust/fault systems, were processed and analyzed. The obtained dataset suggests maximum amount of crustal shortening towards the hinterland in the vicinity of Main Central Thrust (MCT) and Inner Lesser Himalaya, which is also concurrent with the high seismic activity in these parts. The GPS velocities of the sites (in India fixed reference frame) diverge significantly from sub-Himalaya to the Tethys Himalaya. The Sub and Inner Lesser Himalayan parts exhibit low deformation rate while the Inner Lesser and Higher Himalayan parts indicate maximum amount of deformation. The strain analysis reveals some elevated, High & Moderate Strain Zones (HSZ, MSZ) within the compressional regime in various tectonic units of Uttarakhand Himalaya. The HSZ is associated with the locked segment of the MHT, while the seismicity of MSZ is associated with the motion along the localized faults. These zones are also the sectors of active tectonics with maximum number of earthquake epicenters. The highest strain indicates the presence of a locked segment of the Main Himalayan Thrust (MHT) and is responsible for releasing the accommodated stress in the form of earthquakes.

5.3 GPS measurement of rapid subsidence of Gandhinagar, Gujarat (western India) due to groundwater depletion

(P Choudhury, K Gahalaut, R K Dumka, V. K. Gahalaut, A K Singh, S Kumar)

Depletion in groundwater level and deterioration in water quality due to excessive groundwater abstraction for irrigation in the Indo-Gangetic, Punjab and Sindh basins have been highlighted in recent years. Depletion of groundwater is reported in some localised regions also, for example, in Gandhinagar/Ahmedabad, where the groundwater table is depleting at an alarming rate of ~ 1.3 m/y. A continuous GPS measurement site, ISRR, at Gandhinagar documented ~ 5 mm/y of surface subsidence rate during 2009-2016. The observed surface subsidence rate at ISRR is consistent with the ground water depletion reported from Gandhinagar. Interestingly, continuous GPS sites at Lucknow and Varanasi in the Indo-Gangetic plains do not document any significant subsidence, which is also consistent with the in-situ observations of insignificant depletion of groundwater in the region.

5.4 Geodetic evidence of high compression across seismically active Kachchh paleo-rift, India

(V K Gahalaut, K Gahalaut, R K Dumka, P Choudhury, R K Yadav)

During the past 200 years, the Kachchh paleo-rift in western India, a plate interior region, has witnessed unusually large number of strong earthquakes, namely, the 2001 Bhuj (Mw 7.6), 1956 Anjar (Mw 6.0), 1845 Lakhpat (Mw \sim 6) and 1819 Allah Bund (Mw \sim 7.7) earthquake. We report continuous GPS measurements from the Kachchh and adjoining regions during 2009-2016. We find that the ongoing deformation is inconsistent with the postseismic deformation due to the 2001 Bhuj earthquake. The deformation pattern implies that the paleo-rift, bounded by the Kachchh Mainland Fault and other major faults along its southern flank and the Allah Bund fault and Nagar Parker fault along its northern flank, is under compression from both sides at a rate of ~ 4 -5 mm/y, making it seismically one of the most productive paleo-rift zones globally.

5.5 Strong seismic coupling underneath Garhwal-Kumaun region, NW Himalaya, India

(Rajeev Kumar Yadav, Vineet Kumar Gahalaut, Amit Kumar Bansal, SP Sati, Joshi Catherine, Param Gautam, Kireet Kumar, Naresh Rana)

Earthquakes in the Himalaya occur due to the ongoing convergence between the India and Eurasia plates. The frontal part of the plate interface shows brittle behaviour and deforms elastically causing accumulation of strain energy during the interseismic phase of deformation. The seismic hazard potency depends on the extent of the locked portion of the plate interface and the rate of plate convergence. The past geological and geophysical studies suggest that the entire zone of the Himalaya has the potency to generate major to great earthquakes.

Global Positioning System (GPS) is useful to estimate the crustal motion and is an important tool for the monitoring crustal deformation of sub-centimetre level. The recent advancement in the field of tectonic geodesy, made the collection of data easier and thus, provides a better understanding of earthquakes generating processes in the tectonically active region. The continuous GPS measurements (from 2012 to 2016) at twenty-eight stations in the Garhwal-

Kumaun region operated by NGRI, Hyderabad (20 sites), WIHG, Dehradun (5 sites), and GBPIHED, Almora (3 sites) provides several new findings.

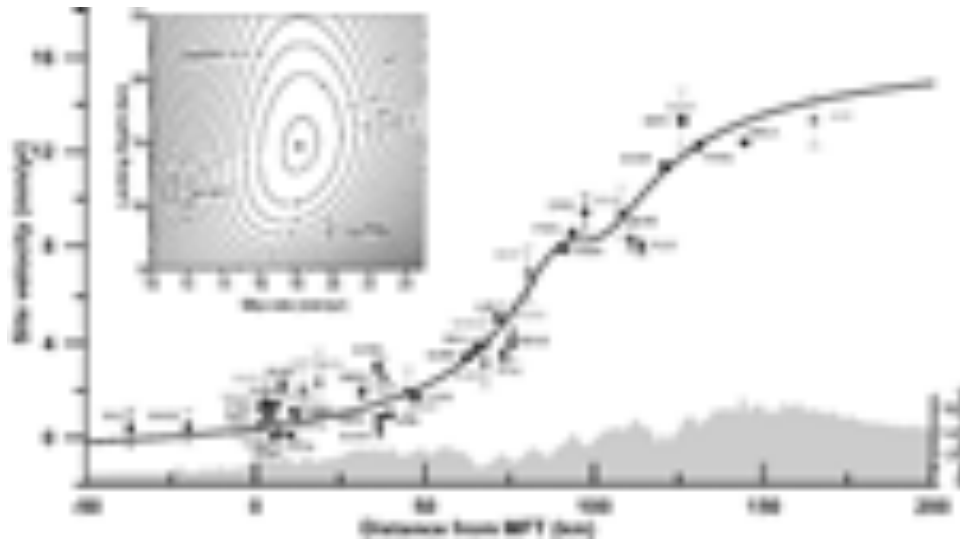


Fig. 5.1: Plate convergence rate in the Garhwal-Kumaun Himalaya. The fault perpendicular site velocity with uncertainty in the estimate of velocity is shown by grey colour (campaign mode) and black colour (permanent mode) square symbol with varying site location from Main Frontal Thrust (MFT). The inset shows the reduced chi square value corresponding the observed and calculated site velocity for varying slip rate and locking depth using grid search approach. Best-fit result gives a shortening rate of 18 mm/yr and locking depth of 15 km (shown by black curve).

The observed GPS time series shows that the site position changes linearly with a constant rate and is modulated by the seasonal perturbations that are periodic in nature. The linear motion is the result of ongoing elastic deformations due to the active plate convergence in the Garhwal-Kumaun Himalaya and the periodic motion represents the seasonal variations in the Himalaya. Strong seasonal variations caused by mass redistribution processes (such as continental water loading, atmospheric pressure loading and non-tidal ocean loading) in all three (North, East, and Vertical) displacement components is observed, which were removed by fitting an analytical function consisting sine and cosine functions with annual and biannual periodicities. In the fixed India plate reference frame, the estimated horizontal velocity varies from 0.5 ± 0.4 mm/yr in the Indo-Gangetic plains and 14 ± 0.3 mm/yr in the Higher and Tethys Himalaya, predominantly towards the south in the arc normal direction (Fig. 5.1). Sites located in the Lesser and Higher Himalaya exhibit uplift with a rate of up to $5-7 \pm 1$ mm/yr.

We applied elastic dislocation theory to estimate the plate convergence. The grid search approach provides the estimate of convergence rate as 18 ± 1 mm/yr and width of the locked zone of shallow Main Himalayan Thrust (MHT) as 100 ± 15 km in the Garhwal-Kumaun Himalaya (Fig. 5.1). Further, we have used the weighted least square inversion approach to derive the interseismic coupling on MHT. **Here, interseismic coupling (Φ) is defined as the ratio between the slip deficit rate during the interseismic period and long-term slip rate derived from relative plate motion. Φ varies between 0 (uncoupled) to 1 (fully coupled). We have divided the MHT into 414 (18 along strike \times 23 along dip) rectangular sub-fault elements of size 20×10 km² and used 18 mm/yr as total convergence rate across the Garhwal-Kumaun.**

We considered a flat-ramp-flat geometry of MHT with a dip angle of 7° for the flat portion and 16° for ramp portion. We have done the inversion of the observed site velocity to derive the arc normal and arc parallel slip on each sub-fault element for an optimal value of smoothing constraint (0.5). The derived coupling map suggests that MHT under the Outer and Lesser Himalaya is strongly coupled ($\Phi > 0.8$) which shows a large rate of strain accumulation (Fig. 5.2). The slip deficit budget in the Garhwal-Kumaun Himalaya since the past devastating earthquakes suggest an overdue of ~ 4 -meter slip on the MHT, which may produce at least one future great earthquake of $M_w \sim 8$.



Fig. 5.2: Interseismic coupling map of Garhwal-Kumaun Himalaya. The black and green colour vector shows the observed and calculated site velocity respectively. Black colour circles show seismicity of the region from 1973 to 2015 (USGS catalogue). Blue colour contour represents the interseismic coupling on decollement with an interval of 0.2. Brown curve show trace of PT2. Top inset shows the geometry of MHT used in the analysis of interseismic coupling.

5.6 Crustal deformation and strain analysis along IBF and ABF

(Rakesh K Dumka, D. SuriBabu, P. Narain)

To analyse the deformation pattern along the Allah Band Fault (ABF) we have used three GPS stations, KHAV, KUAR and VKOT and calculated the strain using best fit calculation, after giving equal weightage to all the three sites. The calculated deformations indicate that the region is experiencing an average deformation of 2.11 ± 0.63 mm/yr. Site KHAV, the southernmost site in this region indicates a maximum amount of deformation (2.46 ± 0.26 mm/yr). Strain analyses along the ABF indicates 0.018μ strain/year with a maximum compression in the NE-SW direction. Detailed analysis reveals that the segmented IBF has a

maximum deformation rate of 2.9 mm/yr towards the Pachham Island and minimum towards the Khadir Island. The computation discloses a maximum seismic moment (M_0) of 2.1×10^{24} dyne-cm in this part which corresponds to an earthquake of \approx Mw 6.0. The calculated maximum strain of 0.04 micro-strain/year is low but significant in the intra-plate region. The postseismic deformation, after the Mw 7.7, 2001 Bhuj earthquake is estimated to be low in this part. The reverse along with strike-slip motion of faults builds up stress in the area and accumulating more strain.

5.7 Observation of Holocene Tectonic activity along KHF

(Rakesh K Dumka, D. SuriBabu, P. Narain)

Paleoseismic and archaeological records of the Kachchh Rift Basin (KRB) of western India indicates that the region became tectonically active during the period of Middle to Late Holocene. To understand the relationship between strain accumulation, earthquake genesis, and landform development, we analyzed uplifted Late Quaternary terraces and archaeological evidence along the Kachchh Mainland Fault (KMF) zone. Dividing the elevation of the bedrock strath at each site by their ages, yields vertical uplift rates of 0.29–1.17 mm/y for the KMF zones. Archaeological data from the excavation of the Kotada Bhadli site suggest that the site was occupied during the Late mature Harappan (2300-2500 BCE) period and abandoned around 1900 BCE. The chronological constraints in geomorphic and archaeological records suggest that the area was hit by an earthquake around 2200 BC (\sim 3.5ka).

5.8 New insight into recent earthquake activity in the North Cambay basin, western India: A linkage between seismicity, focal mechanism and geodetic strain rate

(Pallabee Choudhury, Sumer Chopra, Charu Kamra and Archana Das)

The intra-plate Gujarat region located at the tri-junction of three failed rifts, Kachchh, Narmada and Cambay is seismically one of the most active intra-plate regions of the world. Among these three, the Cambay basin is investigated thoroughly towards petroleum exploration. However, the basin is not studied so far in the seismotectonic perspective. Since the last few years, it is observed that the northern part of the Cambay basin is becoming active with increase in seismicity. In the past 10 years, around 995 earthquakes are recorded from the region, with a maximum magnitude of M4.2. Most of the earthquakes are in the magnitude range 1-3. We attempted to solve the paradox of increasing seismicity in this region using strain rates, deduced from the GPS measurements. It is observed that strain rates \sim 0.02-0.08 micro strain/yr are prevalent in the region and the distribution of high shear strain rates is consistent with the dominant seismicity. The average strain rate is 0.05 microstrain/yr, which translates to a magnitude of 6.4 for the maximum potential earthquake. The focal mechanisms of the earthquakes show mostly normal with strike-slip component, which are well corroborated by the geodetic strain tensors. Most of the seismicity is clustered in the basement ridges, striking along pre-existing Precambrian trends that cross the Cambay basin. The complex geodynamics created around the northern part of the Cambay rift due to various movements along several faults, presence of basement ridges and sub-surface plutonic bodies in a failed rift are creating stresses, causing earthquakes in this part of the rift. Moreover, we suggest that the deep-seated plutonic body is acting as a major stress barrier for the NNE-

SSW compressive motion of the Indian plate and is plausibly facilitating the localized extensional tectonics in the region, where compression is expected.

5.9 Morpho-Structural evidence of Neotectonic activity along the Vigodi Fault, Kachchh, India

(Sneha Mishra, Girish Ch Kothiyari, R. K. Dubey, Gaurav Chauhan, Raj Sunil Kandregula)

In the present study, we analysed geomorphic landform and drainage pattern within the NW-SE oriented, Vigodi Fault (VF) to assess neotectonic deformation. The VF zone is located in the western part of Kachchh Basin that shows a typical wrench geometry, where several compressional and extensional fault segments are present between the Katrol Hill Fault (KHF) and the Kachchh Mainland Fault (KMF). In this study, we present geomorphic evidences along the surface traces of the neotectonically active VF zone. The fault zone is encompassed by several neotectonic landforms such as the development of strath terrace towards the upthrown block and valley fill terrace in the downthrown block of the VF, youthful nature of fault scarps, warping in Quaternary sediments, the formation of slit canyon within Quaternary sediments, knick-points, slickensides, and river offset. Presence of strike and dip parallel slickensides indicates oblique slip motion within the VF zone. We used conventional geomorphic parameters of active tectonics such as stream length-gradient index (SL), steepness index (Ks) to determine the neotectonic variability across the fault zone. Further, we tested a novel method called gradient length anomaly (GLA) to identify the surface deformation pattern within the VF zone. The observed negative and positive values of GLA correspond to the long-term uplift and subsidence associated with the VF. The results of geomorphic, geological and morphometric analyses together show that the area is neotectonically active. The combined observations made from the present investigation can be used to estimate seismic hazard assessment of the study area.

5.10 New insight into some coastal Harappan sites, Saurashtra, Western India: Implications in human-landscape relationship

(Archana Das, S. P. Prizomwala, Aashima Sodhi, Chintan Vedpathak, Nisarg Makwana, Tarun Solanki, and Hema Achyuthan)

In this work, we explore the plausible mechanisms for the demise/de-urbanisation of the **"coastal" Harappan Sites. We examine the hypothesis** revolving around the demise of the civilization in accordance with the climatic/ sea level changes during the Middle-late Holocene time frame (i.e, for the last 6000 years). The sites such as Padri, Lothal, Kuntasi, Rangpur were studied extensively in order to understand the role of the sea level changes, if existing. The present day location (i.e., elevation and inland distance from high water line) and timing of abandonment (2-3 ka BP) of Lothal, Padri and Kuntasi etc. suggest role of sea level in these coastal settlements being dysfunctional/de-urbanised. The study shows the fundamental significance of future studies in integrating the archaeological and palaeo-proxy data for better understanding the response of the one of the most advanced civilizations of their times.

5.11 Cycles of aggradational and incisional events from the Valley fill sequences, South- eastern Saurashtra

(Tarun Solanki and Siddharth Prizomwala)

The fluvial sequences of dryland western India have responded to Late Quaternary climate change, however in a discreet manner (Jain and Tandon, 2003; Juyal et. al., 2006; Das et.

al., 2016). Despite these studies, an understanding of regional aggradation and incision cycles has not been recognized. This lack in understanding is most likely due to the limited chronological support and poor understanding of the fluvial response to such events (Bhaskaran et. al., 1987; Bhatt and Bhonde, 2003; Sharma et. al., 2017). The understanding of aggradational and incision processes is vital for decoupling of the climatic and tectonic imprints in sedimentary deposits (Srivastava et. al., 2008). In the Shetrunji River basin, the time frame ranges from 18 ka to 1 ka. Based on sedimentary architecture, timing and landscape response, we identified three aggradations and three incision cycles associated with external forces (Table 5.1).

Table 5.1: Cycles of aggradation-incision identifying in fluvial sequence from South-eastern Saurashtra

Timing of the event	Site name	Events	Same events in other studies
Late Pleistocene - Early Holocene period (18 ka to 9 ka)	Site-TJ (Unit 1, 2, 3)	Aggradation (Climate)	Depressed monsoonal conditions during LGM in Luni river basin (Kar et al., 2001); 12 ka to 8 ka strong monsoonal conditions with fluctuating climate (Gupta et al., 2003; Enzel and Prasad, 2006; Raj et al., 2015; Prizomwala et al., 2016)
Early Holocene Optima (9 ka to 7.5 ka)	Site-TJ, Site-SL	Incision (Climate) Incision rate 0.5 mm/a	Enhanced monsoon activity, after 9 ka (Thamban et al., 2002), High Holocene optimum occurred during ~9 ka (References there in Thamban et al., 2002)
Middle to Late Holocene period (7.5 ka to 3 ka)	Site-SL (Unit 1 to 10), Site-AM (Unit 1 to 6)	Aggradation (Climate)	Intense monsoon prevailed until 6.4 ka and after 5.4 ka it weakened relatively (Thamban et al., 2002), Steady decline in the monsoonal activity during 8 ka to 3 ka (Gupta et al., 2003; Enzel and Prasad, 2006; Tyagi et al., 2012; Bhattacharya et al., 2014; Raj et al., 2015; Prizomwala et al., 2016; Das et al., 2017).
Middle to Late Holocene period (after 6 ka)	Site-SL	Incision	During 6 ka to 3 ka a sea level marginally higher than present in various parts of Gujarat (Maurya et al. 2008; Deo et al. 2011; Tyagi et al. 2012; Das et al.

		(~ 2 m incision due to falling Sea level)	2017), Incision of 4 m from its Middle Holocene high stand to reach present day level (Das et al. 2017).
Late Holocene period (3 ka to 1 ka)	Site-BH Site-KA Site-DH	Aggradation (Climate)	Stronger conditions of monsoon at around 1 ka which was followed by a period of aridity upto the present day (Ngangom et al., 2012; Bhattacharya et al., 2014)
Recent / Present day period (< 1 ka)	Site-BH Site-DH	Incision (climate/Tectonic ?)	During early Holocene, a tectonic uplift occurred in the entire Mainland Gujarat region (Maurya et al., 2000, Chamyal et al., 2003)

5.12 Characterizing the nature and extent of dryland fluvial response to extrinsic parameters since the Last glacial period: An example from Shetrunji basin (western India)

(Tarun Solanki and Siddharth Prizomwala)

The target of this study is to analyse the sedimentary facies with its natural characteristics. Geochemical analysis is used to interpret its depositional environment and OSL dating to ascertain the timing of the paleo events. By combining all the datasets, we conclude the following:

- The Shetrunji river responded in the form of aggradation during the Late Pleistocene to Early Holocene period (18 to 9 ka), MIS-2, in initial weak to gradual strengthening of the monsoonal conditions. The sea level was rising at a fast pace, but was far below the present-day level during this period.
- The period after 9 ka monsoon intensity increased abruptly, so sediment preservation has not been archived due to high erosive power. Therefore, the period between 9 and 7.5 ka is the period of non-deposition/erosion (?), mainly attributed to high Holocene intense precipitation.
- The period between 7.5 and 3 ka shows overall humid to dry fluctuating climatic conditions. It is the period of aggradation with fluctuating events. This was in response to rising sea level which reached its peak stand above MSL during 4 ka period.
- The period of ~ 3 ka shows gradual decline in the monsoonal condition with relative sea level recession phase, which also started to reach the present day condition. So, during this age the fluvial system experienced an incision phase, at Site-SL, which is located at the mouth of the Shetrunji River basin that shows 2 m incision due to relative sea level lowering supported by geochemical analysis.
- After that, during the period between 3 and 1 ka, a relative improvement in the monsoonal conditions was observed which is reflected by the aggradational phase. Sedimentological characteristics suggest fluctuating climatic conditions during this period.

- The study illustrates the typical valley fill and channel fill sedimentation in the dry land environments, which responded in the form of continued (three cycles) aggradation to the increasing monsoonal condition and oscillated to (2 cycles) incision in response to the relative sea level fall and tectonic activity.

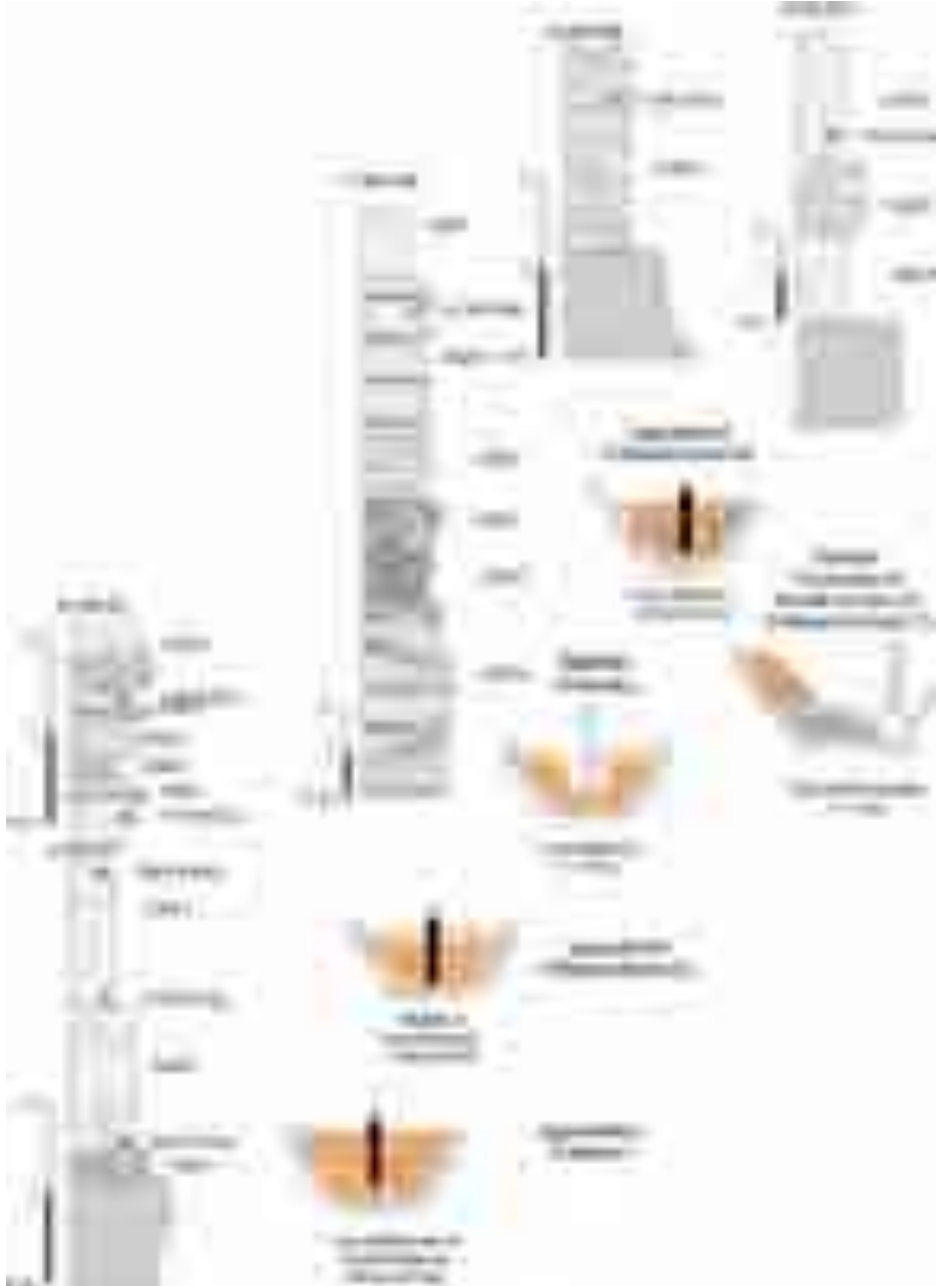


Fig. 5.3: Lithostratigraphy of the Shetrunji River Basin.

6. COMMERCIAL RESEARCH AND DEVELOPMENT

6.1 Magnetotelluric survey in the South Cambay basin

(Kapil Mohan, Peush Chaudhary, Vishal Vats, Pruthul Patel, Dilip Kushwaha, Akash Solanki and Russi Modi)

M/s Mercator Petroleum Limited (Ltd.), Mumbai has requested ISR to conduct the Magnetotelluric (MT) data acquisition, processing and interpretation (API) in a NELP Block in the south Cambay Basin near Bharuch, Gujarat (Fig. 6.1a). A total of 194 MT stations are acquired in the mentioned block, with recording periods of 60 hrs and an interstation spacing of ~0.5km (Fig. 6.1b). The Magnetotellurics data acquisition system ADU-07 (manufactured by M/s Metronix, Geophysics, Germany) has been used for the acquisition of the data. The magnetic field measurements were made using MSF-06e coils, and the electric field measurements were made using Pb-PbCl₂ electrodes. The electric field was measured in two components (Ex and Ey) and the magnetic field was measured in three components (Hx, Hy, and Hz). The location map and acquired sites are shown in Fig. 6.1b.

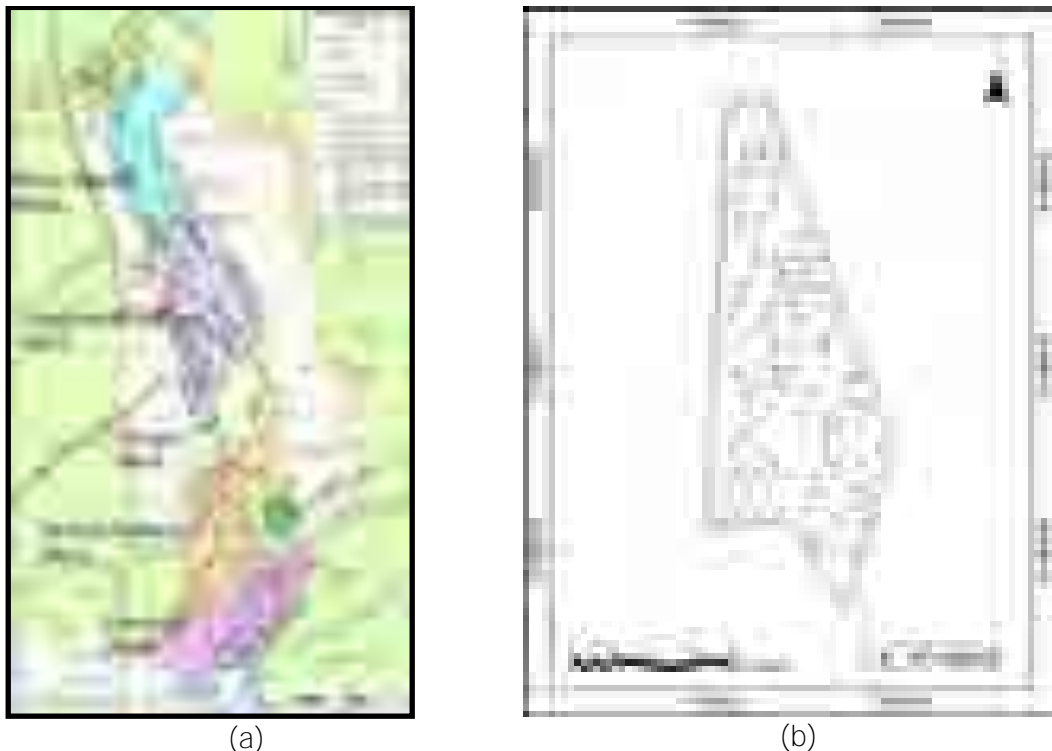


Fig. 6.1: (a) The location of the Block with tectonic map (after Kundu and Wani, 1992) and (b) the location of acquired MT stations.

MT data is processed with MAPROS processing software (M/s Metronix GmbH) to obtain the apparent resistivity and phase curves. The processed MT data at two stations are given in Fig. 6.2. The impedance tensors at all the 194 sites are used for geoelectric strike analysis. The decomposition technique of Becken & Burkhardt (2004) is applied to obtain the geoelectric strike. Using BB decomposition technique, we obtained geoelectric strike as N20°W with 90° ambiguity for a period band of 0.001-1000s. The Rose diagram indicating the regional strike direction obtained after BB approach of three profiles (A, B and C) is shown in Fig. 6.3.



Fig. 6.2: The processed MT data (time series curves)

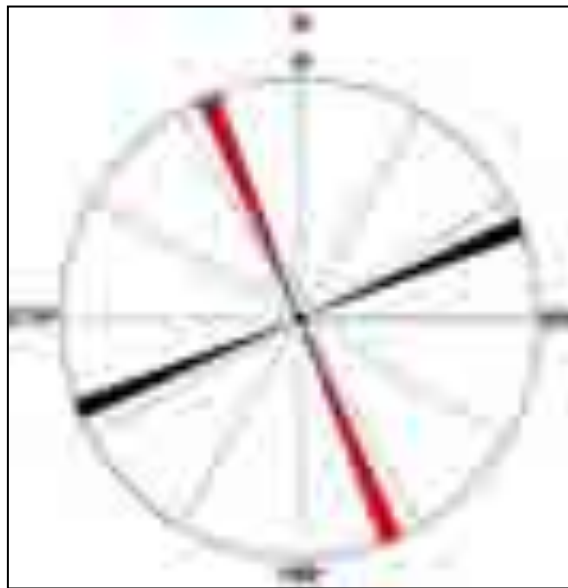


Fig. 6.3: Rose diagram showing the Goelectric strike of N20°W

The calculation of the regional strike facilitates the decoupling of impedance tensor into Transverse magnetic (TM) and Transverse Electric modes (TE). We rotated the recorded MT data to -20° and obtained the respective TE mode (along the strike) and TM mode (across the strike). The respective ellipticities and distortion angle obtained in the analysis supports the 1D/2D nature of the MT data. The distortion angles are very small indicating a rather low degree of distortion in the study area. The ellipticities approximately vanish in this period range and the orientation of telluric vector is found to be independent of period. Thus, 2D analysis seems to be permitted. The recorded MT data is rotated to the estimated strike direction (N20°W), and TE and TM modes are obtained. The rotated apparent resistivity and phase data from 0.001 to 1000s of all the sites were subjected to two dimensional (2D) inversion analysis using the 2D MT inversion code of Rodi and Mackie (2001) available in data modeling package WinGlink for TE (electric field parallel to the strike), TM (electric field perpendicular to the strike) and the combination of TE+TM modes. It discovers regularized solutions (Tikhonov Regularization) to the 2D inversion problem for MT data using the method of non-linear conjugate gradients (NLGG). In the NLGG method, the inversion process is **controlled by a trade off between the data fit and the model smoothness, γ' is the control parameter. We have considered $\gamma'= 7$ (for profile A & C) & $\gamma'= 10$ (for profile B)** appropriate for inversion of data. Error floors of 20 percent for apparent resistivity and 1.5° for the phase

are assigned for the entire profile, which results in down-weighting of the apparent resistivity with respect to the phase and helps in reducing the influence of the static shift in TE Mode. Initially, we ran the inversion using sparse grid and added new columns/rows in the location where significant structures are found. The initial model was a uniform half-space with a resistivity of 100 Ohm.m. The inversions run about 200 iterations before attaining pre-set RMS error levels. The 2D geoelectrical depth sections for profile A for a depth of 6km is given in Fig. 6.4 (a) and the profile lines are shown in Fig. 6.4 (b). In the profile A, the uppermost layer is Tertiary formation having resistivity of ~ 35 Ohm.m. Below this layer, the Tertiary formations are found in two layers (having different resistivity). Deccan traps are found at a depth of approx. 5 km.

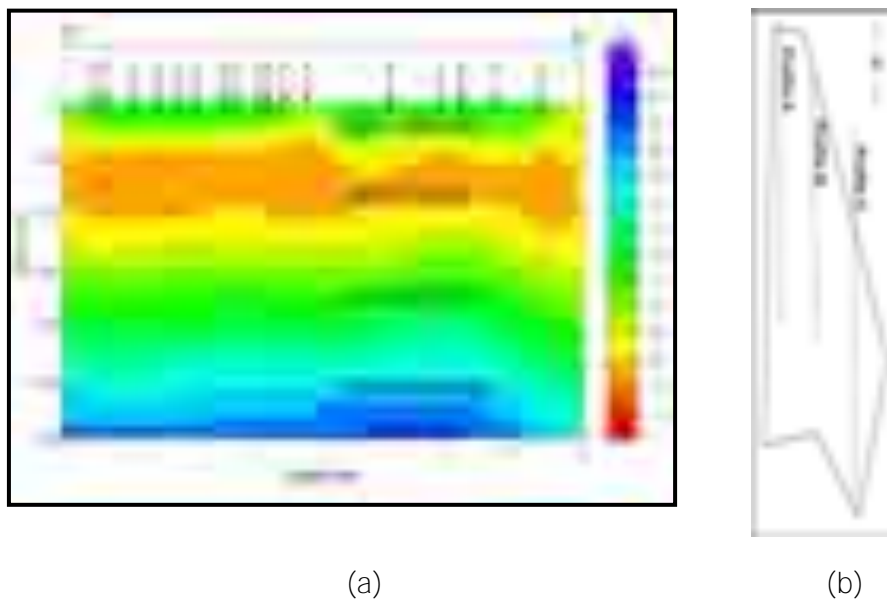


Fig. 6.4: (a) 2D geoelectric depth section of profile A (b) The three profile lines

6.2 Estimation of Mesozoic sediment thickness in the western part of Kachchh (Kapil Mohan, Pruthul Patel, Dilip Kushwaha and Peush Chaudhary)

Magnetotelluric data along a profile from Hajjpir in the north to Lathedi (Total length 80km) in the south was acquired (23 sites) (Fig. 6.5). The data was acquired in broad frequency range of 0.001 Hz to 1000Hz with a recording period of up to 72 hrs. The dimensionality analysis of the processed data has been conducted using WALDIM code. The data is found to be of 1D nature, upto 10 sec. The data was subjected to 1D Occam Inversion (Constable et al., 1987) for up to 10s. The obtained 1D resistivity section is given in Fig. 6.6. From 1-D inversion of MT data, a layer of resistivity 1 to 3 Ohm.m has been found up to a depth of 1.5 km in the northern part of the profile between Hajjpir to Aiyar villages followed by a layer of resistivity of 4 Ohm.m to 12 Ohm.m having thickness of ~ 1.5 to 1.8 km (Fig. 6.6). The first layer is interpreted as Quarternary+Tertiary sediments and the second layer is interpreted as Mesozoics. The Tertiary sediments are also found in the southern part of the profile from Moti Vamoti to Nundhatad villages and Raydhanjar to Lathedi villages (Fig. 6.6). The Mesozoics are found at the surface between Desalpar to Moti Vamoti and Nundhatad to Raydhanjar villages. A small patch of Deccan Trap is found at the surface from Muru to Desalpar villages.



Fig. 6.5: The location map of the MT profile (black triangles)

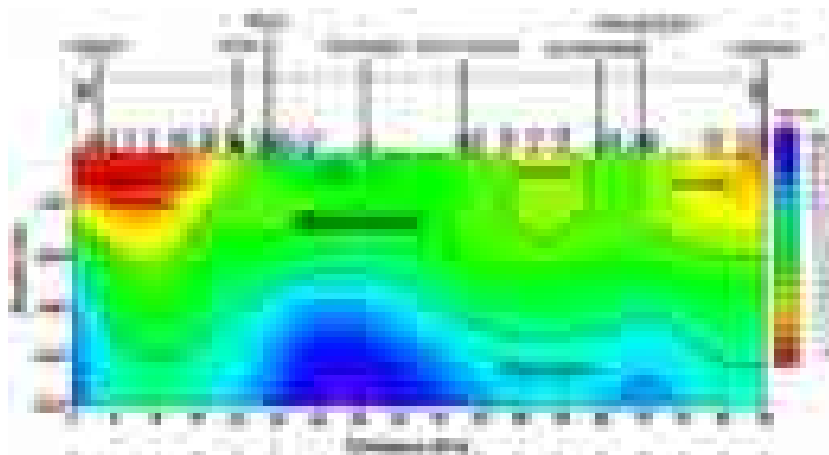


Fig. 6.6: 1-D resistivity section along the profile

6.3 Estimation of sediment thickness (including Mesozoic) considering multiple Magnetotelluric data inversion techniques in the western central part of the Kachchh Basin

(Pruthul Patel, Kapil Mohan and Peush Chaudhary)

A Magnetotelluric survey was conducted along a profile of length 55 km with a station spacing of 2-3 km in the western central Kachchh, from Shervo village in the north to Dujapar village in the south, to estimate the Mesozoic sediment thickness. Three different inverse modelling techniques, namely Occam linearized inversion, Bostick Inversion and smoothed inversion (Zond1DMT) have been applied to the data. Results reveal three different types of subsurface layer sequences. In the northern part of the profile, ~1000 m thick Mesozoic sediments with resistivity in the range of 2-15 Ωm are present beneath the ~700-800 m conductive (from 0.5 Ωm to 2 Ωm), recent (Quaternary-Tertiary) sediments. In the southern part of the profile, ~1500 m thick Mesozoic sediments are observed to be resting on a ~400-500 m thick resistive (from 50 Ωm to 90 Ωm) Deccan basalt. The ~1800-2000 m thick Mesozoic sediments are imaged as a shallow conductive layer overlying the resistive crystalline basement rocks in the

middle of the profile. The Mesozoic sediment thickness is estimated to be ~1500-2000 m in the study area, which correlates well with the lithology from a borehole drilled nearby. The dimensionality analysis reveals a 1D structure <10 s, which is verified by 1D forward modelling. The obtained model is also compared with the drilled borehole in the area (Fig. 6.7). The layered resistivity models from different 1D inversion techniques in the southern, central and northern segments of the MT profile are shown with the generated geological model, in Fig. 6.8.

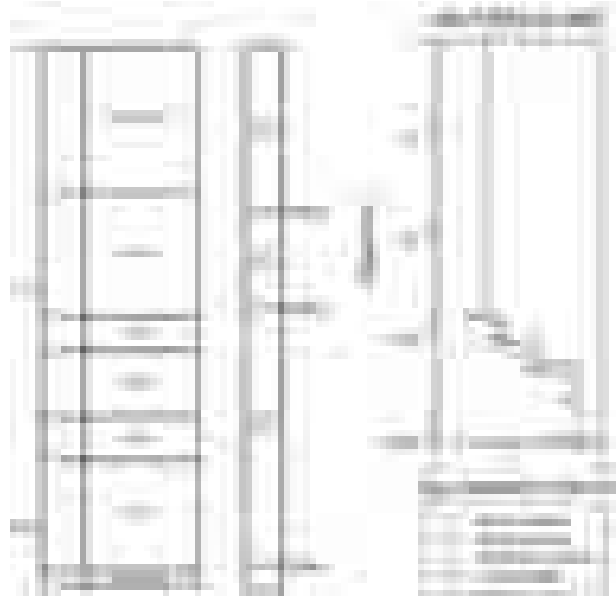


Fig. 6.7: Correlation of layered resistivity model and Nirona ONGC well data.

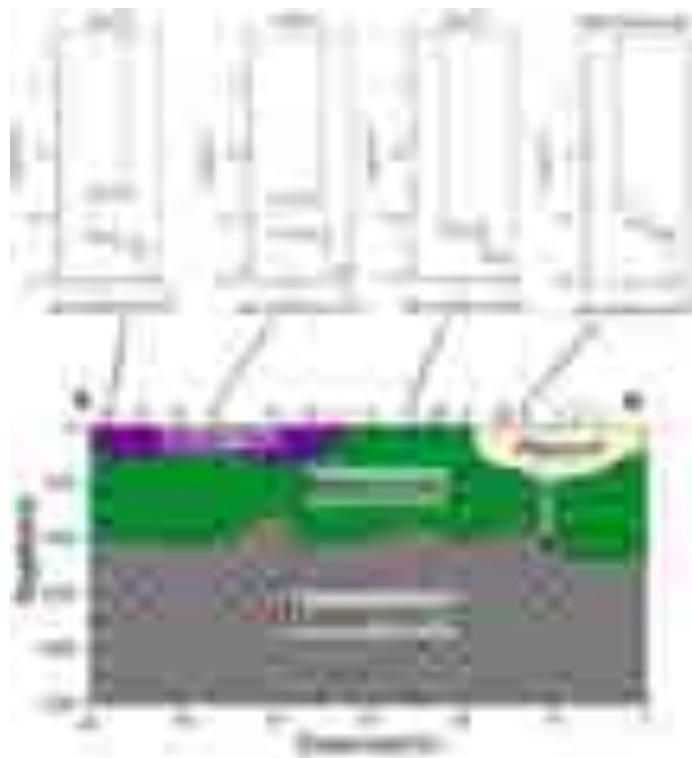


Fig. 6.8: Geological model of the study area with layered resistivity models for the sites representative of southern, central and northern segments of the MT profile is shown on top.

6.4 Site specific seismic hazard assessment and development of ground response spectra for Ammonia Storage tanks at HURL compound Barauni (Bihar)
(Kapil Mohan, Naveen Kumar, Madan Mohan Raut, Neha Tanwar and Sumer Chopra)

M/s. L&T Hydrocarbon Engineering has requested ISR to conduct site specific seismic hazard assessment and develop ground response spectra for ammonia storage tanks at HURL compound Barauni, Bihar (Fig. 6.9). The soil testing at 8 boreholes down to a depth of ~80 m (6 are of ~40.5m depth, 1 of 50.5m and 1 of 80.25m) in the study area and the geotechnical analysis report was prepared by M/s C E Testing Company Pvt. Ltd., Kolkata.

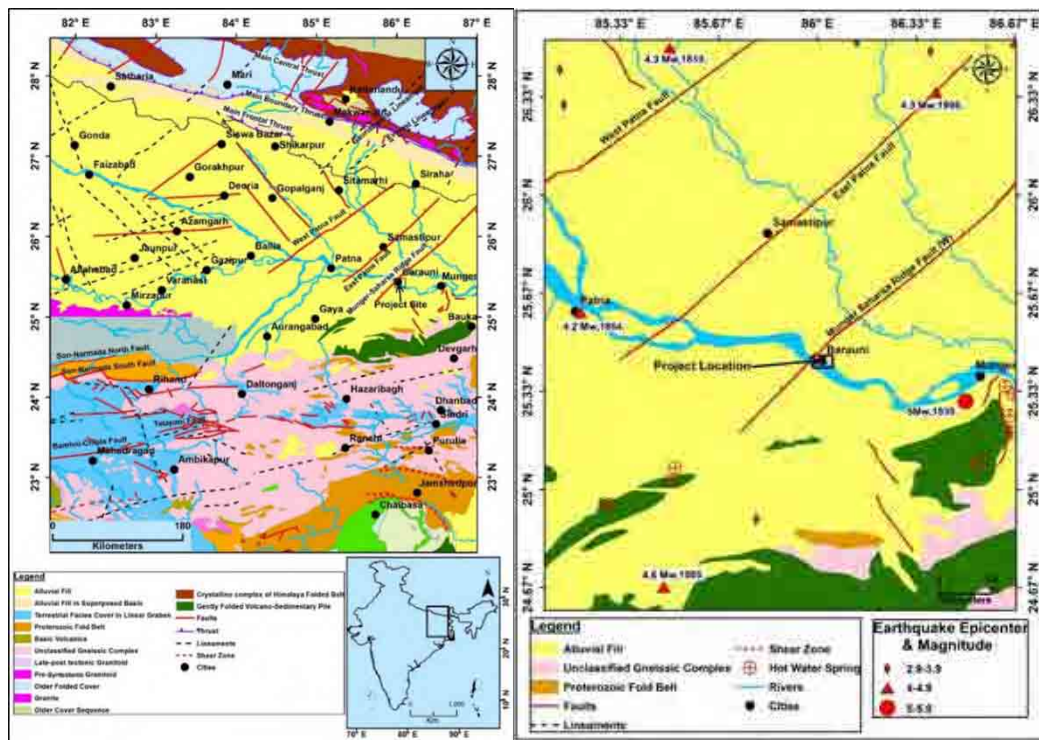


Fig. 6.9: The geological and seismotectonic map of Bihar and Surroundings (left), Barauni Project site and Surroundings (right). The geology is inferred from atlas (GSI, 2000).

ISR has estimated the seismic hazard using both probabilistic and deterministic methodologies. The PSHA has been conducted for 1% (4975 yrs. return period), 2% (2475 yrs. return period) and 10% (475 yrs. return period) probability of exceedance in 50 years for C-type (NEHRP) soil condition. The Deterministic seismic hazard assessment (DSHA) is conducted for three magnitudes, 5.5, 6.0 and 6.2, corresponding to return periods of 475 yrs (Operating Basis Earthquake), 2475yrs (Maximum Credible Earthquake) (SSE-I) and 4975 yrs (Safe Shutdown Earthquake) (SSE-II), respectively.

Detailed calculations are carried out at all the boreholes drilled at the site. The Engineering Bed layer (EBL) is estimated based on the Geophysical (cross-hole survey) and Geotechnical investigations. The EBL is found to vary between 37 and 39 m. The PGAs are estimated corresponding to return periods of 475 yrs, 2475 yrs and 4975 years from PSHA as well as DSHA, at EBL and at the surface. The PGAs estimated through DSHA have been found slightly higher than the PGAs estimated through PSHA for 10% probability of exceedance, and lower

for 1% & 2% probability of exceedance in 50 years. The higher PGA values have been considered for computation of the design spectra. The response spectra estimated at the surface of all boreholes using DSHA for magnitude Mw 6.0 is shown in Fig. 6.10. The higher PGA values were considered for the computation of design spectra.

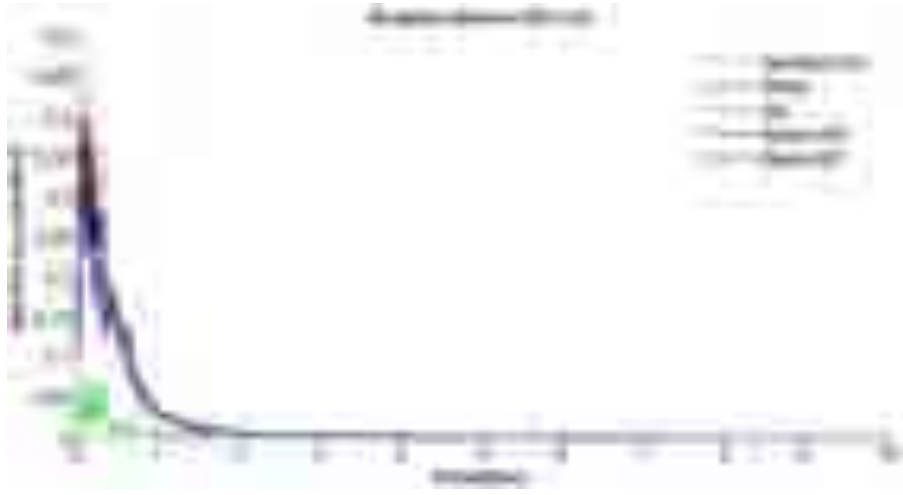


Fig. 6.10: The response spectra (Mean, Mean+SD and Mean-SD) at 5% damping estimated at the surface due to earthquake of magnitude Mw 6.0.

6.5 Seismic hazard assessment and development of site specific ground response spectra for Ammonia Storage tanks at HURL compound Sindri (Jharkhand) (Kapil Mohan, Naveen Kumar, Shruti Dugar, Madan Mohan and Sumer Chopra)

The M/s. L&T Hydrocarbon Engineering Ltd., Jamshedpur, Jharkhand has requested the Institute of Seismological Research to conduct site specific seismic hazard assessment and development of site-specific ground response spectra for Ammonia Storage tanks at HURL compound Sindri (Jharkhand) (Fig.6.11). The Soil Testing report of 10 boreholes up to a depth of ~10m drilled in the study area was provided to ISR. The geotechnical analysis report was prepared by M/s C. E. Testing Company Pvt. Ltd., Kolkata. ISR has conducted both Probabilistic Seismic Hazard Assessment (PSHA) (zoning map has been shown in Fig. 6.12) and Deterministic Seismic Hazard Assessment (DSHA) to estimate the Seismic Hazard at the Ammonia Storage tanks. The PSHA has been conducted for 1% (4975 yrs. return period), 2% (2475 yrs. return period) and 10% probability of exceedance in 50 years (475 yrs. return period) for C-type NEHRP soil condition. The NEHRP amplification factor is applied to estimate the surface Peak Ground Acceleration (PGA).

The Deterministic seismic hazard assessment (DSHA) is conducted for three magnitudes, 5.5, 6.0 and 6.2 estimated from the catalogue prepared from 1100 to 2018 AD corresponding to return periods of 475 yrs, 2475 yrs and 4975 years. An Mw 5.5 earthquake corresponds to a return period of 475 yrs (Operating Basis Earthquake, (OBE), Mw 6.0 is for return period of 2475yrs (Maximum Credible Earthquake) (SSE-I) and Mw 6.2 for return period of 4975 yrs (Safe Shutdown Earthquake) (SSE-II).

The detailed calculations have been carried out at all the boreholes drilled at the site. The Engineering Bed layer (EBL) is estimated based on Geophysical (cross-hole survey) and

Geotechnical investigations. The EBL is found to vary between 2.0 m and 5.5m depth. The PGA and response spectra are estimated at EBL and ground surface. The PGAs have been estimated for return periods of 475 yrs, 2475 yrs and 4975 years from both PSHA as well as DSHA. The PGA estimated through DSHA has been found to be slightly higher than the PGA estimated through PSHA for 10% probability of exceedance, and lower for 1% & 2% probability of exceedance in 50 years. The higher PGA values have been considered for computation of design spectra. The response spectra estimated at the surface of all boreholes using DSHA for magnitude $M_w 6.2$ are given in Fig.6.13. The design spectra corresponding to all three return periods were proposed for the Ammonia Storage Tank site.



Fig. 6.11: (a) SRTM 30arc Model of Bihar, Jharkhand and West Bengal states showing main tectonic units and earthquakes in the region, (b) Geological NWW-SEE cross section along main tectonic units and faults in the study area (modified from Singh et al., 1998).



Fig. 6.12: Seismotectonic map of the study area and its surrounding region. MCT: Main Central Thrust, MBT: Main Boundary Thrust, ISZ: Indus Suture Zone, MF: Moradabad Fault, GBF: Great Boundary Fault, WPF: West Patna Fault, MSRF: Munger Sahasra Ridge Fault, MSRMF: Munger Sahasra Ridge Marginal Fault.



Fig. 6.13: The response spectra (Mean, Mean+SD and Mean-SD) at 5% damping estimated through DSHA at the surface due to earthquake of magnitude Mw 6.2.

6.6 Delineation of freshwater layer at the selected sites in the Anjar Taluka of Kachchh using Time Domain Electromagnetic Survey

(Kapil Mohan, Sumer Chopra, Pavan Gayatri, P. Mahesh, Pruthul Patel, Indu Chaudhary, Rakesh Nikam, Mehul Nagar and Naveen Kumar)

The Gujarat Water Resources Development Corporation (GWRDC) invited the Institute of Seismological Research (ISR) to conduct Time Domain Electromagnetic (TDEM) survey to locate fresh water zones at some of the sites in the Anjar and Bhuj Talukas, with a target depth down to 600 m. ISR carried out TDEM survey at 16 sites for mapping the fresh water aquifer layers and their thickness. The selected sites are located in different geological settings namely, Tertiary, Cretaceous and Deccan Trap. Six sites are located on Tertiary

formations (site no. 1, 3, 4, 10, 12 and 13), five sites on Cretaceous formations (site no. 2, 5, 6, 7 and 9) and three sites on Deccan Traps (site no. 8, 15, 16). The locations where TDEM investigations were carried out are shown in Figure 6.14. Two sites were rejected due to poor data quality/site dimension issue.

The GDP 32-II data acquisition unit (Zonge, USA) together with a transmitter, generator-powered GGT-30 for larger loops system is used to conduct TDEM field survey with 200 m square transmitter loop. The GDP 32-II was positioned at the center of each loop and ferrite-cored antenna is used to take the measurements. Most typical TDEM array is represented by a square loop, in which a trapezoidal (typically square wave form) current waveform is driven. This current induces secondary (eddy) currents within the Earth, the rate of change of which produces an electromotive force (emf) that is picked up by a receiver coil normally located in the loop centre. The amount of current injected in the transmitter loop is 9 Amps for all the TDEM sites. For each loop, the transmitter is operated for a sequence of data repetition frequencies ranging from 32 Hz to 1 Hz (32, 16, 8, 4, 2 and 1Hz). In the early and late times, the apparent resistivity is in general noisy and is removed for further inversion process, whenever necessary. These transient decay curves obtained by the survey were used to find out the depth and subsurface resistivity of the basin fill.

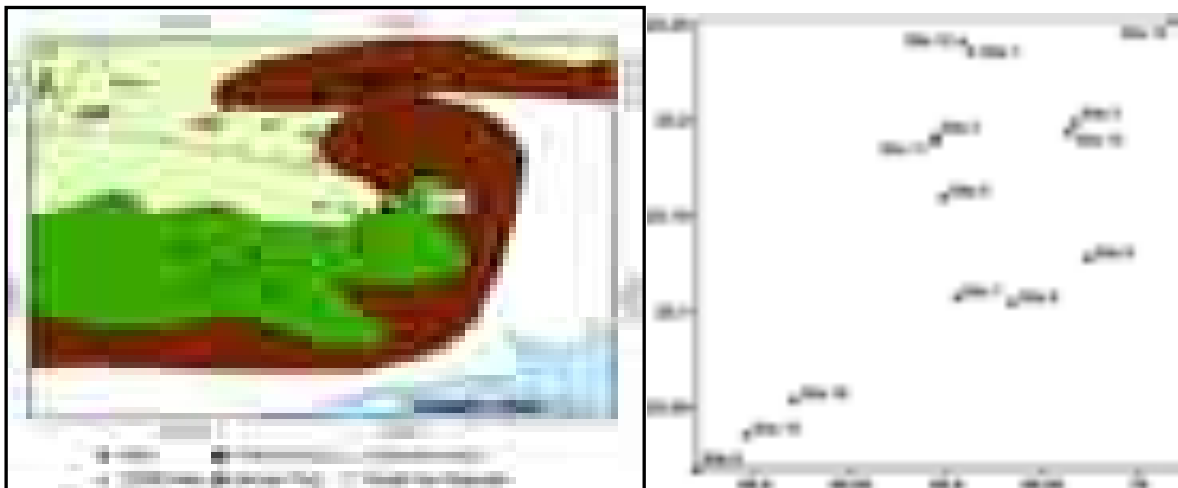


Fig. 6.14: The geological map of the study area overlapped with borewell locations and acquired TDEM sites (left) and (b) Distribution of the TDEM sites (right).

ISR has used the data recorded at 4Hz, 8Hz and 2Hz transmitter frequency for one dimensional (1D) inversion based on quality and depth of penetration. The 1-D modelling of the TDEM soundings derived using STEMINV (Zonge, USA) package is used to prepare layered-earth resistivity models. The program uses an iterative best-fit algorithm to minimize the RMS residuals between the observed and calculated apparent resistivity. After generating the initial model, data points that are either anomalous or could not fit any earth model due to large error bars are selectively discarded from the voltage vs. time decay curve. After removing the anomalous points, the inversion is re-executed to create the best possible model. Inversion results for four sites and the matching between voltage vs. time decay curve are shown in Figure 6.15.

The 1-D models at two sites are shown in Figure 6.16. The resistivity sounding data have been first analysed in terms of resistivity and thickness of the layers. The resistivity data along with the subsurface profile generated from the provided lithologs is shown in Figure 6.17.

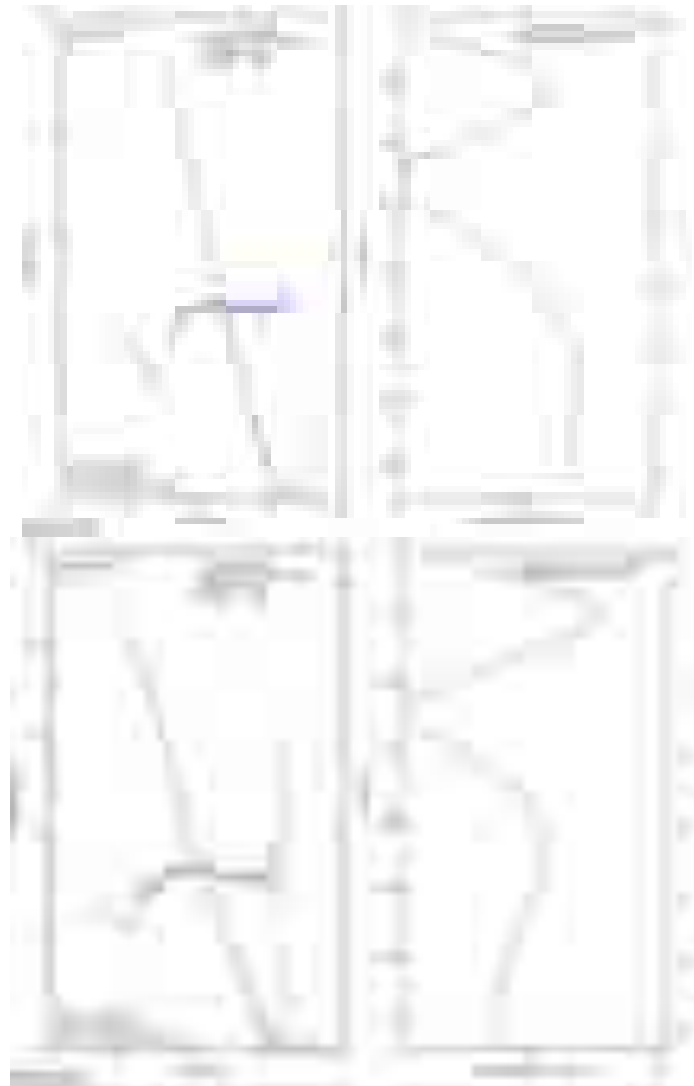


Fig. 6.15: Data fit (right) between observed and computed response using the model obtained from inversion (left).

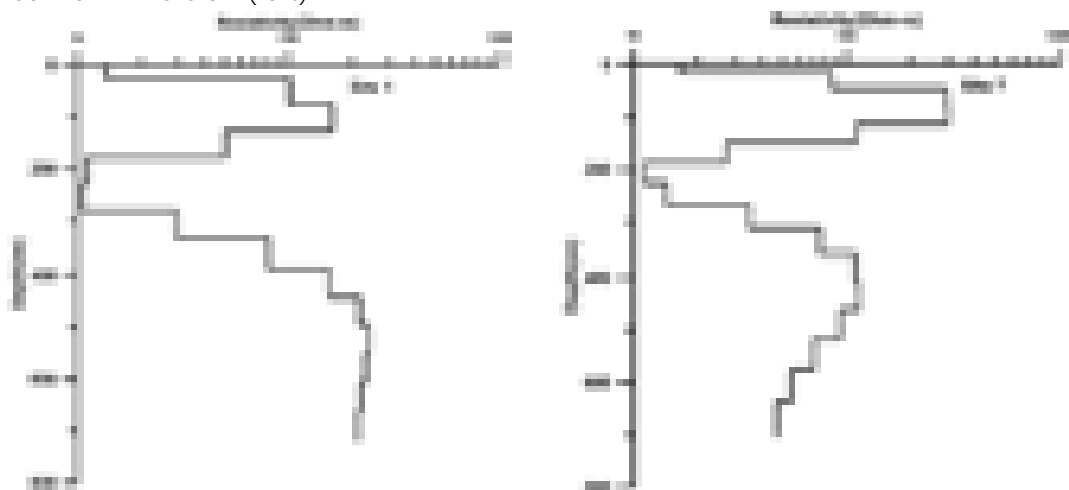


Fig. 6.16: The 1D resistivity structure of the sites 1 and 7.

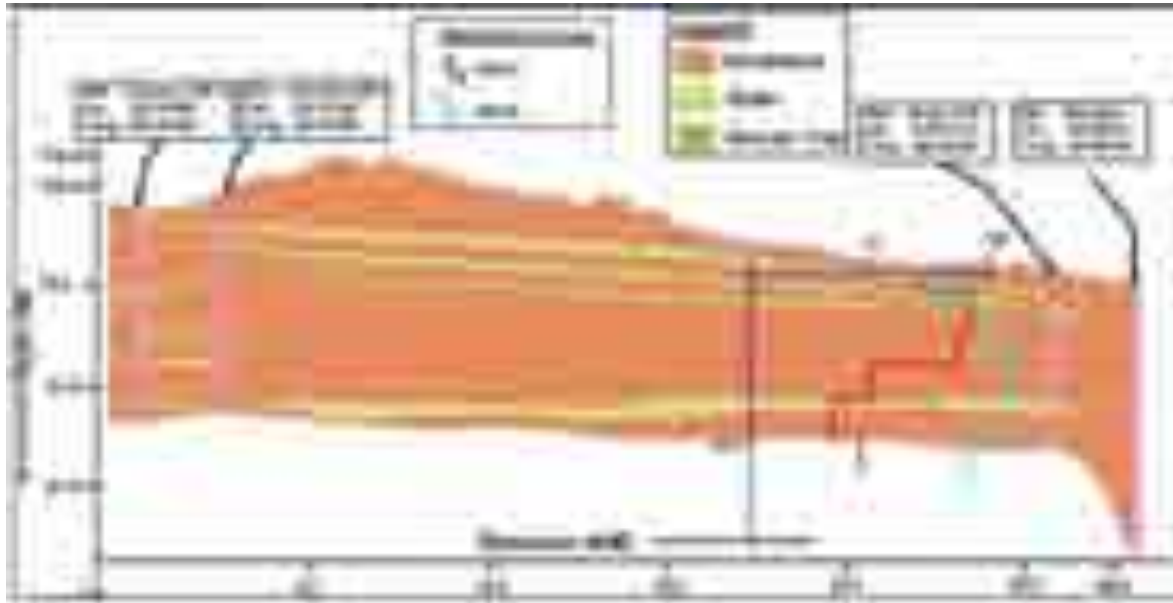


Fig. 6.17: The lithological section (EW) in the central part of the study area overlapped with the 1D resistivity sections of the Site 5 and Site 9.

The area of investigation is covered with three different rock types; Tertiary in the north, Cretaceous in the central and Deccan Trap in the southern part. The borehole data of up to 200 m depth is provided by the GWRDC for validation purpose. The geophysical data interpretation below 200 m depth was done on the basis of lithology suggested in the past literature and resistivity values obtained from the TDEM survey. Three sites were suggested, where freshwater may be present.

6.7 Delineation of Freshwater layer at the selected sites in the Lakhpat, Abdasa and Banni areas of Kachchh using Time Domain Electromagnetic Survey (Kapil Mohan, Pruthul Patel, Mehul Nagar, Akash Solanki and Sumer Chopra)

The Gujarat Water Resources Development Corporation (GWRDC) invited Institute of Seismological Research (ISR) to conduct Time Domain Electromagnetic (TDEM) survey to locate fresh water zones at 32 sites in the Lakhpat, Abdasa, Banni and Mandvi areas of Kachchh (Figure 6.18). The GDP 32-II data acquisition unit (Zonge, USA) together with a transmitter, generator-powered GGT-30 for larger loop system is used to conduct TDEM field survey with 200 m square transmitter loop. The survey was conducted in February-March 2019. The TDEM data was processed for 16Hz, 8Hz and 2Hz transmitter frequency for one dimensional (1D) inversion based on quality and depth of penetration. The 1-D modelling of the TDEM soundings using STEMINV (Zonge, USA) package is undertaken to prepare layered-earth resistivity models. The 1D resistivity models for the Lakhpat and Narayan-Sarovar sites are shown in Figure 6.19. The final interpretation of the data is in progress.



Fig. 6.18: TDEM sites at the various locations of Kachchh on a geological map (Biswas, 2005).

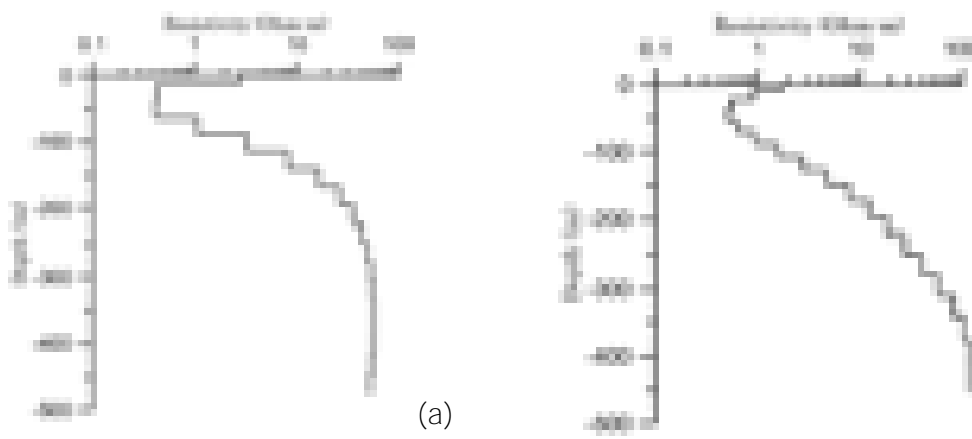


Fig. 6.19: The 1D resistivity structure of the (a) Lakhpat and (b) Narayan Sarovar sites.

6.8 Geophysical survey (Electrical and Time Domain Electromagnetic) for Delineation of groundwater in the Majivana Taluka of Porbandar (Pruthul Patel, Akash Solanki and Kapil Mohan)

The Horticulture department, Government of Gujarat has requested the Institute of Seismological Research to conduct the geophysical survey to delineate ground water level at a site proposed for the Centre of Excellence (CoE) at Majivana (Taluka & District: Porbandar). Therefore, we conducted electrical survey along 3 profiles (using Syscal Pro switch 72 instrument) of lengths ~420 m to 490 m (Figure 6.20) and mapped the subsurface down to a depth of 60 m to 70 m. We have also conducted Time Domain Electromagnetic survey with GDP 32-II data acquisition unit, together with a transmitter, generator-powered GGT-30 (Zonge, USA) at a site where we could retrieve information down to 300 m depth. The electrical data has been processed and the resistivity values are inverted using Res2dinv software. The generated 2D resistivity section is given in Figure 6.21. The TDEM data inversion has been conducted with the STEMINV (Zonge, USA) software. After processing and modelling

the geophysical data, the probable source for groundwater is proposed at >65 m depth in the central part of the CoE.

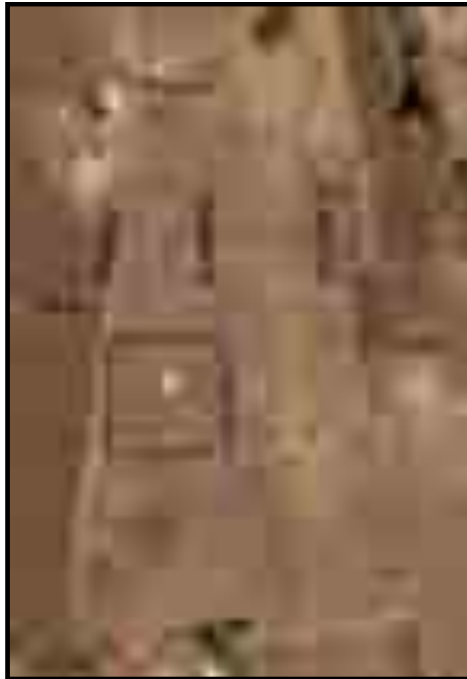


Fig. 6.20: DC- Resistivity profiles (Blue lines) and one TDEM site

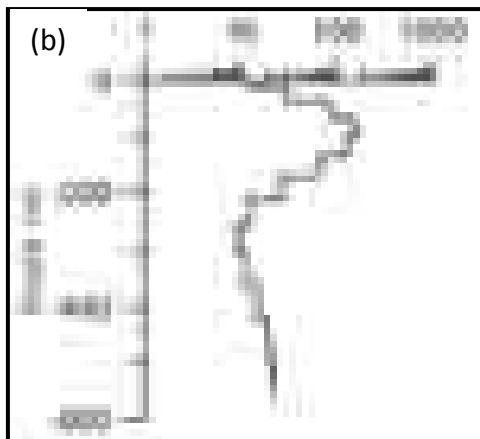
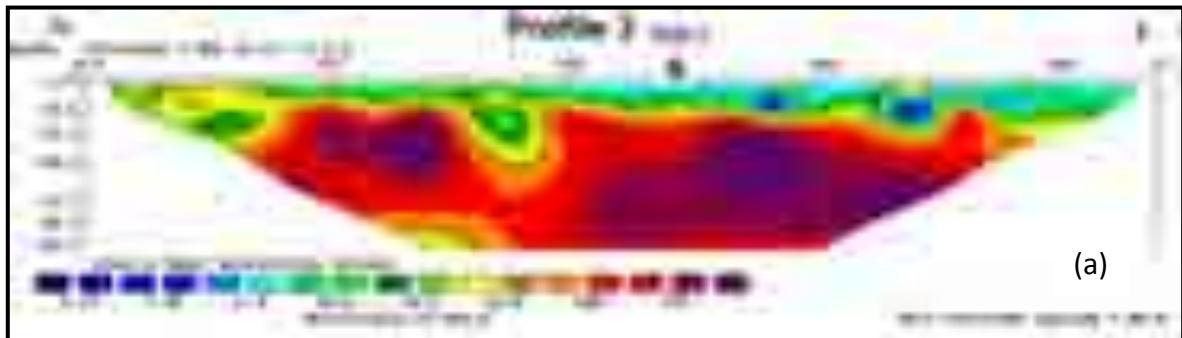


Fig. 6.21: (a) 2D resistivity section generated from the electrical survey and (b) 1D resistivity section generated from the TDEM survey.

PUBLICATIONS

Published

- ✦ Abdul Azeez, K.K., Mohan, K., Veeraswamy, K., Rastogi, B.K., Gupta, A. K., Harinarayana, T. (2018) 3D crustal resistivity structure beneath the Wagad aftershock zone of the 2001 Bhuj earthquake, Kutch, India: Heterogeneous resistivity structure controlled by widespread fluid infiltration and clues to aftershocks pattern, *Tectonophysics*, 747–748, 54–67.
- ✦ Basavaiah, N., Mahesh Babu, J.L.V., Prizomwala, S.P., Achyuthan, H., Siva, V.H.R., Boral, P. (2018) Proxy mineral magnetic and elemental analyses for 2004 tsunami impact deposit along the Muttukadu backwater, East Coast of India: Scope of the palaeotsunami studies, *Quaternary International*, doi: 10.1016/j.quaint.2018.10.038.
- ✦ Bhatt, N., Pancholi, V., Chopra, S., Rout, M. M., Shah, R. D and Kothyari, G. C. (2018) Rapid Seismic Hazard Assessment of Sabarmati River basin Gujarat, using GIS Techniques, *Bulletin of Engineering Geology and the Environment*, <https://doi.org/10.1007/s10064-018-1373-8>.
- ✦ Choudhury P., Chopra S., Kumar M. R. (2018) A review of seismic hazard assessment of Gujarat: A highly active intra-plate region, *Earth-Science Reviews*, doi: <https://doi.org/10.1016/j.earscirev.2018.09.014>.
- ✦ Choudhury, P., Gahalaut, K., Dumka, R. K., Gahalaut, V. K., Singh, A. K., Kumar, S. (2018) GPS measurement of land subsidence in Gandhinagar, Gujarat (Western India), due to groundwater depletion. *Environmental Earth Sciences* 77(22), DOI: 10.1007/s12665-018-7966-5.
- ✦ Chaudhary P., Mohan K. and Chaudhary B.S. (2019) Magnetotellurics study to identify subsurface structure in the eastern part of Kachchh (Little Rann area) of Gujarat, India, *Pure and Applied Geophysics*, <https://doi.org/10.1007/s00024-019-02102-w.2>.
- ✦ Dumka R. K., Chopra, S. and Prajapati S., GPS derived crustal deformation analysis of Kachchh, zone of 2001 (M7.7) earthquake, western India, *Quaternary International*, <https://doi.org/10.1016/j.quaint.2019.01.032>.
- ✦ Dumka, R.K., Choudhury, P., Gahalaut, V.K., Gahalaut, K., Kumar, R., 2018, GPS measurements of deformation caused by seasonal filling and emptying cycles of four hydroelectric reservoirs in India. *BSSA*, 108(5B), 2955–2966.
- ✦ Dumka R. K., Kotlia B. S., Kothyari G. C., Paikray J., Dimri, S. 2018. Detection of High and Moderate Crustal Strain Zones in Uttarakhand Himalaya, India, *Journal of Acta Geodetica*, DOI: 10.1007/s40328-018-0226-z.
- ✦ Dumka, R.K., Kotlia, B.S., Suri Babu, D., Narain, P., Prajapati, S., 2019, Present-day crustal deformation and geodetic strain in the vicinity of Dholavira - Harappan civilization site, Kachchh, the western part of the Indian plate, *Quaternary International*, 507, 324-332.
- ✦ Gayatri, P., Choudhury, I., Nagar, M., Chauhan, A., Prizomwala, S. P., Mahesh, P., Chopra, S. (2018) Transient Electromagnetic investigations in a tectonic domain of the Kachchh intraplate region, western India: A morphotectonic study of the Kachchh Mainland Fault, *Tectonics*, 37 (11), 4239-4260.
- ✦ Joshi N., Singh S., Pant P. D., Kumar M., and Kothyari G. C. (2018). Polyphase Kinematics and Quaternary reactivation of Baijnath Klippe: Western Kumaun Himalaya. *International journal of earth sciences* (accepted).
- ✦ Joshi, V., Chopra, S. and Kumar, S., (2018) A Local Magnitude Scale ML for the Kachchh rift basin: an active intraplate region, Gujarat, India, *BSSA*, doi: 10.1785/0120180138

- ✦ Kothyari, G. C., Joshi N., Taloor A.K., Kandregula R.S., Pant C.C. and Singh R.K. (2019) Landscape evolution and deduction of surface deformation in Soan Dun area of NW Himalaya, India: A Geomorphic approach, Quaternary International, <https://doi.org/10.1016/j.quaint.2019.02.016>.
- ✦ Kothyari, G.C., Kandregula, R.S., Pancholi, V., and Shah, N., (2018) Identification of fluvial stratigraphy using shallow subsurface geophysical and field investigations: a case study from Sabarmati River terraces, mainland Gujarat, Journal of Indian Geophysical Union, 22(6), 659-668.
- ✦ Kothyari, G. C., Srivalkar, P., Kandregulla, R. S., Rawat, Y. S., Dumka, R. K., Joshi, N. (2018) Holocene tectonic activity along Kachchh Mainland Fault: Impact on late mature Harappan civilization, Kachchh, western India, Quaternary International, DOI: 10.1016/j.quaint.2018.10.032.
- ✦ Makwana, N. M., Prizomwala, S. P., Chauhan, G., Phartiyal, B., Thakkar, M. G. (2018) Late Holocene palaeo-environmental change from the Banni Plains, Kachchh, Western India. Quaternary International, <https://doi.org/10.1016/j.quaint.2018.11.028>.
- ✦ Modi R. and Mohan, K., Rapid visual screening of RC frame building in Rambaug area of Ahmedabad, Gujarat, Journal of Indian Geological Union 23(2), 143-151.
- ✦ Mohan, K., Chaudhary, P., Gayatri, P., Kothari, G.C., Choudhary, V., Nagar, M., Patel, P., Gandhi, D., Kushwaha, D. and Rastogi, B.K. 2018. "Magnetotelluric study in Tuwa (Godhra) region, Gujarat, India". Pure and Applied Geophysics. doi: 10.1007/s00024-018-1883-0.
- ✦ Mohan, K., Chaudhary P., Gayatri, P., and Rastogi B.K. (2019) Magnetotelluric investigations in southern end of the Cambay basin near coast, Gujarat, India, Journal of Applied Geophysics, <https://doi.org/10.1016/j.jappgeo.2019.01.011>.
- ✦ Moiya, J.N., Luirei, K., Longkumer, L., Kothyari, G.C. and Thong, G.T. (2019) Late Quaternary deformation in parts of the Belt of Schuppen of Dimapur and Peren districts, Nagaland, NE India, Geological Journal, doi.org/10.1002/gj.3413.
- ✦ Paul, H., Priestley, K. F., Powali, D., Sharma, S., Mitra, S. and Wanchoo, S. (2018) Signatures of the existence of frontal and lateral ramp structures near the Kishtwar Window of the Jammu and Kashmir Himalaya: Evidence from microseismicity and source mechanisms, Geochemistry, Geophysics, Geosystems, doi.org/10.1029/2018GC007597
- ✦ Prizomwala, S. P., Gandhi, D., Bhatt, N. P., Winkler, W., Kumar M. R., Makwana, N., Bhatt, N. Y. (2018) Geological evidence for AD 1008 tsunami along the Kachchh coast, Western India: Implications for hazard along the Makran Subduction Zone, Scientific Reports, 8, 16816.
- ✦ Prizomwala, S. P., Yadav, G., Bhatt, N. P., Sharma, K. (2018) Late Pleistocene relative sea level changes from Saurashtra, west coast of India, Current Science, 115 (12), 2297-2301.
- ✦ Prizomwala, S.P., Yadav, G., Bhatt, N., and Sharma, K., (2018) Late Pleistocene sea level changes from Saurashtra, west coast of India, Current Science, 115(12), 2297-2301.
- ✦ Prizomwala, S. P., Yadav, G., Solanki, T., Das, A., Chauhan, G., Makwana, N. (2018) Style and stages of valley fill aggradation-incision cycles in the Northern Hill Range, Kachchh, Quaternary International, <https://doi.org/10.1016/j.quaint.2018.11.020>.
- ✦ Sairam, B., Singh, A.P., and Kumar, M.R. (2018) Comparison of earthquake source characteristics in the Kachchh Rift Basin and Saurashtra horst, Deccan Volcanic Province, western India. J Earth Syst Sci 127, 55. <https://doi.org/10.1007/s12040-018-0957-9>
- ✦ Sairam, B., Singh, A. P., Patel, V., Pancholi, V., Chopra, S., Dwivedi, V.K., and Kumar, M.R. (2018), Influence of Local Site Effects in the Ahmedabad Mega City on the Damage

Due to Past Earthquakes in Northwestern India, *Bulletin of the Seismological Society of America* 108 (4), 2170-2182.

- ✦ Sharma, J., Kumar, M. R., Roy, K. S., Roy, P. N. S., (2018) Seismic Imprints of Plume-Lithosphere Interaction Beneath the Northwestern Deccan Volcanic Province. *Journal of Geophysical Research: Solid Earth*, 123. doi:10.1029/2018JB01594
- ✦ Singh, A. P., Koulakov, I., Kumar, M. R., Kayal, J. R. (2018) Seismic Velocity Structure and Intraplate Seismicity beneath the Deccan Volcanic Province of Western India, *Physics of The Earth and Planetary Interiors*, 287, 21-36.
- ✦ Singh, D. K., Mohan, K., Nagar, M., (2018) Dimensionality and Directionality Analysis of the Magnetotelluric Data along the Coastal part of Western Saurashtra, Gujarat, *Journal of Indian Geophysical Union*, 23(1):41-54.
- ✦ Sinha, R. K., Vijayan S., Shukla, A. D., Das, P., Bhattacharya, F., 2018. Gullies and debris-flows in Ladakh Himalaya, India: a potential Martian analogue, *Geological Society, London, Special Publications*, 467, <https://doi.org/10.1144/SP467.9>.
- ✦ Solanki, T., Prizomwala, S. P., Solanki, P. M., 2018. Geomorphic Expressions of Active Strike-slip faulting (Girnar Fault), Saurashtra, Western India, *Journal of Indian Geophysical Union* 22 (4), 411-418.
- ✦ Srijayanthi, G., Kumar, M. R., (2019) Subslab anisotropy in the Andaman subduction zone controlled by slab dip?. *Physics of the Earth and Planetary Interiors*, 286, 21-28.
- ✦ Talukdar, R., Kothyari, G. C. and Pant, C. C. (2018) Evaluation of neotectonic variability along major Himalayan thrusts within the Kali River Basin using geomorphic markers, Central Kumaun Himalaya, India, *Geological Journal*, doi: 10.1002/gj.3452.
- ✦ Vemuri, J., Kolluru, S. and Chopra, S., (2018) Surface Level Synthetic Ground Motions for M7.6 2001 Gujarat Earthquake, *Geosciences*, doi.org/10.3390/geosciences8120429
- ✦ Yadav, R.K., Gahalaut, V.K., Bansal, A.K., Sati, S.P., Catherine, J., Gautam, P., Kumar, K. and Rana, N., (2019). Strong seismic coupling underneath Garhwal–Kumaun region, NW Himalaya, India. *Earth and Planetary Science Letters*, 506, pp.8-14.

Under review/ communicated

- ✦ Bhatt, N., Pancholi, V., Chopra, S., Malik, K., Shah, R. D., Naddaf, M. (2018) Co-seismic ground deformation detection of the Mw 7.3 western Iran earthquake of 2017 using SAR Interferometry, *Arabian Journal of Geoscience*.
- ✦ Chouhan, A.K., Choudhury, P., and Pal, S.K., (2018) New evidence for a thin crust and magmatic underplating beneath the Cambay rift basin, Western India through modelling of EIGEN-6C4 gravity data, *Pure and Applied Geophysics*.
- ✦ Chouhan, A.K., Singh, D., Chopra, S. (2018) Structural interpretation over the epicentre zone of 1819 Allah-Bund earthquake, North-western India in an intraplate setup using gravity data, *JGSI*.
- ✦ Das, A., Joseph, J.K., Solanki, T., Makwana, N., Chauhan, G., Thakkar, M.G., (2019) Climate-tectonic interplay from the dryland fluvial landscape of the Southern Kachchh Mainland, Western India: Insights from new OSL and sedimentological datasets. *Geological Journal*.
- ✦ Das A., Prizomwala, S., Makwana, N., Chauhan, G., Vedpathak, C., Sodhi, A., Thakkar, M. G. (2018) A review of Middle Holocene high sea stand deposits from the west coast of India, *Open Quaternary*.
- ✦ Das, A., Prizomwala, S.P., Sodhi, A., Vedpathak, C., Makwana, N., Solanki, T., and Achyuthan, H., (2018) New look into some coastal Harappan sites, Saurashtra, Western India: Implications in human-landscape relationship. *Current Science*.
- ✦ Das, A., Prizomwala, S.P., Solanki, T., Chauhan, G., Thakkar, M.G., Bhatt, N.P., (2018) Relative Assessment of Tectonic Activity along the seismically active Katrol Hill Fault, Kachchh, Western India, *Journal of Geological Society of India*.

- ✦ Dumka, R.K., Chopra, S., Prajapati, S., (2018) GPS derived crustal deformation study of NSL, Journal of Trinova.
- ✦ Dumka, R. K., Suri Babu, D., Prajapati, S. (2018) Characterization of Ionospheric TEC Based on the GPS data between 2009 to 2015 towards western India, Journal of Earth and Space Physics.
- ✦ Dumka, R.K., Paikray, J., Prajapati, S., Disparity in TEC using GPS data during one Himalayan and one Kachchh earthquake (2018) Journal of Remote Sensing.
- ✦ Dwivedi, V. K., Dubey R K., Pancholi, V., Patel V., Sairam B., Chopra, S. (2018) Regression relationship between Standard Penetration Test (SPT) N1(60) and shear wave velocity for different soils in Ahmadabad city, Gujarat, Western India, Natural Hazards.
- ✦ Gahalaut, V.K., Gahalaut, K., Dumka, R.K., Choudhury, P., Yadav, R.K., (2018) Geodetic evidence of high compression across seismically active Kachchh paleo-rift, India, GRL.
- ✦ Haldar, C., Kumar, P., Kumar, M.R., and Ray, L., (2018) On the nature of Indian Moho, J. Geophys. Res.
- ✦ Haldar, C., Kumar, P., Kumar, S., (2018) Widespread crustal magmatism in the Kachchh region— Evidence from shear wave velocity contrast across Moho, Solid Earth.
- ✦ Kothiyari, G., Talukdar, R., Kotlia, B. S., Pant, C. C. (2018) Evidences of Neotectonic activity along the longitudinal length of Goriganga River Higher Central Kumaun Himalaya, International Journal of Earth Sciences.
- ✦ Kumar, N., Mohan, K., Dumka, R.K., Chopra, S., Evidence of Neotectonism in Quaternary Sediments From Dadra and Nagar Haveli, Western India (2018) Quaternary International.
- ✦ Kumar, P., and Mahender (2018), Transient electromagnetic imaging of Khari River Palaeochannel, Bhuj, Western India. J. A. Earth Sci.
- ✦ Kotlia, B.S., Dumka, R.K., Bisht, H., etc. Holocene tectonic activity along MBT in the Kumaun Himalaya, India (2018) Journal of Geomorphology.
- ✦ Mishra, S., Kothiyari, G. C., Dubey, R. K., Chauhan, G., Kandregula, R. S. (2018) Morpho-Structural evidence of Neotectonic activity along the Vigodi Fault, Kachchh, India, Journal of Geosciences Frontier.
- ✦ Misra, A., Agrawal, K.K., Talukdar, R., Kothiyari, G.C., (2018) An integrated approach for identifying active deformation in the foreland region of Central Indo-Nepal Himalaya: A geomorphic approach”, Geomorphology journal.
- ✦ Patel P., Mohan K., Chaudhary P., Estimation of Mesozoic thickness in the western central part of Kachchh Basin, Gujarat (India) using Magnetotellurics. Journal of applied geophysics (under review).
- ✦ Pancholi, V., Bhatt, N., Chopra, S., Singh, P (2018) Multi-criteria approach using GIS for macro-level seismic hazard assessment of Kachchh intraplate region, Gujarat, Western India— First step towards earthquake disaster mitigation, Journal of Environmental science.
- ✦ Pancholi, V., Bhatt, N.Y., Dwivedi, V.K., Choudhury, P., and Chopra, S., (2018) Estimation of the Liquefaction potential index for the capital city of Gujarat state, Western India, International Journal of Earthquake Engineering.
- ✦ Rout, M.M., Chopra, S., and Sairam, B. 2018, Probabilistic seismic hazard assessment at surface level for Gujarat state, Western India-an active intraplate region. Soil dynamics and earthquake engineering.
- ✦ Sairam, B., Kothiyari, G.C., Pavan Kumar, G., Patel, V., and Pancholi, V., Geophysical Investigations for Paleochannels and Possible Sources for Groundwater: A Case Study from Kachchh, Western Peninsular India.

- ✦ Sairam, B., Singh, A.P., Patel,V., Chopra, S., Kumar, M.R., (2018) VS30 Mapping and Site Characterization in the seismically active intraplate region of Western India - Implications for Risk Mitigation. Earthquake Spectra.
- ✦ Sateesh, A., Mahesh, P., Singh, A.P., Kumar, S., Chopra, S., Kumar, M.R., Monsoon, M., induced Earthquake Swarms in South Gujarat, Northwest Deccan Volcanic Province of India, Environmental Earth Sciences.
- ✦ Shreyasvi, C., Venkataramana, K., Chopra, S., Rout, M. M. (2018) Probabilistic Seismic Hazard Assessment of Mangalore and Its Adjoining Regions, A Part of Indian Peninsular, Pure and applied Geophysics.
- ✦ Solanki, A., and Mohan, K., The Scenario based Seismic Risk Assessment in the commercially important zone (sector 21) of Gandhinagar city, Gujarat, India" accepted in Journal of Indian Geophysical Union (JIGU).

Technical Reports

- ✦ **Final report of the project titled "Comparative seismic hazard assessment of Mumbai and GIFT City, Gandhinagar for establishment of Disaster Recovery Sites (DRS) by Multi Commodity Exchange of India Limited, Project PI: Dr. Kapil Mohan; Project coordinator: Dr. Sumer Chopra; Major contributors: Naveen Kumar and Shruti Dugar submitted to M/s Multi Commodity Exchange of India Limited, GIFT City, Gandhinagar, ISR Technical Report No.123, submitted in July 2018.**
- ✦ Mahesh, P.,Santosh Kumar, A.P. Singh, Ravi Kumar, M., Chpora, S., (2018). Earthquake data processing and interpretation of MEQ data collected during Jan. to Dec. 2017 for study the of Seismogenic sources around the Subansiri lower H.E. project, ISR Technical Report No. 124.
- ✦ A.P.Singh,Maynak Dixit, Ketan Singha Roy, Sumer Chopra, M. Ravi Kumar (2018) A report on low frequency passive seismic studies at hydrocarbon reservoir sites in Mansa and Jotana areas, Gujarat, (ISR Technical Report No. 125), Submitted to Oil Natural Gas Corporation, Kolkata, Vadodara, Gujarat.
- ✦ **Final report of the project "Site specific seismic hazard assessment and development of site specific ground response spectra for Ammonia Storage tanks at HURL compound Barauni (Bihar), Project PI: Dr. Kapil Mohan; Project coordinator: Dr. Sumer Chopra; Major contributors: Co-PI: Naveen Kumar Project contributor: Dr. Madan Mohan, Ms. Shruti Dugar and Ms. Neha Tanwar submitted to M/s L&T Hydrocarbon Engineering Limited, Patna, Bihar, ISR Technical Report No.126, in October 2018.**
- ✦ **Final report of the project "Site specific seismic hazard assessment and development of site specific ground response spectra for Ammonia Storage tanks at HURL compound Sindri, Jharkhand, Project PI: Dr. Kapil Mohan; Project coordinator: Dr. Sumer Chopra; Major contributors: Co-PI: Naveen Kumar Project contributor: Dr. Madan Mohan and Ms. Shruti Dugar submitted to M/s L&T Hydrocarbon Engineering Limited, Jamshedpur, Jharkhand, Technical Report No.127, in November 2018.**
- ✦ **Final Report of the project entitled "Magnetotelluric (MT) data acquisition, processing and interpretation (API) in the NELP Block no.- CB-ONN-2005/9", Project PI: Dr. Kapil Mohan, Co-PI: Peush Chaudhary, Project Participants: Pruthul Patel, Dilip Kushwaha, Vishal Vats, Russi Modi and Akash Solanki, ISR Technical Report 128, submitted to M/s Mercator Petroleum Ltd., Mumbai.**
- ✦ A.P.Singh, Harsh Limbachiya, Jai Pandit, Ketan Singha Roy, Sumer Chopra, M. Ravi Kumar (2019) A report on Feasibility study of Low Frequency Passive Seismic (LFPS) survey in NELP Block WB-ONN-2005/4, MBA Basin, Kolkata ONGC, ISR Technical Report No. 129, January 2019, Submitted to Oil Natural Gas Corporation, Kolkata, W. Bengal.

- ✦ Mahesh, P., Santosh Kumar, A.P. Singh, Ravi Kumar, M., Chpora, S., (2019). Earthquake data processing and interpretation of MEQ data collected during Jan. to Dec. 2018 for study the of Seismogenic sources around the Subansiri lower H.E. project, ISR Technical Report No. 130.
- ✦ Third Progress Report (October 2017-**March 2018**) of the project entitled "**Operational definition of seismic risk and intervention Technique for strategic buildings: an integrated system on HPC platform**", submitted by Dr. Kapil Mohan.
- ✦ **Annual Progress Report (March 2017 to April 2018)** of the project entitled "**To map the subsurface nature and extension of the Kachchh Mainland Fault (KMF) through magneto-telluric and geoelectrical methods along the entire length of the KMF zone**" PI: Dr. Kapil Mohan; Co-PI: Mr. Pavan Gayatri and Dr. Rakesh Dumka submitted to Ministry of Earth Sciences, Govt. of India.

NOTABLE EVENTS

Awards/Recognition

- ✦ P. Narain has been awarded 2nd in the Best Poster Competition category during in the **second National conference on "Recent studies on the geology of Kachchh basin"** organised by KSKV University, Bhuj during 29-31 December, 2018.
- ✦ Sneha Mishra has been awarded 3rd in the Best Poster Competition category in the **second National conference on "Recent studies on the geology of Kachchh basin"** organised by KSKV University, Bhuj during 29-31 December, 2018.

Meetings/ conferences attended/ papers presented

- ✦ Neha Joshi attended the Advanced Training Course on Geological Mapping in **"Sedimentary Terrain" for Officers of GSI and State DGMs, other organizations and University scholars** held during April 16-30, 2018.
- ✦ P. Narain, attended a 2 weeks training course on Microwave Remote Sensing, organized by National Remote Sensing Centre, ISRO, Hyderabad from 16th to 27th April 2018.
- ✦ **Sh. Akash Solanki and Sh. Russi Modi has attended Training Workshop on "Urban Risk Reduction and Resilience: Capacity Development for Making Cities Resilient to Disasters"** at Gujarat Institute of Disaster Management, Gandhinagar from 17-20 April, 2018.
- ✦ An international school on use of **e-infrastructure in Seismology" was organized in** collaboration with the Department of Engineering and Architecture (DEA), Trieste University during 23-26 April, 2018, funded by the Friuli Venezia Giulia Region, Italy, Coordinators: Dr. Kapil Mohan, ISR Gandhinagar (India) and Prof. Fabio Romanelli, DEA (Italy).
- ✦ Dr. Kapil Mohan has attended meetings on Science, Technology and Innovation Policy, Government of Gujarat on 18.04.2018 at GUJCOST, Gandhinagar and on 02.06.2018 at Science City, Ahmedabad.
- ✦ Dr. Kapil Mohan attended meeting for the Seismic hazard assessment of Bhadbhut Barrage site with Sh. Tushar Shah and Sh. N.R. Patel, Assistant engineers, KALPSAR Department on 02.05.2018 and 21.06.2018.
- ✦ Dr. Kapil Mohan has presented the extended proposal for Seismic hazard assessment of Devni Mori sit at the office of principal Secretary, Tourism and Devsthanam office in Gandhinagar on 07.05.2018.
- ✦ Dr. Kapil Mohan presented the project proposal entitled **"Seismic Hazard Assessment and salinity ingress monitoring for the proposed Barrage across River Narmada near Bhadbhut, Distt. Bharuch"** in Scientific audit Committee meeting of KALPSAR and water resource department, Government of Gujarat on 29.05.2018.
- ✦ **Pallabee Choudhury delivered a talk on "Role of ISR in monitoring seismic activity and seismic micro-zonation of areas prone to earthquakes" at GIDM on 30.05.2018.**
- ✦ K K S Thingbaijam delivered an invited talk on Advancing Knowledge of Earthquake Source, at Department of Earth Sciences, Indian Institute of Technology Kanpur on 04.06.2018.
- ✦ Dr. A. P. Singh delivered a lecture titled **"Disaster Resistant Construction Technologies and Practices"** at GIDM from 18 – 20th June 2018 in the training program at Gujarat Institute of Disaster Management (GIDM), Gandhinagar.
- ✦ Dr. Kapil Mohan attended meeting with MD, Tourism Corporation of Gujarat Ltd. (TCGL) on 20.06.2018 regarding extended proposal of site specific seismic hazard assessment of Devni Mori site.

- ✦ Dr. Kapil Mohan has delivered an expert talk on "Seismic Microzonation" at Gujarat Institute of Disaster Management (GIDM), Gandhinagar Dtd. 26.06.2018 in a training program on "DRR inclusion in WASH and Health Institutions (Structural / Non-structural Safety).
- ✦ Dr. Sumer Chopra has attended a meeting at NDMA as an expert regarding installation of EEW systems in parts of India.
- ✦ Dr. A. P. Singh delivered a lecture as a Resource Person on **"An Introduction to Earthquakes & Earthquake Hazards"** in the training program held at GIDM, Gandhinagar on 6th July 2018.
- ✦ Rakesh K Dumka, attended a MoES-PAMC meeting, and presented the progress of **project entitled "GPS study along KHF in Kachchh" under the AFM program of MoES** during 16-17 July 2018.
- ✦ Dr. Kapil Mohan has attended the 5th PAC meeting at IIT Kanpur on AFM Program of MoES, New Delhi and presented the progress of the project entitled "To map the subsurface nature and extension of the Kachchh Mainland Fault (KMF) through magneto-telluric and geoelectrical methods along the entire length of the KMF zone".
- ✦ **Dr. Kapil Mohan delivered the presentation entitled "Magnetotellurics Capacity of ISR"** to a delegation from ONGC on 24 July 2018.
- ✦ Dr. Kapil Mohan has delivered an expert talk on "Seismic Microzonation of Gujarat" at Gujarat Institute of Disaster Management (GIDM), Gandhinagar, on 25 July 2018 in a training program on "Structural and Non-structural Mitigation for Schools".
- ✦ Rakesh K Dumka, attended a DST-PAMC meeting, and presented the progress of the **project entitled "Identification of progressively growing crustal strain zones along MCT in Uttarakhand Himalaya using GPS geodesy" during 27-28 July 2018.**
- ✦ **Mr. Avinash Chouhan attended the Summer School on "Earth Surface Dynamics 2018"** organised by University of Potsdam, Germany during 10 August - 02 September 2018.
- ✦ D. Suri Babu and Sandip Prajapati attended a workshop on "Advances in GNSS Technologies and its applications" at Osmania University, Hyderabad during 16-19, August 2018.
- ✦ P. Narain attended a two days seminar on GIS for geomorphologic studies at PAN India, Noida during 12-13 September 2018.
- ✦ Dr. M. Ravi Kumar, Dr. Sumer Chopra, Dr. A. P. Singh, Mr. Ketan Singha Roy and Mr. Mayank Dixit attended meeting on low frequency passive seismic studies at hydrocarbon reservoir sites in Mansa and Jotana areas, Gujarat at Oil and Natural Gas Corporation Limited Mehsana, 19th September 2018
- ✦ Pallabee Choudhury, Siddharth Prizomwala and Falguni Bhattacharjee visited Indian Institute of Remote Sensing (IIRS) Dehradun during 19-22 September 2018.
- ✦ Dr. Kapil Mohan attended the Scientific Audit Committee meeting of Kalpsar deptment on during **10-11 October 2018, related to the project "Seismic Hazard Assessment and Salinity Ingression Monitoring at Bhadbhut barrage site"**.
- ✦ Ms. Neha Tanwar and Mr. Pruthul Patel have attended a short-term course on **"High-Performance Computing (HPC) and Deep Learning"** held by Electronics & ICT Academy of IIT Roorkee from 21st to 25th October, 2018.
- ✦ Archana R.K, Nandini Nagarajan and Kusumita Arora, Evaluation of Prompt penetration effects on Equatorial Electrojet in the Indian sector, International Symposium on Equatorial Aeronomy (ISEA) at PRL held at PRL during 22th – 26th October, 2018.
- ✦ **C.P.Simha delivered a talk on "Earthquake Precursory Research at MPMO, ISR"**, in a workshop on recent trends and future perspectives of earthquake precursory analysis and geodynamics held at IIRS, Dehradun on 26th Oct 2018.
- ✦ Avinash Kumar Chouhan, attended the AEG-2018 at IIT Bombay, held during Nov 1-3, 2018 and presented a poster on **"Integrated geophysical studies to delineate the structural features over the Ambaji mineralization zone, Gujarat, NW India"**.

- ✦ Dr. Rajeev Yadav attended the NISAR Science Workshop on 16th November 2018 at Space Application Centre, Ahmedabad.
- ✦ Pallabee Choudhury attended the NISAR Science Workshop on 16th November 2018 at **Space Application Centre, Ahmedabad and delivered a talk on "ISR GPS network and results"**.
- ✦ N. Bhavani, C.P.Simha, Shivam Joshi, K. M. Rao and K. V. Swami, Anomalous Geomagnetic variations associated with the 2016 New Zealand Earthquake (M7.8), 55th Annual convention of IGU 2018, held in RTU, Bhopal during 5th-7th Dec 2018.
- ✦ C.P.Simha, K.M.Rao and R.K.Dumka, Spatial and temporal behaviour of Ionospheric VTEC during the shallow earthquake of New Zealand (M 7.8) on 13th November 2016, 55th Annual convention of IGU 2018, held in RTU, Bhopal during 5th-7th Dec 2018.
- ✦ Archana R.K, Geomagnetic data characterisation and analysis of seasonal trend of Solar quiet time current at low latitude sites of Indian sector during different phase of solar cycle-24, 55th Annual convention of IGU 2018, held in RTU, Bhopal during 5th-7th Dec 2018.
- ✦ **Naveen Kumar presented a poster on "Lineaments and faults study in Dadra and Nagar Haveli, Western India: implication to Seismotectonic of the study area" in the 55th Annual convention of Indian Geophysical Union on Changing Water Cycle & Water Resources held during December 5-7, 2018.**
- ✦ Pawan Kumar Singh attended the 55th Annual convention of Indian Geophysical Union on Changing Water Cycle & Water Resources held during December 5-7, 2018.
- ✦ **Kapil Mohan has delivered an expert talk on "Seismic Microzonation" during FT Seminar, exhibition and design competitions at CEPT University, Ahmedabad under the session Advanced Analysis Technique in Earthquake engineering" held on 7th Dec 2018.**
- ✦ **Kapil Mohan presented a paper on "Kachchh Mainland Fault: Characterization and associated seismic hazard" in the 2nd International conference on Recent studies on the Geology of Kachchh Basin held at KSKV Kachchh University during 30-31st Dec. 2018.**
- ✦ **R. K. Dumka, attended and presented a paper entitled "Crustal deformation studies of Kachchh (western India) using GPS" in the second National conference on "Recent studies on the geology of Kachchh basin" organised by KSKV University, Bhuj during 29-31 December, 2018.**
- ✦ **P. Narain, attended and presented a poster entitled "Crustal deformation study using GPS and InSAR techniques in Kachchh, Western India" in the second National conference on "Recent studies on the geology of Kachchh basin" organised by KSKV University, Bhuj during 29-31 December 2018.**
- ✦ **D. Suri Babu, attended the second National conference on "Recent studies on the geology of Kachchh basin" organised by KSKV University, Bhuj during 29-31 December 2018.**
- ✦ **Nisarg Makhwana attended Second National Conference and Field workshop on "The Recent Studies on Geology of Kachchh Basin" at KSKV, Kachchh University during Dec 30, 2018- Jan 01, 2019 and participated in the poster presentation.**
- ✦ Sneha Mishra attended the Second national conference and field workshop on "Recent Studies on the Geology of Kachchh Basin" in Kachchh University during Dec 29, 2018- Jan 1, 2019 and **presented poster on "Morpho-Structural evidence of Neotectonic activity along the Vigodi Fault, Kachchh, India"**.
- ✦ Avinash Kumar Chouhan, attended second national conference and field workshop on recent studies on the geology of Kachchh basin during Dec 29, 2018- Jan 1, 2019 **organized by K.S.K.V. Kachchh University, Bhuj and presented a paper on "Utilization of EGM 2008 gravity data for crustal architectural study over the 1819 Allah-Bund earthquake"**.

- ✦ P. Narain and D. Suri Babu attended field trip as a part of the National conference on recent studies on the geology of Kachchh basin, organised by KSKV University, Bhuj on 1 January 2019.
- ✦ Dr. K.M. Rao represented our Department 'DST, Government of Gujarat' during Indian Science Congress held at Jalandhar, Punjab during January 2-7 2019. Our state was award the best among all states in Indian Science Congress-2019. The award was given by Hon'ble Chancellor of LPU.
- ✦ Dr. Kapil Mohan attended the meeting with representative of Gujarat Water Resource and Development Corporation (GWRDC) (Dr. R. C. Jain and Dr. D. Saha (Advisors) and Sh. Gor and Sh. Garva (Geologists)) on groundwater mapping in Kachchh at deeper depths on 04.01.2019.
- ✦ P. Narain attended 25 days training at NCESS, Trivandrum Kerala for SAR data processing in the month of January 2019.
- ✦ Dr. Kapil Mohan and Dr. Sumer Chopra visited the project site of Bhadbhut Barrage for site inspection on 9 January 2019.
- ✦ **Dr. Kapil Mohan has delivered a talk on "Magnetotelluric study to characterize the sediment thickness (including Mesozoic) and major faults in Kachchh (Gujarat)" in Society of Petroleum Geophysicist (SPG) Ahmedabad Chapter on 22 January 2019 at ISR, Gandhinagar.**
- ✦ Rakesh K Dumka, delivered an invited lecture on GPS geodesy and its application for deformation studies, as a part of the main syllabus of M.Sc. degree (Geology) in KSKV, University Bhuj, during 24-25 January 2019.
- ✦ Dr. Kapil Mohan attended the joint meeting of GWRDC and ISR on discussion of conducted geophysical survey in Kachchh for fresh water mapping Dtd. 25.01.2019.
- ✦ Dr. Kapil Mohan attended the **Pre-bid meeting of the tender entitled "Geotechnical and Geophysical investigations of eight cities (Patna, Meerut, Amritsar, Agra, Varanasi, Lucknow, Kanpur, and Dhanbad) on 28 January 2019.**
- ✦ Ashima Sodhi presented a paper at the 35th Convention of Indian Association of Sedimentologist (IAS), held at Dr. Hari Singh Gaur University, Sagar, Madhya Pradesh during 28-30 January 2019.
- ✦ Mr. Pruthul Patel and Mr. Dilip Kushwaha have presented the Ph.D. progress report for August 2018 to January 2019 on 29 January 2019 and Mr. Naveen Kumar has presented 3rd half yearly Ph.D. Progress in Gujarat University Ahmedabad on 30 January 2019.
- ✦ Dr. Kapil Mohan delivered visiting lectures to M.Sc. Geology, SEM-II students, under the subject Geophysical Exploration (CCGE-210) in KSKV Kachchh University, Bhuj during 4-5 February 2019.
- ✦ **Tarun Solanki presented a poster on "Characterizing the nature and extent of dryland fluvial response to extrinsic parameters since the Last glacial period: An example from Shetrunji basin (western India)" at the 7th meeting of the Scientific Advisory Committee (SAC) of the ISR, held on 18 February 2019.**
- ✦ **Sh. Dilip Kushwaha has presented a poster entitled "Magnetotelluric Investigation in the Talala Region of Saurashtra, Gujarat" in the 7th SAC meeting held on 18 February 2019 at ISR.**
- ✦ **Sh. Russi Modi has Presented a poster titled "Estimation of Building Damage State using Rapid Visual Screening in the 2001 Bhuj Earthquake-affected Zone, Ahmedabad City, Gujarat" in the 7th SAC meeting held on 18 February 2019 at ISR.**
- ✦ **C.P. Simha, Jayashree Bulsu, Kusumita Arora and K.M. Rao, "Identification of Geomagnetic Pulsations associated with the Geomagnetic storm, Quiet and Earthquake Days" (Poster Presented at before SAC 2019 committee on 18th Feb 2019)**

- ✦ Archana R.K, K. Arora, K.M Rao, "Geomagnetic data characterization and study of seasonal pattern of Sq current" (Poster Presented at before SAC 2019 committee on 18th Feb 2019)
- ✦ P. Narain attended special outreach session conducted by IIRS Dehradun on "Principles of Polarimetric SAR Remote Sensing and its Processing" during 18 February -01 March 2019.
- ✦ Dr. Kapil Mohan has delivered a lecture on "Role of Geophysical, Geological and Geotechnical investigations for seismic resistant designing" to the M.Tech. (Civil Engineering) students of Charusat University on 26 February 2019 at ISR.
- ✦ Dr. Kapil Mohan has attended a meeting of the project entitled "Study of Geothermal processes in Gujarat using Remote Sensing and Geophysical techniques: A potential to Martian analogue with collaborators" from SAC, ISRO, Ahmedabad on 19.03.2019.
- ✦ Dr. Kapil Mohan has presented the draft report of the project entitled "Seismic Microzonation of Bhuj City (Kachchh), Gujarat during the 6th PAMC meeting (25 -26 March 2019) of Ministry of Earth Sciences, New Delhi held at NGRI, Hyderabad.
- ✦ Rakesh K Dumka, D. Suri Babu, Sandip Prajapati, attended an introduction, installation, running and operations of newly procured GPS online Software, given by Trimble, during 25-29 March 2019.
- ✦ Sneha Mishra visited IIT(ISM) Dhanbad during 25-30 March 2019 for the academic discussions on paleostress methods with Prof. R.K. Dubey and Prof. Sharda Mohanty.
- ✦ Dr. B. Sairam demonstrated the MASW and Microtremor techniques to the participants of two-days symposium on "Current Challenges for Safe and Sustainable Structural Development" which was organized by the department of Civil Engineering, PDPU, Gandhinagar on 27 March 2019.
- ✦ Dr. Vasu Pancholi delivered a talk on "Importance of the Seismic Hazard & Seismic Microzonation" in the seminar "Seismic Hazard Assessment - Need & Techniques" (SPECTRUM-19) at Anand, Gujarat.
- ✦ Dr. K.M. Rao presided as a judge in the 26th KVS National Children Science Congress - 2018. Students from 45 Kendriya Vidyalayas of Ahmedabad Region participated in NCSC-2018.
- ✦ Dr. K.M. Rao, presided as a judge to evaluate the project/ activities of KVS 46th Jawaharlal Nehru National Science, Mathematics and Environment Exhibition for Children 2019. Students from 47 Kendriya Vidyalayas of Ahmedabad Region participated in JNNSMEE-2019.

Distiguished Visitors

- ✦ A team of ONGC officials visited ISR on 27/04/2018
- ✦ Dr. V.M. Tiwari (Director, NGRI), Dr. P.C. Rao (Director, NCESS), Dr. Vineet Gahalaut (Director, NCS), Prof. D.C. Srivastava (Head, Earth Science Dept., IIT Roorkee), Prof. Sunil Kumar Singh (Director, NIO) and Dr S. K. Som (Director, GSI) visited ISR to attend the 6th Scientific Advisory Committee (SAC) meeting of ISR on 06/06/2018
- ✦ A team of ONGC officials visited ISR on 24/07/2018
- ✦ Dr. Afroz Ahmad, Member, Narmada Control Authority visited ISR on 01/08/2018
- ✦ Shri D. Chakrapani, IAS (Retd.) Director General- APHRDI visited ISR on 30/08/2018
- ✦ Prof. S. K. Verma, Ex: Director Grade Scientist & Raja Ramanna Fellow, CSIR-NGRI and Expert advisor Heliborne Surveys to Map Aquifers, Groundwater Group (NGRI) visited ISR on 08/10/18 and deliver a talk on "Novel Applications of Time-domain Electromagnetic methods".
- ✦ The Scientific Audit Committee members and senior staff members (Gandhinagar office) of the Kalpsar department, Government of Gujarat (total 20 persons) visited ISR on 11/10/2018.

- ✦ Dr. Dhaval Joshi, Veer Narmada South Gujarat University, Surat visited ISR on 11/01/2019
- ✦ Dr. V.M. Tiwari (Director, NGRI), Dr. P.C. Rao (Director, NCESS), Dr. Vineet Gahalaut (Director, NCS), Prof. D.C. Srivastava (Head, Earth Science Dept., IIT Roorkee), and Dr P. K. Khan (Professor, ISM- Dhanbad) visited ISR to attend 7th Scientific Advisory Committee (SAC) meeting of ISR on 18/02/2019.
- ✦ **Hon'ble Chief Secretary, Gujarat State and Secretary, DST, GoG visited ISR on 14/03/2019.**

Visit of Student Groups

- ✦ A group of 10 students of Civil and Computer Science Engg. Department with their faculty members from BITS Pilani visited ISR on 23/05/2018.
- ✦ A group of 40 students of Civil Engineering Department along with their faculty members from Marwadi University, Rajkot visited ISR on 07/07/2018.
- ✦ A group of 54 M.Tech. students along with their faculty member from CEPT University, Ahmedabad visited ISR on 25/07/2018.
- ✦ A group of 40 students of Civil Engineering Department along with their faculty member from Rai University, Ahmedabad visited ISR on 26/07/2018.
- ✦ A group of 26 students of M.Tech. Structural Engineering Department along with their faculty member from CEPT University, Ahmedabad visited ISR on 14/08/2018
- ✦ A group of 49 students of 1st Sem. Computer Engg. department with their 3 faculty members from B&B Institute of Technology, Vallabh Vidhyanagar, Anand visited ISR on 05/09/2018.
- ✦ A group of 35 students of 1st Sem. and 3rd Sem. M.Sc. Geoinformatics department with their 2 faculty members from ISTAR College, Vallabh Vidhyanagar, Anand visited ISR on 18/09/2018.
- ✦ A group of 33 students of 3rd and 5th Sem B.E. Civil Engg. department with two faculty members from B.H.G.C.E.T, Rajkot visited ISR on 18/09/2018.
- ✦ A group of 58 students of 3rd and 5th Sem Electronics and Communication Engg. department with 4 faculty members from B&B Inst. of Tech., Vallabh Vidhyanagar, Anand visited ISR on 20/09/2018.
- ✦ A group of 38 students of 5th Sem B.E. Civil Engg. Department with their 2 faculty members from G.H. Patel College of Engg. & Tech., Vallabh Vidhyanagar, Anand visited ISR on 04/10/2018.
- ✦ A group of 40 students of Sangam University, Bhilwara, Rasjsthan visited ISR on 06/10/2018.
- ✦ A group of 58 students of Jamnabai Narsee School visited ISR on 30/10/2018.
- ✦ A group of 56 students of 8th Sem B.E. Civil Engg. department with two faculty members from HJD institute of technical education and research, Gujarat visited ISR on 11/01/2019.
- ✦ A group of 45 students of 6th Sem diploma in Civil Engg. department with two faculty members from HJD institute of technical education and research, Gujarat visited ISR on 17/01/2019.
- ✦ A group of 20 students of 2nd Sem M.Tech. Civil-Structural Engineering department with two faculty members from CSPIT, Charusat, Changa visited ISR on 26/02/2019.
- ✦ A group of 25 students of 2nd Sem M.Tech. Civil Engineering department with their 2 faculty members from Nirma University, Ahmedabad visited ISR on 25/03/2019.

SOCEITAL OUTREACH

GSDMA organized the School Safety Week from 25th June to 29th June July 2018, to create awareness among school children about the various hazards due to Earthquakes, Floods, Fire etc and their mitigation. ISR participated in the School Safety Week for Earthquake awareness. Three teams of ISR were deputed to provide information about Earthquake, Tsunami and what to do before, during and after an earthquake. Around 16726 students of 52 schools of Banaskantha, Navsari and Kachchh districts were given the earthquake awareness tips.

Training/supervision of students

- ✦ K K S Thingbaijam trained Ms Shivani Gupta, a student of M.Sc Tech Applied Geophysics, IIT-ISM Dhanbad, during the period May 21-June 30, 2018. The topics include: (1) seismic source and path characterization, (2) use of open data: source models and strong ground-motion recordings, and (3) rudimentary MATLAB programming.
- ✦ B Sairam supervised the dissertation work of Bhawesh Chandra Pandey, a 6th Semester student of B.Tech Geoscience, Department of Petroleum Engineering and Earth Sciences, **University of Petroleum and Energy Studies. The topic of dissertation is "Estimation of S-wave Velocity Surface Wave Method".**
- ✦ Sh. Kulin Dave (Civil Engg, B.Tech. Sem VIII), Nirma University has completed his Major Project-Dissertation, One dimensional ground response analysis for Rapar City (Kachchh) subjected to strong ground motion from 01.01.2018 to 14.05.2018 under the supervision of Dr. Kapil Mohan.
- ✦ Ms. Ashu Kanwar (M.Tech. Applied Geophysics-IIIyr), Kurukshetra University, **Kurukshetra completed her dissertation on " Seismic Hazard assessment of Dadra and Nagar Haveli (U.T.)." from 01.03.2018- 18.06.2018** under the supervision of Dr. Kapil Mohan.
- ✦ Six B.E students of Civil Engineering Department from Birla Institute of Technology and science, Pilani completed their dissertation on **"Seismic hazard assessment of Gujarat with GIS techniques"** under guidance of Sh. Vasu Pancholi.
- ✦ Falguni Bhattacharya supervised three students from Kachchh University for their M.Sc. dissertation work.
- ✦ Pallabee Choudhury guided Mr Hardeep Panchal, a student from Kurukshetra University for his MTech dissertation work. The title of his work is **"Estimation of Crustal Strain using Least Square Collocation Method".**
- ✦ Dr. Santosh Kumar guided Sh. Tony Saini from Kurukshetra University, Kurukshetra for his dissertation work on **"Estimation of Earthquake Source Parameters of Small Earthquakes in Arunachal Pradesh and its Adjoining region of NE, India".**
- ✦ Ms. Athira C. P., a second year student of M.Sc. (4th Sem) in Marine Geology, Cochin University of Science and Technology has completed her dissertation under Dr Archana Das on "Paleoenvironmental Changes During The Middle To Late Holocene Period : A Study From Lothal Region ~ A Harappan Dockyard, Mainland Gujarat".
- ✦ Ms. Layana .V. K., a second year student of M.Sc. (4th Sem), in Marine Geology, Cochin University of Science and Technology has completed her dissertation on "Application of

Total Foraminifera Number in Paleoenvironmental Reconstruction: An Example of Lothal" under the guidance of Dr Archana Das.

- ✦ Eight students from different institutes did their internship at ISR. The topics are listed below:

Name	Institute	Topic
Vishnu Kant Verma	IIT, Bombay	Seismological signal processing
Anupam Patel	IIT (ISM), Dhanbad	Earthquake location using Geiger's method and magnitude determination
Rigvita Sharma	BITS Pilani	Preparation of synthetic seismograms using wavenumber integration and modal summation technique
Poorav Parekh	BITS Pilani	Determination of earthquake moment tensor solution using damped weighted least-square inversion method by singular value decomposition
Sarthak Agarwal	BITS Pilani	Use of Seisan for estimation of epicentral parameters
Piyush Garg	BITS Pilani	Time lag between earthquake energy releases for different regions of Himalaya
Mr. Vaibhav Joshi	UPES, Dehradun	Preparation of SQL database containing earthquake information
Vishvendra Singh	IIT, Roorkee	Preparation of webpage showing earthquake information

- ✦ Six students from BITS Pilani of B-tech did their dissertation on "First order Seismic Hazard Assessment of Gujarat Region" from May 21 to July 13, 2018 under guidance of Dr. Vasu Pancholi
- ✦ One student from UPES university did MTech dissertation from May to July 2018 on **"Developing regression relationship between SPT N and shear wave velocity"** under guidance of Dr. Vasu Pancholi.
- ✦ Dr. B Sairam supervised dissertation work of Bhawesh Chandra Pandey, a 6th Semester student of B.Tech Geoscience, Department of Petroleum Engineering and Earth Sciences, UPSE during May - **July 2018. The topic of dissertation is "Estimation of S-wave velocity surface wave method"**.
- ✦ Pallabee Choudhury has imparted **training on "Strong motion data analysis"** to Ms. Santhoshi Panamareddy, a 2nd year student of MSc Geophysics from Adikavi Nannaya University. Duration of the training: Dec 21, 2018- Jan 30, 2019.
- ✦ Ms. Puja Kutafale, Swami Ramanand Teerth Marathwada University, Nanded, Maharashtra attended summer training during Dec 3- 31, 2018 at ISR.
- ✦ Dr. B Sairam is supervising M Sc. dissertation work of Ms. V. Muthulakshmi, a final student of Applied Geophysics, the Center for Geotechnology, Manonmaniam Sundaranar

University, Tirunelveli, Tamilnadu. The topic of the work is **“Two-Dimensional Reflection Land Seismic Data Processing and Interpretation”**.

- ✦ Dr. B Sairam has supervised the M Sc dissertation work of Mr. P. Balachandar, a final student Applied Geophysics, the Center for Geotechnology, Manonmaniam Sundaranar University, Tirunelveli, Tamilnadu. The topic of the work is **“Processing of Two-Dimensional Reflection Land Seismic Data of Alaska Oil field data using Seismic Unix”**.
- ✦ Dr Vasu Pancholi has guided six students (three students of M.Sc Geology, Earth Science Department of the Gujarat University and three students of M.Sc Geology from Bundelkhand University) for their M.Sc dissertation.
- ✦ Mr. Maripireddi Ashok, a 2nd Year M.Sc (Geophysics) student from Department of Geology, Adikavi Nannaya University, Rajamahendravaram, Andhra Pradesh, has successfully completed his dissertation work under guidance of Dr. A.P. Singh during the period from 08 December to 31st January 2019, at the Institute of Seismological Research, Gandhinagar.
- ✦ Ms. M. Rema Vaishali, a 2nd Year M.Sc (Applied Geophysics) student from the Center for Geotechnology, Manonmaniam Sundaranar University, Tamilnadu, has successfully completed her dissertation work under guidance of Dr. A.P. Singh during the period from 4th January to 24th March 2019, at the Institute of Seismological Research, Gandhinagar.
- ✦ Ms. Ramalakshmia 2nd Year M.Sc (Applied Geophysics) student from the Center for Geotechnology, Manonmaniam Sundaranar University, Tamilnadu, has successfully completed her dissertation work under guidance of Dr. Srijayanthi G during the period from 4th January to 24th March 2019, at the Institute of Seismological Research, Gandhinagar.

CAMPUS NEWS AND EVENTS



International School on **“Operational definition of seismic risk and intervention techniques for strategic buildings: an integrated system on HPC platform”**, held at ISR during 23-26 April 2018



A team of ONGC officials visited ISR on 27/04/2018



12th Foundation Day Celebration of ISR on 20/05/2018



Poster Presentation during the 6th SAC meeting, held on 06/06/2018



Independence Day Celebration at ISR on 15/08/2018



Republic Day Celebration at ISR on 26/01/2019



ISR Scientist Dr. Archana Das receiving GSA - Prof. M.P. Patel Best Ph.D thesis Award in Geology for the Year 2018, given by Gujarat Science Academy on 03/02/2019.



Scientific presentation during 7th SAC meeting, held on 18/02/2019



Poster presentation during the 7th SAC meeting, held on 18/02/2019



ISR staff with SAC members



Hon'ble Chief Secretary, Gujarat State and Secretary, DST, GoG visited ISR on 14/03/2019



Hon'ble Chief Secretary, Gujarat State and Secretary, DST, GoG visited ISR on 14/03/2019

List of Projects received

Sl. no	Name of Funding Agency	Title
1.	Dept of Science & Technology, Govt. of Gujarat	Human Response to Landscape Dynamics during the last 20,000 years and Future Implications
2.	Mercator Petroleum Ltd., Mumbai	Magnetotelluric Data acquisition, processing and interpretation in the NELP Block no. CB-ONN-2005/9
3.	Space & Application Centre, Ahmedabad	Study of Geothermal processes in Gujarat using Remote Sensing and Geophysical techniques: A potential to Martian analogue (ISRO 06)
4.	Multi commodity Exchange of India Limited	Comparative seismic hazard assessment of Mumbai and GIFT City, Gandhinagar for establishment of Disaster Recovery Sites
5.	Ministry of Earth Sciences, Govt. of India	Structure, style and rates of deformation along the Himalayan Frontal Fault (HFT) zone, northeast Himalaya using an integrated geophysical and geological approach: Implications for seismic hazard scenario
6.	Saurashtra Enviro Projects Pvt. Ltd.	Strong Motion Investigation at SEPPL-Kutch
7.	L & T Chiyoda Limited	Development of site specific spectra for IOCL Bongaigaon refinery, Assam state, India
8.	Tourism Corporation of Gujarat Ltd	Site Specific Seismic Hazard Assessment of Devni Mori site, Near Mesow Dam, District Sabarkantha, Gujarat
9.	L&T Hydrocarbon Engineering Limited	Site specific seismic hazard assessment and development of site specific ground response spectra for Ammonia Storage tanks at cosidering DSHA and PSHA at HURL Barauni Project
10.	L&T Hydrocarbon Engineering Limited	Site specific seismic hazard assessment and development of site specific ground response spectra for Ammonia Storage tanks at cosidering DSHA and PSHA at HURL Sindri Project
11.	Adani Green Energy Ltd.	Site specific seismic study to develop site site specific response spectrum at Khavda wind mill site, Kachchh (Gujarat)
12.	National Hydroelectric Power Corporation (NHPC) Limited	MEQ Data Processing, Interpretation and report preparation of earthquake data generated for 2017
13.	Narmada, Water Resources, Water Supply and Kalpsar Department, Govt. of Gujarat	Seismic Hazard Assessment and Salinity Ingress monitoring for proposed Bhadbhut Barrage Project across river Narmada near Bharuch, Gujarat
14.	Oil and Natural Gas Corporation (ONGC), Vadodara	Low Frequency Passive Seismic (LFPS) survey in Mansa, Jotana and Linch, Cambay basin
15.	Narmada, Water Resources, Water Supply and Kalpsar Department, Govt. of Gujarat	Geophysical investigation in the Kachchh district - Groundwater exploration
16.	Gujarat Horticulture Mission, Govt. of Gujarat	Groundwater exploration at Majivana Dist. Porbandar